Zeiger, Lucas (2022) *Targeting PI3-kinase signalling in genetically engineered mouse models of intestinal cancer.* PhD thesis.

https://theses.gla.ac.uk/83180/

Copyright and moral rights for this work are retained by the author

A copy can be downloaded for personal non-commercial research or study, without prior permission or charge

This work cannot be reproduced or quoted extensively from without first obtaining permission in writing from the author

The content must not be changed in any way or sold commercially in any format or medium without the formal permission of the author

When referring to this work, full bibliographic details including the author, title, awarding institution and date of the thesis must be given

Enlighten: Theses
https://theses.gla.ac.uk/
research-enlighten@glasgow.ac.uk

Targeting PI3-Kinase Signalling in Genetically Engineered Mouse Models of Intestinal Cancer

Lucas Zeiger,
BSc, MSc.

Supervisor: Owen Sansom

Thesis Submitted to the University of Glasgow for the Degree of Doctor of Philosophy (PhD)

College of Medical, Veterinary, and Life Sciences

May 2022

University of Glasgow

CANCER RESEARCH UK | BEATSON INSTITUTE

CRUK Beatson Institute
Garscube Estate
Switchback Road
Glasgow
G61 1BD
United Kingdom

Abstract

PI3-Kinase signalling is frequently dysregulated in human colorectal cancer (CRC), but its role in cancer initiation, progression to malignant disease, and subsequent impact upon response to treatment are not fully understood.

In order to address these ongoing clinical concerns, I have developed and characterised a novel collection of genetically engineered mouse models of intestinal cancer, driven by hyperactivation of the PI3-Kinase signalling pathway. Targeted expression of oncogenic *Pik3ca*^{H1047R} or deletion of the negative regulator *Pten* in the intestinal epithelium result in rampant acceleration of tumourigenesis in models driven by loss of the tumour suppressor *Apc*. Moreover, PI3-Kinase and *Kras* mutations, which co-occur in human CRC, strongly synergise to drive intestinal tumour initiation and alter the transcriptional landscape.

Using these advanced preclinical models as a platform, I have now interrogated the therapeutic impact of targeted inhibition of key PI3-Kinase/MAPK/mTOR signalling nodes. From these studies, a number of key observations were made, in particular, oncogenic *Kras* mutations drives resistance to PI3-Kinase alpha inhibition, irrespective of concomitant PI3-Kinase mutation. Moreover, models which were driven by activation of PI3-Kinase signalling in the absence of *Kras* mutation were acutely sensitive to mTORC1 inhibition, with *Kras* mutation again seen to drive resistance. The therapeutic approaches tested here indicate that combination approaches may be the most effective means of driving therapeutic benefit in CRC, particularly in the context of *KRAS* mutation.

Through the research described here, I have developed a set of mouse models which will hopefully aid the development of novel therapeutic approaches for a large proportion of CRC patients, particularly those for whom current therapeutic options are limited.

Table of Contents

Targeting PI3-Kinase Signalling in Genetically Engineered Mouse Models of Intestinal Cancer 1
Abstract 2
Table of Contents 3
List of Tables 6
List of Figures 7
Acknowledgement 14
Author's declaration 15
Definitions/Abbrevations 16
Chapter 1 Introduction 19
1.1 The intestine 19
1.1.1 Intestinal epithelial homeostasis 21
1.2 Colorectal cancer initiation and progression 22
1.3 Cellular and organismal growth regulation, and their dysregulation in cancer 25
1.3.1 Wnt signalling 26
1.3.2 MAPK signalling 29
1.3.3 PI3-Kinase signalling 33
1.3.4 mTOR signalling 43
1.3.5 Signalling pathway interactions 47
1.4 Aims 49
Chapter 2 Materials and Methods 51
2.1 *In Vivo* experiments 51
2.1.1 Mouse Housing and Ethics 51
2.1.2 Genetic Alleles (Mice) 51
2.1.3 In Vivo Inductions 52
2.1.4 In Vivo drug treatments 52
2.2 Tissue Sampling and Processing 53
2.3 Immunohistochemistry and RNA in situ hybridisation 54
2.4 Tumour scoring 55
2.5 Slide Scanning and BrdU quantification 56
2.6 Tissue processing and RNA-sequencing 56
2.6.1 RNA Extraction 56
2.6.2 RNA-Sequencing and Data Analysis 56
2.7 Organoid/Spheroid Isolation and Culture 58
2.8 PCR detection of recombined *Rictor*^{fl} allele 59
2.9 Western blot to detect RICTOR 61
2.10 Statistical analyses 61
2.11 Illustrations 61
Chapter 3 PI3-Kinase signalling hyperactivation in mouse models of intestinal cancer 62
3.1 PI3-Kinase-activating mutation in *Apc*-loss predisposed mice 63
3.1.1 Intestine-specific heterozygous Apc knock-out leads to tumour formation 63
3.1.2 Heterozygous Pik3ca^{H1047R} mutation does not alter survival, but promotes adenoma to adenocarcinoma progression in Villin-CreER^{T2}; Apc$^{fl/wt}$ mice 66
3.1.3 Homozygous Pik3ca^{H1047R} mutation drives small intestinal tumour initiation, but not adenoma to adenocarcinoma progression 70
3.1.4 Discussion 75

3.2 *Pten*-KO in *Apc*-loss predisposed mice 77
3.2.1 Intestine-specific heterozygous knock-out of Pten leads to earlier clinical endpoint in Apc-loss predisposed mice 77
3.2.2 Homozygous Pten knock-out leads to rapid small intestinal tumour formation 82
3.2.3 Discussion 85
3.3 PI3-Kinase hyperactivation in $Apc^{fl/fl}$ mice 86
3.3.1 Discussion 91
3.4 Combined *Pten*-KO and $Pik3ca^{H1047R}$ mutation in *Apc*-loss dependent intestinal cancer 92
3.4.1 Heterozygous $Pik3ca^{H1047R}$ mutation in Villin-$CreER^{T2}$; $Apc^{fl/wt}$; $Pten^{fl/wt}$ accelerates clinical endpoint and progression to invasive adenocarcinoma 93
3.4.2 Homozygous Pik3ca mutation further accelerates the Villin-$CreER^{T2}$; $Apc^{fl/wt}$; $Pten^{fl/wt}$ model 95
3.4.3 Heterozygous $Pik3ca^{H1047}$ mutation accelerates small intestinal tumour formation in Villin-$CreER^{T2}$; $Apc^{fl/wt}$; $Pten^{fl/fl}$ mice 97
3.4.4 Discussion 102
3.5 PI3-Kinase hyperactivation in *Apc* wildtype mice 103
3.5.1 Discussion 108
3.6 PI3-Kinase-activating mutation in context of KRAS mutation 110
3.6.1 $Kras^{G12D}$ mutation results in small intestinal, and colonic tumour initiation in Villin-$CreER^{T2}$; $Apc^{fl/wt}$ mice 110
3.6.2 Heterozygous $Pik3ca^{H1047R}$ mutation further reduces survival in $Kras^{G12D}$ mutant mice by accelerating small intestinal tumour initiation. . 112
3.6.3 Homozygous $Pik3ca^{H1047R}$ mutation further accelerates the Villin-$CreER^{T2}$; $Apc^{fl/wt}$; $Kras^{G12D/wt}$ model 114
3.6.4 Discussion 118
3.7 *Pten*-KO in context of KRAS mutation 119
3.7.1 Discussion 121
3.8 PI3-Kinase signalling hyperactivation in $Apc^{fl/fl}$; $Kras^{G12D}$ mice 122
3.8.1 $Kras^{G12D}$ mutation in Villin-$CreER^{T2}$; $Apc^{fl/fl}$ mice 122
3.8.2 PI3-Kinase hyperactivation in Villin-$CreER^{T2}$; $Apc^{fl/fl}$; $Kras^{G12D/wt}$ mice 125
3.8.3 Discussion 131
3.9 Discussion 133
Chapter 4 Targeted inhibition of the PI3K/MAPK/MTOR signalling network in PI3-Kinase signalling hyperactive intestinal cancer GEMMs 136
4.1 Targeting PI3-Kinase isoforms in intestinal cancer GEMMs 137
4.1.1 PI3-Kinase beta/delta inhibition does not prevent outgrowth of Pten deficient intestinal cancer models 138
4.1.2 PI3-Kinase alpha inhibition delays tumour formation in Villin-$CreER^{T2}$; $Apc^{fl/wt}$; $Pten^{fl/fl}$ ageing mice 139
4.1.3 $Pik3ca^{H1047R}$ mutant mice still respond to PI3-Kinase alpha inhibition 141
4.1.4 Discussion 144
4.1.5 Kras mutation drives resistance to PI3-Kinase alpha inhibition 146
4.1.6 PI3-Kinase beta/delta inhibition prolongs survival in Villin-$CreER^{T2}$; $Apc^{fl/wt}$; $Kras^{G12D/wt}$ mice, likely not through the Rac1/CDC42 axis 152
4.1.7 Discussion 154
4.2 Targeting mTOR in PI3-Kinase hyperactive GEMMs 156
4.2.1 Rictor KO does not prevent outgrowth of tumours in Villin-$CreER^{T2}$; $Apc^{fl/wt}$; $Pten^{fl/fl}$ mice 157

4.2.2 Rictor KO is dispensable for PI3-Kinase mutant intestinal cancer outgrowth, but limits occurrence of invasive adenocarcinoma 160
4.2.3 AKT inhibition does not prevent outgrowth of Pten deficient intestinal tumours 164
4.2.4 Rapamycin rescues late stage PI3-Kinase driven intestinal cancer models 166
4.2.5 mTOR kinase inhibition extends survival in late stage Pten-KO models 171
4.2.6 Discussion 173
4.3 Targeting mTOR signalling in *Kras* mutant intestinal cancer models ... 174
4.3.1 Rictor-KO dependent survival benefit in Villin-CreER^{T2}; Apc$^{fl/wt}$; Kras$^{G12D/wt}$ mice 175
4.3.2 Kras mutant/PI3-Kinase signalling high models are resistant to Rapamycin treatment 176
4.3.3 Discussion 179
4.4 Targeting MEK1/2 in intestinal cancer models 180
4.4.1 MEK1/2 inhibition does not provide a clear benefit in late stage Villin-CreER^{T2}; Apc$^{fl/wt}$; Pten$^{fl/fl}$ mice 181
4.4.2 MEK1/2 inhibition is effective when treated from early, but not from late in Kras and PI3-Kinase pathway co-mutated models 183
4.4.3 Discussion 189
4.5 Combination treatment approaches in intestinal cancer models 191
4.5.1 PI3-Kinase beta/delta inhibition does not synergize with MEK1/2 or mTOR kinase inhibition in Villin-CreER^{T2}; Apc$^{fl/wt}$; Pten$^{fl/fl}$ mice 191
4.5.2 Combined MEK1/2 and mTOR kinase inhibition shows synergy in Villin-CreER^{T2}; Apc$^{fl/wt}$; Pten$^{fl/fl}$ mice 193
4.5.3 MEK1/2 inhibition is needed to achieve synergy in drug combinations in Kras mutant models 194
4.5.4 Discussion 202
4.6 Discussion 203
Chapter 5 Discussion and Outlook 206
Bibliography 214

List of Tables

Table 2-1: Details of Antibodies used for Immunohistochemistry 54
Table 2-2: List of "HALLMARK" gene sets from the Molecular Signatures Database (MSigDB) 58
Table 2-3: Primers used to detect the recombined *Rictor*^{fl} allele 60
Table 3-1: Co-occurrence and Mutual exclusivety between PI3-Kinase and MAPK signalling components. Data from the Metastatic Colorectal Cancer (MSK) cohort, generated using cBioportal. 102
Table 3-2: MSK Metastatic colorectal cancer cohort mutual exclusivety analysis. Input: *KRAS* and *PIK3CA*. Data generated using cBioportal. 112
Table 4-1: Small molecule inhibitors used in this thesis 136

List of Figures

Figure 1-1: Schematics of human and mouse colons, indicating anatomical differences. 20
Figure 1-2: A small intestinal crypt villus axis, compromised of different cell types and growth factor gradients. 20
Figure 1-3: Initiation and progression of colorectal cancer in humans. 22
Figure 1-4: Frequency of selected mutations in the Memorial Sloan Kettering (MSK)- Metastatic Colorectal Cancer patient cohort and their associations to cellular signalling pathways. 25
Figure 1-5: Wnt signalling schematic depicting activated and inhibited states, and upon loss of functional APC. 26
Figure 1-6: Ras signalling diverges upon multiple effector pathways. 29
Figure 1-7: PI3-Kinase and MAPK signalling stimulate mTOR activity 33
Figure 1-8: Ras and Rho family proteins differentially regulate PI3-Kinase isoforms. 36
Figure 1-9: Domain structure of PIK3CA and prominent mutation hotspots in MSK metastatic CRC cohort. 39
Figure 2-1: RNA-scope based detection of EYFP mRNA in *Pik3ca*^{H1047R} mutant small intestinal epithelial tissue, including tumours. 51
Figure 2-2 Difference between adenoma and adenocarcinomas observed in the SIs of intestinal cancer models. 55
Figure 3-1: Summary of crosses presented in this thesis 62
Figure 3-2: Villin-CreER^{T2}; *Apc*$^{fl/wt}$ mice develop signs of intestinal cancer. 64
Figure 3-3: Villin-CreER^{T2} *Apc*$^{fl/wt}$ mice develop mostly small intestinal tumours, with occasional colonic polyps. 64
Figure 3-4: Tumours in Villin-CreER^{T2}; *Apc*$^{fl/wt}$ mice rarely progress to invasive adenocarcinoma. 65
Figure 3-5: Tumour cells in Villin-CreER^{T2}; *Apc*$^{fl/wt}$ mice are high for nuclear ß-catenin 65
Figure 3-6: Heterozygous Pik3ca^{H1047R} mutation does not modulate survival of Villin-CreER^{T2}; *Apc*$^{fl/wt}$ ageing mice. 66
Figure 3-7: Heterozygous *Pik3ca*^{H1047R} mutation does not lead to increased tumour initiation. 67
Figure 3-8: Mice with heterozygous PI3-Kinase mutation have a higher proportion of invasive adenocarcinoma 67
Figure 3-9: Tumour cells in Villin-CreER^{T2}; *Apc*$^{fl/wt}$; *Pik3ca*$^{H1047R/wt}$ mice are nuclear ß-catenin high in SI adenomas and colon, while adenocarcinomas can contain mixed populations. 68
Figure 3-10: IHC characterisation of PI3-Kinase-wildtype and mutant tumours reveals high basal mTORC1 activation, no apparent pAKT-S473 engagement. 69
Figure 3-11: PI3-Kinase-wildtype and mutant tumours have high levels of PTEN. 70
Figure 3-12: Homozygous *Pik3ca*^{H1047R} mutation accelerates the Villin-CreER^{T2}; *Apc*$^{fl/wt}$ model 71
Figure 3-13: Similar tumour number in *Pik3ca*^{H1047R} mutant ageing mice at endpoint. 72
Figure 3-14: Homozygous *Pik3ca*^{H1047R} mutation leads to increased small intestinal tumour initiation. 72
Figure 3-15: Homozygous PI3-Kinase-mutation does not further increase invasive adenocarcinoma formation. 73

Figure 3-16: IHC characterisation of *Pik3ca*^{H1047R}-homozygous mutant guts reveals mTORC1 and pAKT-S473 activation in SI tumours. 74
Figure 3-17: Tumour cells in Villin-CreER^{T2}; *Apc*$^{fl/wt}$; *Pik3ca*$^{H1047R/H1047R}$ mice at endpoint are high for nuclear ß-catenin. 75
Figure 3-18: Heterozygous *Pten* knock-out leads to earlier clinical endpoint in Villin-CreER^{T2}; *Apc*$^{fl/wt}$ mice. 78
Figure 3-19: Heterozygous *Pten* knock-out in Villin-CreER^{T2}; *Apc*$^{fl/wt}$ mice does not increase overall tumour number 79
Figure 3-20: Heterozygous *Pten* knock-out leads to increased invasive adenocarcinoma formation in Villin-CreER^{T2}; *Apc*$^{fl/wt}$ mice. 79
Figure 3-21: PTEN LoH in SI tumours in Villin-CreER^{T2}; *Apc*$^{fl/wt}$; *Pten*$^{fl/wt}$ mice. .. 80
Figure 3-22: PTEN loss results in high PI3-Kinase and mTOR signalling. 81
Figure 3-23: Occurrence of PTEN negative crypts in Villin-CreER^{T2}; *Apc*$^{fl/wt}$; *Pten*$^{fl/wt}$ mice. 81
Figure 3-24: Homozygous *Pten* knock-out leads to vastly accelerated clinical endpoint in Villin-CreER^{T2}; *Apc*$^{fl/wt}$ mice. 83
Figure 3-25: Homozygous Pten knock out leads to increased small intestinal tumour formation in Villin-CreER^{T2}; *Apc*$^{fl/wt}$ mice. 83
Figure 3-26: Nuclear localisation of ß-catenin in SI tumours from Villin-CreER^{T2}; *Apc*$^{fl/wt}$; *Pten*$^{fl/fl}$ mice. 84
Figure 3-27: *Pten* deletion leads to high mTORC1 and pAKT-S473 signalling in tumours. 84
Figure 3-28: Impact of PI3-Kinase-hyperactivation on proliferation immediately post *Apc*-loss. 87
Figure 3-29: Differentially expressed genes in Villin-CreER^{T2}; *Apc*$^{fl/fl}$ vs PI3-K-hyperactive mice. 88
Figure 3-30: Summary of RNA sequencing experiment in PI3-Kinase hyperactive short term mice. 88
Figure 3-31: Reactome pathways upregulated in *Apc*$^{fl/fl}$; *Pik3ca*$^{H1047R/wt}$ vs Villin-CreER^{T2}; *Apc*$^{fl/fl}$ and genes driving the top four pathways. 89
Figure 3-32: Gene-set enrichment analysis for the Hallmark gene sets. 90
Figure 3-33: Heterozygous Pik3ca^{H1047R} mutation accellerates the Villin-CreER^{T2}; *Apc*$^{fl/wt}$; *Pten*$^{fl/wt}$ model. 94
Figure 3-34: Heterozygous *Pik3ca*^{H1047R} mutation does not drive tumour initiation in Villin-CreER^{T2}; *Apc*$^{fl/wt}$; *Pten*$^{fl/wt}$ mice. 94
Figure 3-35: Occurrence of invasive adenocarcinoma in Villin-CreER^{T2}; *Apc*$^{fl/wt}$; *Pten*$^{fl/wt}$; *Pik3ca*$^{H1047R/wt}$ mice. 95
Figure 3-36: Slightly higher frequency of PTEN loss of heterozygosity (LoH) in tumours from PI3-Kinase mutant mice. 95
Figure 3-37: homozygous Pik3ca mutation in Villin-CreER^{T2}; *Apc*$^{fl/wt}$; *Pten*$^{fl/wt}$ mice. 96
Figure 3-38: Homozygous *Pik3ca*^{H1047R} mutation drives tumour initiation in Villin-CreER^{T2}; *Apc*$^{fl/wt}$; *Pten*$^{fl/wt}$ mice. 97
Figure 3-39: Occurrence of invasive adenocarcinoma in Villin-CreER^{T2}; *Apc*$^{fl/wt}$; *Pten*$^{fl/wt}$; *Pik3ca*$^{H1047R/H1047R}$ mice. 97
Figure 3-40: Heterozygous *Pik3ca*^{H1047R} mutation in Villin-CreER^{T2}; *Apc*$^{fl/wt}$; *Pten*$^{fl/fl}$ mice leads to accelerated time to clinical endpoint. 98
Figure 3-41: Heterozygous *Pik3ca*^{H1047R} mutation drives small intestinal tumour initiation in Villin-CreER^{T2}; *Apc*$^{fl/wt}$; *Pten*$^{fl/fl}$ mice. 99
Figure 3-42: Homozygous PIK3CA mutation accellerates the Villin-CreER^{T2}; *Apc*$^{fl/wt}$; *Pten*$^{fl/fl}$ model even further. 99
Figure 3-43: Homozygous *PIK3CA*^{H1047R} mutation does not further increase tumour numbers in Villin-CreER^{T2}; *Apc*$^{fl/wt}$; *Pten*$^{fl/fl}$ mice. 100

Figure 3-44: Tumour numbers in Villin-CreER^{T2}; *Apc*$^{fl/wt}$; *Pten*$^{fl/fl}$; *Pik3ca*$^{H1047R/H1047R}$ mice at endpoint. 100
Figure 3-45: *Pik3ca*^{H1047R} mutation does not further modulate mTOR signalling markers in Villin-CreER^{T2}; *Apc*$^{fl/wt}$; *Pten*$^{fl/wt}$ and Villin-CreER^{T2}; *Apc*$^{fl/wt}$; *Pten*$^{fl/fl}$ mice based on IHC. 101
Figure 3-46: Villin-Cre^{ERT2}; Pten$^{fl/fl}$ and Villin-CreER^{T2}; *Pten*$^{fl/fl}$ Pik3ca$^{H1047R/wt}$ mice develop signs of intestinal cancer with long latency. 104
Figure 3-47: Concomittant *Pten* loss and *Pik3ca* mutation results in increased tumour burden in an *Apc*-loss independent model 104
Figure 3-48: Tumour distribution in small intestines of Villin-Cre^{ERT2}; Pten$^{fl/fl}$; Pik3ca$^{H1047R/wt}$ decreases along its axis. 105
Figure 3-49: Adenoma and adenocarcinoma arising in Villin-CreER^{T2}; *Pten*$^{fl/fl}$; *Pik3ca*$^{H1047R/wt}$ 105
Figure 3-50: Adenoma in Villin-CreER^{T2}; *Pten*$^{fl/fl}$; *Pik3ca*$^{H1047R/wt}$ mouse stained for ß-catenin reveals nuclear localisation. 106
Figure 3-51: Invasive adenocarcinoma of Villin-CreER^{T2}; *Pten*$^{fl/fl}$; *Pik3ca*$^{H1047R/wt}$ mouse stained for ß-catenin reveals heterogeneous nuclear localisation. 107
Figure 3-52: Tumouroid culture from Villin-CreER^{T2}; *Pten*$^{fl/fl}$; *Pik3ca*$^{H1047R/wt}$ SI tumour requires full growth factor mix to grow efficiently. 108
Figure 3-53: *Kras*^{G12D} mutation in Villin-CreER^{T2}; *Apc*$^{fl/wt}$ mice results in reduced survival. 111
Figure 3-54: *Kras*^{G12D} mutation drives small intestinal and colonic tumour initiation. 111
Figure 3-55: Nuclear localisation of ß-catenin in Villin-CreER^{T2}; *Apc*$^{fl/wt}$; *Kras*$^{G12D/wt}$ tumour cells. 112
Figure 3-56: Strong pERK staining in *Kras*^{G12D} mutant tumours and surrounding intestinal epithelium. 112
Figure 3-57: Heterozygous *Pik3ca*^{H1047R} mutation accelerates the Villin-CreER^{T2}; *Apc*$^{fl/wt}$; *Kras*$^{G12D/wt}$ model. 113
Figure 3-58: PIK3CA^{H1047R} mutation drives small intestinal tumour initiation in Villin-CreER^{T2}; *Apc*$^{fl/wt}$; *Kras*$^{G12D/wt}$ mice. 113
Figure 3-59: Nuclear localisation of ß-catenin in Villin-CreER^{T2}; *Apc*$^{fl/wt}$; *Kras*$^{G12D/wt}$; *Pik3ca*$^{H1047R/wt}$ tumour cells. 114
Figure 3-60: Homozygous *Pik3ca*^{H1047R} mutation further accelerates the Villin-CreER^{T2}; *Apc*$^{fl/wt}$; *Kras*$^{G12D/wt}$ model. 115
Figure 3-61: Homozygous *Pik3ca*^{H1047R} mutation drives small intestinal and colonic tumour initiation. 115
Figure 3-62: Nuclear localisation of ß-catenin in Villin-CreER^{T2}; *Apc*$^{fl/wt}$; *Kras*$^{G12D/wt}$; *Pik3ca*$^{H1047R/H1047R}$ tumour cells. 116
Figure 3-63: Representative images and quatification of PTEN IHC in intestinal tumours from Villin-CreER^{T2}; *Apc*$^{fl/wt}$ (APC), Villin-CreER^{T2}; *Apc*$^{fl/wt}$; *Kras*$^{G12D/wt}$ (APC KRAS), Villin-CreER^{T2}; *Apc*$^{fl/wt}$; *Kras*$^{G12D/wt}$; *Pik3ca*$^{H1047R/wt}$ (APC KRAS PIK3CA^{HET}), and Villin-CreER^{T2}; *Apc*$^{fl/wt}$; *Kras*$^{G12D/wt}$; *Pik3ca*$^{H1047R/H1047R}$ (APC KRAS PIK3CA^{HOM}). 117
Figure 3-64: Similar abundance of Pten ISH-probe (mmPTEN) in tumours from various mouse models. 118
Figure 3-65: Villin-CreER^{T2}*Apc*$^{fl/wt}$; *Kras*^{G12D}; *Pten*$^{fl/fl}$ mice develop rapid signs of intestinal cancer. 120
Figure 3-66: *Pten*-KO in the context of *Kras* mutation drives small intestinal and colonic tumour initiation. 121
Figure 3-67: Concomitant *Pten*-KO and *Kras* mutation leads to increased small intestinal and colonic tumour initiation. 121

Figure 3-68: Similar amounts of proliferations upon *Kras* mutation in the short term model. 123
Figure 3-69: Number of significantly altered genes and volcano plot visualization in wildtype vs *Kras* mutant RNA-sequencing experiment. 123
Figure 3-70: Significantly altered Reactome pathways in wildtype vs *Kras* mutant RNA-sequencing experiment. 124
Figure 3-71: Gene-set enrichment analysis for the hallmark gene sets..... 125
Figure 3-72: Impact of PI3-Kinase-hyperactivation on proliferation immediately post *Apc*-loss in the context of *Kras* mutation. 126
Figure 3-73: Number of significantly altered genes and volcano plot visualization in wildtype vs PI3-Kinase hyperactive models from RNA-sequencing experiment in the context of *Kras* mutation. 127
Figure 3-74: Reactome pathways upregulated in Villin-CreER^{T2}; *Apc*$^{fl/fl}$; Kras^{G12D} vs Villin-CreER^{T2}; *Apc*$^{fl/fl}$; Kras^{G12D}; *Pten*$^{fl/fl}$. 128
Figure 3-75: Reactome pathways downregulated in Villin-CreER^{T2}; *Apc*$^{fl/fl}$; Kras^{G12D} vs Villin-CreER^{T2}; *Apc*$^{fl/fl}$; Kras^{G12D}; *Pten*$^{fl/fl}$ and genes driving enrichment for the extracellular matrix organisation pathway..... 128
Figure 3-76: Reactome pathways upregulated in Villin-CreER^{T2}; *Apc*$^{fl/fl}$; Kras^{G12D} vs Villin-CreER^{T2}; *Apc*$^{fl/fl}$; Kras^{G12D}; *Pik3ca*$^{H1047R/wt}$. 129
Figure 3-77: Reactome pathways downregulated in Villin-CreER^{T2}; *Apc*$^{fl/fl}$; Kras^{G12D} vs Villin-CreER^{T2}; *Apc*$^{fl/fl}$; Kras^{G12D}; *Pik3ca*$^{H1047R/wt}$. 130
Figure 3-78: Gene-set enrichment analysis for the hallmark gene sets..... 131
Figure 3-79: Occurrence of SI tumours per day survival post-induction in the models presented in this results chapter. 134
Figure 3-80: Occurrence of SI tumours per day survival post-induction in the models presented in this results chapter. 135
Figure 4-1: Targeted PI3-Kinase/MAPK/mTOR pathway inhibition by genetics and small molecule inhibitors..... 137
Figure 4-2: PI3-Kinase beta/delta inhibition does not extend survival of Villin-CreER^{T2}; *Apc*$^{fl/wt}$; *Pten*$^{fl/fl}$ ageing mice. 138
Figure 4-3: Similar amount of tumours at endpoint after AZD8186 treatment from day 5 post-induction in Villin-CreER^{T2}; *Apc*$^{fl/wt}$; *Pten*$^{fl/fl}$..... 139
Figure 4-4: AZD8835 prolongs survival of Villin-CreER^{T2}; *Apc*$^{fl/wt}$; *Pten*$^{fl/fl}$ mice.140
Figure 4-5: Similar amount of tumours at endpoint after AZD8835 treatment from day 5 post-induction in Villin-CreER^{T2}; *Apc*$^{fl/wt}$; *Pten*$^{fl/fl}$..... 140
Figure 4-6: AZD8835 prolongs survival of Villin-CreER^{T2}; *Apc*$^{fl/wt}$; *Pten*$^{fl/fl}$; *Pik3ca*$^{H1047R/wt}$ mice. 141
Figure 4-7: Similar amount of tumours at endpoint, less when adjusted for longer survival after AZD8835 treatment from day 5 post-induction in Villin-CreER^{T2}; *Apc*$^{fl/wt}$; *Pten*$^{fl/fl}$; *Pik3ca*$^{H1047R/wt}$ 142
Figure 4-8: AZD8835 prolongs survival of Villin-CreER^{T2}; *Apc*$^{fl/wt}$; *Pten*$^{fl/fl}$; *Pik3ca*$^{H1047R/H1047R}$ mice. 143
Figure 4-9: Reduced amount of tumours at endpoint after AZD8835 treatment from day 5 post-induction in Villin-CreER^{T2}; *Apc*$^{fl/wt}$; *Pten*$^{fl/fl}$; *Pik3ca*$^{H1047R/wt}$ .. 143
Figure 4-10: No signalling changes in AZD8835 treated small intestinal tumours in PI3-K high models. 144
Figure 4-11: PI3-Kinase alpha inhibition does not extend survival of Villin-CreER^{T2}; *Apc*$^{fl/wt}$; *Kras*$^{G12D/wt}$ ageing mice. 147
Figure 4-12: Increased SI tumour, decreased colon tumour number in AZD8835-treated Villin-CreER^{T2}; *Apc*$^{fl/wt}$; *Kras*$^{G12D/wt}$ mice at endpoint. 148
Figure 4-13: PI3-Kinase alpha inhibition does not extend survival of Villin-CreER^{T2}; *Apc*$^{fl/wt}$; *Kras*$^{G12D/wt}$; *Pik3ca*$^{H1047R/wt}$ ageing mice. 149

Figure 4-14: Increased SI tumour, decreased colon tumour number in AZD8835-treated Villin-CreER^{T2}; *Apc*$^{fl/wt}$; *Kras*$^{G12D/wt}$; *Pik3ca*$^{H1047R/wt}$ mice at endpoint .. 149
Figure 4-15: PI3-Kinase alpha inhibition does not extend survival of Villin-CreER^{T2}; *Apc*$^{fl/wt}$; *Kras*$^{G12D/wt}$; *Pik3ca*$^{H1047R/H1047R}$ ageing mice. 150
Figure 4-16: Less BrdU positive cells per half crypt in AZD8835 treated CreER^{T2}; *Apc*$^{fl/fl}$ *Kras*$^{G12D/wt}$ and Villin-CreER^{T2}; *Apc*$^{fl/fl}$; *Kras*$^{G12D/wt}$; *Pik3ca*$^{H1047R/wt}$ mice, compared to untreated control. 151
Figure 4-17: PI3-Kinase beta/delta inhibition extended survival of Villin-CreER^{T2}; *Apc*$^{fl/wt}$; *Kras*$^{G12D/wt}$ ageing mice. 152
Figure 4-18: PI3-Kinase beta Ras-binding domain mutation did not confer a survival benefit to Villin-CreER^{T2}; *Apc*$^{fl/wt}$; *Kras*$^{G12D/wt}$ ageing mice 153
Figure 4-19: Similar tumour numbers in Villin-CreER^{T2}; *Apc*$^{fl/wt}$; *Kras*$^{G12D/wt}$; *Pik3cb-RBD*^{Mut} models..... 154
Figure 4-20: Genetic depletion of *Rictor* does not alter time to clinical endpoint in the Villin-CreER^{T2}; *Apc*$^{fl/wt}$; *Pten*$^{fl/fl}$ ageing model. 158
Figure 4-21: Increased amount of SI tumours at endpoint after *Rictor*-KO in the Villin-CreER^{T2}; *Apc*$^{fl/wt}$; *Pten*$^{fl/fl}$ model 158
Figure 4-22: PCR amplification of recombined *Rictor*^{fl} allele..... 159
Figure 4-23: Western blot against RICTOR reveals absence of RICTOR protein in organoids/spheroids generated from tumours arising in Villin-CreER^{T2}; *Apc*$^{fl/wt}$; *Pten*$^{fl/fl}$; *Rictor*$^{fl/fl}$ mice. 160
Figure 4-24: Genetic depletion of *Rictor* does not alter time to clinical endpoint in the Villin-CreER^{T2}; *Apc*$^{fl/wt}$; *Pik3ca*$^{H1047R/wt}$ ageing model. 161
Figure 4-25: Increased amount of SI tumours at endpoint after *Rictor*-KO in the Villin-CreER^{T2}; *Apc*$^{fl/wt}$; *Pik3ca*$^{H1047R/wt}$ model 161
Figure 4-26: Increased gene-dosage of *Pik3ca*^{H1047R} reduces survival of Villin-CreER^{T2}; *Apc*$^{fl/wt}$; *Rictor*$^{fl/fl}$ mice. 163
Figure 4-27: *Pik3ca*^{H1047R} mutation dependent small intestinal tumour initiation in *Rictor* deficient mice..... 163
Figure 4-28: *Rictor*-KO limits *Pik3ca*^{H1047R} dependent occurrence of invasive adenocarcinoma. 164
Figure 4-29: Villin-CreER^{T2}; *Apc*$^{fl/wt}$; *Pten*$^{fl/fl}$ mice did not get a survival benefit from AZD5363 mediated AKT inhibition. 165
Figure 4-30: Increased amount of SI tumours at endpoint, after AZD5363 treatment from day 5 post-induction in the Villin-CreER^{T2}; *Apc*$^{fl/wt}$; *Pten*$^{fl/fl}$ model 165
Figure 4-31: Rapamycin treatment rescues late stage survival of Villin-CreER^{T2}; *Apc*$^{fl/wt}$; *Pten*$^{fl/fl}$ ageing mice..... 167
Figure 4-32: Similar number of tumours in Rapamycin treated Villin-CreER^{T2}; *Apc*$^{fl/wt}$; *Pten*$^{fl/fl}$ mice, less when adjusted for the time of sampling. 167
Figure 4-33: Rapamycin treatment rescues late stage survival of Villin-CreER^{T2}; *Apc*$^{fl/wt}$; *Pten*$^{fl/fl}$; *Pik3ca*$^{H1047R/wt}$ ageing mice. 168
Figure 4-34: Similar number of tumours in Rapamycin treated Villin-CreER^{T2}; *Apc*$^{fl/wt}$; *Pten*$^{fl/fl}$; *Pik3ca*$^{H1047R/wt}$ mice, less when adjusted for the time of sampling. 169
Figure 4-35: Immunohistochemical analysis of PI3-K/mTOR signalling targets reveal Rapamycin dependent signalling changes. 170
Figure 4-36: A BrdU positive cell population remains in tumours under Rapamycin treatment. 171
Figure 4-37: Rapamycin treatment extends survival of Villin-CreER^{T2}; *Apc*$^{fl/wt}$; *Pten*$^{fl/fl}$ ageing mice. 172
Figure 4-38: Similar number of tumours in AZD2014 treated Villin-CreER^{T2}; *Apc*$^{fl/wt}$; *Pten*$^{fl/fl}$ mice, also when adjusted for the time of sampling. 172

Figure 4-39: Genetic depletion of Rictor delays time to clinical endpoint in Villin-CreER^{T2}; *Apc*$^{fl/wt}$; *Kras*$^{G12D/wt}$ mice. 175
Figure 4-40: No impact on tumour numbers upon *Rictor*-KO in Villin-CreER^{T2}; *Apc*$^{fl/wt}$; *Kras*$^{G12D/wt}$ mice. 176
Figure 4-41: Shorter time to clinical endpoint in Rapamycin-treated Villin-CreER^{T2}; *Apc*$^{fl/wt}$; *Kras*$^{G12D/wt}$; *Pik3ca*$^{H1047R/wt}$ ageing mice, compared to untreated controls. 177
Figure 4-42: Less tumours at endpoint, but similar tumour number adjusted for time to endpoint in Rapamycin vs untreated Villin-CreER^{T2}; *Apc*$^{fl/wt}$; *Kras*$^{G12D/wt}$; *Pik3ca*$^{H1047R/wt}$ mice. 178
Figure 4-43: Shorter time to clinical endpoint in Rapamycin-treated Villin-CreER^{T2}; *Apc*$^{fl/wt}$; *Kras*$^{G12D/wt}$; *Pten*$^{fl/fl}$ ageing mice, compared to vehicle-treated controls. 179
Figure 4-44: Mek inhibition does not extend survival of Villin-CreER^{T2}; *Apc*$^{fl/wt}$; *Pten*$^{fl/fl}$ ageing mice. 182
Figure 4-45: Similar number of tumours in AZD6244 treated Villin-CreER^{T2}; *Apc*$^{fl/wt}$; *Pten*$^{fl/fl}$; mice, lower when adjusted for days post-induction. 182
Figure 4-46: MEK1/2 inhibition extended survival of Villin-CreER^{T2}; *Apc*$^{fl/wt}$; *Kras*$^{G12D/wt}$; *Pik3ca*$^{H1047R/wt}$ ageing mice when treated from day 5 post-induction. 184
Figure 4-47: Reduced tumour number in AZD6244 treated Villin-CreER^{T2}; *Apc*$^{fl/wt}$; *Kras*$^{G12D/wt}$; *Pik3ca*$^{H1047R/wt}$ mice. 184
Figure 4-48: MEK1/2 inhibition extended survival of Villin-CreER^{T2}; *Apc*$^{fl/wt}$; *Kras*$^{G12D/wt}$; *Pik3ca*$^{H1047R/H1047R}$ ageing mice when treated from day 5 post-induction. 185
Figure 4-49: Reduced tumour number in AZD6244 treated Villin-CreER^{T2}; *Apc*$^{fl/wt}$; *Kras*$^{G12D/wt}$; *Pik3ca*$^{H1047R/H1047R}$ mice. 186
Figure 4-50: Diminished effect of MEK1/2 inhibition on survival of Villin-CreER^{T2}; *Apc*$^{fl/wt}$; *Kras*$^{G12D/wt}$; *Pik3ca*$^{H1047R/wt}$ ageing mice when treated from day 21 post-induction. 187
Figure 4-51: Reduced tumour number in AZD6244 treated Villin-CreER^{T2}; *Apc*$^{fl/wt}$; *Kras*$^{G12D/wt}$; *Pik3ca*$^{H1047R/wt}$ mice from d21 post-induction. 187
Figure 4-52: MEK1/2 inhibition extended survival of Villin-CreER^{T2}; *Apc*$^{fl/wt}$; *Kras*$^{G12D/wt}$; *Pten*$^{fl/fl}$ ageing mice when treated from day 10 post-induction. ... 188
Figure 4-53: Reduced tumour number in AZD6244 treated Villin-CreER^{T2}; *Apc*$^{fl/wt}$; *Kras*$^{G12D/wt}$; *Pten*$^{fl/fl}$ mice from d10 post-induction. 189
Figure 4-54: MEK1/2 and mTOR kinase inhibition did not synergize with AZD8186 in Villin-CreER^{T2}; *Apc*$^{fl/wt}$; *Pten*$^{fl/fl}$ mice from day 25. 192
Figure 4-55: No further reduction in combination treatments driven by AZD8186 in Villin-CreER^{T2}; *Apc*$^{fl/wt}$; *Pten*$^{fl/fl}$; mice. 192
Figure 4-56: MEK1/2 and mTOR kinase inhibitor co-treatment results in a further survival benefit in Villin-CreER^{T2}; *Apc*$^{fl/wt}$; *Pten*$^{fl/fl}$ mice when treated from day 25 post-induction. 193
Figure 4-57: Similar total tumour number, reduction in tumour number per day post-induction in AZD6244/2014 combination treated Villin-CreER^{T2}; *Apc*$^{fl/wt}$; *Pten*$^{fl/fl}$ mice 194
Figure 4-58: No added benefit of PI3-Kinase beta/delta (AZD8186) and mTOR-Kinase (AZD2014) inhibitors in Villin-CreER^{T2}*Apc*$^{fl/wt}$; *Kras*^{G12D}; *Pten*$^{fl/fl}$ mice from day 10 post-induction. 195
Figure 4-59: Increased SI tumour number in AZD2014 and AZD2014/AZD8186 treated Villin-CreER^{T2}*Apc*$^{fl/wt}$; *Kras*^{G12D}; *Pten*$^{fl/fl}$ mice, similar colon tumour number. 196

Figure 4-60: PI3-Kinase beta/delta (AZD8186) and MEK1/2 (AZD6244) inhibitor combination robustly extends survival in Villin-CreER^{T2}*Apc*$^{fl/wt}$; *Kras*^{G12D}; *Pten*$^{fl/fl}$ mice from day 10 post-induction. 197
Figure 4-61: AZD6244 dependent reduction in SI and Colon in Villin-CreER^{T2}*Apc*$^{fl/wt}$; *Kras*^{G12D}; *Pten*$^{fl/fl}$ mice treated from day 10 post-induction. .. 198
Figure 4-62: PI3-Kinase beta/delta (AZD8186) inhibitor does not add benefit to MEK1/2 (AZD6244) inhibitor treatment in Villin-CreER^{T2}*Apc*$^{fl/wt}$; *Kras*^{G12D}; *Pik3ca*$^{H1047R/H1047R}$ mice from day 10 post-induction. 199
Figure 4-63: AZD6244 dependent reduction in SI and Colon in Villin-CreER^{T2}*Apc*$^{fl/wt}$; *Kras*^{G12D}; *Pik3ca*$^{H1047R/H1047R}$ mice treated from day 10 post-induction. 200
Figure 4-64: MEK1/2 (AZD6244) and mTOR (AZD2014) inhibitors synergize to extend survival in Villin-CreER^{T2}*Apc*$^{fl/wt}$; *Kras*^{G12D}; *Pten*$^{fl/fl}$ mice from day 10 post-induction. 201
Figure 4-65: AZD6244 dependent reduction in SI and Colon in Villin-CreER^{T2}*Apc*$^{fl/wt}$; *Kras*^{G12D}; *Pten*$^{fl/fl}$ mice treated from day 10 post-induction. .. 201
Figure 4-66: Summary of treatments trialled in Villin-CreER^{T2}; *Apc*$^{fl/wt}$; *Pten*$^{fl/fl}$ mice. Data generated for this graph were presented in chapter 4 of this thesis.Therapeutic benefit was defined as change in median survival in treated vs vehicle/untreated cohorts. Fill pattern in mTORC1 treatment indicates that these mice did not reach clinical endpoint and were sampled at timepoint. Dashed line separates single from combination therapies. Two stars (**) represent P-value <0.01. 204
Figure 5-1: SLC7A5 ISH reveals increased positivity upon PI3-Kinase hyperactivation in *Apc*$^{fl/fl}$ *Kras*^{G12D} short term models. 212
Figure 5-2: Preliminary data indicates diminishing effect of *Slc7a5*-KO in Villin-CreER^{T2}; *Apc*$^{fl/wt}$; *Kras*$^{G12D/wt}$; *Pik3ca*$^{H1047R/H1047R}$mice..... 212

Acknowledgement

I want to thank my supervisor Owen Sansom, who has supported my throughout my time at the CRUK Beatson Institute, first during a summer-internship and now PhD studentship. Owen was always keen to discuss findings, guide future experiments, and helped me develop to be a better scientist than I otherwise might have been. He has also continued to support me during long ill-health related absences, which I am very grateful for.

I want to thank Andrew Campbell for valuable advice, discussion, and support throughout this PhD studentship and for critically reading this thesis prior to submission. I want to thank Catriona Ford for her help during the aforementioned absences, as otherwise this thesis would not have been in the shape it is now. I want to thank Rachel Ridgway for guidance especially in regards to managing the mouse work. I want to thank all R18 lab members, past and present, for their help, for creating a welcoming environment, and making this a great place to do science. Especially during the COVID-19 pandemic, when working as a team was crucial, their effort was invaluable.

Without the fantastic facilities at the Institute, much of the work contained in this thesis would not have been possible. I want to thank Colin Nixon, Mark Hughes, and the whole Histology team for dealing with all sorts of (sometimes urgent) requests and Herculean tasks. The animal unit staff, and the animals themselves, deserve unending thanks as without their efforts none of this work would have been possible. I want to thank William Clark, Robin Shaw, and Kathryn Gilroy, who facilitated the RNA-sequencing analysis. Furthermore, I also want to thank the Beatson Central Services and the mouse transgenic team.

I want to thank my parents and family for unconditional support in all life situations for as long as I can remember. I want to thank my partner Dominika for endless support (including PCR troubleshooting!). I want to thank my friends back in Austria who have been understanding in times without contact, but always provide a warm welcome and a sense of home when I do manage to travel home. Finally, I want to thank the friends I made during this PhD studentship for the time spent together and memories made – people indeed make Glasgow.

Author's declaration

I confirm that the contents of this thesis are my own work unless stated otherwise.

The work contained in this thesis does not form part of any other degree.

Definitions/Abbrevations

4E-BP1 - Eukaryotic Translation Initiation Factor 4E (eIF4E)-Binding Protein 1

AMPK - AMP-Activated Protein Kinase

APC – Adenomatous Polyposis Coli

BMP – Bone Morphogenic Protein

CBC - Crypt Base Columnar Cells

CK1 – Casein Kinase 1

CMS – Consensus Molecular Subtype

CRC – Colorectal Cancer

CRIS - CRC Intrinsic Subtypes

DUSP - Dual Specific Phosphatase

DVL - Dishevelled

EGFR – Epidermal Growth Factor

EMT – Epithelial to Mesenchymal Transition

ENU - N-ethyl-N-nitrosourea

ERBB – Epidermal Growth Factor Receptor Family

ERK – Extracellular Signal Regulated Kinase

EtOH - Ethanol

EYFP – Enhanced Yellow Fluorescent Protein

FABP1 – Fatty Acid-Binding Protein 1

FAP – Familial Adenomatous Polyposis

FGFR – Fibroblast Growth Factor Receptor

FOX – Forkhead Box Transcription Factor Family

FZD - Frizzled

GEF – Guanine Nucleotide Exchange Factors

GEMM – Genetically Engineered Mouse Model

GPCR – G-Protein Coupled Receptor

GRB2 - Growth Factor Receptor-Bound Protein 2

GSK3 – Glycogen Synthase Kinase 3

H&E – Hematoxilin and Eosin

HIF – Hypoxia Inducible Factor

HPMC - Hydroxypropyl Methylcellulose

IGFR – Insulin-like Growth Factor Receptor

IP - Intraperitoneal

ISH – *In-situ* hybridisation

JNK - c-Jun N-terminal Kinases

KRAS – Kirsten Rat Sarcoma Virus

LGR5 - Leucine-rich Repeat-containing G-protein Coupled Receptor 5

LOF – Loss of Function

LRP5/6 - Low-density Lipoprotein Receptor-related Proteins 5/6

LTB_4 – Leukotriene B4

MAPK – Mitogen Activated Protein Kinase

MIN – Multiple Intestinal Neoplasia

MLH1 - MutL Homolog 1, Colon Cancer, Nonpolyposis Type 2

mLST8 - Mammalian Lethal with SEC13 Protein 8

MSH2 - MutS Homolog 2

mTOR – Mechanistic Target of Rapamycin

NDRG1 – n-Myc Downregulated Gene 1

NF1 – Neurofibromatosis 1

NRF2 - Nuclear Factor Erythroid 2-related Factor 2

PDGFR – Platelet-derived Growth Factor Receptor

PH – Plekstrin Homology

PI3-K – Phosphatidylinositol-3-phosphate Kinase

PIP3 - phosphatidylinositol(3,4,5)phosphate; PI(3,4,5)P3

PKC – Protein Kinase C

PTEN – Phosphatase and Tensin Homolog

Rag - Ras-Related GTPase

RAPTOR - Regulatory-associated Protein of mTOR

RBD – Ras Binding Domain

RCC – Renal Cell Carcinoma

RTK – Receptor Tyrosine Kinase

S6K – Ribosomal Protein S6 Kinase

SGK1 – Serum/Glucocorticoid Regulated Kinase 1

SI – Small Intestine

SOS1 - Son of Sevenless Homolog 1

SREBP1/2 – Sterol Regulatory Element Binding Protein 1/2

TA – Transit Amplifying

TCF/ LEF - T-cell factor/Lymphoid Enhancer-binding Factor

TGFb-beta – Transforming Growth Factor Beta

TP53 – Tumour Protein 53

TSC – Tuberosis Sclerosis Complex

VEGFR – Vascular Endothelial Growth Factor

Chapter 1 Introduction

According to Cancer Research UK data, Colorectal cancer (CRC) is the 4th most common cancer in the UK, accounting for around 16,600 annual deaths making it the second most common cause of cancer death (CRUK, 2022).

First line treatment of CRC depends on the stage of the disease at diagnosis. If possible, surgical resection can lead to curative treatment without the need for systemic chemotherapy (*NICE Guidelines Colorectal Cancer*, 2022). In cases where this is not possible, or where the disease is diagnosed at an advanced stage, patients undergo systemic chemotherapy. Widespread personalized medicine is yet to be implemented for this disease.

As this introduction will show, our understanding of CRC has far outpaced the application of anticancer drugs in the clinic. My work aims to narrow this gap by characterizing the impact of genetic alterations in clinically relevant genetically engineered mouse models (GEMMs) of intestinal cancer and trialling targeted therapy to identify vulnerabilities – or resistances.

1.1 The intestine

The intestine as an organ is conserved throughout multicellular organisms, as the efficient uptake and distribution of nutrients is a requirement to thrive. Anatomically, both human and mouse intestines can be divided into two main parts, the small intestine (SI) and colon. Proximal to distal, the SI is further sub-divided into Duodenum, Jejunum, and Ileum, with the shared goal of absorbing nutrients from the intestinal lumen. Microscopic finger-like protrusions – villi – increase the surface area of the SI for this purpose. Intestinal crypts, also referred to as crypts of Lieberkühn, are situated at the base of villi and together they form functional units of the SI. The human colon is divided into caecum, ascending-, transverse-, descending colon, and Rectum. These anatomic distinctions are not as pronounced in mice. (Figure 1-1). While humans have a poorly defined caecum, it is a bacteria-filled pouch in mice, which is always filled and aids digestion of plant matter (Kararli and Searle, 1995). The functional role of the colon is to re-absorb water and volatile fatty acids, and absence of villi differentiates it structurally from the SI.

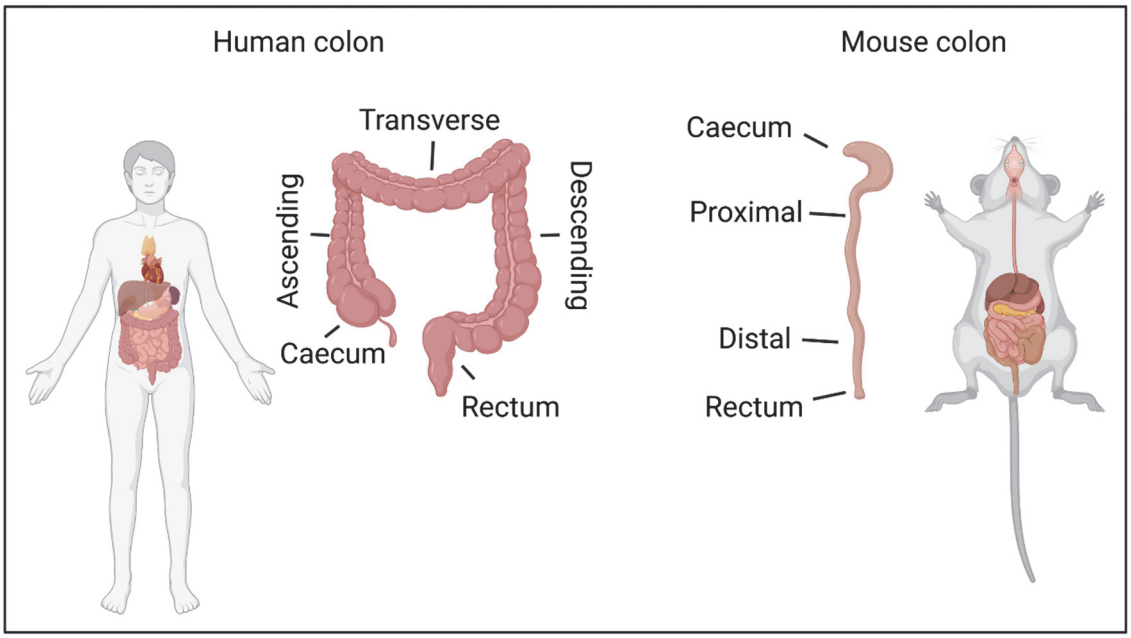

Figure 1-1: Schematics of human and mouse colons, indicating anatomical differences. The human Colon is subdivided into Caecum, Ascending, Transverse, Descending Colon, and Rectum. The mouse Colon is lacking these anatomical distinctions. Mice have a large Caecum, and their Colon can be sub-divided into Proximal- and Distal Colon, and Rectum. Image was generated using biorender.com.

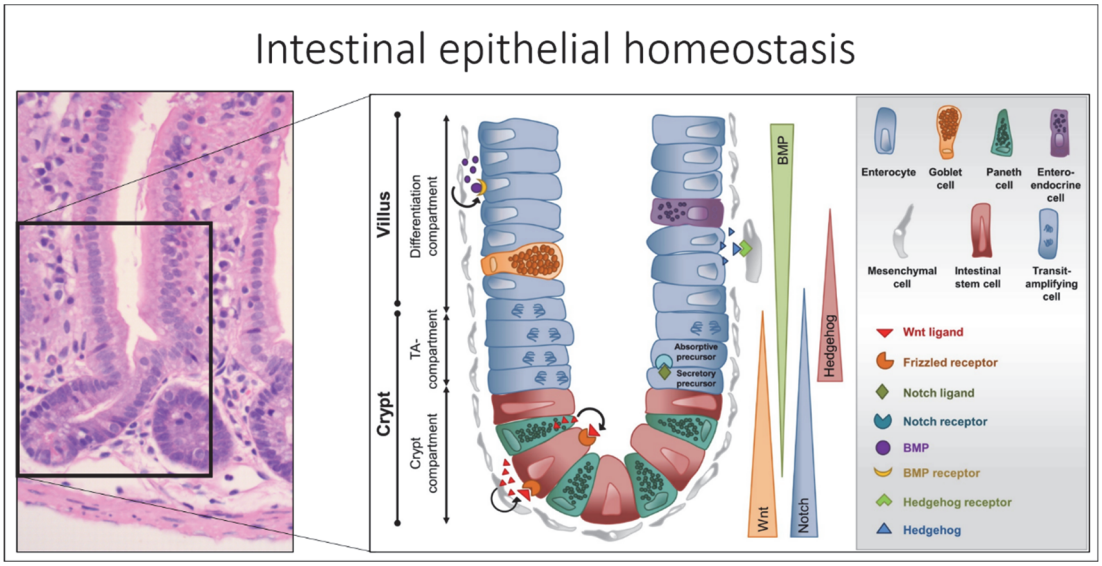

Figure 1-2: A small intestinal crypt villus axis, compromised of different cell types and growth factor gradients. Left: HE image of a small intestinal crypt. Right: Schematic of an intestinal crypt-villus axis. Abundant cell types of the small intestine, including Enterocytes, Goblet cells, Paneth cells, Enteroendocrine cells, Mesenchymal cells, Intestinal stem cells, and transit amplifying cells. Wnt, BMP, Notch, and Hedgehog growth factor gradients are indicated. Mesenchymal and Paneth cells secret Wnt-ligands. Adapted from Martini et al., 2017.

1.1.1 Intestinal epithelial homeostasis

Homeostasis of the single-layered intestinal epithelium requires the generation of multiple differentiated cell lineages from a single progenitor stem population. In summary, cells within the crypt are proliferative, with their progeny subject to lateral migration, differentiation, and eventual loss through sloughing into the intestinal lumen.

The base of the intestinal crypt is host to multipotent slowly-dividing intestinal stem cells termed crypt-base columnar cells (CBCs), interspersed with secretory Paneth cells (or deep secretory cells in the colon) (Cheng and Leblond, 1974). Together with surrounding stromal cells, this is commonly referred to as the intestinal stem cell niche (Sphyris, Hodder and Sansom, 2021). Both Paneth-, and stromal cells at the intestinal crypt base secrete Wnt ligands (Wnt signalling is discussed in detail later), which have a key role in maintenance of the the stem-cell phenotype of CBCs. Leucine-rich repeat containing G-protein coupled receptor (Lgr5) is a Wnt-target gene commonly expressed in adult stem cell populations, and known to be exclusively expressed by the CBC population in the intestine. As a result, it is widely used marker of this population (Barker *et al.*, 2007). In addition to the canonical CBC population, a second "reserve" stem cell, termed the +4 stem cell, has been identified. These cells express *Bmi1* and are able to compensate for specific ablation of Lgr5 positive cells (Tian *et al.*, 2011). More recently, evidence emerged that intestinal cells can be re-programmed to a foetal-like state during intestinal regeneration, driven by YAP/TAZ signalling (Yui *et al.*, 2018).

As epithelial progenitor cells transit upwards from the crypt base, they enter the rapidly dividing transit-amplifying (TA) zone, through which they are responsible for populating the intestinal epithelium and for its relatively fast turnover. The concentration of Wnt-ligands exists as a gradient across the crypt-villus axis, with the highest concentration found at the crypt base, reducing as one traverses upwards towards the villus. This is contrasted by a gradient of bone-morphogenic protein (bmp) abundance which is low at the base of the crypt and increases toward the villus tip (Leedham *et al.*, 2012). These and additional opposing gradients are at least in part responsible for the subsequent differentiation of cells into the cell types responsible for the organismal function of the gut in

nutrient absorption, mucus secretion, microbial defense, and endocrine secretion. These cell types include mature enterocytes, goblet cells, rare M-cells, Tuft cells, and entero-endocrine cells (Figure 1-2).

1.2 Colorectal cancer initiation and progression

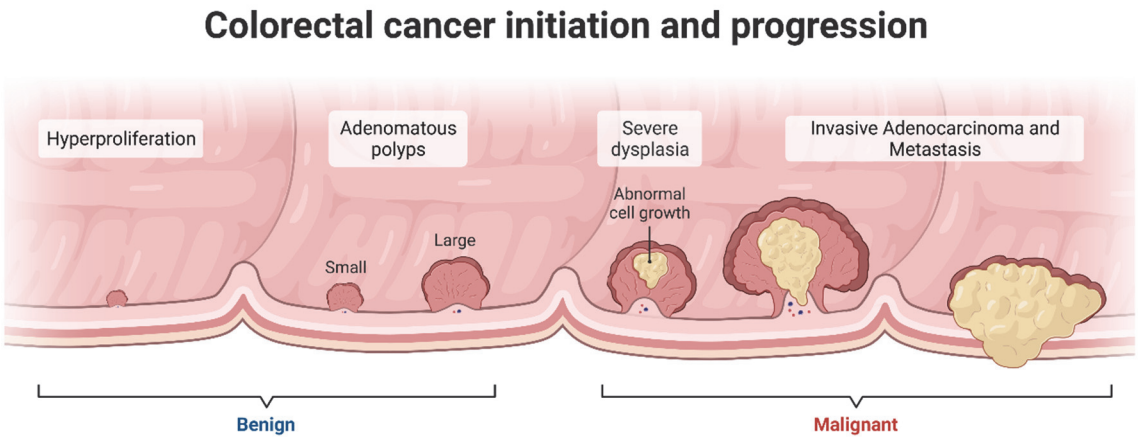

Figure 1-3: Initiation and progression of colorectal cancer in humans. Colorectal lesions were described as progressing through an initially benign adenomatous polyp stage to invasive adenocarcinoma and eventual metastasis. Image was generated using biorender.com.

Human colorectal cancers arise either sporadically or due to hereditary factors. Among the hereditary forms of CRC, heterozygous loss-of-function (LOF) mutations in the adenomatous polyposis coli (*APC*) gene are most common. These mutations give rise to an autosomal dominant disorder termed *Familial adenomatous polyposis* (FAP) (OMIM #175100), which is characterized by predisposition to intestinal cancer via sporadic loss of the healthy copy of the *APC* gene. Over time, these lesions tend to progress further to adenocarcinoma resulting in a dramatically reduced life expectancy and requiring drastic surgical intervention (colectomy) for clinical management (Okamura *et al.*, 2020). The second most common form of hereditary CRC is Lynch syndrome (OMIM #120435), also known as hereditary non-polyposis colorectal cancer. The majority of cases (>90%) are due to mutations in MSH2 and MLH1, both part of the DNA mismatch repair machinery (Barrow *et al.*, 2008).

Sporadic CRC is more common than hereditary forms and its occurrence is influenced by multiple factors such as diet, obesity, inflammatory bowel disease,

smoking, the microbiome, alcohol, and more (Murphy *et al.*, 2019). The initiation and progression of sporadic CRC was first described in 1990 by Fearon and Vogelstein. They proposed that genetic mutations conferring cells with aberrantly high Wnt signalling – most commonly in the *APC* gene – resulted in the formation of initially benign polyps in the colon. This was followed by sequential acquisition of genetic alterations in kirsten rat sarcoma viral oncogene homolog (*KRAS*), tumour protein P53 (*TP53*), and transforming growth factor beta (TGFbeta) signalling components, which drive progression to adenocarcinoma and eventually metastasis (Fearon and Vogelstein, 1990). Reality is likely more chaotic than this step-wise progression, with Sottoriva et al. more recently proposing the "big-bang" model of CRC initiation, characterised by a rapid burst of growth and mutation in the beginning of cancer formation, which does not follow stringent selection and can dictate the outcome of the tumour (Sottoriva *et al.*, 2015).

While tumours initiated by APC mutations can be thought of as the "classical" route for CRC initiation and progression, an alternative initiating process known as the "serrated" route is known to occur, whereby mutations which amplify MAPK signalling lead to the development of saw-tooth-like serration of intestinal villi, which exhibit reduced Wnt signalling at initiation when compared to classical adenomas (Rex *et al.*, 2012).

With the advent of large-scale genomics, it has also become feasible to interrogate the frequency of mutations and copy number alterations in large cohorts of CRC patients (Yaeger *et al.*, 2018). Although exact numbers vary slightly between cohorts, these efforts have confirmed that loss-of-function *APC* mutations are the most common genetic alteration in CRC, occurring in around 70-80%. Next most common is *TP53*, mutated in around 55-75% and *KRAS* mutations in around 40-50% of patients. TGF-ß pathway mutations, *SMAD4* being the most commonly altered gene, are present in ca 30% of tumours (Muzny *et al.*, 2012). These very common mutations give insights into major cellular pathways relevant for CRC initiation and progression, namely Wnt-, p53-, mitogen-activated kinase (MAPK), and TGF-ß signalling.

Phosphatidylinositol 3-Kinase (PI3-Kinase) signalling pathway mutations are common in CRC (Muzny *et al.*, 2012). Activating mutations in PIK3CA, encoding for the p110α catalytic subunit of PI3-Kinase, are present in around 15-20% of

patients. The main negative regulator *PTEN* is mutated in ca 5-10% of CRC. These commonly recurring mutations indicate that PI3-Kinase signalling has functional relevance in human CRC and impact of its hyperactivation in mouse models of intestinal cancer will be the central focus of this thesis.

While these genomic sequencing efforts and identification of key driver mutations have provided insight into the mechanisms which underlie the development and progression of colorectal cancer, to date they have proved to be relatively poor predictors of prognosis or therapeutic response. In order to address this problem, recent efforts have focussed upon using transcriptional profiling of human tumour material to develop a much more detailed understanding of the molecular biology which drives CRC. To this end, Guinney et al. applied RNA-sequencing to clinical CRC samples and described four consensus-molecular subtypes (CMS) (Guinney *et al.*, 2015). CMS1 tumours were hypermutated, encompassed most microsatellite-instable samples, and had a strong immune-inflitrate. CMS2 tumours were Wnt- and Myc-signalling high and displayed epithelial differentiation. CMS3, termed the metabolic subtype, was enriched for *KRAS* mutations and multiple metabolism-related signatures. CMS4 tumours, associated with the worst prognosis for patients, displayed high levels of epithelial to mesenchymal transition (EMT) and higher infiltration of non-cancer cells such as fibroblasts. Since samples were taken from bulk tumours, this transcriptional analysis included stromal cells. Following this, Isella et al published CRC intrinsic subtype classifiers (CRIS), derived from RNA-sequencing of patient derived xenografts, identifying five distinct epithelial-cell intrinsic subtypes. CRIS-A and CRIS-B displayed EMT, were associated with inflammatory traits, and most similar to CMS1. CRIS-C displayed ERBB1/3 acitvation and moderate WNT, while CRIS-D was characterized by high IGFR, FGFR, and WNT signalling activity. CRIS-E also displayed high WNT signalling, but was enriched for a paneth-like phenotype, while CRIS-D was enriched for an LGR5 signature indicating abundance of stem cells (Isella *et al.*, 2017).

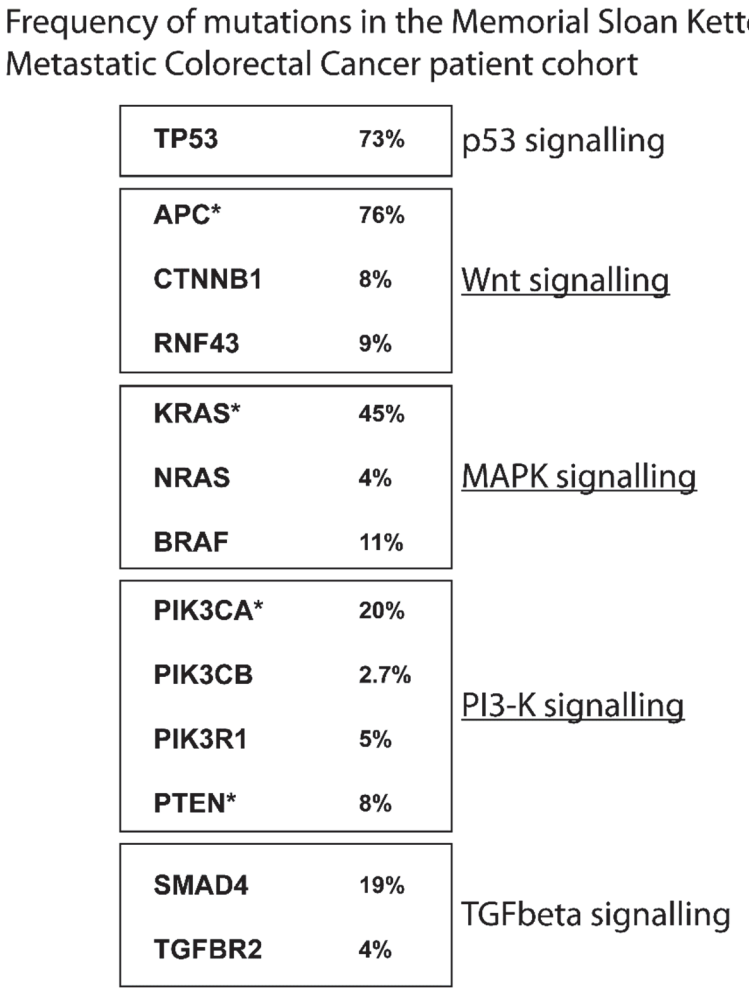

Figure 1-4: Frequency of selected mutations in the Memorial Sloan Kettering (MSK)-Metastatic Colorectal Cancer patient cohort and their associations to cellular signalling pathways. cBioportal was used to query the MSK metastatic CRC dataset for the genes indicated in the figure. Pathways specifically investigated in this thesis were underlined. Asterisks indicate genes investigated in this thesis. n = 1099. Original publication: (Yaeger *et al.*, 2018).

1.3 Cellular and organismal growth regulation, and their dysregulation in cancer

In the preceding section, I have described our current understanding of the genetic basis of CRC formation and subsequent progression. In the following section, I will go on to describe cellular pathways that are influenced by common recurring mutations in colorectal cancer, and which are thought to play a key role in tumour cell growth and survival (Figure 1-4). In brief, the research outlined in this thesis has focussed upon four key signalling pathways, each of which is thought to play a role in CRC development and progression. These are the Wnt signalling pathway, the mitogen-activated protein kinase (MAPK) pathway, the Phosphatidylinositide 3-kinase (PI3-K) pathway, and the mammalian target of rapamycin (mTOR) pathway. *KRAS* mutations within the MAPK signalling pathway confer CRCs therapy

resistance and are therefore an unmet need (Misale *et al.*, 2012). Active Ras has a broad effector network and over the years research in the lab has focussed on dissecting those, including RalGTPase signalling (Johansson *et al.*, 2019) and Rac1 signalling (Myant *et al.*, 2013; Pickering *et al.*, 2021). Both PI3-Kinase- and mTOR signalling can be seen as effectors of KRAS. Focus in this thesis was to understand their relative functional importance, and how they interact to drive intestinal cancer in mouse models.

1.3.1 Wnt signalling

1.3.1.1 Physiology

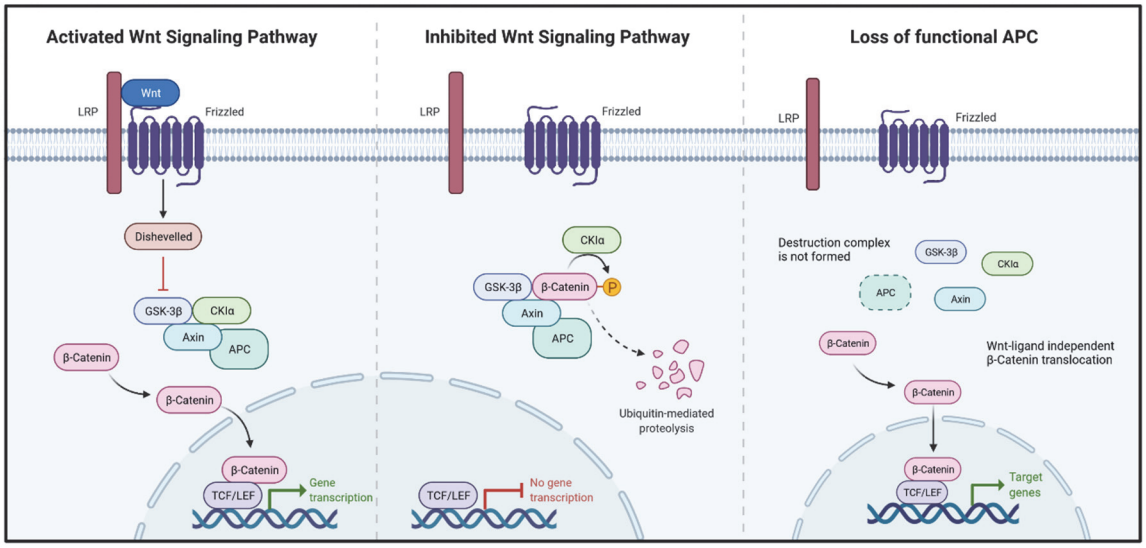

Figure 1-5: Wnt signalling schematic depicting activated and inhibited states, and upon loss of functional APC. Wnt signalling is activated by Wnt-ligands and their recognition by cell surface receptors (Frizzled and LRP). Disheveled transduces this information to the β-Catenin destruction complex (DC), consisting of GSK3-beta, CK1alpha, Axin, and APC. Under high Wnt-signalling conditions, β-Catenin is not degraded, accumulates, and translocates to the nucleus where it activates TCF/LEF transcription factors resulting in gene transcription. In low Wnt conditions, the DC is active and induces degradation of β-Catenin. Upon loss of functional APC, β-Catenin can accumulate, translocate to the nucleus, and aid transcription of Wnt-target genes. Illustration was generated using Biorender.com

In a nutshell, Wnt-signalling is an evolutionarily conserved growth-stimulating pathway which directs not only embryonal development, but also somatic tissue homeostasis (Rim, Clevers and Nusse, 2022).

By default, where Wnt-ligand abundance is low, Wnt signalling is in an “off” state, and can be switched to “on” in the presence of Wnt ligands. Control of cellular abundance and localisation of free ß-catenin protein is the ultimate impact of

Wnt-signalling. In the “Off” state, ß-catenin undergoes constant phosphorylation and subsequent ubiquitination by the so-called ß-catenin “destruction complex” (DC), which leads to its proteasomal degradation. The DC is composed of the scaffold protein Axin2, APC, Casein Kinase 1 (CK1), and glycogen synthase kinase 3 (GSK3) (Liu *et al.*, 2002; Van Noort *et al.*, 2002).

Cells recognize Wnt-ligands by heterodimeric cell-surface receptors, composed of frizzled (FZD) and low-density lipoprotein receptor-related proteins 5, and 6 (LRP5/6) (Bhanot *et al.*, 1996; Pinson *et al.*, 2000; Cong, Schweizer and Varmus, 2004). Upon Wnt-ligand binding, these receptors can bind to dishevelled (DVL), which provides a platform to bind and recruit the DC to the plasma membrane, where ß-catenin is localized. In this state, it can phosphorylate, but not ubiquitinate ß-catenin. This leads to accumulation and translocation of ß-catenin to the nucleus, where it can promote transcriptional activity of Wnt-target genes, such as *MYC*, *AXIN-2, or NOTUM,* through TCF and LEF transcription factors (Hernández, Klein and Kirschner, 2012). Levels of nuclear ß-catenin are commonly used to assess cellular wnt-pathway engagement.

1.3.1.2 Pathophysiology and intestinal cancer GEMMs

Aberrantly activated Wnt signalling appears to be a near-obligate step in the development of CRC, most commonly by loss of functional APC (Figure 1-4) (Fearon, 2011). This results in destabilisation of the DC, and accumulation of ß-catenin in the nucleus in a ligand-independent manner (Figure 1-5).

One of the earliest mouse models of intestinal tumourigenesis was developed through an *in vivo* screen using the potent carcinogen ENU (N-ethyl-N-nitrosourea). A proportion of the F2 progeny generated from an individual ENU treated mouse were noted to develop apparently heritable adult-onset anaemia, associated with the development of numerous intestinal tumours, leading to use of the term “multiple intestinal neoplasia” or MIN to describe this strain (Moser, Pitot and Dove, 1990). Around the same time, the mutation responsible for the human polyposis syndrome FAP was mapped to chromosome 5q.21, and ultimately to the *APC* gene locus (Kinzler *et al.*, 1991), and the gene responsible for the MIN phenotype was found to be the murine homologue of *APC* (Su *et al.*, 1992). Later studies aimed at development of a functional understanding of the role played by

the *Apc* gene in early tumourigenesis demonstrated that loss of APC in the murine small intestine resulted in an immediate and marked perturbation of many features of normal intestinal physiology and crypt architecture (Sansom *et al.*, 2004). Moreover, this phenotype was associated with the adoption of a characteristic, tumour-associated, Wnt-driven transcriptional programme, with both histopathological phenotype and transcriptional programme found to be highly dependent upon the transcription factor *cMyc* (Sansom *et al.*, 2007).

More recently, refined targeted transgenic mouse models have been developed to allow spatio-temporal control of *Apc* mutation. I have taken advantage of this system for generation of the transgenic mouse models described in this thesis. Briefly, and as an example, this approach takes advantage of a transgenic, tamoxifen inducible Cre-recombinase, expressed under the control of the intestinal epithelium-specific *Villin1* promoter, allowing targeted genetic recombination at defined genetic sequences ("loxP" sites) engineered into specific gene loci, such as *Apc* (Maunoury *et al.*, 1992; El Marjou *et al.*, 2004). In mice harbouring both the Villin-Cre^{ERT2} and a single copy of a targeted conditional *Apc* allele such as Apc^{Tm1tno}/Apc^{580S} (henceforth referred to as Apc^{fl}), systemic administration of tamoxifen or the active metabolite 4-hydroxytamoxifen results in targeted deletion of a single copy of *Apc* throughout the intestinal epithelium. In turn, a sporadic process driven by loss-of-heterozygosity (LOH) at the *Apc* locus in individual intestinal stem cells leads to the formation of small intestinal and colonic tumours. Similarly, in mice where the conditional targeted *Apc* allele has been bred to homozygosity, targeted recombination results in the generation of the previously mentioned crypt-expansion and hyperproliferation phenotype (data shown in results chapter 3).

Oncogenic mutations in ß-catenin in human CRC often occur in conserved phosphorylation sites on Exon 3, leading to stabilisation of the protein. By expression of such a stable mutant of ß-catenin, Leedham et al. could show that wnt-ligand abundance and stem cell number can also influence the rate and quality of small intestinal and colonic tumorigenesis. In the proximal SI, where Wnt-ligand abundance is highest, expression of stable ß-catenin resulted in high-grade dysplasia and nuclear localisation of ß-catenin. The severity of this phenotype was gradually reduced towards the distal end of the gut. APC truncating mutations in human patients occur in distinct areas, indicating that the level of

APC truncation is selected for in part due to the aforementioned regional differences (Leedham *et al.*, 2012).

While these Wnt-pathway dependent models accurately recapitulate the polyposis/tumourigenesis observed in conditions such as FAP, they fail to faithfully capture multiple aspects of sporadic CRC, such as occurrence of invasive adenocarcinomas or metastasis.

1.3.2 MAPK signalling

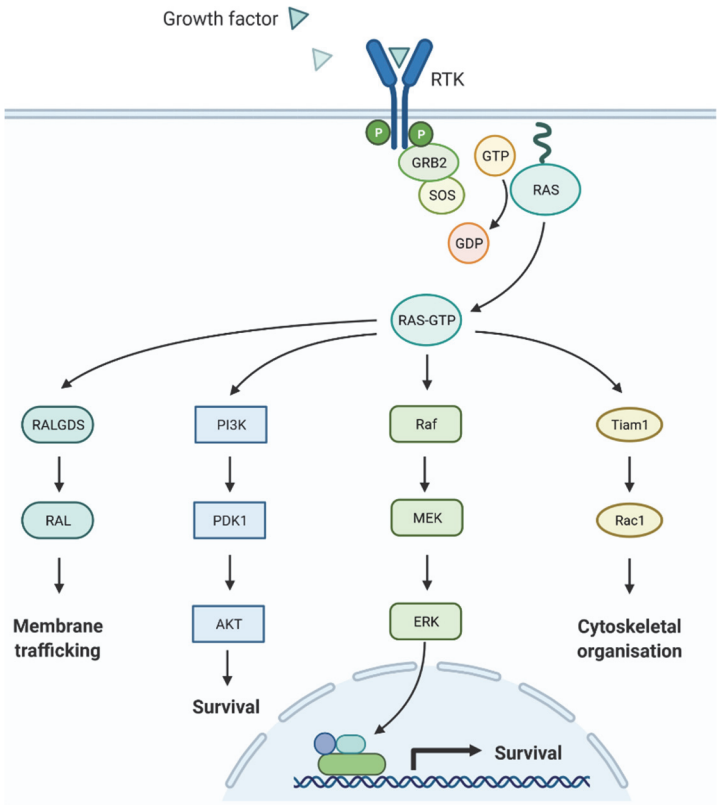

Figure 1-6: Ras signalling diverges upon multiple effector pathways. Upon growth factor binding to receptor tyrosine kinases (RTK) at membranes, Ras is loaded with GTP by its guanosine exchange factors, including SOS1 (SOS). This leads to a conformational change and allows activation of multiple effector pathways. These include Ral signalling via RALGDS, PI3-Kinase signalling via PIK3CA, canonical MAPK signalling via Raf, and Rac1 signalling via Tiam1. Canonical MAPK signalling results in transcriptional activation of multiple programs, resulting in increased cell survival. Illustration was generated using Biorender.com.

1.3.2.1 Physiology

As the name implies, mitogen-activated protein kinase signalling is a cellular response mechanism to mitogens, such as growth factors. There are four major MAPK pathways in mammals, which lead to the activation of extracellular signal-regulated kinase (ERK), p38, c-Jun N-terminal kinase (JNK), and extracellular

signal-regulated kinase 5 (ERK5). Activation of those is highly context dependent and relies on signal amplification to transduce information from the cell surface to multiple effectors, influencing cell behaviour through control of transcriptional programmes and crosstalk with other key pathways. ERK signalling is most robustly activated by growth factor/mitogen signalling and will be introduced below (Whitmarsh, 2007).

The MAPK signalling cascade is initiated at growth factor receptors, such as epidermal growth factor receptor (EGFR). These are usually receptor tyrosine kinases (RTKs), which undergo dimerization, autophosphorylation, and thereby allow formation of signalling complexes. These complexes include adapter proteins such as Growth Factor Receptor Bound Protein 2 (GRB2). Guanine exchange factors (GEF), most notably son of sevenless 1 (SOS1), localize there and can induce GTP-loading of the small GTPase RAS, leading to its activation (Lowenstein *et al.*, 1992; Pierre, Bats and Coumoul, 2011). This active, GTP bound RAS molecule, can then bind to a multitude of binding partners, initiating signalling to divergent downstream effectors (Figure 1-6). These include 1) canonical MAPK signalling through binding to RAF (Matallanas *et al.*, 2011), 2) PI3-Kinase signalling through its catalytic p110 subunit (Cuesta, Arévalo-Alameda and Castellano, 2021), 3) RAL-GTPases through binding of its GEFs (Koyama and Kikuchi, 2001), and 4) Rac through binding of its GEF (Lambert *et al.*, 2002).

In the canonical MAPK signalling cascade, active RAS-GTP (dimer) binds to, phosphorylates, induces dimerization, and consequently activates MAPKKK/mitogen activated kinase kinase kinases such as BRAF (alternatively ARAF/CRAF) (Chong, Lee and Guan, 2001; Lavoie and Therrien, 2015). This in turn leads to phosphorylation and activation of the downstream target MAPKK/mitogen activated kinase kinases, MEK1/2, which ultimately leads to phosphorylation and activation of the effector MAPK/mitogen activated kinase ERK1/2 (Fanger, Johnson and Johnson, 1997; Braicu *et al.*, 2019). These activated ERK kinases are then able to phosphorylate effector proteins in the cytosol, and are translocated to the nucleus, where they can influence a broad array of targets, including transcription factors such as c-FOS, resulting in local chromatin acetylation and transcriptional changes (Chow and Davis, 2006; Olsen *et al.*, 2006; Kosako *et al.*, 2009; Vermeulen *et al.*, 2009; Yang, Sharrocks and Whitmarsh, 2013). Recent

publications also describe larger, multimeric structures termed signalosomes (Mysore *et al.*, 2021).

Multiple negative regulators of MAPK signalling exist. Kinase Suppressor of Kras (KSR) is a scaffolding protein, appropriate levels of which are necessary to transduce signal from growth factor receptors or mutant KRAS (Therrien *et al.*, 1995; Lozano *et al.*, 2003) The intrinsic GTPase activity of Ras is stimulated by GTPase activating proteins, such as neurofibromin 1 (NF-1) (Daston *et al.*, 1992; Chaker-Margot *et al.*, 2022). Additionally, the group of dual-specificity phosphatases (DUSPs) contains several proteins termed MAPK-phosphatases (MKP) that dephosphorylate and thereby inactivate MAPK proteins in various cellular compartments (Caunt and Keyse, 2013). Of note, DUSP6 is a cytoplasmic Erk-specific phosphatase (Groom *et al.*, 1996).

1.3.2.2 MAPK pathophysiology and intestinal cancer GEMMs

MAPK signalling has an undisputed role in driving human cancer, especially given the high frequency of MAPK activating mutations observed in CRC patients (Figure 1-4). Highlighting the impact on CRC biology, the only molecular biomarkers used to stratify patients routinely are *KRAS* and *BRAF* mutations (*NICE Guidelines Colorectal Cancer*, 2022). RAS mutant patients are known to be poorly responsive to targeted EGFR inhibition (a standard of care treatment for KRAS wildtype CRC) (Misale *et al.*, 2012), while recent clinical trial data has indicated promising responses to MAPK targeting combination therapies in BRAF-mutant cancers (Kopetz *et al.*, 2019).

This biological impact is also reflected in GEMMs of intestinal cancer. Although expression of mutant KRAS in the murine intestine by itself does not have an immediate tumour phenotype, two studies from 2006 showed that KRAS mutation in the context of APC-loss predisposed mice to increased tumour formation, and resulted in an increased incidence of adenocarcinoma (Janssen *et al.*, 2006; Sansom *et al.*, 2006).

As previously discussed, the serrated route to CRC is initiated by a high MAPK drive, such as KRAS or BRAF mutation, and are associated with loss of functional p53 signalling, rather than a canonical *APC* mutation. This is reflected in mouse

models which are driven by transgenic expression of KRAS-G12D and BRAF-V600E in combination with deletion of *Trp53* or *Cdkn2a* (p16ink4a/p19arf), which are prone to intestinal adenocarcinoma formation (Bennecke *et al.*, 2010; Rad *et al.*, 2013). Additional epithelial NOTCH1 hyperactivation in *Kras* mutant/*TP53*-KO intestinal cancer GEMMs was recently shown to drive metastasis with 100% penetrance (Jackstadt *et al.*, 2019).

As I will show in chapter 3, *Kras* mutation accelerates APC-loss mediated intestinal tumour initiation. In multiple recent publications, our group has also shown key differences between *Kras* wildtype and mutant intestinal cancer models, once tumours are formed. *Kras* mutation alters cellular metabolism (Najumudeen *et al.*, 2021) and cell signalling (Knight *et al.*, 2021; Pickering *et al.*, 2021) in intestinal cancer GEMMs.

1.3.2.3 MAPK targeted drugs

Direct inhibition of KRAS has been challenging to say the least, and it has long been termed undruggable (Cox *et al.*, 2014). Recently, direct KRAS-G12C inhibitors have entered clinical trials, but G12C mutation only affects a small subset of CRC patients, and will need further research to determine effective (combination) treatment regimens (Amodio *et al.*, 2020). KRAS-G12D specific inhibitors and pan-KRAS (KRAS-SOS1-interaction) inhibitors are also in development, which, if effective, would impact a larger patient segment in CRC (Hofmann *et al.*, 2021; Wang *et al.*, 2022). While pre-clinical results look promising, these compounds may result in intrinsic or acquired resistance in cancer cells akin to BRAF-V600E inhibitors (Das Thakur *et al.*, 2013). Identifying resistance mechanisms and efficacious combination therapies prior to clinical trials would be beneficial, which highlights the importance of using pre-clinical models.

Downstream MAPK signalling inhibitors have been in development for some time, given the historic inability to target RAS directly. In this thesis, I have made use of the Mek1/2 inhibitor AZD6244 (Selumetinib) (IC50: 14nM for Mek1), which has been characterized extensively in pre-clinical models (Davies *et al.*, 2007), and has been evaluated in clinical trials, although only 1/5 completed studies in CRC has results as of May 2022 (*ClinicalTrials.gov*, 2022). In the study with results,

AZD6244 was trialled in combination with the AKT inhibitor MK-2206. Its primary outcome, >70% target biomarker reduction of pAKT and pERK, was not achieved (Do *et al.*, 2015). In the SELECT-1 phase III trial in lung cancer, selumetinib in combination with docetaxel did not provide any benefit over placebo+docetaxel in locally advanced KRAS mutant NSCLC (Jänne *et al.*, 2017). Therefore finding treatments that would be effective when combined with Mek-inhibition would be very beneficial for cancer management. PI3-Kinase co-targeting has been shown to be promising (Jaaks, Elizabeth A Coker, *et al.*, 2022) and that signalling pathway will be subject of the next part of this introduction.

1.3.3 PI3-Kinase signalling

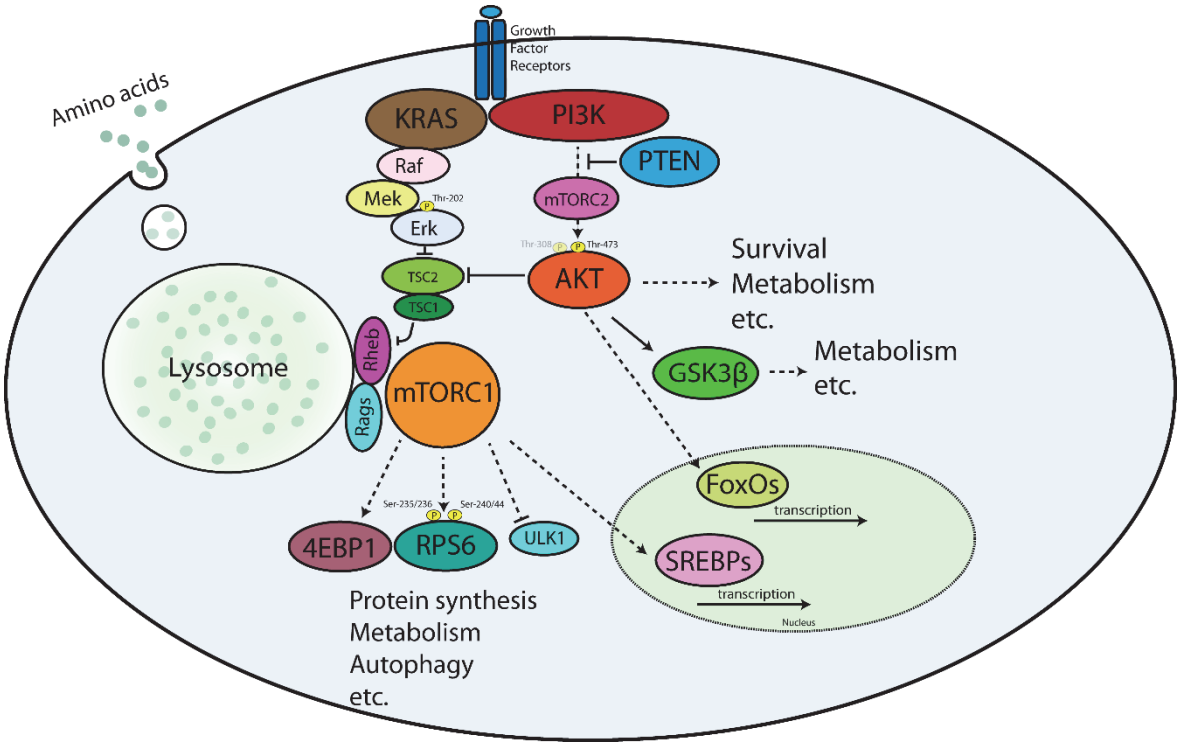

Figure 1-7: PI3-Kinase and MAPK signalling stimulate mTOR activity MAPK and PI3-Kinase signalling can be initiated at growth factor receptors. Signalling cascades diverge initially before converging upon mTORC1 to activate protein synthesis, cellular metabolism, inhibition of autophagy via direct phosphorylation and transcriptional program activation.

In this section, I will introduce the key aspects of PI3-Kinase signalling pertinent to the research outlined in this thesis, and will go on to discuss their relevance in organismal and cellular insulin and growth factor mediated signalling.

1.3.3.1 Classes and structure of PI3-Kinases

PI3-Kinase is a broad term describing a family of kinases that phosphorylate the 3' position on the membrane lipid species phosphatidylinositol. They are part of a vast network of phospholipid kinases and phosphatases responsible for regulation of key cellular lipid signalling events (Román-Fernández *et al.*, 2018). Multiple PI3-kinase isoforms have been described, and classified based on their substrates. This research project has exclusively focused on Class 1A PI3-Kinases. This class has been grouped together due to their shared ability to generate phosphatidylinositol(3,4,5)phosphate ($PI(3,4,5)P_3$ = PIP3), which is recognized by a distinct subset of proteins containing plekstrin homology (PH) and other domains. There are four Class 1A PI3-K isoforms - alpha (PI3-Kα), beta (PI3-Kβ), gamma (PI3-Kγ) delta (PI3-Kδ), encoded by four discreet genes - PIK3CA, PIK3CB, PIK3CG and PIK3CD respectively. In this research project, I have focussed mostly upon the roles of epithelial PI3-Kα and PI3-Kβ in tumour initiation, progression and therapeutic response. This is because PI3-Kγ and PI3-Kδ are predominantly expressed in immune cells, although recent literature suggests that PI3-Kδ may play a previously under-appreciated role in different cancer types, including colorectal cancer (Jean and Kiger, 2014; Xenou and Papakonstanti, 2020).

1.3.3.2 Physiology - Organismal

On an organismal-scale, Class 1A PI3-Kinases are involved in insulin/glucose homeostasis. Briefly, β-cells within the endocrine pancreas secrete insulin in response to elevated blood-glucose levels. This stimulates glucose uptake in cells in peripheral tissues. In hepatocytes, the balance between gluconeogenesis and glycogen synthesis is shifted towards the latter. It is therefore a mechanism to convey the message that there is a systemic abundance of glucose.

To elucidate the functional relevance of PI3-Kα in this process, Foukas et al. generated PI3-Kα Kinase-dead knock-in mice. Homozygotes for the transgene were embryonically lethal, while heterozygotes were viable, but showed blunted signalling through insulin-receptor substrate proteins, leading to organismal-scale phenotypes such as stunted growth, glucose intolerance, and hyper-insulinaemia. This positions PI3-Kα as a critical regulator of metabolism at an organismal scale. Meanwhile, using a PI3-Kβ-specific inhibitor, they were also able to demonstrate

that the transduction of information from the insulin receptor is primarily a PI3-Kα dependent process in this setting (Foukas *et al.*, 2006). Beyond insulin signalling, PI3-Kα also transduces information from other RTKs, such as EGFR, VEGFR1 and 2, and PDGFR, in a context dependent manner (Bjorge *et al.*, 1990; Zeng, Dvorak and Mukhopadhyay, 2001; Zhang *et al.*, 2007). Especially in the context of EGFR signalling, its direct interaction with KRAS was shown to amplify PI3-Kα signalling and can maintain tumour growth in the absence of oncogenic Ras (Lim and Counter, 2005). Oncogenic activation of this pathway can be intuitively understood, as the dissociation of cell growth from organism- or tissue-scale regulation is a key feature of cancer.

While PI3-Kα appears to be the predominant isoform responsible for transduction of signals emanating from receptor tyrosine kinases (RTKs), Guillermet-Guibert et al. found that PI3-Kβ preferentially responds to activation of G-protein coupled receptors (GPCRs), such as sphingosine-1-phosphate-, or lysophosphatic acid receptors. Furthermore, they established functional redundancy between PI3-Kβ and PI3-Kγ. Given the ubiquitous expression of PI3-Kβ, compared to the immune-cell specific expression of γ, this positions PI3-Kβ predominantly as a GPCR effector in epithelial cell populations (Guillermet-Guibert *et al.*, 2008). In addition, Kulkarni et al. generated transgenic knock-out and kinase-dead, non-functional knock-in PIK3CB alleles to better understand the function of PI3-Kβ. Although ubiquitously expressed, the dominant phenotype observed in this study was a non-redundant role in neutrophil activity in response to formation of immune complexes, through low-affinity receptors. Moreover, PI3-Kβ was observed to bind the G-protein coupled receptor of LTB_4, a pro-inflammatory lipid. PI3-Kβ can therefore be seen as an integrator of signals from RTKs and GPCRs, in a context-dependent manner (Kulkarni *et al.*, 2011).

1.3.3.3 Physiology - Cellular

As previously mentioned, PI3-Kinase is responsible for signal transduction at receptor tyrosine kinases, such as insulin receptors. Functional PI3-Kinase consists of a catalytic subunit termed p110, and a scaffold subunit p85. The p110 subunit has a RAS-binding domain (RBD), which is specific for PI3-K isoforms. While the RBD of PIK3CA binds Ras, Fritsch et al. found that the RBD of PIK3CB does not bind

RAS proteins itself, rather to the related small GTPases Rac1 and CDC42 (Figure 1-8)(Fritsch *et al.*, 2013).

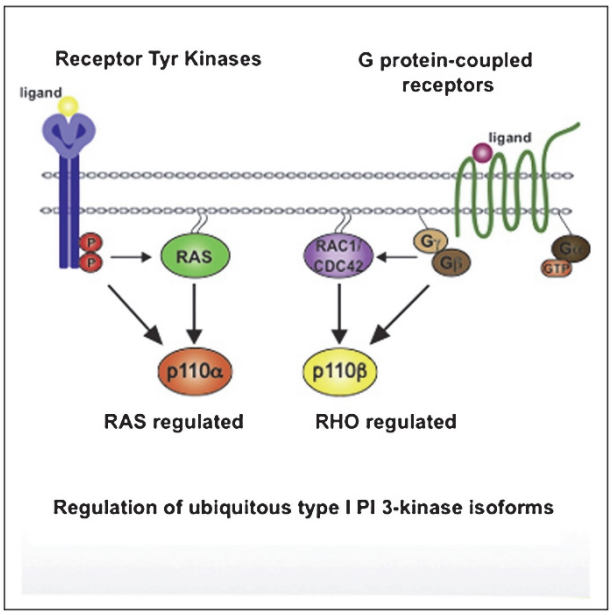

Figure 1-8: Ras and Rho family proteins differentially regulate PI3-Kinase isoforms. While RAS GTPases directly bind and activate the p110α subunit of PI3-Kinase in the context of RTKs, RAC1 and CDC42 can bind p110β upon activation by G protein-coupled receptors. Original publication: (Fritsch *et al.*, 2013).

PI3-Kinase is a lipid kinase that generates PIP3 as a second messenger from PIP2 at cellular membranes. The phosphates provide a negative charge for proteins with PH-domains (and others) to bind and form signalling complexes. There are multiple context dependent outputs of PI3-Kinase signalling, typically through downstream effector molecules including PDK1, AKT, and mTOR. PDK1 and AKT are serine/threonine kinases which can in turn phosphorylate, and hence influence the behaviour of a large array of substrates (Madsen and Vanhaesebroeck, 2020). In the presence of PIP3, AKT can be phosphorylated and activated by PDK1 at T308 (Alessi *et al.*, 1996), and then subsequently phosphorylated and fully activated in a context-dependent manner by a secondary protein kinase complex, mTORC2 at S473. This forms an important overlap between PI3-Kinase and mTOR signalling and was shown to be important for the full activation of AKT (Sarbassov *et al.*, 2005).

The best described role of PDK1 is the aforementioned activation of AKT. This however, is just the tip of the iceberg, as PDK1 also phosphorylates and thereby activates additional prominent AGC family protein kinases, including p70

ribosomal S6 kinase (S6K), serum- and glucocorticoid-induced protein kinase (SGK) and protein kinase C (PKC). The biological effect of those phosphorylation events are generally pro-survival, growth and proliferation, and anabolic processes (Mora *et al.*, 2004). Jiang et al. recently demonstrated that S6K1, controlled by mTORC1, can inhibit the activity of PDK1 towards AKT, making this signalling network even more convoluted (Jiang *et al.*, 2022).

There are three AKT isoforms conserved in mammalian genomes: AKT1, AKT2, and AKT3 with similar domain structure, but subtly different context dependent functions (Basu and Lambring, 2021). Once activated, AKT has a broad effector network as indicated by over 100 reported substrates from various functional classes. Grouped into functions, AKT signalling results in a pro-survival, proliferation, cell growth, and glycolytic-metabolism phenotype (Manning and Toker, 2017). Glycogen-synthase kinase 3 beta (GSK3β) is a notable target of AKT, on which it exerts an inhibitory phosphorylation on S9 (Frame, Cohen and Biondi, 2001). GSK3β has multiple context-dependent targets that are generally inhibited or degraded upon phosphorylation. Targets include the pro-survival protein MCL-1, metabolic enzymes such as its namesake glycogen synthase, and transcription factors such as c-Myc, SREBP1, HIF1α, or NRF2 that globally regulate cellular metabolism (Kaidanovich-Beilin and Woodgett, 2011a). Of note, its association with the aforementioned Wnt-signalling pathway by association to the DC is deemed to be independent of PI3-Kinase/AKT signalling (McManus *et al.*, 2005). In addition to GSK3β, Forkhead box O (FOXO) family transcription factors have been shown to be important AKT effectors. They control processes in the adaptation to fasting and IGF1 signalling and integrate this information with stress stimuli (Webb and Brunet, 2014). Finally, mTORC1 is an important effector of AKT and will be discussed later.

Phosphoinositide signalling is terminated by a complex network of phosphatases (Román-Fernández *et al.*, 2018). Phosphatase and tensin homolog (PTEN) is the best-characterized direct negative regulator of PI3-Kinase signalling (Li *et al.*, 1997). It recognizes PIP3 and catalyses hydrolysis of the phosphate on the 3' position on PIP3 to revert it to PIP2, which is recognized by a different set of proteins, and does not have the same biological output. More recently, Malek et al have shown that PTEN not only phosphorylates $PI(3,4,5)P_3$, but is also a $PI(3,4)P_2$ 3-phosphatase. This appears to have functional relevance in driving invasion in

prostate cancer cells (Malek *et al.*, 2017). Regulation of PTEN itself has been subject of intense study over the years. There are multiple levels of PTEN regulation: Transcription; mRNA stability and translation; and protein localisation, stability, and function (Brito, Goulielmaki and Papakonstanti, 2015). In addition to PTEN, SHP1 and 2 by interruption of p85 and p110 subunits of PI3-Kinase and INPPL1/SHIP2 by de-phosphoryolation of PIP3 at the 5' position have also been described to negatively regulate PI3-Kinase signalling (Cuevas *et al.*, 2001; Edimo *et al.*, 2016; Song *et al.*, 2022).

1.3.3.4 Pathophysiology

Broadly speaking, because of the complex regulatory mechanisms involved, hyperactivation of the PI3-Kinase pathway in cancer can occur through multiple mechanisms, including through loss-of-function mutations in negative regulators of the pathway, or gain-of-function mutations or amplifications of the PI3-Kinase subunits and effector kinases.

PIK3CA-related overgrowth spectrum (PROS) disorders are the result of somatic PI3-Kinase hyperactivating mutations in the developing body. The common phenotype of those syndromes, dependent upon the initially mutated cell, are mosaic benign overgrowth. Prominent syndromes include macrodactyly (OMIM #155500), congenital lipomatous overgrowth, vascular malformations, epidermal nevi, and skeletal/spinal abnormalities syndrome (CLOVES) (OMIM # 612918), and Cowden syndrome , which is characterized by outgrowth of benign hamartoma tumours in multiple organ systems (OMIM #612918). Loss of PTEN can also lead to autism disorders (Rademacher and Eickholt, 2019).This said, PI3-Kinase hyperactivation is prevalent in many types of cancer with variable incidence, indicating tissue specificity. PI3-Kinase hyperactivation is for example particularly common in gynaecological cancers, but rare in haematological cancers (Castel *et al.*, 2021). It is notable that while both PIK3CA and PIK3CB are expressed ubiquitously and functionally similar, PIK3CA mutations in cancer are much more frequent (Kim *et al.*, 2016). PIK3CA mutations occur in two distinct hotspots, located on the helical and kinase domain of the protein (Figure 1-9). The helical domain interacts with the p85 scaffold subunit of PI3-Kinase and mutations in this domain are thought to promote scaffold-independent activation of PI3-Kinase that still requires binding to Ras-GTP. Kinase domain mutations result in a hyperactive

kinase which is dependent on p85 binding, but are somewhat independent of Ras-binding (Zhao and Vogt, 2008). Helical and kinase domain mutations were also shown to act in a synergistic manner to drive cellular transformation, a feature that was recently affirmed in a clinical study looking at PIK3CA mutations in cis, which resulted in increased PI3-K inhibitor sensitivity (Vasan *et al.*, 2019). Given the frequency of *PIK3CA* H1047R mutations in human cancers, this mutant protein has been subject of substantial research, aimed at elucidating why it results in hyperactivity (Samuels *et al.*, 2004). In summary, the mutation leads to enhanced binding of p110α to membranes, loss of auto-inhibition, and conformational change of His917 pointing towards the active site, leading to increased activity (Gkeka *et al.*, 2014a). While activating mutations in the catalytic p110 protein are most common, PIK3R1 (encoding for the p85 subunit) mutations can also result in a dominant activation of PI3-Kinase signalling (Lucas *et al.*, 2014).

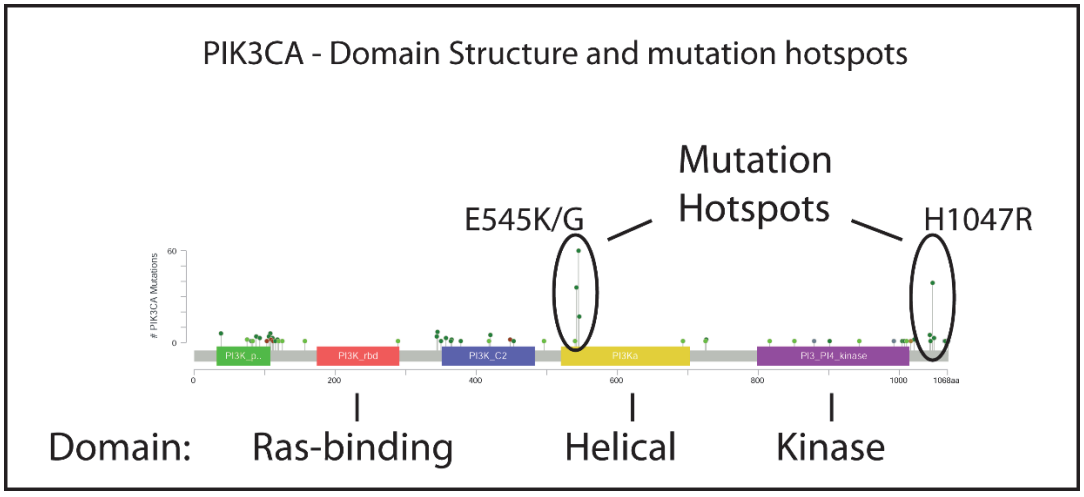

Figure 1-9: Domain structure of PIK3CA and prominent mutation hotspots in MSK metastatic CRC cohort. PIK3CA protein has five main domains, including the Ras-binding, Helical, and Kinase domains. Sequencing of clinical samples revealed two main mutation hotspots: One in the helical, and one in the kinase domain of the gene/protein. Helical domain mutations are most common on amino acid position 545, while kinase domain mutations are most common on position 1047R. The H1047R mutation is the mutation studied in this thesis.

Multiple clinical investigations into the role of PIK3CA mutations in human colorectal cancer have been conducted (Ogino *et al.*, 2013). PIK3CA mutations are more common in the proximal colon than in rectal tumours (Yamauchi *et al.*, 2012). PIK3CA mutant cancers tend to be high for p-AKT and pS6, and *KRAS*-mutated (Nosho *et al.*, 2008). High levels of pAKT were associated with low stage and favourable outcome in a cohort of 717 CRCs (Baba *et al.*, 2011). *PIK3CA* amplification has also been described and seems to result in longer overall survival

than in non-amplified cancers (Jehan *et al.*, 2009). Despite their prevalence in cancer, in a systematic review and meta-analysis from 2016, Mei et al. found no impact of PIK3CA mutation on overall survival and progression free survival, analysing 12,747 CRC cases (Mei *et al.*, 2016).

PTEN-loss or reduced function of PTEN can be relevant and the result of genetic mutation or deletion. Furthermore, promoter methylation and subtle reduction of protein have been reported to play a role in various cancer contexts (Trotman *et al.*, 2003; Alimonti *et al.*, 2010; Álvarez-Garcia *et al.*, 2019). In a study of 746 human cancer genomes, *PTEN* was identified as the locus with the highest selection pressure for homozygous loss, highlighting the relevance of the gene across cancer types (Bignell *et al.*, 2010). PTEN is frequently mutated in colorectal cancer, exhibiting a broad spectrum of mutations (Serebriiskii *et al.*, 2022). It was also found to be downregulated on a protein level in colorectal adenocarcinoma and precancerous lesions (Waniczek *et al.*, 2013). The same trend was observed by Colakoglu et al. in cancer vs pre-cancerous lesions (Colakoglu *et al.*, 2008). Data from 1,093 CRCs indicates that both PIK3CA mutant and PTEN deficient cancers are related to proximal colonic disease, and are generally associated with the sessile-serrated pathway, characterized by microsatellite instability, CpG island methylation, and *BRAF* mutations (Day *et al.*, 2013).

As discussed previously, while *KRAS* and *BRAF* mutational status is commonly used to predict EGF-R inhibitor resistance in CRC, there is also evidence that PIK3CA mutations confer resistance to this class of drugs, although the impact may be smaller than these canonical MAPK mutations and the evidence is not conclusive (Prenen *et al.*, 2009; Siena *et al.*, 2009; Mao *et al.*, 2012; Jhaveri *et al.*, 2020).

Given the clear functional association between PI3-Kinase pathway activation and control of cellular growth, and the somewhat ambiguous relationship between PI3-Kinase pathway activating mutations and development, progression and response to therapy in human CRC, accurate preclinical research *in vivo* is an absolute necessity.

1.3.3.5 Previous attempts at modelling hyperactive PI3-K signalling in GEMMs

In 2012, Leystra and Deming et al. generated a transgene encoding a chimeric protein containing the SH-domain of the p85 protein fused to the N-terminus of the PI3-Kα p110 subunit and termed this PIK3ca* (PIK3CA constitutively active). This protein exhibits dominant active behaviour over its wildtype counterpart and was expressed heterozygously from the Fatty Acid Binding Protein 1 (Fabp1) promoter. Human FABP1 is mostly expressed in differentiated enterocytes (both SI and Colon) and liver cells, but also to an extent in undifferentiated intestinal cells (Karlsson *et al.*, 2021). These mice presented with moderately differentiated, diffusely invasive mucinous proximal colonic tumours with short latency of 40-60d. As might be expected, the tumours exhibited high levels of phosphorylated AKT, although lacked obvious nuclear accumulation of ß-Catenin, suggestive of a WNT-independent route to tumorigenesis without an intermediate benign adenoma stage. While this study demonstrates that aberrantly activated PI3-Kinase signalling can induce colonic cancer, the caveat remains that this fusion protein escapes physiological regulation such as transcriptional regulation and membrane dynamics (A. A. Leystra *et al.*, 2012). This was addressed later by Yueh et al, which demonstrated that colon cancer could also be initiated by expression of $PIK3CA^{H1047}$ expressed under the Fabp1 promoter. Tumours arising in these mice were invasive adenocarcinomas and lacked nuclear ß-Catenin, again suggestive of a Wnt-independent route to tumour initiation (Yueh *et al.*, 2016). In a follow-up study, Deming et al. showed that tumours driven by PIK3ca* were sensitive to mTOR inhibition by Rapamycin for two weeks. Tumours growing out were high for pS6 (Deming *et al.*, 2013).

In 2014, the same group showed that expression of PIK3ca* leads to increased tumour initiation in $APC^{Min/+}$ mice in the SI and Colon, leading to the conclusion that APC-loss and hyperactive PI3-Kinase signalling synergize to drive intestinal cancer. The tumours in $APC^{Min/+}$ mice were again advanced adenocarcinomas, compared to mostly adenomas in PI3-Kinase wildtype mice, and had mixed populations of ß-Catenin nuclear and membranous cells (Deming *et al.*, 2014). Further studies utilizing 3D cell cultures generated from APC PIK3ca* as allografts showed that while PI3-Kinase-inhibition was ineffective in this setting, dual PI3-K/mTOR(1/2) inhibition was efficacious (Foley *et al.*, 2017). Similarly, Fricke et al. showed that while everolimus mediated mTORC1 inhibition was not sufficient

to slow growth in APC deficient, *Pik3ca*^{H1047R} mutant spheroids, mTORC1/2 inhibition was efficacious (Fricke *et al.*, 2019).

In addition to modelling activating mutations in PIK3CA, models of intestinal tumorigenesis driven by loss of PTEN have also been generated. He and colleagues generated conditional *Pten*-KO mice, driven by the musashi promoter, and showed increased formation of polyps. They propose a mechanism in which Akt-mediated phosphorylation of ß-catenin may lead to nuclear localisation and hence activation of Wnt-transcriptional targets (He *et al.*, 2007). In contrast to this, intestinal epithelium-specific depletion of *Pten*, using the Villin1 promoter, did not perturb intestinal homeostasis and only led to polyps in about 20% of mice (Byun *et al.*, 2011). Furthermore, using *Ah*CRE (*Cyp1a1* aryl hydrocarbon-responsive promoter CRE) and Villin1-CRE, intestinal epithelial *Pten* loss was shown to be dispensible in homeostasis, but was necessary to suppress *Apc*-loss mediated tumour formation. In a more advanced system, a recent study indicated that concurrent intestine-specific loss of *Apc*, expression of a *Kras*^{G12V} oncogenic mutant, and deletion of *Pten* led to formation of invasive adenocarcinomas without metastasis. Moreover, in the same study, in the context of *Apc* proficiency, KRAS activation and PTEN loss synergized to drive hyperplastic polyps, dysplastic sessile serrated adenomas and metastasizing adenocarcinomas indicating that these lesions may mirror the serrated path to CRC in humans (Davies *et al.*, 2014).

In summary, intestinal tumour initiation driven by hyperactive of PI3-Kinase signalling mouse models seems to be dependent on how and where it is hyperactivated. Expression of the constituitive active PIK3ca* allele resulted in a far more dramatic phenotype than e.g. *Pten* KO. Targeted mutation at the endogenous locus of *Pik3ca* and comparative analysis to *Pten*-KO in intestinal epithelial cells in the same genetic background was used in this thesis to refine these models.

1.3.3.6 PI3-Kinase targeting drugs

Multiple compounds targeting Class 1A PI3-Kinases have been developed and proceeded into clinical trials. Early drugs, such as the fungal metabolite wortmannin or buparlisib were pan-PI3-K inhibitors (Vanhaesebroeck *et al.*, 2021). In recent years, isoform-specific inhibitors were developed. In this thesis, I have

taken advantage of two isoform-specific PI3-Kinase inhibitors developed by AstraZeneca: AZD8835 and AZD8186.

AZD8835 is an inhibitor of PI3-Kα and PI3-Kδ (IC50: 6.2/5.7 nM) with selectivity over PI3-Kβ and PI3-Kγ (IC50: 431/90 nM) and inhibits H1047R mutant PI3-Kα at an IC50 of 5.8nM (Barlaam, Cosulich, Delouvrié, *et al.*, 2015; Hudson *et al.*, 2016). It has entered Phase 1 clinical trial to test the maximum tolerated dose in 2014, although no results were posted as of yet (Clinical trial NCT02260661, 2014).

AZD8186 is an inhibitor of PI3-Kβ and PI3-Kδ (IC50 4/12 nM) (Barlaam, Cosulich, Degorce, *et al.*, 2015). Hancox et al. showed that the compound inhibited growth of PTEN deficient prostate cancer cell lines, and showed synergy with docetaxel (Hancox *et al.*, 2015). AZD8186 has been taken into the clinic in a phase I clinical trial, for advanced castrate resistant prostate cancer, squamous non-small cell lung cancer, and triple negative breast cancer. No results were posted yet (Clinical trial NCT01884285, 2020).

1.3.4 mTOR signalling

Mechanistic target of Rapamycin (mTOR) has made its way to mainstream media as a major regulator of the ageing process. Administration of the naturally occurring inhibitor Rapamycin extends the lifespan of mice, flies, and worms (Wilkinson *et al.*, 2012). mTOR signalling acts as an evolutionarily conserved cellular mechanism for integrating information from multiple cell signalling pathways related to availability of nutrients and energy (Kim and Guan, 2019). mTOR itself is a kinase, and forms part of at least two protein complexes with distinct subunits, subcellular localisations and downstream effector pathways: mTOR complex 1 (mTORC1) and mTOR complex 2 (mTORC2) (Szwed, Kim and Jacinto, 2021).

The vast majority of research to date has focussed upon the role of mTORC1, both in normal physiology, and in cancer. This is in part due to the ability of Rapamycin to exclusively, and directly block the function of mTORC1, although it also suppresses mTORC2 indirectly following prolonged exposure (Schreiber *et al.*, 2015). mTORC2 is less well studied, as historically there was no specific inhibitor available.

1.3.4.1 mTORC1

The core mTORC1 is a ca. 1MD protein complex formed by mTOR kinase, Raptor (regulatory-associated protein of mTOR), and mLST8 (mammalian homolog of protein Lethal with Sec Thirteen). The structure of mTORC1 has been resolved with cryo-electron microscopy to 5.9Å and 4.4Å in 2016 and revealed that dimers of two complexes with a large cavity are formed (Aylett *et al.*, 2016; Yang *et al.*, 2016).

The impact of mTORC1 activity on cellular physiology can hardly be overstated. Broadly speaking, its activation leads to a pro-survival, cell growth, anabolic phenotype. This is mediated by activation of downstream effector pathways including mRNA translation, ribosomal biogenesis, inhibition of autophagy, anti-apoptotic pathways, lipid and cholesterol synthesis. Low mTORC1 signalling on the other hand can result in cell cycle arrest, increased autophagy/catabolism, and decreased cell growth (Kim and Guan, 2019).

As mentioned earlier, mTORC1 integrates information from cell signalling pathways and nutrient-availability to determine cell fate. The main cell growth pathways that feed into mTORC1 activation are PI3-K and MAPK signalling. ERK and AKT can phosphorylate and thereby inhibit the tuberous sclerosis complex (TSC), which is formed by TSC1 and TSC2. TSC is a GAP for the small GTPase Rheb, which directly binds and activates mTORC1 (Long *et al.*, 2005). Inhibition of TSC therefore leads to mTORC1 activation. (Manning *et al.*, 2002; Potter, Pedraza and Xu, 2002; Garami *et al.*, 2003; Tee *et al.*, 2003). High AKT activity can also activate mTORC1 activity through PRAS40 (Sancak *et al.*, 2008; Yang *et al.*, 2017).

Cellular energy levels are sensed by AMP-activated protein kinase (AMPK), which can also directly phosphorylate TSC2, which is required for the response to energy deprivation (Inoki *et al.*, 2002).

mTORC1 localizes to lysosomes, which provide first-hand information on environmental nutrient abundance. Lysosomal arginine is recognized by SLC38A9 (Jung, Genau and Behrends, 2015; Rebsamen *et al.*, 2015; Wang *et al.*, 2015; Wyant *et al.*, 2017). Lysosomal v-ATPase undergoes a conformational change depending on lysosomal amino acid concentration (Zoncu *et al.*, 2011). In addition

to lysosomal contents, cytosolic amino acids are also sensed. Cytosolic methionine, after incorporation into S-adenosyl methionine, is recognized by SAMTOR (Gu *et al.*, 2017). Sestrin2 senses cytosolic leucine (Wolfson *et al.*, 2016), and Castor proteins sense cytosolic arginine (Chantranupong *et al.*, 2016). These processes lead to mTORC1 activation through the Ras-related GTPase (Rag) family of proteins (Kim *et al.*, 2008; Sancak *et al.*, 2008). Rags are localized to lysosomal membranes, activated by their GEF Ragulator (Sancak *et al.*, 2010; Bar-Peled *et al.*, 2012), and inhibited by the GAP protein complex GATOR (Bar-Peled *et al.*, 2013). Solute carriers such as SLC7A5/SLC3A2 and SLC1A5 alter levels of these amino acids and can thereby directly influence mTORC1 activity (Nicklin *et al.*, 2009; Najumudeen *et al.*, 2021).

This description does not even capture the true complexity of mTORC1 activation as molecular details are omitted for brevity and clarity, or are simply not uncovered yet.

Accumulation of biomass is essential for cell proliferation. As protein synthesis is the most energy-consuming cellular process, cells need to regulate this process tightly. mTORC1 regulates protein synthesis on multiple levels. mRNA is translated at ribosomes, biosynthesis of which is regulated by mTORC1 in a S6-K1-phosphorylation dependent manner by upregulating expression of both 47S rRNA and 5S rRNA (Hannan *et al.*, 2003; Shor *et al.*, 2010). mRNA translation is a multi-step process that involves translation initiation, elongation, termination, and ribosome recycling. mTORC1 affects both translation initiation and elongation by phosphorylation of two distinct proteins. Translation initiation is primarily controlled by eukaryotic initiation factors (eIFs). In this context, mTORC1 most notably phosphorylates and thereby inactivates eiF4E-binding protein 1 (4EBP-1). This allows binding of eIF4E to the scaffold protein eIF4G, which allows formation of the initiation complex and protein synthesis (Pause *et al.*, 1994). I used phosphorylation of 4EBP on Thr-37 as a marker for mTORC1 dependent control of translation initiation. Translation elongation is primarily regulated by eukaryotic elongation factor F2 (eEF2), activity of which is activated by eEF2 Kinase (eEF2K). mTORC1 activates eEF2K by phosphorylation, but also other factors such as Ca^{2+} and AMPK influence its activity (Karakas and Ozpolat, 2020). In this study, I have used phosphorylation of eEF2 at Thr-56 to assess mTORC1-mediated regulation of translation elongation, and additionally phosphorylation of RPS6 at Ser235/236

and Ser240/244 as a read-out for mTORC-mediated activation of S6K1, although others and I have shown that biologically, these phosphorylations seem to be merely markers of activity and have yet to be assigned a specific function.

Besides regulation of protein synthesis, mTORC1 has additional roles in cellular physiology, generally by promoting anabolic processes. These include stimulation of lipid synthesis through SREBPs, nucleotide synthesis via IMDPH, and inhibition of autophagy via ULK1 (Porstmann *et al.*, 2008; Park *et al.*, 2016; Eid *et al.*, 2017; Valvezan *et al.*, 2017)

1.3.4.2 mTORC2

mTORC2 shares two subunits with mTORC1: The mTOR kinase itself and mLST8. Instead of Raptor, the Rapamycin insensitive companion of mTOR (RICTOR) acts as a scaffold protein and confers, as the name suggests, insensitivity to Rapamycin. Finally, mTORC2 features an additional subunit, SIN1, which has a Ras-binding domain and a PH domain. The structure and composition of mTORC2 has been solved using cryo-electron microscopy by multiple groups in 2018. Similarly to mTORC1 it functions as a dimer (Chen *et al.*, 2018).

mTORC2 is less-well characterized and its function in different tissues and contexts is still being evaluated. Activity of mTORC2 is also regulated by growth factor signalling and nutrients, but the logic behind this seems to be more convoluted. As mentioned previously, SIN1 has a PH-domain which can functionally bind PIP3, leading to its activation (Liu *et al.*, 2015). In a recent publication, Thobe et al. have worked through the logic of five proposed models of mTORC2 activation, and established that PI3-K is an essential regulator of mTORC2 (Thobe, Sers and Siebert, 2017).

mTORC2 is reported to regulate actin dynamics and phosphorylate a subset of AGC-class kinases. One of these is AKT, which was shown to be phosphorylated co-translationally at S473, and thereby fully activated. In this study, this has been used as a biomarker of PI3-Kinase activation. SGK1 is another phosphorylation target of mTORC2 (García-Martínez and Alessi, 2008). SGK1 in turn phosphorylates multiple targets, including NDRG1, function of which still needs to be fully elucidated. I use phosphorylation at T346 as a marker of mTORC2 activation.

1.3.4.3 mTOR inhibitors

Rapamycin is a complex antifungal metabolite produced by Streptomyces hygroscopicus, discovered on the island Rapa Nui. It was initially described as having immunosuppressive function, and the newest generation of its analogue drugs (Rapalogues) are still used as such in transplantation medicine. Mechanistically, Rapamycin induces dimerization of two proteins: FK506-binding protein (FKBP12) and the FKBP-rapamycin-associated protein (FRAP), resulting in mTORC1 inhibition (Choi *et al.*, 1996). It is approved for treatment of Renal Cell Carcinoma (RCC) (Li, Kim and Blenis, 2014).

AZD2014 is an mTOR-kinase inhibitor (IC50 2.8 nM). In contrast to Rapamycin, it inhibits the 4E-BP axis in addition to S6-Kinase, as well as inhibits mTORC2 signalling, read out by pAKT-S473 and pNDRG1-T346 positivity. It was shown to be effective at growth inhibition and biomarker-reduction in cell lines, in particular in ER+ breast cancer lines (Guichard *et al.*, 2015). It has been evaluated in clinical trials, but has not been very effective in patients, as multiple studies have been terminated due to either adverse effects, or lack of efficacy (*https://clinicaltrials.gov/ct2/results?term=AZD2014*, accessed 26/05/2022).

1.3.5 Signalling pathway interactions

Multiple interconnections between the previously mentioned growth signalling pathways exist. I have mentioned the cross regulation of mTOR by PI3-Kinase and MAPK signalling earlier and want to point out additional studies here on the interplay between PI3-Kinase, MAPK, and Wnt-signalling.

1.3.5.1 PI3-Kinase and MAPK signalling interaction

PI3-Kinase signalling has been established as an important Ras-effector pathway (Castellano and Downward, 2011; Cuesta, Arévalo-Alameda and Castellano, 2021). Active Ras can bind to the p110α subunit of PI3-Kinase at RTKs upon growth factor stimulation (Sjolander *et al.*, 1991; Rodriguez-Viciana, Sabatier and McCormick, 2004). Binding of active Ras to PI3-Kinases generally stimulates production of PIP3 (Pacold *et al.*, 2000). As oncogenic mutations in Ras result in a higher abundance of active protein, this results in more Ras/PI3-K interaction in the cell. This interaction has been shown to be functionally relevant in different contexts *in*

vivo. Neutrophils seem to rely on Ras/PI3-Kinase gamma interaction to fully engage in chemotaxis (Suire *et al.*, 2006). PI3-Kα Ras-binding domain mutant mice suffered from a growth defect, attributed to failure to respond appropriately to EGF or FGF2 stimuli (Gupta *et al.*, 2007). Especially Ras-induced AKT signalling, which can be regulated by Raf, seems to be important to efficiently drive survival and cell cycle progression (Downward, 2004).

There is also evidence for functional synergy of *Ras* and *Pik3ca* co-mutation to drive cancer in mouse models. In a GEMM of lung cancer, mutant *Pik3ca*^{H1047R} failed to initiate tumours when expressed by itself, but accelerated initiation and outgrowth when co-expressed with mutant *Kras*^{G12D}. In this setting, the PI3-Kinase inhibitor BYL719 could effectively block outgrowth of *Kras*^{G12D}/*Pik3ca*^{H1047R} mutant tumours and thereby reverse the impact of concomitant Kras/Pik3ca mutation (Green, Trejo and McMahon, 2015). Induction of *Apc*$^{fl/fl}$ *Kras*$^{G12D/wt}$ *Pik3ca*^{p110*} mice via adenoviral introduction of Cre recombinase into the colon resulted in invasive adenocarcinoma, although compound mutation was not too different from *Apc*$^{fl/fl}$ plus single mutation. (Hadac *et al.*, 2015). In human colorectal cancer, concomitant *PIK3CA* and *KRAS* mutations were associated with aggressive clinicopathological features and poorer overall survival (Luo *et al.*, 2020)

1.3.5.2 PI3-Kinase/mTOR and Wnt signalling

As discussed earlier, hyperactive PI3-Kinase signalling was shown to drive colonic cancer in mice upon expression of a dominant active form of the protein. No concomitant nuclear ß-catenin was observed, indicating a Wnt-independent mechanism (Alyssa A Leystra *et al.*, 2012). Most colorectal cancers have some form of Wnt-signalling alteration though (Figure 1-4). Therefore the interplay between PI3-Kinase-, and by extension mTOR signalling, and Wnt signalling has been subject to study (Prossomariti *et al.*, 2020). The importance of functional mTORC1 signalling in *Apc* deficient intestinal cancer has been established, indicating that once Wnt signalling is aberrantly hyperactivated, cells rely on mTORC1 driven translation elongation (Hardiman *et al.*, 2014; Faller *et al.*, 2015). Both Wnt-and PI3-Kinase/mTOR signalling are regulated by multiple feedback mechanisms, some of which are cross-regulated. A prominent signalling node present in both PI3-Kinase- and Wnt signalling networks is GSK3ß. It has multiple subcellular locations and functions, and is generally regulated by inhibitory phosphorylation

(Kaidanovich-Beilin and Woodgett, 2011b). In Wnt-signalling it promotes degradation of ß-Catenin, while in PI3-Kinase signalling it promotes anabolic metabolic processes (Beurel, Grieco and Jope, 2015). While AKT phosphorylates GSK3ß on S9 and thereby inhibits it, this was shown to be uncoupled from Wnt-signalling regulation (Ding, Chen and Mccormick, 2000; Doble *et al.*, 2007).

PI3-Kinase pathway inhibition has so far not been successful in colorectal cancer. In the context of PI3-Kinase and AKT inhibitor resistance, high nuclear ß-Catenin has been implicated as a resistance mechanism in colorectal cancer cells. Reduction of nuclear ß-Catenin levels using a Wnt/tankyrase inhibitor rendered cells sensitive to PI3-Kinase and AKT inhibition. On the flipside, PI3-K/AKT-regulated nuclear localisation of FOXO3A transcription factors conferred resistance to Wnt/tankyrase inhibitors. Indeed, FOXO transcription factors and ß-Catenin have been previously shown to interact functionally and regulate responses e.g. to oxidative stress (Essers *et al.*, 2005). This indicates that the two pathways can compensate for each other in conferring cells survival properties and co-targeting might be beneficial (Tenbaum *et al.*, 2012; Solberg *et al.*, 2018)

1.4 Aims

Colorectal cancer is a worldwide health burden, yet patient stratification beyond *KRAS* and *BRAF* mutational profiling is not widely performed and translated to personalized therapeutic approaches. Modelling human disease in mice has proven invaluable to understand the fundamental processes in disease initiation and progression to advanced disease. PI3-Kinase signalling hyperactivation either through aberrant activation of the kinase itself, or loss of negative regulation is common in CRC, but functional relevance of this is still incompletely understood.

In **Chapter 3** I present characterisation of novel mouse models of intestinal cancer, driven by human disease-relevant mutations in the Wnt, PI3-Kinase and MAPK pathway. I aimed to understand the effect that these mutations have on cancer initiation and progression from benign to malignant disease, their impact on gene transcription and abundance of signalling markers. Furthermore I generated complex models to understand interplay between multiple oncogenic mutations within and outwith the same pathway.

In **Chapter 4** I made use of additional genetic models and clinically relevant small molecule inhibitors to inhibit PI3-Kinase, MAPK, and mTOR signalling pathway components to identify vulnerabilities or resistances in the newly generated models.

Chapter 2 Materials and Methods

2.1 *In Vivo* experiments

2.1.1 Mouse Housing and Ethics

Mice were housed in accordance with UK Home Office Regulations. Animals were fed a standard chow diet and given drinking water *ad libidum*. All experiments were performed in accordance with the UK Home Office guidelines under project licences 70/8646 and PP3908577 and were reviewed and approved by the University of Glasgow Animal Welfare and Ethical Review Board.

2.1.2 Genetic Alleles (Mice)

Mice used were on a C57BL/6J background (N≥9) for following alleles: Villin-CreER^{T2} transgene (El Marjou *et al.*, 2004), *Apc*^{fl} (Shibata *et al.*, 1997), *Kras*^{G12D} (Jackson *et al.*, 2001), *Pten*^{fl} (Suzuki *et al.*, 2001), *Pik3ca*$^{fl\text{-}H1047R\text{-}T2A\text{-}EYFP\text{-}NLS}$ (hereafter *Pik3ca*^{H1047R}) (Herms *et al.*, 2021), p110ß-RBD-DM (hereafter *Pik3cb*-RBD^{mut}) (Fritsch *et al.*, 2013); and mixed C57BL/6J background (N≥6) for *Rictor*^{fl} (Bentzinger *et al.*, 2008). For genotyping, mice were ear notched upon weaning and tissue was sent to Transnetyx (Cordova, TN) using the established genotyping procedure for the individual alleles.

Efficient expression from the *Pik3ca*$^{fl\text{-}H1047R\text{-}T2A\text{-}EYFP\text{-}NLS}$ allele was confirmed by ISH, using an RNA-scope® probe against EYFP mRNA, which was absent in *Pik3ca* wildtype tissue, but robustly expressed in *Pik3ca*^{H1047R} mutant tissue (Figure 2-1). Halo image analysis was used to better visualize abundance of probes in the outlined areas of interest, as the signal can appear faint.

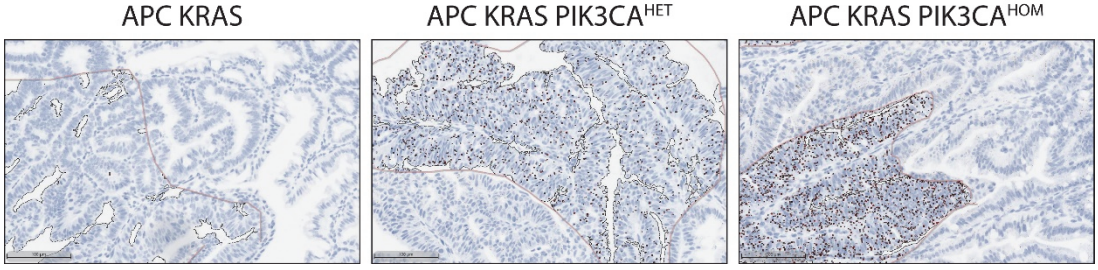

Figure 2-1: RNA-scope based detection of EYFP mRNA in *Pik3ca*^{H1047R} mutant small intestinal epithelial tissue, including tumours. *Pik3ca*^{H1047R} mutant intestinal epithelial tissue was processed and in-situ hybridisation (RNA-scope®) for EYFP mRNA was performed. Halo

image analysis was used to visualize abundance of detected probes in areas of interest (outlined). Scale bars 100µm.

2.1.3 In Vivo Inductions

Two types of experiments were performed: “ageing” and “acute”. In ageing experiments, transgenes were induced by a single intraperitoneal injection of 2mg (80mg/kg) tamoxifen and sampled either at a defined clinical endpoint, or at a pre-defined timepoint. In the acute setting, *Apc*$^{fl/fl}$; *Kras* wildtype mice were intraperitoneally injected 2mg (80mg/kg) tamoxifen on two consecutive days for, while *Apc*$^{fl/fl}$; *Kras*^{G12D} mutant mice received one 2mg (80mg/kg) dose of tamoxifen.

In ageing experiments, mice were monitored daily and routinely weighed according to the licence. Unless stated as a timepoint sampling, mice were sampled at clinical endpoint. This was defined as a combination of any of the following: weight loss (sudden, due to bowel obstruction, or gradual, due to tumour burden), hunching, and paling.

2.1.4 In Vivo drug treatments

Tamoxifen (Sigma, #T5648 was dissolved in EtOH abs to a stock solution of 100mg/ml. This was diluted in corn oil (Sigma, #C8267) to a final working concentration of 10mg/ml for intraperitoneal injection.

AZD6244 (AstraZeneca) – was reconstituted in 0.5% hydroxypropyl methylcellulose (HPMC) + 0.1% Tween-80 and mice were dosed 25mg/kg 2x daily by oral gavage.

AZD2014 (AstraZeneca) - was reconstituted in 0.5% hydroxypropyl methylcellulose (HPMC) + 0.1% Tween-80 and mice were dosed 15mg/kg 1x daily by oral gavage.

AZD5363 (AstraZeneca) – was reconstituted in 100% DMSO at a concentration of 400mg/ml, further diluted 1:5 in sterile water, and finally diluted 1:2 in 50% Kleptose HPB solution for a working concentration of 40mg/ml. AZD5363 was administered orally at 200mg/kg.

AZD8835 (AstraZeneca) - was reconstituted in 0.5% hydroxypropyl methylcellulose (HPMC) + 0.1% Tween-80 and mice were dosed 25mg/kg 2x daily by oral gavage.

AZD8186 (AstraZeneca) - was reconstituted in 0.5% hydroxypropyl methylcellulose (HPMC) + 0.1% Tween-80 and mice were dosed 50mg/kg 2x daily by oral gavage.

For combination treatments, drugs were reconstituted together at appropriate concentrations and co-administered at the same frequency. For example AZD6244/AZD2014 combination treated mice would receive AZD6244/AZD2014 1x daily AM and AZD6244 1x daily PM.

Upon reconstitution, AZD6244, AZD2014, AZD5363, AZD8835, and AZD8186 were stored at RT under constant stirring.

2.2 Tissue Sampling and Processing

Upon dissection, intestines were flushed with water, opened longitudinally and pinned on wax plates. The pinned-out guts were then fixed using one of the following methods:

“Quick Fix” for optimal ß-Catenin IHC staining: Guts were submerged in 10% neutral buffered formalin (NBF) on the wax plate at 4C, rolled into “swiss rolls”, and transferred to tubes containing NBF after at least 5h for a total of 16-24h of fixation.

“Optimal Fix” – optimal for general purpose IHC: Guts were submerged in 10% NBF on the plate, rolled into “swiss rolls”, and transferred to tubes containing 70% Ethanol after 24-72h of fixation.

“Long Fix” – when unable to perform Optimal Fix: Guts were submerged in 10% neutral buffered formalin (NBF) on the plate, rolled into “swiss rolls”, and transferred to tubes containing 70% Ethanol or 10% NBF after more than 72h of fixation.

“Methacarn Fix” – mostly used for short term experiments because of good BrdU IHC staining: Guts were spread out on Whatman filter paper and submerged in a mixture of 1:2:4 Acetic Acid (Sigma, #695092): Chloroform (Fisher Scientific, #C4960/PB17): Methanol (Sigma, #32213) for 3-24 hours at room temperature, after which they were “swiss rolled” and transferred to 10% NBF for processing.

For ageing experiments, tumour number, location, and size was recorded during the process of rolling guts into “swiss rolls”. It was taken note when further microscopic tumours were expected and those were scored after processing.

Following fixation, samples were processed by the CRUK Beatson Institute Histology Department and embedded into paraffin wax using standard histological techniques. 3-4µm sections were cut for Hematoxilin and Eosin (H&E), and IHC or *in situ* hybridisation techniques (RNAscope®). H&E staining was performed using standard protocols.

2.3 Immunohistochemistry and RNA in situ hybridisation

IHC stainings were performed either by myself or by the CRUK Beatson Institute Histology Department using the following primary antibodies: ß-catenin (BD Biosciences, #610154), BrdU (BD Biosciences, #347580), pAKT-S473 (Cell Signalling, #4060); p4E-BP1-T37/46 (Cell Signalling, #2855); pEEF2-T56 (Cell Signalling, #2331); pNDRG1-346 (Cell Signalling, #5482); pS6-S235/236 (Cell Signalling, #4858); pS6-S240/244 (Cell Signalling, #5364); PTEN (Cell Signalling, #9559) (Table 2-1).

Table 2-1: Details of Antibodies used for Immunohistochemistry

Antibody	Cat. #	Supplier	Secondary	Antibody Retrieval	Dilution
B-Catenin	610154	BD Transduction	Anti-Mouse	Vector Citrate pH6	1/500
BrdU	347580	BD Biosciences	Envision Mouse	Tris-EDTA pH10	1/250
p4E-BP1-T37/46 (236B4)	2855	Cell Signalling	Envision Rabbit Bond™	ER2 pH 9 20mins	1/250
pAKT (S473)(9DE)	4060	Cell Signalling	Envision Rabbit	Tris-EDTA pH10	1/45
pEEF2-T56	2331	Cell Signalling	Envision Rabbit Bond™	ER2 pH 9 20mins	1/100
pS6-S235/236 (D57.2.2E)	4858	Cell Signalling	Envision Rabbit	Tris-EDTA pH10	1/75
pS6 Ser240/244 (D68F8)	5364	Cell Signalling	Envision Rabbit Bond™	ER2 pH 9 20mins	1/1000
PTEN	9559	Cell Signalling	Envision Rabbit Bond™	ER2 pH 9 20mins	1/70
pNDRG1-T346	5482	Cell Signalling	Envision Rabbit	Tris-EDTA pH10	1/400

The CRUK Beatson Institute Histology Department performed RNA *in situ* hybridisation (ISH) on a Leica Biosystems BOND RX automated IHC/ISH stainer using the RNAscope 2.5 LSReagent Kit–BROWN (Advanced Cell Diagnostics, #322100). Mm-PPIB probe (Advanced Cell Diagnostics, #313918) were run as a positive control to confirm integrity of RNA. dabP probe (Advanced Cell Diagnostics, #312038) was used as a negative control. RNAscope® probes used: EYFP (Advanced Cell Diagnostics, cat# 312131), murine PTEN - mmPTEN (Advanced Cell Diagnostics, cat #464338).

2.4 Tumour scoring

For models in which no microscopic tumours were expected and observed, tumours were scored during the "swiss rolling". Most models presented in this thesis had additional microscopic tumours and tumour numbers were scored under the microscope.

Invasive adenocarcinomas were defined as such, when the basal membrane was broken, tumours had a clear stromal component, and architecture was lost to some degree. Example is shown in (Figure 2-2). This scoring diverges from the TNM staging system used for human colorectal cancer, as the murine small intestine is not directly comparable to human colon.

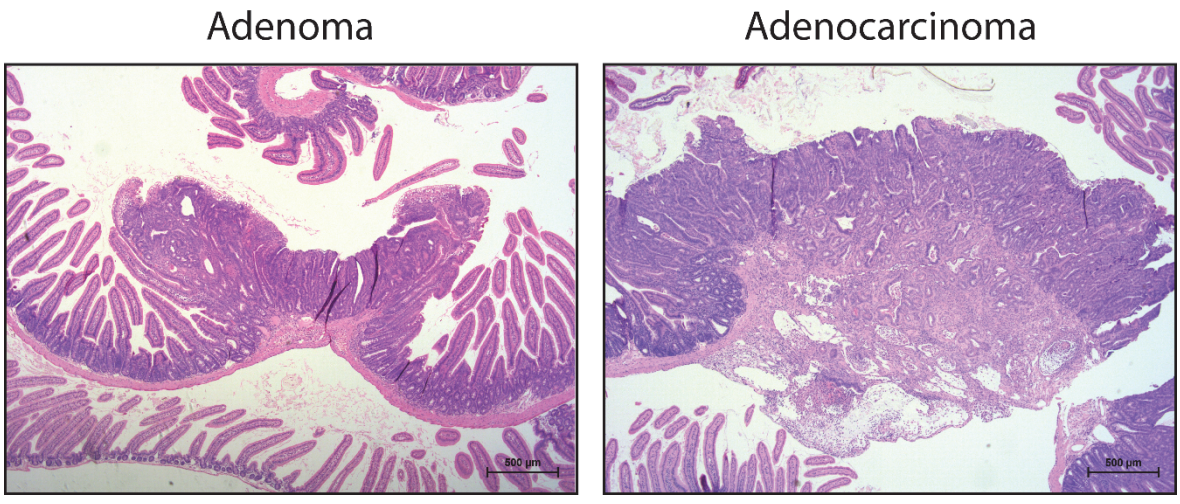

Figure 2-2 Difference between adenoma and adenocarcinomas observed in the SIs of intestinal cancer models. Benign adenomas have an intact basal membrane and conserved glandular structure with high grade of differentiation and little stromal infiltrate. Adenocarcinomas are characterized by broken basal membrane, rich stromal infiltrate and loss of architecture.

2.5 Slide Scanning and BrdU quantification

Slides were scanned by the CRUK Beatson Institute Histology Department using a SCN400F Leica Slide Scanner at x20 magnification. Halo software (V3.4.2986, Indica Labs) was used to quantify BrdU positive tumour cells. First, regions of interest were drawn on tumours. Total cell number was determined by quantification of stained nuclei. BrdU staining was identified based on brown staining and BrdU positive/total cell ratio was determined. This was done using an adaptation of the CytoNuclear V 2.0.9 algorithm.

2.6 Tissue processing and RNA-sequencing

2.6.1 RNA Extraction

Tissue for RNA sequencing was snap frozen in RNAlater (Sigma, #R0901) and stored at -80C until processing. Tissue samples were homogenized using ceramic bead filled tubes (Precellys, #03961-1-00) in a Precellys Evolution tissue homogenizer. RNA was isolated using the RNAeasy kit (Qiagen, #74104) according to the manufacturer's protocol and ß-mercaptoethanol (Sigma, #M6250) was used during this process to preserve RNA integrity.

2.6.2 RNA-Sequencing and Data Analysis

Purity of RNA was confirmed by determining the ratio of absorbance at 260nm/280nm and was subsequently diluted to 1µg/50µl for sequencing. The Agilent 2200 Tapestation in combination with RNA ScreenTape (Agilent, #5067-5576) was used to validate purity and quality of RNA. cDNA libraries were prepared using an Illumina TruSeq RNA LT Kit and quality was validated using the Agilent 2200 Tapestation. DNA library sequencing was performed on the Illumina Next Seq 500 using the High Output 75-cycle kit (2x36 cycles). Raw sequence quality was assessed using the FastQC algorithm version 0.11.8, the sequences were trimmed to remove adaptor sequences and low-quality base calls, defined by a Phred score of <20, using the Trim Galore tool version 0.6.4. The trimmed sequences were aligned to the mouse genome build GRCm38.98 using HISAT2 version 2.1.0, then raw counts per gene were determined using FeatureCounts version 1.6.4. Differential expression analysis was performed using the R package DESeq2 version 1.22.2. Reactome pathway analysis was performed using the R packages

ReactomePA version 1.28.0 and org.mM.eg.db version 3.8.2. Gene set expression analysis was conducted using GSEA v4.1.0 [build 27] using standard settings. HALLMARK gene sets were downloaded from the Molecular Signatures Database (MSigDB) (https://www.gsea-msigdb.org/gsea/msigdb/collections.jsp) (Table 2-2). Four biological replicates were used for all experimental conditions. William Clark performed Tapestation analysis, library preparation, and library sequencing. Robin Shaw and Kathryn Gilroy processed data and facilitated data analysis.

Table 2-2: List of "HALLMARK" gene sets from the Molecular Signatures Database (MSigDB)

HALLMARK gene sets	
ADIPOGENESIS	INTERFERON_ALPHA_RESPONSE
ALLOGRAFT_REJECTION	INTERFERON_GAMMA_RESPONSE
ANDROGEN_RESPONSE	KRAS_SIGNALING_DN
ANGIOGENESIS	KRAS_SIGNALING_UP
APICAL_JUNCTION	MITOTIC_SPINDLE
APICAL_SURFACE	MTORC1_SIGNALING
APOPTOSIS	MYC_TARGETS_V1
BILE_ACID_METABOLISM	MYC_TARGETS_V2
CHOLESTEROL_HOMEOSTASIS	MYOGENESIS
COAGULATION	NOTCH_SIGNALING
COMPLEMENT	OXIDATIVE_PHOSPHORYLATION
DNA_REPAIR	P53_PATHWAY
E2F_TARGETS	PANCREAS_BETA_CELLS
EPITHELIAL_MESENCHYMAL_TRANSITION	PEROXISOME
ESTROGEN_RESPONSE_EARLY	PI3K_AKT_MTOR_SIGNALING
ESTROGEN_RESPONSE_LATE	PROTEIN_SECRETION
FATTY_ACID_METABOLISM	REACTIVE_OXYGEN_SPECIES_PATHWAY
G2M_CHECKPOINT	SPERMATOGENESIS
GLYCOLYSIS	TGF_BETA_SIGNALING
HEDGEHOG_SIGNALING	TNFA_SIGNALING_VIA_NFKB
HEME_METABOLISM	UNFOLDED_PROTEIN_RESPONSE
HYPOXIA	UV_RESPONSE_DN
IL2_STAT5_SIGNALING	UV_RESPONSE_UP
IL6_JAK_STAT3_SIGNALING	WNT_BETA_CATENIN_SIGNALING
INFLAMMATORY_RESPONSE	XENOBIOTIC_METABOLISM

2.7 Organoid/Spheroid Isolation and Culture

Organoid isolation was performed according to an adapted protocol established by Sato et al. (Sato *et al.*, 2009). Upon dissection, part (≥3x3mm) of a single intestinal tumour was excised and placed in ice-cold sterile PBS. It was cut into fragments using forceps and a scissor and washed 2x with ice-cold sterile PBS. Fragments were incubated in 5ml trypsin (5 mg/ml; Gibco) and 200 U recombinant DNAse I (Roche, #04716728001) at 37C in a water bath for 30min. After this, they were shaken vigorously and subsequently centrifuged for 5min at 260g. Supernatant was aspirated, pellet was resuspended in 10ml ADF and passed through a 70µm cell strainer. This was repeated with additional 5ml of ADF to collect residual material. The flow-through was centrifuged at 260g and resuspended in 20µl matrigel® (BD Bioscience, #354234) domes. Organoids/spheroids were passaged 1-2 times per week. For this, matrigel domes were scraped off the plate using a P1000 pipette and sterile PBS. They were washed in PBS and centrifuged at 260g for 5min, before

being dissociated further using a ADF and a P200 pipette. They were washed once more in sterile PBS before resuspension and seeding in fresh matrigel®. They were typically expanded at a 2:1 ratio. Cells were cultured in complete ADF in a humidified atmosphere of 5% CO_2 at 37C.

ADF - Advanced DMEM/F12 (Gibco, #12634-028): This was supplemented with 100U/ml penicillin/streptomycin (ThermoFisher Scientific, #15140122), 10mM HEPES (ThermoFisher Scientific, #15630080), 2 mM L-glutamine (ThermoFisher Scientific, #25030081). Additional supplements: 1:100 N2-supplement (ThermoFisher Scientific, #17502001) and 1:50 B27-supplement (ThermoFisher Scientific, #17504044), 50ng/ml recombinant murine EGF (Peprotech, #AF-100-15), 100 ng/ml recombinant murine Noggin (Peprotech, #250-38).

Full growth factor mix: 500 ng/ml recombinant mouse Rspondin-1 (R&D systems, #3474-RS), 2.5µM CHIR99021 (GSK3 inhibitor) (Sigma, #SML1046), 1 µM valproic acid (Sigma, #P4543), and 10 µM 62Y-27632 (ROCK inhibitor) (Cambridge Bioscience, #SMO2-1), 10nM Gastrin (Sigma-Aldrich, G9145), 50ng/ml Wnt-3A (R&D Systems, 5036-WN), 1µM A83-01 (TGFBR1 inhibitor) (Tocris Bioscience, 2939), 10µM SB2022190 (p38 MAPK inhibitor) (Sigma-Aldrich, S7067), 4mM Nicotinamide (Sigma-Aldrich, N0636), 5ng/ml FGF basic (Peprotech, 100-28A), 5ng/ml FGF10 (Peprotech, 100-26A), and 2.5 µM Prostaglandin E2 (Tocris Bioscience, 2296).

2.8 PCR detection of recombined *Rictor*^{fl} allele

3 days post-seeding, organoids/shperoids were collected as described above in the context of passaging. Genomic DNA from cell pellets of one well of a 6-well plate of organoids/spheroids was prepared using a Qiagen QIAamp® DNA Kit (Cat. No. 51304) according to manufacturer's instructions. For tail DNA samples, tail tips of mice were lysed using the lysis buffer from a Gentra Puregene DNA extraction Kit (Flowgen Cat. No. FD-50K2) and added proteinase K (Roche, Cat no. 03115844001) overnight at 37C. Protein was precipitated using protein precipitation solution (Flowgen Cat no. FD-50K3). Finally, DNA was precipitated in isopropanol before resuspension in water. To detect the recombined *Rictor*^{fl} allele, a primer pair described in the original publication of the allele was used (Bentzinger *et al.*,

2008) (Table 2-3). Reactions were set up using a GoTaq G2 DNA polymerase kit (Promega: Cat No M7841):

- 5x buffer 10µl
- $MgCl_2$ 4µl
- dNTPs 1µl
- 10µM fwd primer 5µl
- 10µM rev primer 5µl
- Polymerase 0.25µl
- Template 1µl
- H_2O 23.75µl

PCR was run using following settings:

1. 95°C 5min
2. 95°C 45sec
3. 47°C 30sec
4. 72°C 20sec
5. Repeat steps 2-4 30X
6. 72°C 10min
7. 4°C Inf.

DNA concentration and purity was measured and ca 600ng of DNA per sample was loaded on a 1% agarose Gel containing Ethidium Bromide and images were taken upon UV exposure.

Table 2-3: Primers used to detect the recombined *Rictor*^{fl} allele

Rictor-KO fwd	5' TTA TTA ACT GTG TGT GGG TTG
Rictor-KO rev	5' CAG ATT CAA GCA TGT CCT AAG C

2.9 Western blot to detect RICTOR

One well of a 6-well plate, which typically contains ca. 5x10E5 cells of organoids/spheroids were harvested as described above, but on ice, on day 2 post-seeding. Cells were lysed on ice using RIPA buffer and phosphatase and proteinase inhibitors. BCA assay was done to determine protein concentration and gel electrophoresis using NuPAGE4-12% gradient Bis-Tris Gels was performed using 20µg of protein, 10X reducing agent, 4X loading buffer, and RIPA buffer to fill up to 30µl per sample. Samples were heated to 95°C for 5min before loading and MOPS buffer was used to fill the tank. Gels were run for 50min at 200V. Protein was transferred to PVDF membranes using wet transfer in methanol containing transfer buffer at 30V for 1.5h. Membranes were blocked using 5% BSA in TBS-T for 1h at room temperature. Total protein levels (relative to one another) were determined using Revert™ 700 Total Protein Stain Kit (Licor, P/N 926-11016). Anti-RICTOR primary antibody (Santa Cruz, sc-271081) was diluted 1:500 in 5% BSA in TBS-T and membranes were incubated overnight on a rotary shaker. Subsequently, membranes were washed 3x in TBS-T and incubated in secondary Alexa-fluor488-conjugated anti-mouse antibody (Thermo Fischer Scientific, A32723) for 1h at room temperature. Membranes were washed 3x with TBS-T and fluorescence was detected using the Licor Odyssey™ system.

2.10 Statistical analyses

All statistical analyses except for differential expression analysis in DESeq2 was performed using GraphPad Prism 9.

2.11 Illustrations

Some illustrations were generated using Biorender.com, which was indicated in the figure caption where applicable.

Chapter 3 PI3-Kinase signalling hyperactivation in mouse models of intestinal cancer

In the introduction to this thesis, I outlined the physiological role and cancer-related pathophysiology of Wnt-, PI3-Kinase-, MAPK-, and mTOR signalling. In light of the common mutations found in these pathways in colorectal cancer and their impact upon outcomes and therapeutic response, I have developed multiple genetically engineered mouse models of intestinal tumorigenesis driven by mutations in the Wnt-, PI3-Kinase-, and MAPK signalling pathways.

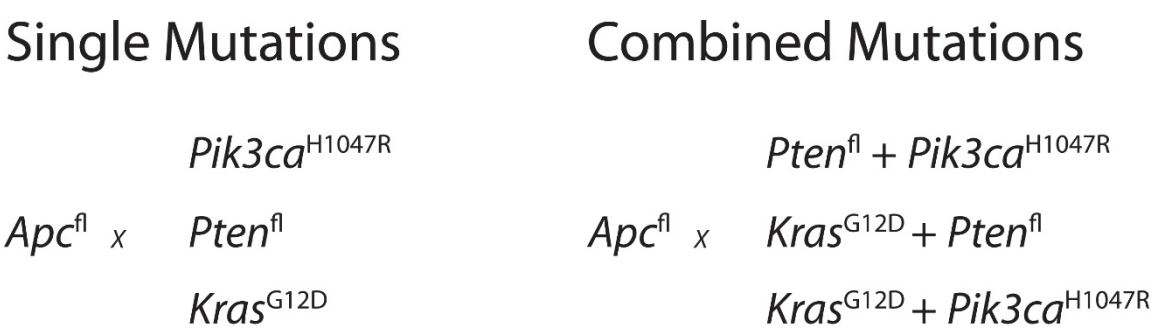

Figure 3-1: Summary of crosses presented in this thesis The *Apc*^{fl} allele was used heterozygously to predispose mice to intestinal cancer initiation and multiple oncogenic alleles were crossed to this background (described in the materials and methods section) as single and combined mutations.

The majority of studies were carried out in two experimental settings: 1) Ageing/tumorigenesis experiments, where PI3-Kinase signalling and/or MAPK driving mutations were combined with heterozygous deletion of *Apc*. In this setting, sporadic loss of the second copy of *Apc* drives tumour formation. 2) Short-term/acute experiments, where biallelic deletion of *Apc* in combination with the same mutations allows assessment of the impact of oncogenic expression directly upon oncogenic transformation. Finally, I carried out a study on the potential of

PI3-Kinase hyperactivation to drive intestinal cancer in the absence of transgenic *Apc* mutation.

3.1 PI3-Kinase-activating mutation in *Apc*-loss predisposed mice

3.1.1 Intestine-specific heterozygous Apc knock-out leads to tumour formation

Before assessing the impact of hyperactivated PI3-Kinase signalling, it was important to establish a baseline of intestinal cancer initiation and progression driven solely by loss of functional APC. To do so, I took advantage of Cre-lox technology to generate a model incorporating a tamoxifen inducible Cre-recombinase under control of the intestinal epithelium-specific *Villin1* promoter (Villin-CreER^{T2}), and an allele that allowed targeted deletion of exon 14 of *Apc* (*Apc*^{fl}). In this model, genetic recombination was driven by induction of Cre activity through intraperitoneal (IP) administration of 80mg/kg tamoxifen. This resulted in loss of one copy of *Apc* throughout the intestinal epithelium, and drove a predisposition to intestinal tumour formation. Following induction, mice were aged up to a defined clinical endpoint (weight loss, paling feet due to anaemia, and hunching) and then sampled. Villin-CreER^{T2}; *Apc*$^{fl/wt}$ mice were sampled at a median of 178-days post-induction (range: 83 to 358 days) (Figure 3-2), and were observed to develop tumours predominantly in their small intestines, with occasional formation of colonic polyps (Figure 3-3).

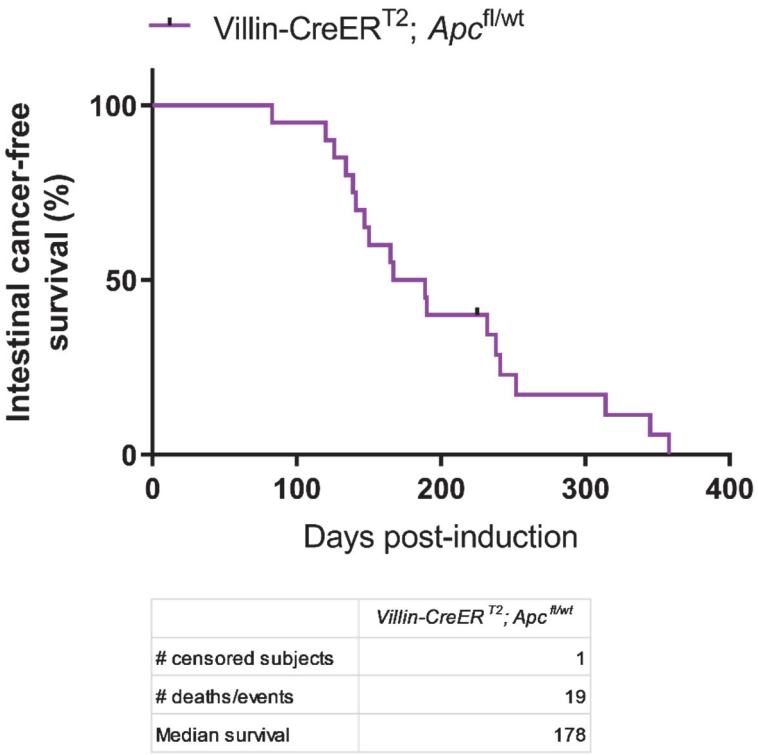

	Villin-CreER ^{T2}; Apc $^{fl/wt}$
# censored subjects	1
# deaths/events	19
Median survival	178

Figure 3-2: Villin-CreER^{T2}; *Apc*$^{fl/wt}$ mice develop signs of intestinal cancer. Survival curve of Villin-CreER^{T2}; *Apc*$^{fl/wt}$ mice (n=20) post-induction by administration of 80mg/kg tamoxifen. Median survival: 178 days.

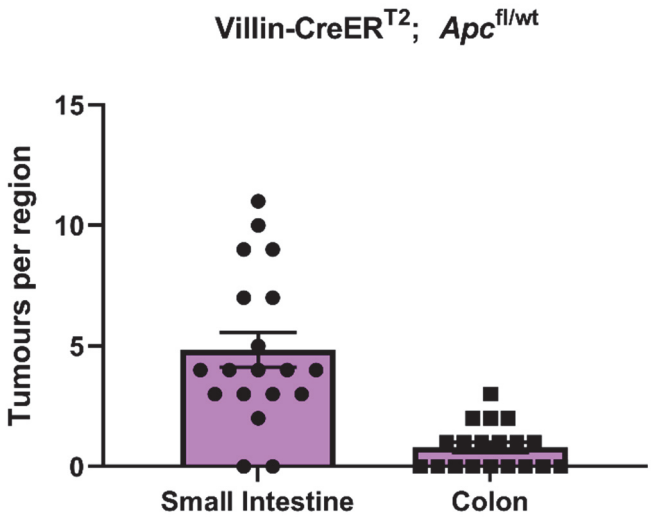

Figure 3-3: Villin-CreER^{T2} *Apc*$^{fl/wt}$ mice develop mostly small intestinal tumours, with occasional colonic polyps. Villin-CreER^{T2} *Apc*$^{fl/wt}$ mice (n=19) were sampled at endpoint and tumours were scored from the processed H&E stained histological samples. Mean ± s.e.m.

To initially characterize the tumours that arose in these mice, they were assessed histopathologically using haemotoxylin and eosin (H&E) stained sections. Most

mice exclusively developed benign-looking adenomas, while 2/19 mice developed an adenocarcinoma with invasive features (Figure 3-4).

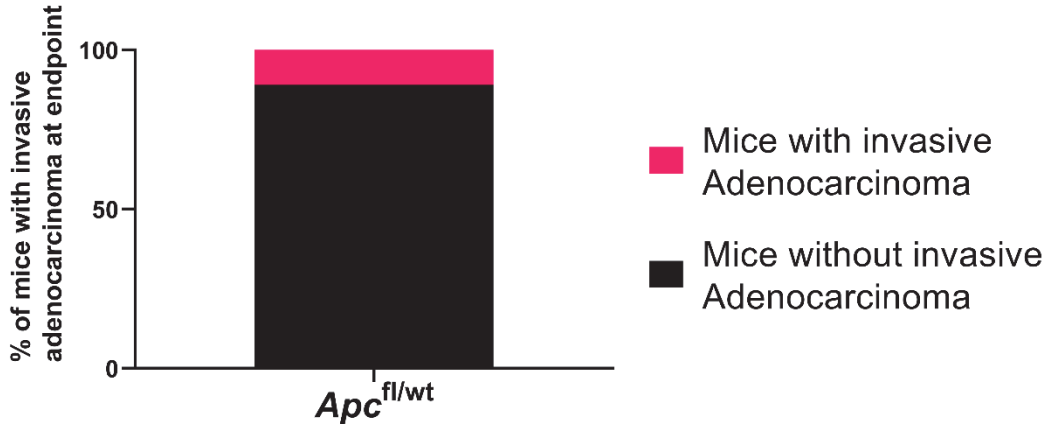

Figure 3-4: Tumours in Villin-CreER^{T2}; *Apc*$^{fl/wt}$ mice rarely progress to invasive adenocarcinoma. Histological assessment of tumours in Villin-CreER^{T2} *APC*$^{fl/wt}$ guts (n=19) at endpoint revealed tumours with adenomatous morphology in 17/19 of mice (89%), while 2/19 (11%) developed adenocarcinomas with invasive features as described in the Materials and Methods section.

Given that these tumours are thought to arise through loss of functional APC, and consequent hyperactivation of the Wnt-signalling pathway, a hallmark of APC-deficient intestinal cancer, I sought to assess Wnt-activation in this model through immunohistochemical staining against ß-catenin. Where the Wnt pathway is active, ß-catenin can be seen to accumulate in the nucleus, therefore assessment of the subcellular localisation of ß-catenin can be used to quantify Wnt activity. It is notable that as expected, the stem compartment of non-transformed epithelium exhibited high levels of nuclear stain, and the differentiated epithelium low levels, while nuclear ß-catenin was strikingly high in transformed cells within adenomatous tissue (Figure 3-5).

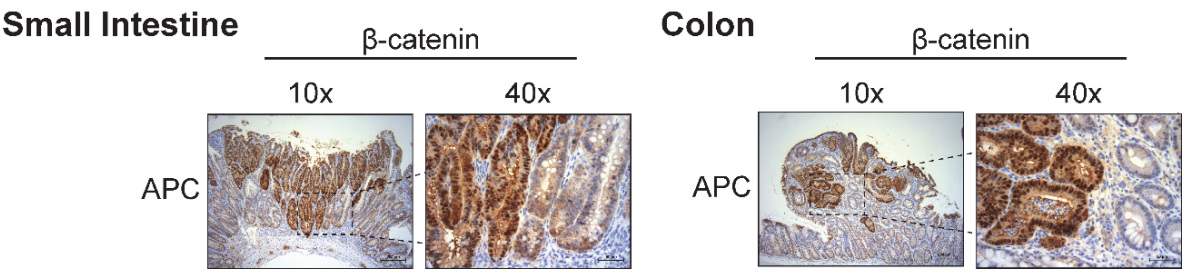

Figure 3-5: Tumour cells in Villin-CreER^{T2}; *Apc*$^{fl/wt}$ mice are high for nuclear β-catenin IHC-staining of β-catenin in SI and Colon tumours from Villin-CreER^{T2}; *Apc*$^{fl/wt}$ mice sampled at clinical endpoint. Scale bars 200µm (10x), and 50µm (40x).

3.1.2 Heterozygous *Pik3ca*^{H1047R} mutation does not alter survival, but promotes adenoma to adenocarcinoma progression in Villin-CreER^{T2}; *Apc*$^{fl/wt}$ mice

Having established a baseline model incorporating *Apc* loss in the intestinal epithelium, I then went on to assess the impact of compounding mutations in the PI3-Kinase pathway. Initially, I crossed Villin-CreER^{T2}; *Apc*$^{fl/wt}$ mice to animals bearing the *Pik3ca*^{H1047R} allele, thus generating Villin-CreER^{T2}; *Apc*$^{fl/wt}$; *Pik3ca*$^{H1047R/wt}$ mice. After administration of tamoxifen, these mice were aged and sampled at clinical endpoint, which they reached at a median of 155 days (range: 57 to 352 days). This was not significantly different from Villin-CreER^{T2}; *Apc*$^{fl/wt}$ ageing mice (Figure 3-6). Moreover, histopathological analysis of the intestinal tissue from these mice indicated that PI3-Kinase had no significant effect on occurrence and distribution of tumours (Figure 3-7).

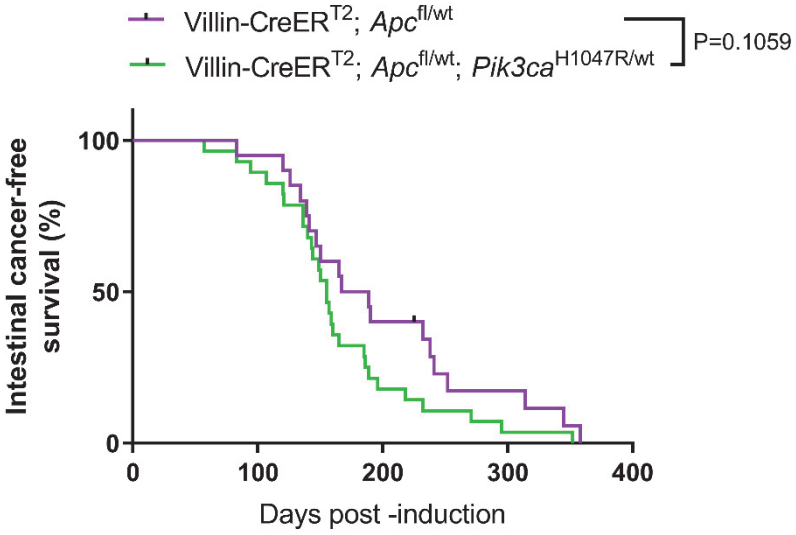

Genotype	Villin-CreER^{T2}; *Apc*$^{fl/wt}$	Villin-CreER^{T2}; *Apc*$^{fl/wt}$; *PIK3CA*$^{H1047R/wt}$
# censored subjects	1	0
# deaths/events	19	28
Median survival	178	155

Figure 3-6: Heterozygous Pik3ca^{H1047R} mutation does not modulate survival of Villin-CreER^{T2}; *Apc*$^{fl/wt}$ ageing mice. Survival curve of Villin-CreER^{T2}; *Apc*$^{fl/wt}$ (n=20, purple) and Villin-CreER^{T2}; *Apc*$^{fl/wt}$; *Pik3ca*$^{H1047R/wt}$ (n=28, green, median survival =155 days) mice post-induction by administration of 80mg/kg tamoxifen. Log-rank test.

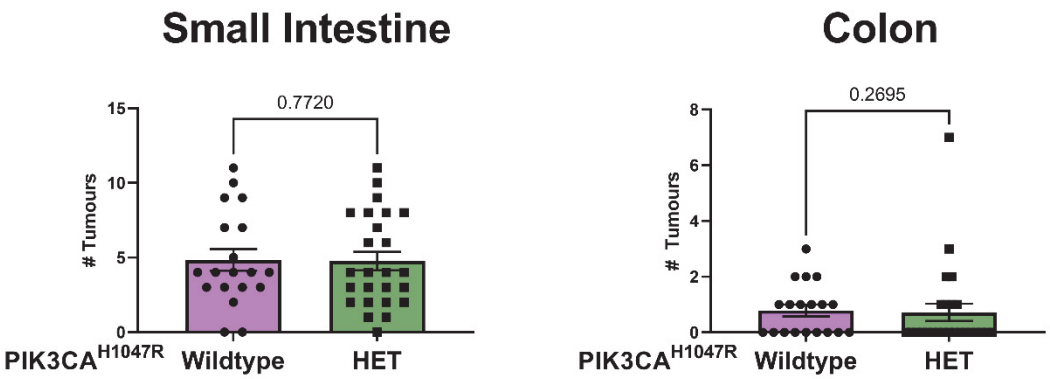

Figure 3-7: Heterozygous *Pik3ca*^{H1047R} mutation does not lead to increased tumour initiation. Villin-CreER^{T2}; *Apc*$^{fl/wt}$; *Pik3ca*$^{H1047R/wt}$ mice were sampled at endpoint and tumours were scored from the processed H&E stained samples. Mean ± s.e.m. Two-sided Mann-Whitney U test.

Despite these obvious similarities, it was notable that previous publications demonstrated a faster adenoma-to-adenocarcinoma progression driven by PI3-Kinase mutation (Deming *et al.*, 2014). I therefore went on to examine the intestines of Villin-CreER^{T2}; *Apc*$^{fl/wt}$; *Pik3ca*$^{H1047R/wt}$ mice at endpoint to assess the relative proportion of mice that developed invasive adenocarcinoma in Villin-CreER^{T2}; *Apc*$^{fl/wt}$ versus Villin-CreER^{T2}; *Apc*$^{fl/wt}$; *Pik3ca*$^{H1047R/wt}$. This proportion was significantly higher in PI3-Kinase mutants than in their PI3-Kinase-wildtype counterparts (Figure 3-8).

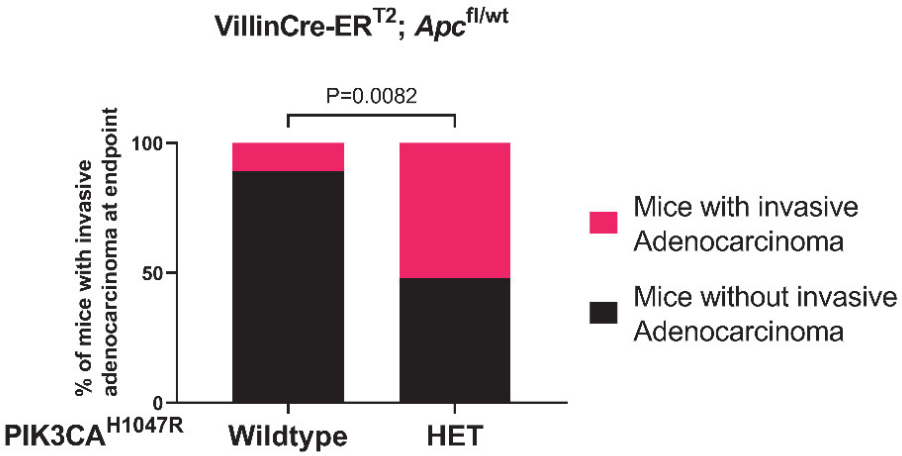

	No Invasive Tumour	Invasive Tumour
APC	17	2
APC PIK3CA^{HET}	12	13

Figure 3-8: Mice with heterozygous PI3-Kinase mutation have a higher proportion of invasive adenocarcinoma Histological assessment of tumours in Villin-CreER^{T2}; *Apc*$^{fl/wt}$; *Pik3ca*$^{H1047R/wt}$ guts (n=23) at endpoint revealed increased occurrence of invasive adenocarcinomas (n=12, 52%) compared to Villin-CreER^{T2}; *Apc*$^{fl/wt}$ mice (n=2, 11%). Fisher's exact test.

As done previously, to determine whether tumours arising in *Pik3ca*-mutant mice are high for Wnt signalling, I went on to assess ß-catenin nuclear localisation (Figure 3-9). Large adenocarcinomas in PI3-Kinase mutant mice tended to have mixed populations of cells exhibiting high- and low-levels of nuclear ß-catenin, while cells in adenomas had uniformly nuclear localisation of ß -catenin. This indicates that there are Wnt-signalling-high and low populations within Villin-CreER^{T2}; *Apc*$^{fl/wt}$; *Pik3ca*$^{H1047R/wt}$ adenocarcinomas.

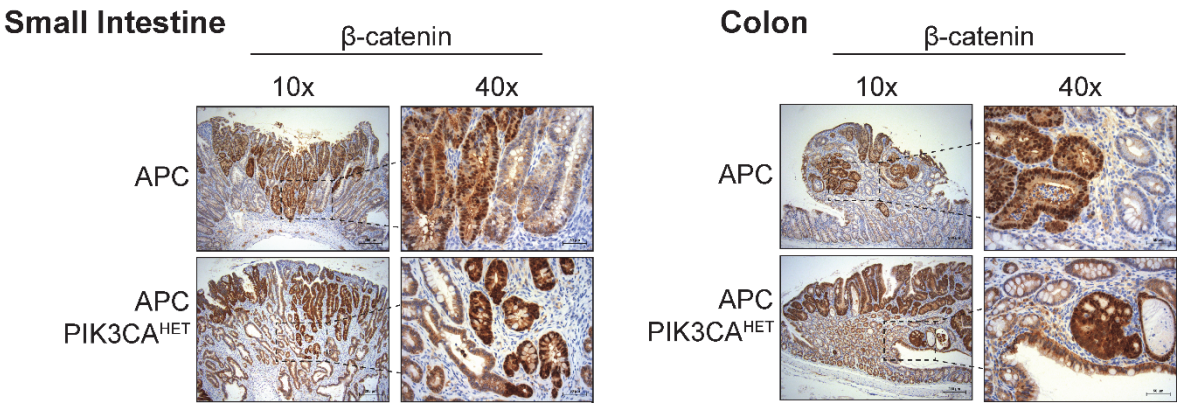

Figure 3-9: Tumour cells in Villin-CreER^{T2}; *Apc*$^{fl/wt}$; *Pik3ca*$^{H1047R/wt}$ mice are nuclear β-catenin high in SI adenomas and colon, while adenocarcinomas can contain mixed populations. IHC-staining of β-catenin in SI and colonic tumours from Villin-CreER^{T2}; *Apc*$^{fl/wt}$ and Villin-CreER^{T2}; *Apc*$^{fl/wt}$; *Pik3ca*$^{H1047R/wt}$ mice taken at endpoint. Scale bars 200µm (10x), and 50µm (40x).

Further to this characterisation of Wnt-pathway activity in this model, I then went on to assess the impact of Pik3ca mutation upon cellular signalling *in vivo*. To this end, I undertook immunohistochemical staining for key downstream targets of the PI3-Kinase pathway. I have grouped these into mTORC1 (pS6-S235/236, pS6-S240/244), and mTORC2 (pAKT-473, pNDRG1-T346) dependent targets. Tumours from Villin-CreER^{T2}; *Apc*$^{fl/wt}$ mice were generally high for mTORC1 targets, but low for mTORC2 targets (Figure 3-10). Similar observations were made in Villin-CreER^{T2}; *Apc*$^{fl/wt}$; *Pik3ca*$^{H1047R/wt}$ mice, where adenomas and adenocarcinomas did not exhibit increased mTOR pathway activation at the phosphoprotein level (Figure 3-10).

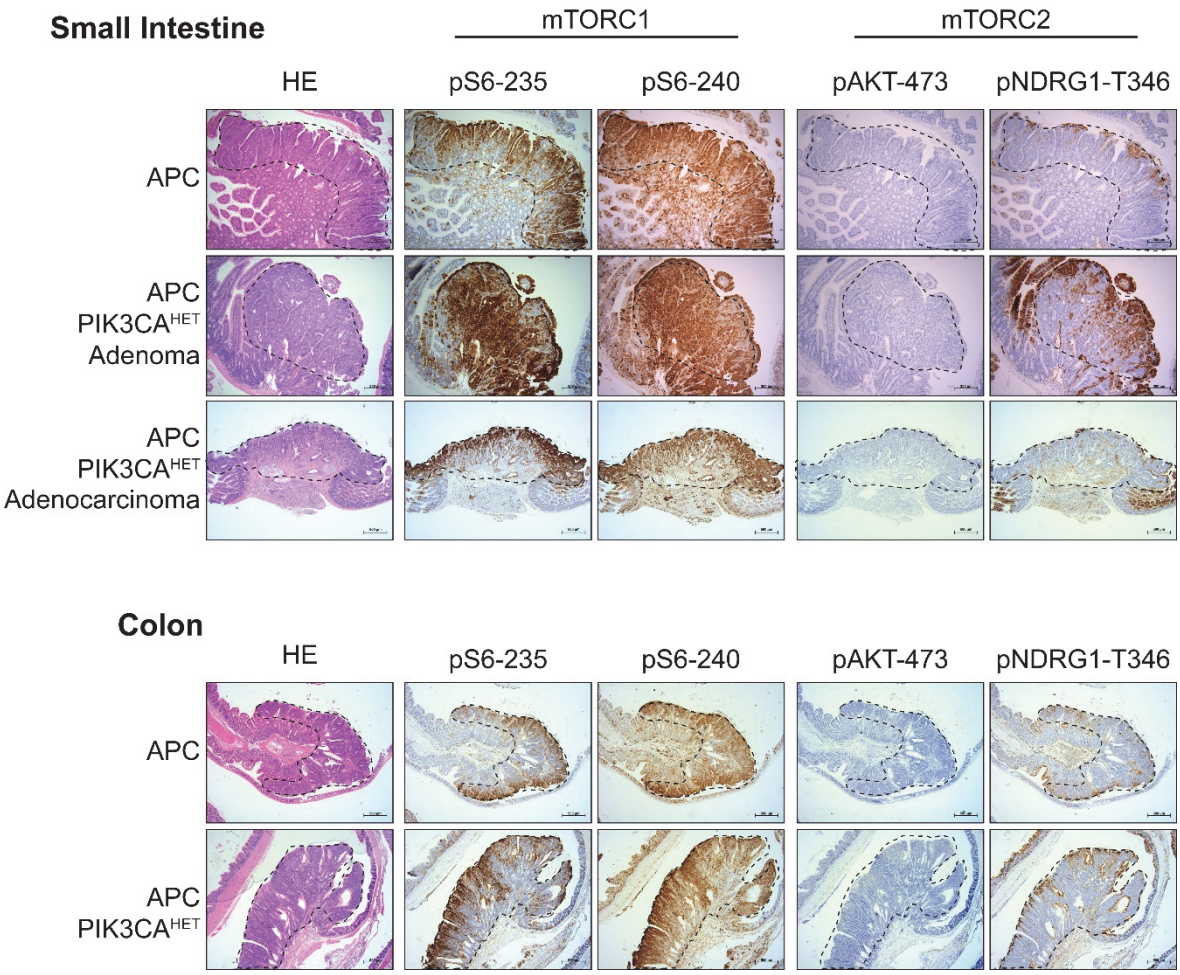

Figure 3-10: IHC characterisation of PI3-Kinase-wildtype and mutant tumours reveals high basal mTORC1 activation, no apparent pAKT-S473 engagement. Representative images of immunohistochemistry of tumours from Villin-CreER^{T2}; *Apc*$^{fl/wt}$ *(APC)* and Villin-CreER^{T2}; *Apc*$^{fl/wt}$; *Pik3ca*$^{H1047R/wt}$ (APC PIK3CA^{HET}) mice, stained with H&E, or against pS6-235, pS6-240, pAKT-473, and pNDRG1-T346. Scale bars 200µm and 500µm.

The apparent lack of impact upon canonical downstream targets of the PI3-Kinase pathway in these models may be related to the function of the tumour suppressor PTEN, whose function is to counteract the generation of PIP3 by PI3-K directly. It was notable that PTEN expression was generally high in tumours of both PI3-K wildtype, and mutant animals (Figure 3-11), providing a ready explanation for the lack of a more substantial difference between these genotypes. PTEN expression is not uniform in invasive adenocarcinomas arising in *Pik3ca* mutant mice, suggestive of some form of context-specific regulation. While there were too few colonic tumours in this experimental cohort to make a clear statement on the distribution of PTEN in this setting, it was generally high.

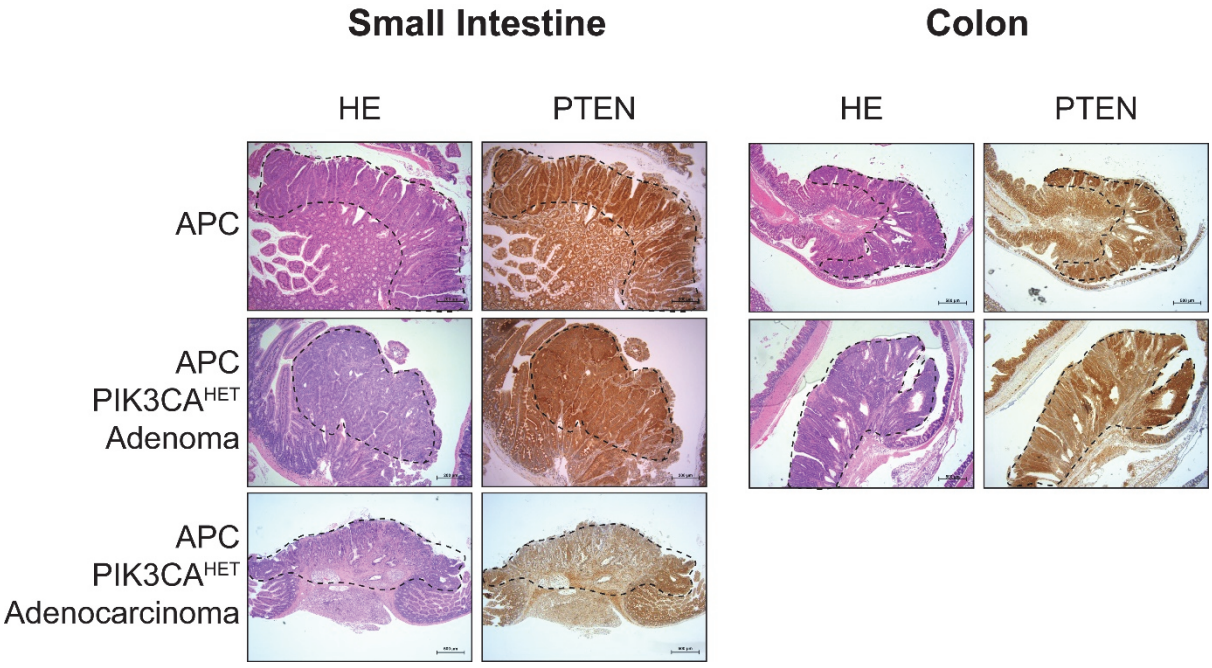

Figure 3-11: PI3-Kinase-wildtype and mutant tumours have high levels of PTEN. Representative images of tumours from Villin-CreER^{T2}; *Apc*$^{fl/wt}$ (APC) and Villin-CreER^{T2}; *Apc*$^{fl/wt}$; *Pik3ca*$^{H1047R/wt}$ (APC PIK3CA^{HET}) mice, stained with H&E, or against PTEN. Scale bars 200µm and 500µm.

3.1.3 Homozygous Pik3ca^{H1047R} mutation drives small intestinal tumour initiation, but not adenoma to adenocarcinoma progression

A previous publication from the Vanhaesebroeck lab indicated that human inducible pluripotent stem cells tolerate heterozygous *PIK3CA*^{H1047R} mutation, but cannot be differentiated into all lineages when the mutant PI3-Kinase is expressed homozygously, suggesting that gene-doseage might be important in penetrance of phenotypes driven by this mutation (Madsen *et al.*, 2019). To determine whether gene-doseage of *Pik3ca* mutation has a role in intestinal cancer initiation in my models, I bred the *Pik3ca*^{H1047R} allele to homozygosity in the context of Villin-CreER^{T2}; *Apc*$^{fl/wt}$, thus generating Villin-CreER^{T2}; *Apc*$^{fl/wt}$; *Pik3ca*$^{H1047R/H1047R}$ mice. When subjected to ageing experiments as described earlier, these mice reached clinical endpoint at a median of 126 days post-induction (range: 28 to 198 days), significantly earlier than PI3-K wildtype and heterozygous mutants (Figure 3-12).

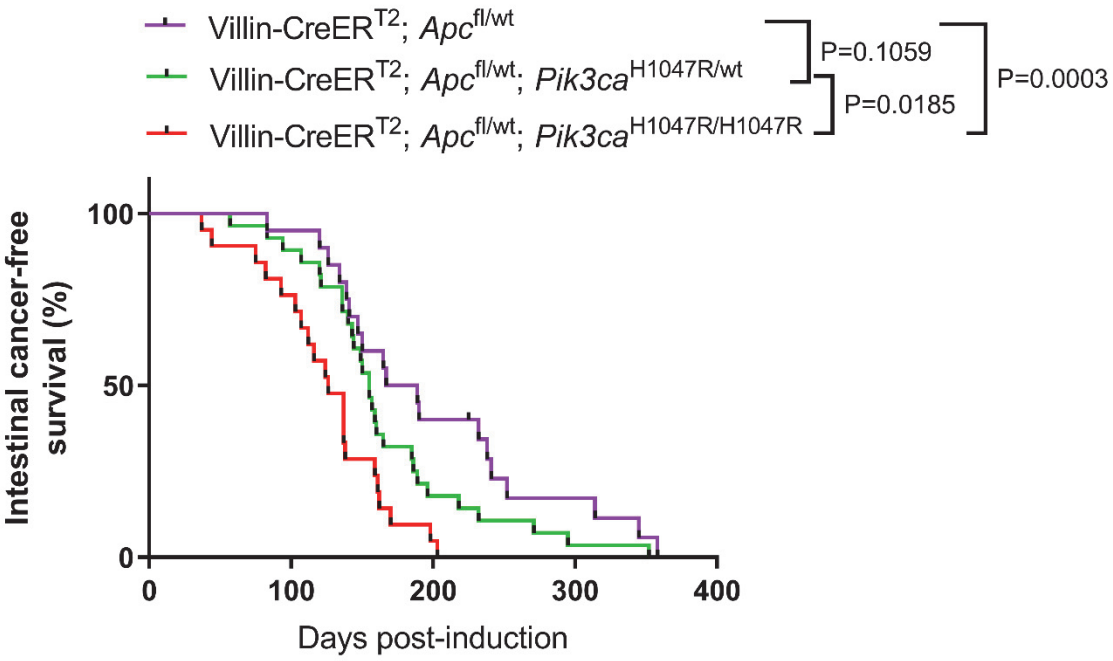

	Villin-CreER^{T2}; *Apc*$^{fl/wt}$	Villin-CreER^{T2}; *Apc*$^{fl/wt}$; *Pik3ca*$^{H1047R/wt}$	Villin-CreER^{T2}; *Apc*$^{fl/wt}$; *Pik3ca*$^{H1047R/H1047R}$
# censored subjects	1	0	0
# deaths/events	19	28	21
Median survival	178	156	126

Figure 3-12: Homozygous *Pik3ca*^{H1047R} mutation accelerates the Villin-CreER^{T2}; *Apc*$^{fl/wt}$ model Survival curve of Villin-CreER^{T2}; *Apc*$^{fl/wt}$ (n=20, purple), Villin-CreER^{T2}; *Apc*$^{fl/wt}$; *Pik3ca*$^{H1047R/wt}$ (n=28, green), and Villin-CreER^{T2}; *Apc*$^{fl/wt}$; *Pik3ca*$^{H1047R/H1047R}$ (n=21, red, median survival = 126 days) mice post-induction by administration of 80mg/kg tamoxifen. Log-rank test.

I hypothesized that this decrease in overall survival might be associated with an increase in tumour initiation, and therefore compared intestinal tumour number at clinical endpoint in Villin-CreER^{T2}; *Apc*$^{fl/wt}$; *Pik3ca*$^{H1047R/H1047R}$ versus Villin-CreER^{T2}; *Apc*$^{fl/wt}$; *Pik3ca*$^{H1047R/+}$ and Villin-CreER^{T2}; *Apc*$^{fl/wt}$ mice, but surprisingly observed no significant difference (Figure 3-13).

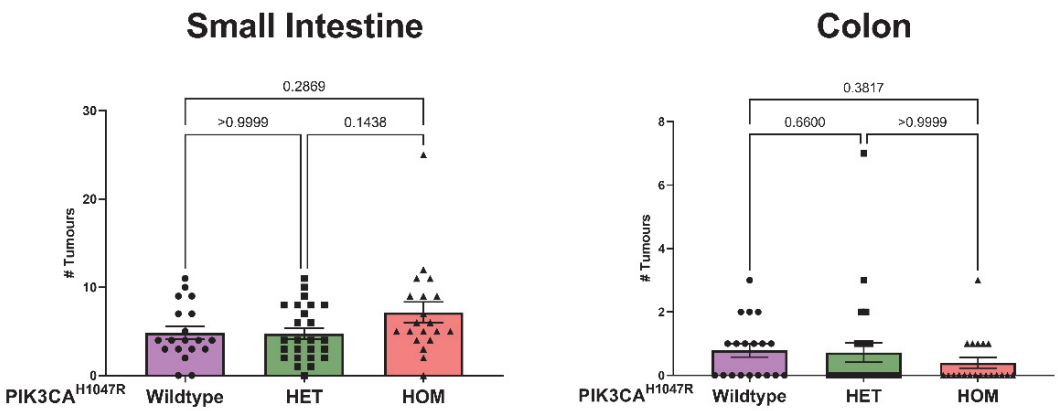

Figure 3-13: Similar tumour number in *Pik3ca*^{H1047R} mutant ageing mice at endpoint. Villin-CreER^{T2}; *Apc*$^{fl/wt}$; *Pik3ca*$^{H1047R/H1047R}$ mice were sampled at endpoint and tumours were scored from the processed H&E stained samples. Mean ± s.e.m. Kruskal-Wallis test and Dunn's multiple comparisons test.

Given that the process of sporadic tumour initiation is thought to occur progressively throughout the experiment, to account for the earlier clinical endpoint of *Pik3ca*$^{H1047R/H1047R}$ mice, I normalized the tumour number of each mouse by their days post-induction to endpoint, which results in a significant difference between the *Pik3ca*^{H1047R} wildtypes and heterozygotes vs homozygotes (Figure 3-14).

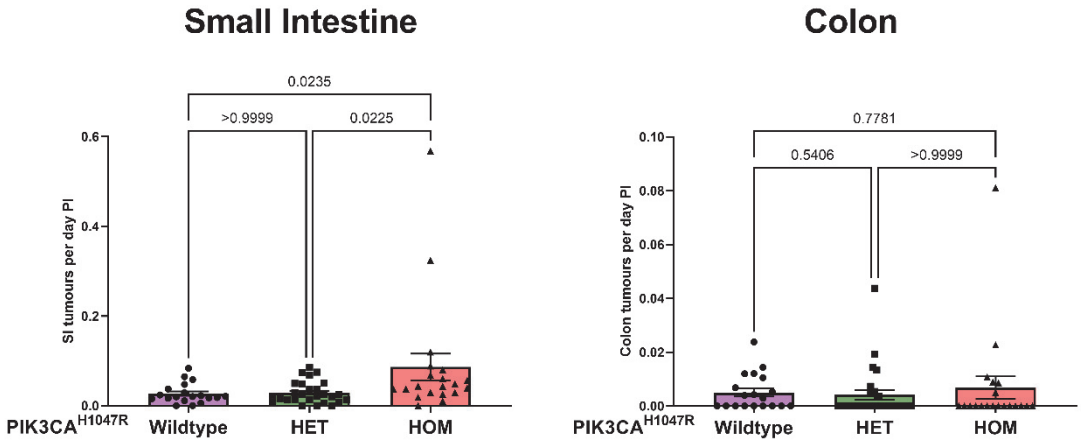

Figure 3-14: Homozygous *Pik3ca*^{H1047R} mutation leads to increased small intestinal tumour initiation. Number of SI and Colon tumours were divided by time to clinical endpoint, normalizing the rate of intestinal tumour initiation to the time to endopoint in individual mice. Mean ± s.e.m. Kruskal-Wallis test and Dunn's multiple comparisons test.

Given the increase in the invasive nature of tumours following heterozygous expression of *Pik3ca*^{H1047R}, it was surprising that *Pik3ca*$^{H1047R/H1047R}$ mice did did not develop more invasive adenocarcinoma than their wildtype counterparts (Figure

3-15). Furthermore, the tumours with invasive adenocarcinoma features were usually not as large and stroma-rich as the ones in *Pik3ca*^{H1047R} heterozygous mice.

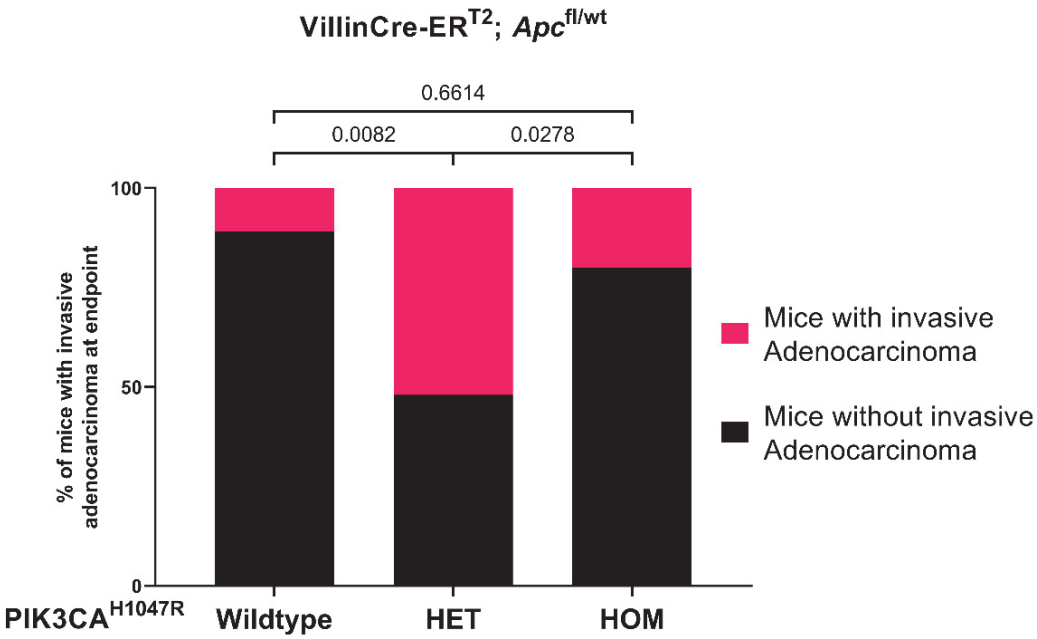

	No Invasive Tumour	Invasive Tumour
APC	17	2
APC PIK3CA ^{HET}	12	13
APC PIK3CA ^{HOM}	16	4

Figure 3-15: Homozygous PI3-Kinase-mutation does not further increase invasive adenocarcinoma formation. Histological assessment of tumours in Villin-CreER^{T2}; *Apc*$^{fl/wt}$; *Pik3ca*$^{H1047R/H1047R}$ guts (n=14) at endpoint revealed no increase in occurrence of invasive adenocarcinomas (n=4, 20%) compare to *Pik3ca* wildtypes. Fisher's exact tests.

As previously, to determine whether homozygous *Pik3ca*^{H1047R} mutation had any impact upon modulation of downstream targets, I stained for the same mTORC1 (pS6-S235/236, pS6-S240/244), and mTORC2 (pAKT-473, pNDRG1-T346) dependent targets (Figure 3-16). mTORC1 targets were strongly engaged. In contrast to the previously described genotypes, pAKT-473 was upregulated in SI tumours of homozygotes, potentially indicating more robust PI3-Kinase pathway activation.

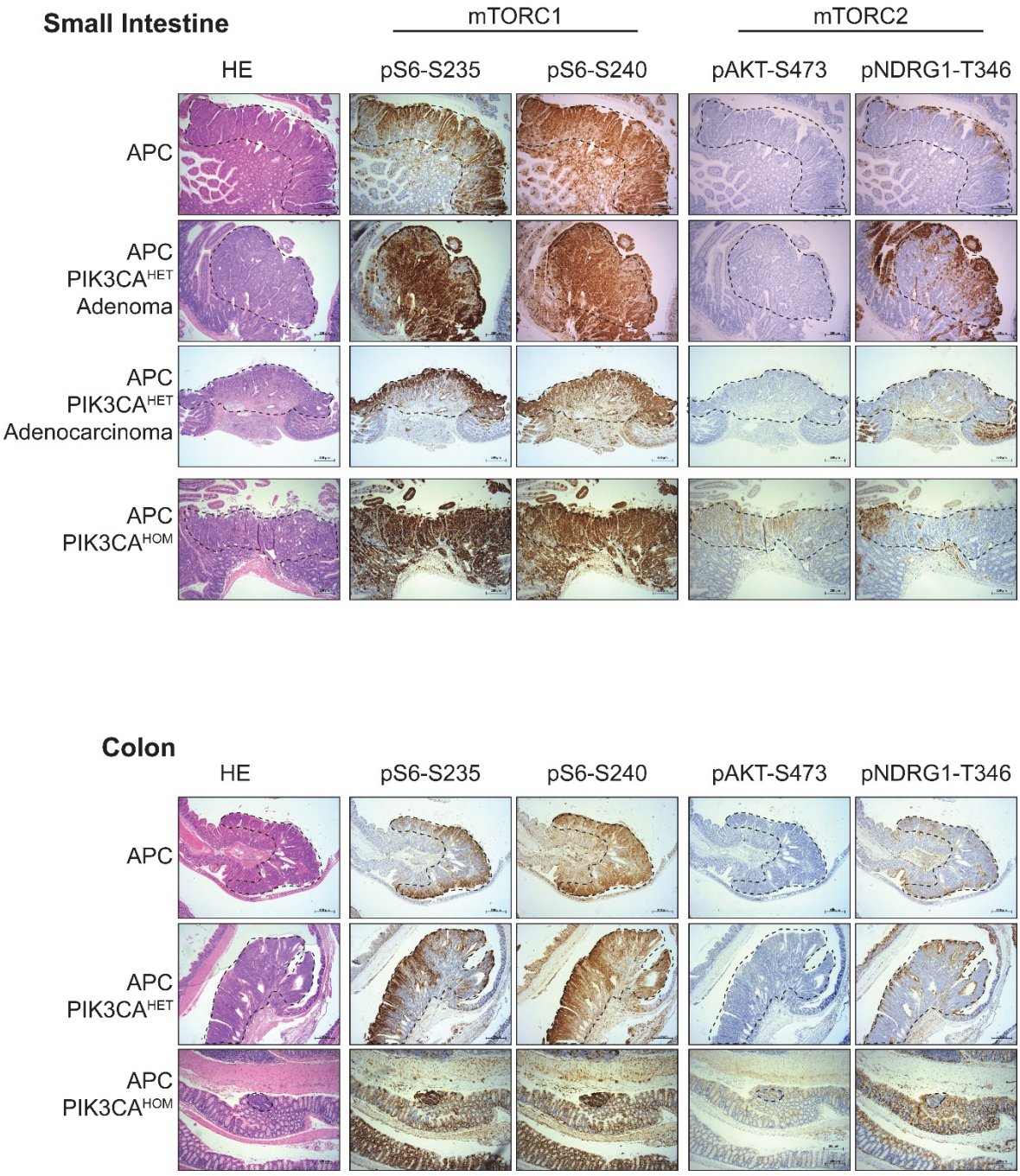

Figure 3-16: IHC characterisation of *Pik3ca*^{H1047R}-homozygous mutant guts reveals mTORC1 and pAKT-S473 activation in SI tumours. Representative images of immunohistochemistry of tumours from Villin-CreER^{T2}; *Apc*$^{fl/wt}$ (APC) and Villin-CreER^{T2}; *Apc*$^{fl/wt}$; *Pik3ca*$^{H1047R/wt}$ (APC PIK3CA^{HET}) mice, and Villin-CreER^{T2}; *Apc*$^{fl/wt}$; *Pik3ca*$^{H1047R/H1047R}$ (APC PIK3CA^{HOM}), stained with H&E, or against pS6-235, pS6-240, pAKT-473, and pNDRG1-T346. Scale bars 200µm and 500µm.

Tumour cells in Villin-CreER^{T2}; *Apc*$^{fl/wt}$; *Pik3ca*$^{H1047R/H1047R}$ mice also exhibited high levels of nuclear ß-catenin accumulation, indicating activated Wnt signalling (Figure 3-17).

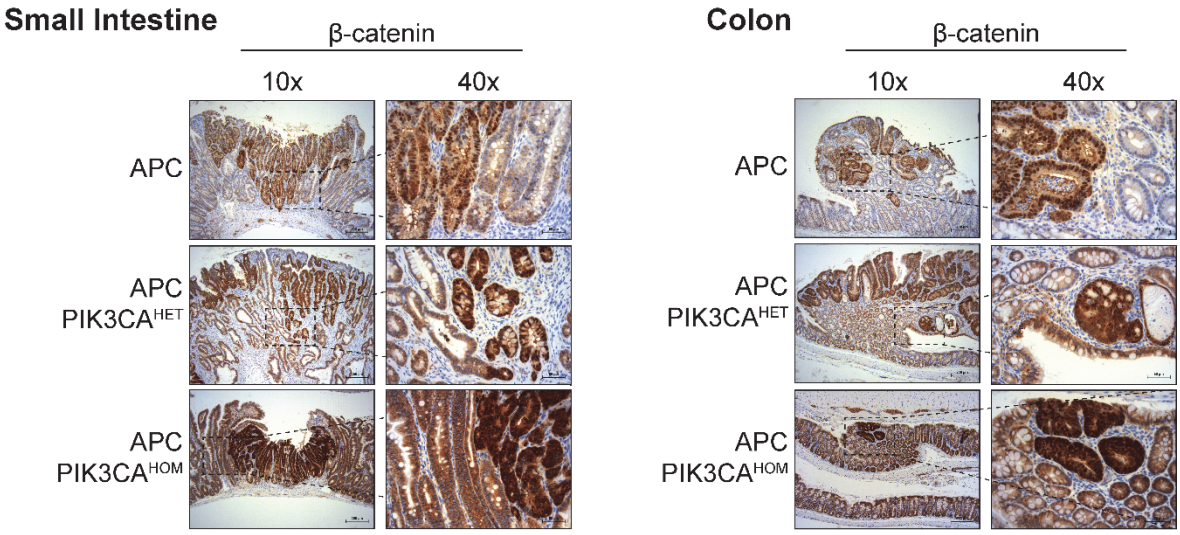

Figure 3-17: Tumour cells in Villin-CreER^{T2}; *Apc*$^{fl/wt}$; *Pik3ca*$^{H1047R/H1047R}$ mice at endpoint are high for nuclear β-catenin. IHC-staining of β-catenin in tumours from Villin-CreER^{T2}; *Apc*$^{fl/wt}$,Villin-CreER^{T2}; *Apc*$^{fl/wt}$; *Pik3ca*$^{H1047R/wt}$, and Villin-CreER^{T2}; *Apc*$^{fl/wt}$; *Pik3ca*$^{H1047R/H1047R}$ mice taken at endpoint. Scale bars 200µm (10x), and 50µm (40x).

3.1.4 Discussion

In summary, I have shown that *Pik3ca*^{H1047R} mutation has an allele-dose dependent effect in the context of *Apc*-loss mediated intestinal cancer. When expressing a single mutant allele, mice tended to develop advanced tumours with variable levels of nuclear ß-catenin that did not show obvious additional PI3-Kinase/mTOR pathway activation. When mutated homozygously, mice developed small intestinal tumours at a faster rate. These tumours were generally benign-looking polyps, expressed nuclear beta catenin, and showed high PI3-Kinase/mTOR pathway activation.

While the higher proportion of advanced cancer in *Pik3ca*^{H1047R} heterozygous mutants was somewhat expected, lack of increased occurrence in homozygotes was unexpected. An obvious explanation for the less advanced tumours is shorter time until endpoint. As results in chapter 3.4.1 will show, this is unlikely to be the reason because mice with a similar latency can develop invasive adenocarcinoma. Recent unpublished data generated in our lab related to oncogenic *Kras* driven disease, has shown that gene doseage can be critical, and in some circumstances, the wildtype copy of *Kras* can in effect act as tumour suppressor. In the PI3-Kinase mutant setting, the wildtype PI3-Kinase protein might also have an independent function, loss of which might prevent formation of advanced cancer in bi-allelic mutants. There could also be a threshold of PI3-Kinase signalling that determines

the fate of tumours: too much PI3-Kinase signalling could cause tumours to remain in a relatively benign state. In the introduction to this thesis, I discussed one study which showed that increased pAKT was associated with less advanced tumours and better overall survival, which would be in favour of this hypothesis (Baba *et al.*, 2011). Further analysis of other pathways that play a key role in intestinal homeostasis and colorectal cancer development, such as TGF-beta or Notch signalling, may be necessary to elucidate the mechanism behind this phenotype.

I previously mentioned studies in which a dominant active PI3-Kinase fusion gene (PIK3ca*) was expressed from the fabp1 promoter in mice (A. A. Leystra *et al.*, 2012). This resulted in a much stronger phenotype, even in the absence of *Apc* mutation, as mice in these experiments had to be sampled at 40-60 days due to invasive mucinous tumours. The authors of that paper detected strong PI3-Kinase pathway activation by IHC. Furthermore, tumours did not progress through a benign polypoid stage, but directly to advanced cancer without nuclear ß-catenin localisation. This fusion gene is expressed in addition to two copies of wildtype *Pik3ca* and escapes both transcriptional and post-translational regulation. Therefore, it may be a suboptimal model to study the effect of dysregulated PI3-Kinase. Here I express the point-mutated *Pik3ca* from its endogenous locus, which may be more relevant to human disease. Large adenocarcinomas arising in *Pik3ca* heterozygous mutant mice showed mixed populations of cells expressing nuclear and membranous ß-catenin. This was observed to occur in clinical samples, in particular in the invasive front of colorectal tumours (Brabletz *et al.*, 1998; Baldus *et al.*, 2004). Further analysis using e.g. RNA-ISH on Exon 14 of *Apc* would be useful to determine whether all epithelial cells present in tumours have recombined the *Apc* allele or whether untransformed epithelial cells are part of those tumours in addition to the stromal infiltrate.

My inability to detect a robust activation of PI3-Kinase signalling in *Pik3ca* heterozygotes may have been due to a technical limitation of this study, since the use of IHC as a read-out of pathway activation involves non-linear signal amplification and can mask subtle differences. Western blot or reverse-phase protein array (RPPA) on tumour samples would enable quantification of PI3-Kinase/mTOR hyperactivation more precisely.

3.2 *Pten*-KO in *Apc*-loss predisposed mice

3.2.1 Intestine-specific heterozygous knock-out of Pten leads to earlier clinical endpoint in Apc-loss predisposed mice

While oncogenic *PIK3CA* mutations provide a gain-of-function by increasing kinase activity, common loss-of-function mutations in the tumour suppressor PTEN can also elicit increased PI3-Kinase pathway activation. PTEN directly counteracts PI3-Kinase activity through lipid phosphatase activity targeted specifically at the 3' phosphate of PIP3. Since PTEN levels in APC-deficient tumours are generally high, I sought to evaluate the effect of genetic depletion of *Pten* in *Apc*-loss predisposed mice and therefore generated Villin-CreER^{T2}; *Apc*$^{fl/wt}$; *Pten*$^{fl/wt}$ mice. These mice reached clinical endpoint at a median of 128.5 days (range: 36 to 268 days) post-induction with tamoxifen (Figure 3-18). This was significantly shorter than in *Pten* wildtype mice. A caveat here is that these two ageing cohorts were carried out in independent breeding colonies, albeit on a matched genetic background – N≥9 C57Bl/6.

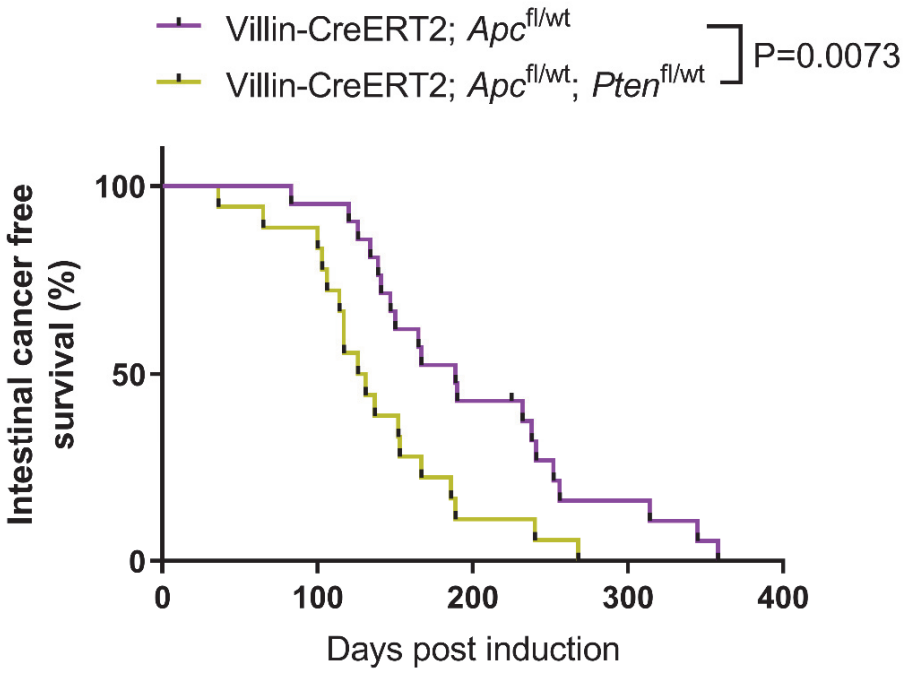

	VillinCre-ER^{T2}; Apc$^{fl/wt}$	VillinCre-ER^{T2}; Apc$^{fl/wt}$; Pten$^{fl/wt}$
# censored subjects	1	0
# deaths/events	19	18
Median survival	178	128.5

Figure 3-18: Heterozygous *Pten* knock-out leads to earlier clinical endpoint in Villin-CreER^{T2}; *Apc*$^{fl/wt}$ mice. Survival curve of Villin-CreER^{T2}; *Apc*$^{fl/wt}$ mice (n=20, purple), and Villin-CreER^{T2}; *Apc*$^{fl/wt}$; *Pten*$^{fl/wt}$ mice (n=18, yellow, median survival 128 days) post-induction by administration of 80mg/kg tamoxifen. Log-rank test.

Despite the difference in overall survival, the number of tumours arising in the small intestines of these mice at endpoint were not significantly different between the two models, while *Pten* heterozygous mice had fewer colonic tumours. (Figure 3-19). Interestingly, in light of the invasive phenotype associated with Villin-CreER^{T2}; *Apc*$^{fl/wt}$; *Pik3ca*$^{H1047R/+}$, the incidence of invasive adenocarcinomas was increased in Villin-CreER^{T2}; *Apc*$^{fl/wt}$; *Pten*$^{fl/wt}$ mice (Figure 3-20).

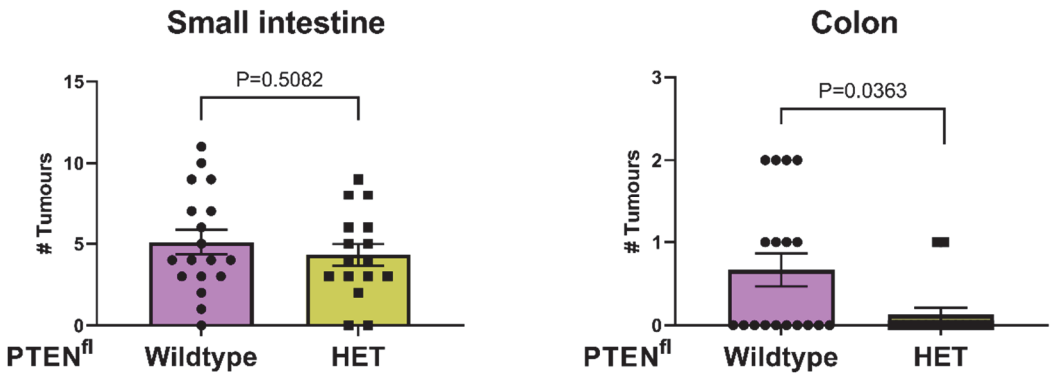

Figure 3-19: Heterozygous *Pten* knock-out in Villin-CreER^{T2}; *Apc*$^{fl/wt}$ mice does not increase overall tumour number Villin-CreER^{T2}; *Apc*$^{fl/wt}$; *Pten*$^{fl/wt}$ mice were sampled at endpoint and tumours were scored from the processed H&E stained samples. Mean ± s.e.m. Two-sided Mann-Whitney U test.

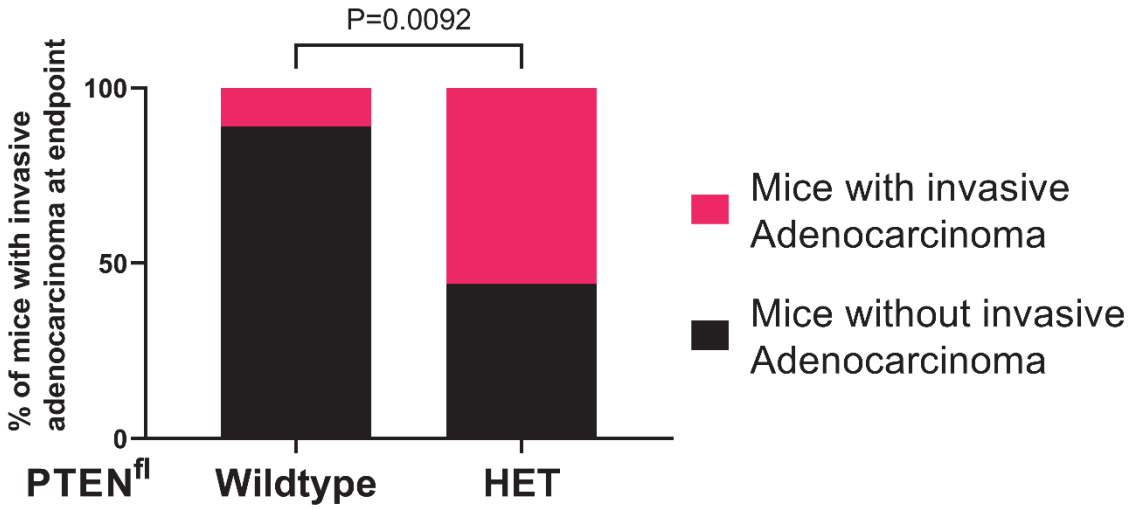

Figure 3-20: Heterozygous *Pten* knock-out leads to increased invasive adenocarcinoma formation in Villin-CreER^{T2}; *Apc*$^{fl/wt}$ mice. Histological assessment of tumours in Villin-CreER^{T2}; *Apc*$^{fl/wt}$; *Pten*$^{fl/wt}$ guts (n=16) at endpoint revealed tumours with adenomatous morphology in 7/16 of mice (44%), while 9/16 (56%) developed adenocarcinomas with invasive features. Fisher's exact test.

Interestingly, despite its known role as a tumour suppressor, tumours that arose in *Pten*$^{fl/wt}$ mice had not in all cases lost PTEN expression. In fact, IHC staining for PTEN revealed that tumours were either PTEN positive, negative, or exhibited mixed popuations of positive and negative cells (Figure 3-22 shows a mixed tumour). In light of this observation, I then assessed the frequency of *Pten* deficiency in tumours arising in this model. Scoring 48 tumours from eight individual mice, 50% were positive for PTEN, 27% were mixed, and 23% were fully negative (Figure 3-21).

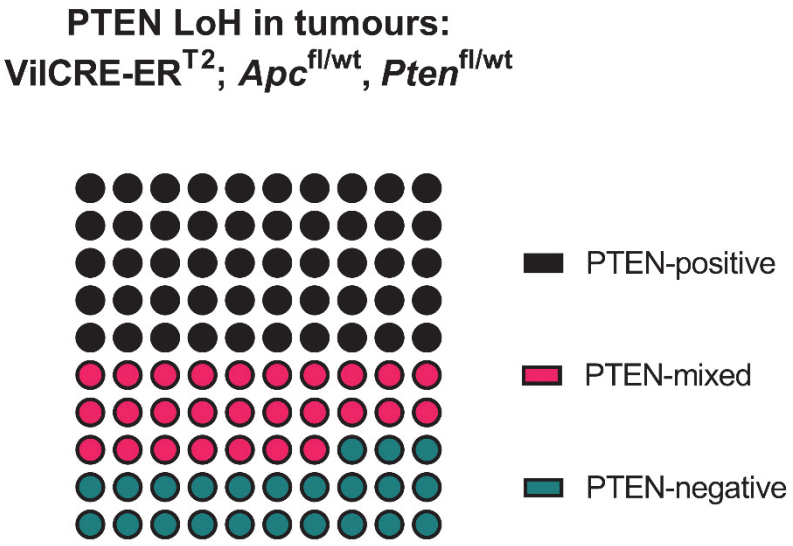

Figure 3-21: PTEN LoH in SI tumours in Villin-CreER^{T2}; *Apc*$^{fl/wt}$; *Pten*$^{fl/wt}$ mice. Sections of intestines of Villin-CreER^{T2}; *Apc*$^{fl/wt}$; *Pten*$^{fl/wt}$ mice were stained for PTEN and tumours were scored for their PTEN status. They were binned into PTEN positive, mixed, or negative. N=48 from 8 animals.

Tumours that exhibited mixed populations of PTEN proficient and deficient cells provided an excellent opportunity to understand the impact of PTEN loss upon PI3-kinase effector activation. This could be achieved through comparison of PTEN deficient cells to the surrounding proficient ones. To this end, I stained these tissue by IHC against PTEN, alongside mTORC1 (pS6-S235/236, pS6-S240/244), and mTORC2 (pAKT-473, pNDRG1-T346) dependent targets (Figure 3-22). As discussed previously, *Pten* wildtype tumours are strongly positive for mTORC1 signalling markers. Interestingly, and in contrast to *Pik3ca* mutant tumours, the mTORC2 dependent phosphorylation of AKT at S473 was prominent in PTEN deficient tumour areas, suggestive of a specific role for PTEN in limiting mTORC2 dependent phosphorylation of AKT, and by extension increased PI3-Kinase signalling activation.

The sporadic nature of loss of the second copy of PTEN in this model was highlighted by the common observation of *Pten* also being lost in single intestinal crypts (Figure 3-23). This suggests that *Pten* can be lost independently of tumour formation, and in isolation has no significant impact upon crypt homeostasis.

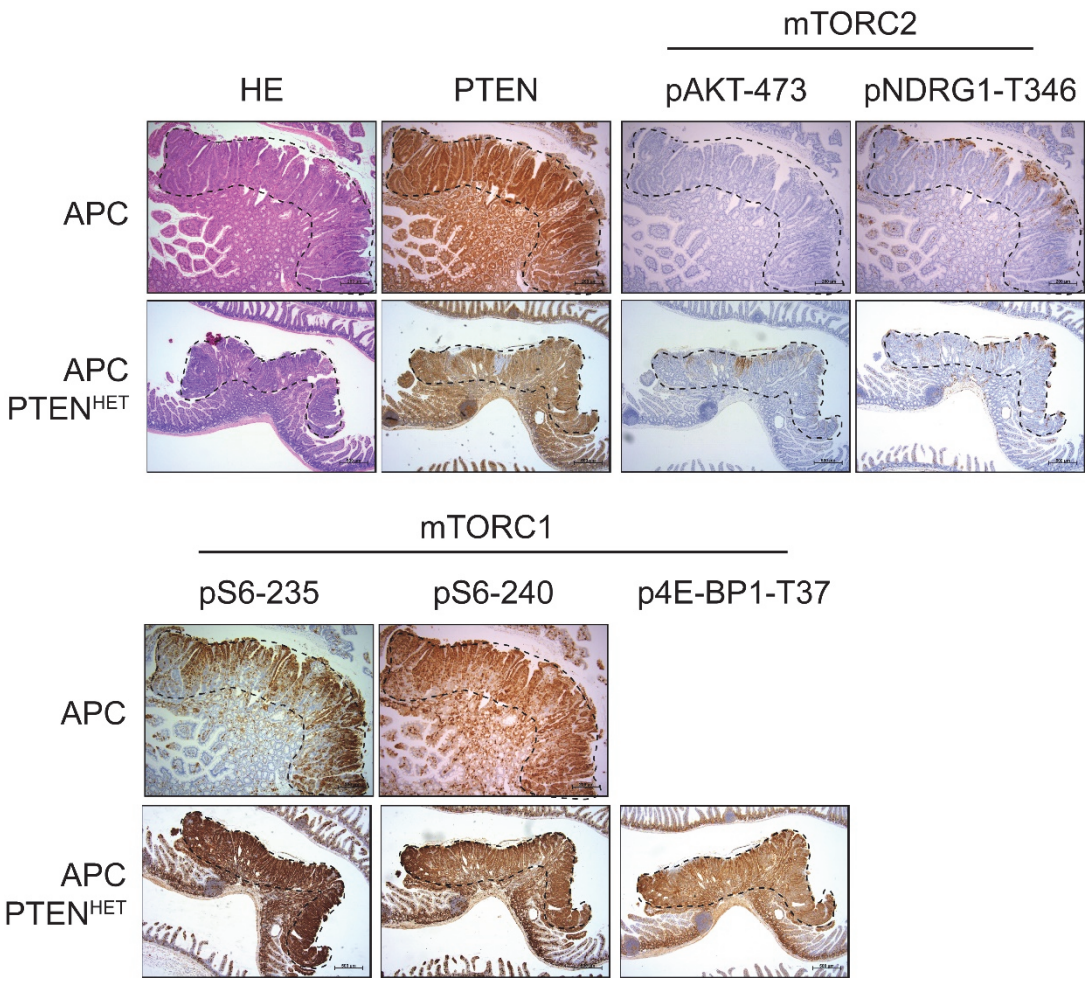

Figure 3-22: PTEN loss results in high PI3-Kinase and mTOR signalling. Representative images of immunohistochemistry of tumours from Villin-CreER^{T2}; *Apc*$^{fl/wt}$ (APC) and Villin-CreER^{T2}; *Apc*$^{fl/wt}$; *Pten*$^{fl/wt}$ (APC PTEN^{HET}) mice, stained with H&E, or against pAKT-473, pNDRG1-T346, pS6-235, pS6-240, or p4E-BP1-T37. Arrowhead points at PTEN deficient tissue. Scale bars 200µm and 500µm.

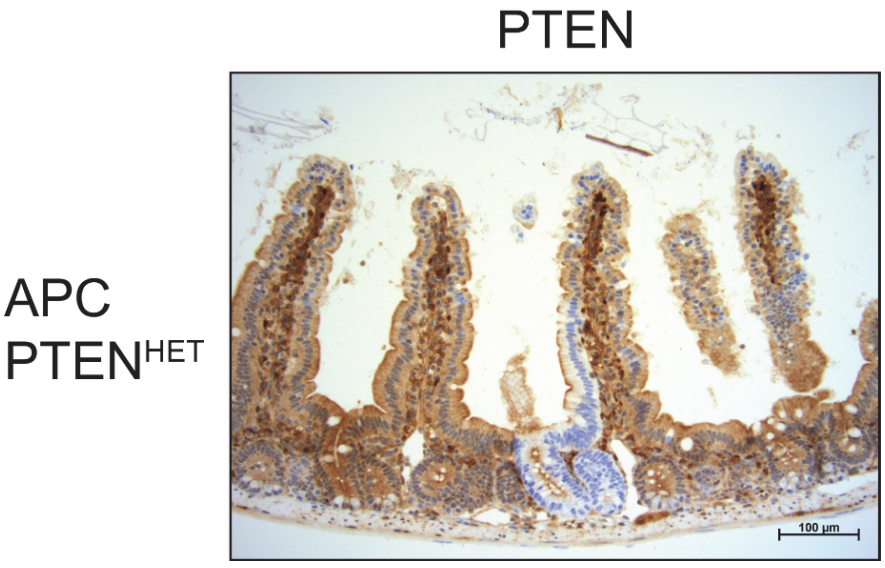

Figure 3-23: Occurrence of PTEN negative crypts in Villin-CreER^{T2}; *Apc*$^{fl/wt}$; *Pten*$^{fl/wt}$ mice. SI sections of Villin-CreER^{T2}; *Apc*$^{fl/wt}$; *Pten*$^{fl/wt}$ mice sampled at endpoint were stained for PTEN. Scale bar 100um.

3.2.2 Homozygous Pten knock-out leads to rapid small intestinal tumour formation

Given the observed impact of PTEN deficiency upon downstream targets of the PI3-Kinase pathway, I next sought to assess the impact of these changes upon tumour formation through complete ablation of *Pten* in the context of APC loss. To achieve this, I generated Villin-CreER^{T2}; *Apc*$^{fl/wt}$; *Pten*$^{fl/fl}$ mice and carried out ageing experiments as described earlier in this chapter. These mice reached clinical endpoint at a median of 37 days post-induction with tamoxifen (range: 16 to 46 days) (Figure 3-24), significantly earlier that the previously discussed Villin-CreER^{T2}; *Apc*$^{fl/wt}$ or Villin-CreER^{T2}; *Apc*$^{fl/wt}$; *Pten*$^{fl/wt}$ models. The early clinical endpoint in *Pten*$^{fl/fl}$ mice was associated with, and may be a result of, rapid formation of small intestinal tumours (Figure 3-25). Moreover, tumours in these mice did not progress to invasive adenocarcinoma, presumably due to the short latency of the model.

Tumour cells in Villin-CreER^{T2}; *Apc*$^{fl/wt}$; *Pten*$^{fl/fl}$ mice were generally high for nuclear ß-catenin, indicative of the expected aberrant activation of the Wnt signalling pathway (Figure 3-26). Meanwhile, characterisation of the impact that PTEN deficiency has upon PI3-Kinase target activation revealed that, in line with PTEN deficient areas observed in Villin-CreER^{T2}; *Apc*$^{fl/wt}$; *Pten*$^{fl/wt}$ tumours, tumours arising in Villin-CreER^{T2}; *Apc*$^{fl/wt}$; *Pten*$^{fl/fl}$ were PTEN deficient, and exhibited robust mTORC1 and mTORC2 target engagement via RPS6 and 4E-BP1 and AKT (Ser-473) phosphorylation respectively (Figure 3-27).

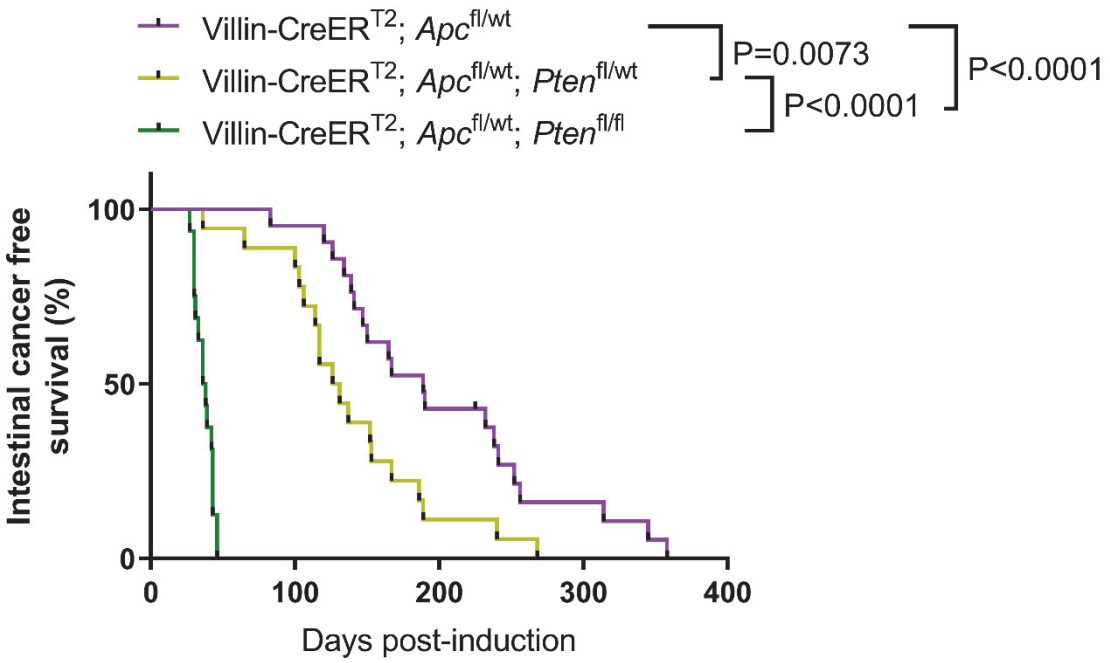

	VillinCre-ER^{T2}; *Apc*$^{fl/wt}$	VillinCre-ER^{T2}; *Apc*$^{fl/wt}$; *Pten*$^{fl/wt}$	VillinCre-ER^{T2}; *Apc*$^{fl/wt}$; *Pten*$^{fl/fl}$
# censored subjects	1	0	0
# deaths/events	19	18	16
Median survival	178	128.5	37

Figure 3-24: Homozygous *Pten* knock-out leads to vastly accelerated clinical endpoint in Villin-CreER^{T2}; *Apc*$^{fl/wt}$ mice. Survival curve of Villin-CreER^{T2}; *Apc*$^{fl/wt}$ (purple), Villin-CreER^{T2}; *Apc*$^{fl/wt}$; *Pten*$^{fl/wt}$ (yellow), and Villin-CreER^{T2}; *Apc*$^{fl/wt}$; *Pten*$^{fl/fl}$ mice (n=16, green, median survival=37 days) post-induction by administration of 80mg/kg tamoxifen. Log-rank test.

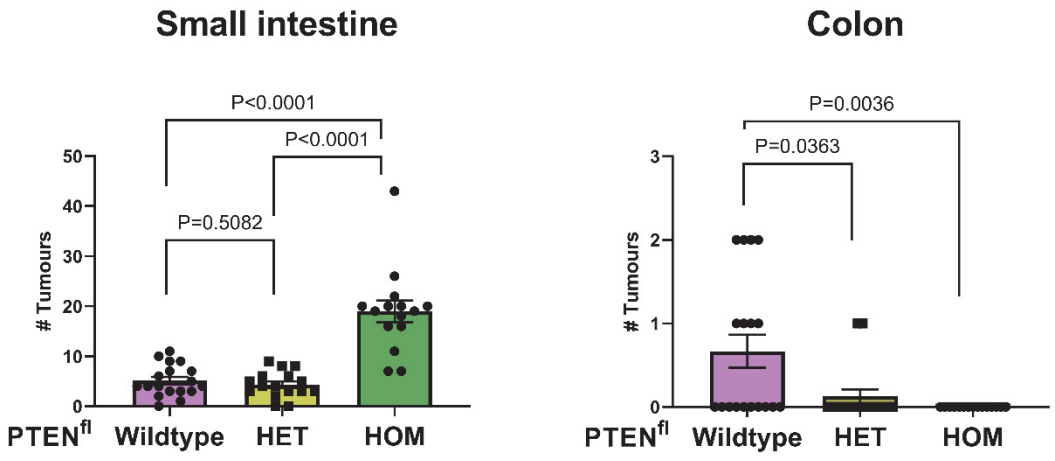

Figure 3-25: Homozygous Pten knock out leads to increased small intestinal tumour formation in Villin-CreER^{T2}; *Apc*$^{fl/wt}$ mice. Villin-CreER^{T2}; *Apc*$^{fl/wt}$; *Pten*$^{fl/fl}$ mice were sampled at endpoint and tumours were scored from the processed H&E stained samples. Mean ± s.e.m. Two-sided Mann-Whitney U test.

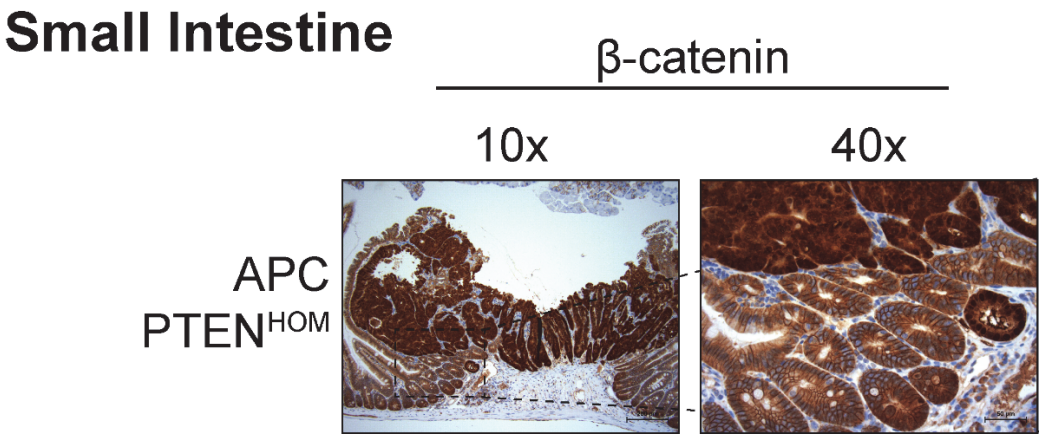

Figure 3-26: Nuclear localisation of β-catenin in SI tumours from Villin-CreER^{T2}; *Apc*$^{fl/wt}$; *Pten*$^{fl/fl}$ mice. IHC-staining of β-catenin in tumours from Villin-CreER^{T2}; *Apc*$^{fl/wt}$; *Pten*$^{fl/fl}$ mice taken at endpoint. Scale bars 200μm (10x), and 50μm (40x).

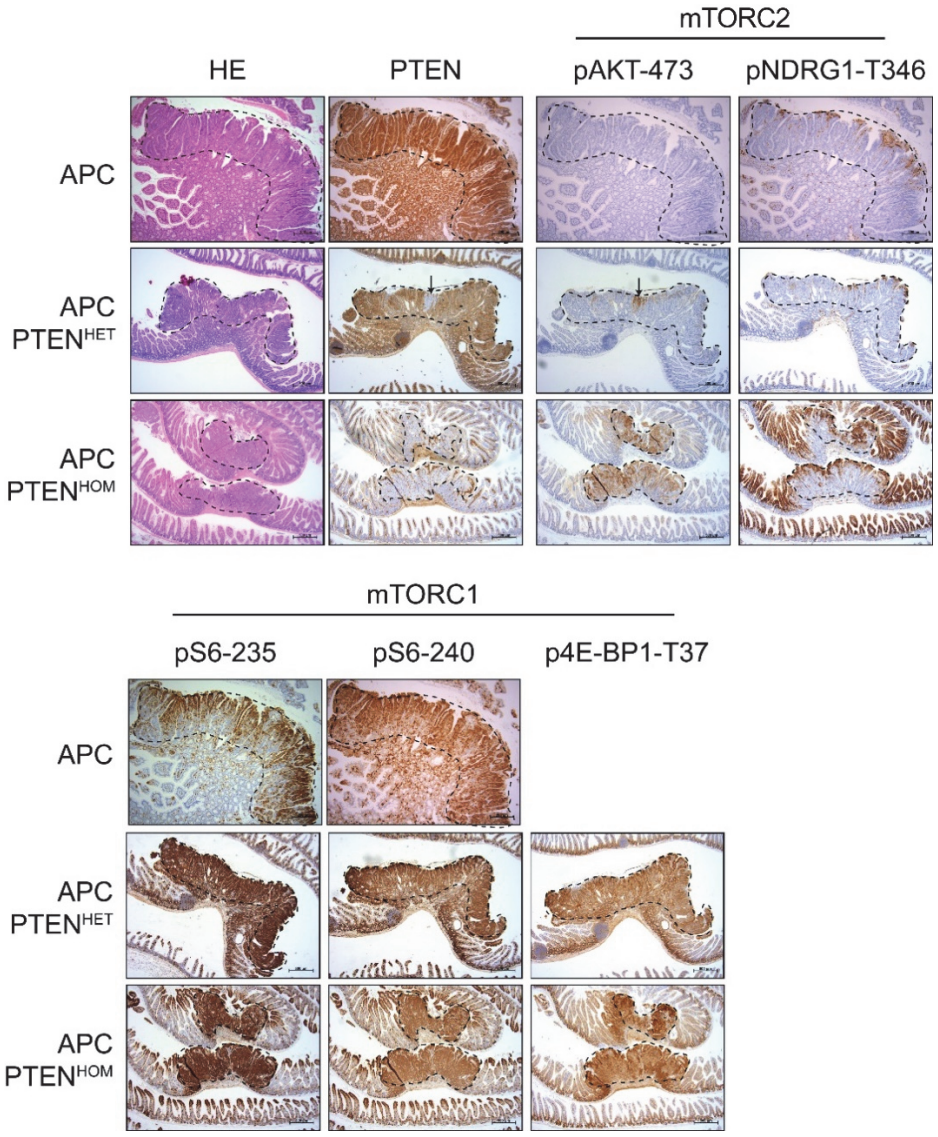

Figure 3-27: *Pten* deletion leads to high mTORC1 and pAKT-S473 signalling in tumours. Representative images of immunohistochemistry of tumours from Villin-CreER^{T2}; *Apc*$^{fl/wt}$ (APC), Villin-CreER^{T2}; *Apc*$^{fl/wt}$; *Pten*$^{fl/wt}$ (APC PTEN^{HET}), and Villin-CreER^{T2}; *Apc*$^{fl/wt}$; *Pten*$^{fl/fl}$ (APC PTEN^{HOM}) stained with H&E, or against pAKT-473, pNDRG1-T346, pS6-235, pS6-240, or p4E-BP1. Scale bars 200μm and 500μm.

3.2.3 Discussion

In summary, I have shown that genetic depletion of *Pten* had an allele-dose dependent effect on the initiation and progression of *Apc*-loss driven intestinal cancer. Heterozygous *Pten* KO led to initiation of earlier, but more advanced small intestinal cancer in *Apc*-loss predisposed mice. This mirrored heterozygous *Pik3ca*^{H1047R} mutation. Homozygous depletion of *Pten* led to rapid small intestinal tumour initiation, which was presumably too fast to allow for development of invasive adenocarcinomas.

Literature suggests that PTEN levels are frequently downregulated in human pre-cancerous lesions and adenocarcinomas (Waniczek *et al.*, 2013). My data shows that reduction in *Pten* gene dosage can increase the progression to adenocarcinoma. It may be important to determine the exact level of PTEN protein depletion in the intestinal epithelium of *Pten*$^{fl/wt}$ mice using a different method. The phenotype might also be due to inability to respond to certain stimuli, rather than a change in PTEN levels in homeostasis. Furthermore, pAKT-S473 was not upregulated in *Pten*$^{fl/wt}$ mice, unless the second copy of *Pten* was lost and the protein was obviously depleted. The effect of heterozygous *Pten* KO may therefore be more subtle, and small reductions in protein might lead to a small increase in signalling with biological relevance. A recent study showed monoallelic mutations in PTEN, leading to reduction in protein function are common and may therefore play a role in the initiation and progression of sporadic CRC (Serebriiskii *et al.*, 2022).

As shown in Figure 3-22, Tumour cells in the *Pten*$^{fl/wt}$ model frequently lose the wildtype copy of *Pten*, which results in increased pAKT-S473 staining and may further alter cellular physiology. Interestingly, only a fraction of tumours displays this phenotype and it is therefore not a prerequisite for tumour initiation in this model. 23% of tumours were PTEN negative, either because of *Pten* loss at a very early stage, or because they initiated in *Pten* negative crypts. Given the tumour initiation phenotype in Villin-CreER^{T2}; *Apc*$^{fl/wt}$; *Pten*$^{fl/fl}$ mice, it is likely that *Pten* negative crypts are prone to *Apc*-loss mediated tumour initiation. Mixed population tumours are interesting as well, as it indicates that loss of heterozygosity is a common event in these tumours. Especially in the case of *Pten*

one would expect that tumour cells gain a survival benefit. Nuclear localisation of ß-catenin indicates that these tumours follow the classical path of CRC initiation.

3.3 PI3-Kinase hyperactivation in *Apc*$^{fl/fl}$ mice

Over many years, a central approach taken in our laboratory to understand the molecular and pathological impact of APC-loss in the intestinal epithelium, and to characterise genetic alterations which promote or suppress transformation driven by APC deficiency, has been to assess their acute impact following homozygous deletion of *Apc*. To study the impact of PI3-Kinase pathway activation in this setting, I generated Villin-CreER^{T2}; *Apc*$^{fl/fl}$; *Pten*$^{fl/fl}$ and Villin-CreER^{T2}; *Apc*$^{fl/fl}$; *Pik3ca*$^{H1047R/wt}$ mice. Due to the well-characterised impact of acute *Apc* loss upon normal intestinal epithelial homeostasis (Sansom *et al.*, 2004; Najumudeen *et al.*, 2021), these mice, alongside Villin-CreER^{T2}; *Apc*$^{fl/fl}$ controls were sampled at day 4 post-induction. A key feature of this model is increased proliferation within the intestinal crypt. To establish whether PI3-Kinase hyperactivation impacts this proliferative phenotype, I assessed proliferation through scoring of BrdU positive cells per half-crypt in the small intestines of these mice (Figure 3-28). BrdU is a synthetic nucleotide, which can incorporate into the DNA of rapidly dividing cells during S-phase, is bioavailable *in vivo*, and can therefore be used to trace proliferating cells. While there appeared to be little impact upon proliferation driven by *Apc* loss upon further genetic deletion of *Pten*, *Pik3ca*^{H1047R} mutation resulted in increased BrdU incorporation, and therefore was associated with increased proliferation.

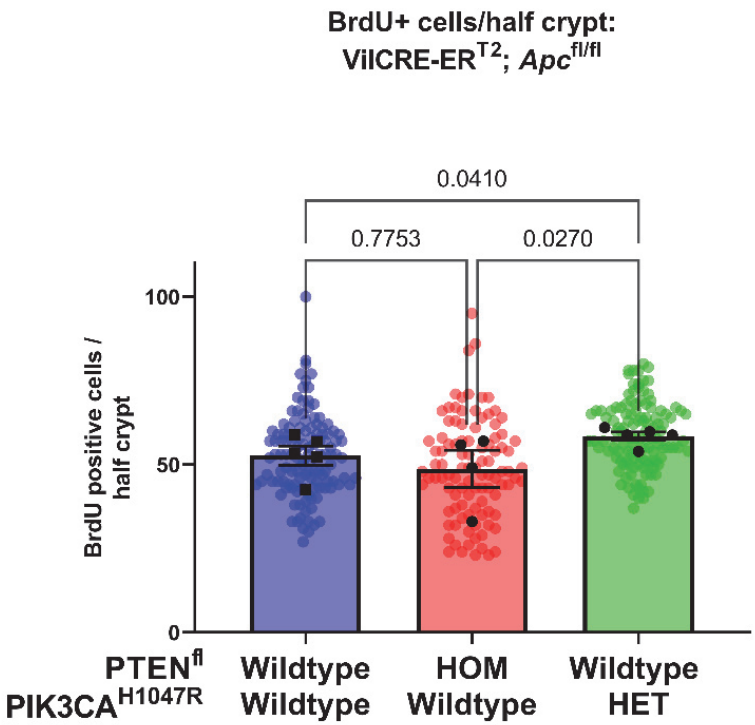

Figure 3-28: Impact of PI3-Kinase-hyperactivation on proliferation immediately post *Apc*-loss. Villin-CreER^{T2}; *Apc*$^{fl/fl}$, Villin-CreER^{T2}; *Apc*$^{fl/fl}$; *Pten*$^{fl/fl}$, and *Apc*$^{fl/fl}$; *Pik3ca*$^{H1047R/wt}$ were administered 80mg/kg tamoxifen on day 0 and 1. BrdU was administered IP on day 4 post-first induction, 2h before sampling. BrdU positive cells per half crypt (n=25) were quantified off histological samples. Pale coloured dots represent single half-crypts, black dots are means of biological replicates. Kruskal-Wallis test, uncorrected Dunn's multiple comparison test.

In concert with the increased proliferation and altered differentiation characteristic of *Apc* deletion in the intestine, this approach drives a number of characteristic Wnt- and proliferation-associated transcriptional programmes. To determine whether these (or other pro-tumorigenic) programmes were affected by PI3-Kinase pathway activation, I conducted transcriptional profiling by RNA-sequencing on RNA extracted from the proximal small intestine of cohorts of mice from each group. Subsequent analysis of differential gene expression analysis from this experiment revealed surprisingly few differentially regulated genes between tissue extracted from Villin-CreER^{T2}; *Apc*$^{fl/fl}$; *Pten*$^{fl/fl}$ (34 up-, 29 downregulated) and *Apc*$^{fl/fl}$; *Pik3ca*$^{H1047R/wt}$ (42 up, 30 downregulated), when compared to Villin-CreER^{T2}; *Apc*$^{fl/fl}$ controls (Figure 3-29).

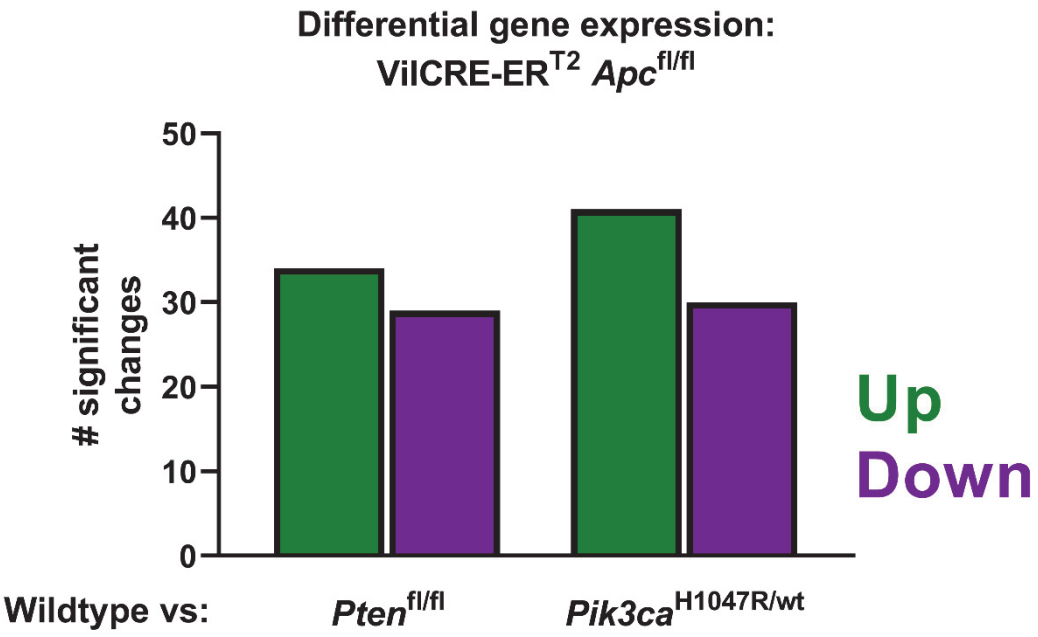

Figure 3-29: Differentially expressed genes in Villin-CreER^{T2}; *Apc*$^{fl/fl}$ vs PI3-K-hyperactive mice. Bar graph showing number of differentially regulated genes (adjusted p-value <0.05) following RNA-sequencing of small intestinal samples from Villin-CreER^{T2}; *Apc*$^{fl/fl}$, Villin-CreER^{T2}; *Apc*$^{fl/fl}$; *Pten*$^{fl/fl}$, and Villin-CreER^{T2}; *Apc*$^{fl/fl}$; *Pik3ca*$^{H1047R/wt}$. n=4 mice used per experimental condition. Robin Shaw and Kathryn Gilroy contributed to the generation of these data.To visualize the output from this experiment, I generated volcano plots, highlighted significantly altered genes (p≤0.05) in red, and added gene names for some of the notable changes (Figure 3-30). There wasn't an obvious pattern for up- or downregulated genes that led to immediate investigation of a specific signalling pathway or transcription factor activation.

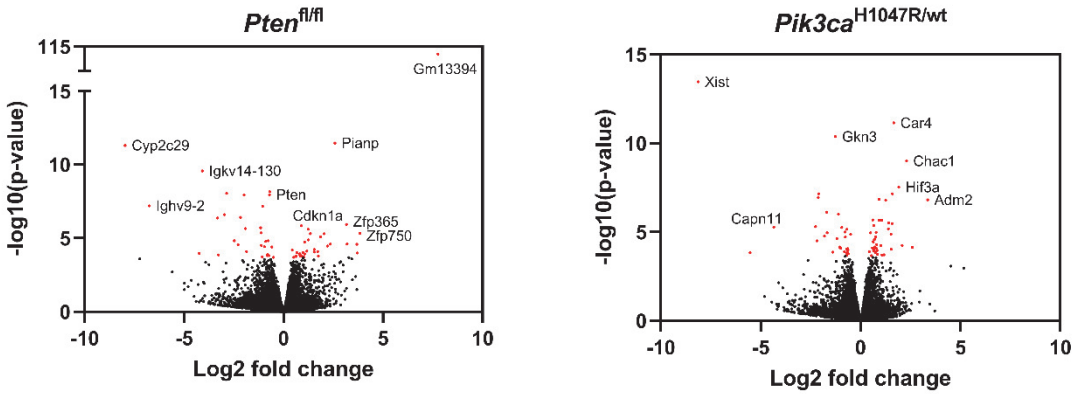

Figure 3-30: Summary of RNA sequencing experiment in PI3-Kinase hyperactive short term mice. SI samples of mice were subjected to RNA sequencing. Individual genes are highlighted next to their position.

Differentially expressed genes may be part of larger functional gene expression networks. The Reactome database is an open-source, open access, manually curated and peer-reviewed pathway database (*https://reactome.org*, accessed 26/05/2022). Associations with gene expression networks or biological processes can be made by analysing the amount of differentially regulated genes in a given pathway. Upregulated genes in *Pik3ca* mutant tissue were enriched for pathways centred on biological oxidations (Figure 3-31). Of note, *Mgst1* and 2 encode for Microsomal Glutathione S-Transferases, which are involved in the defence against reactive oxygen species at membranes (Shi *et al.*, 2012). There were no significantly enriched pathways in the *Pten* deficient condition.

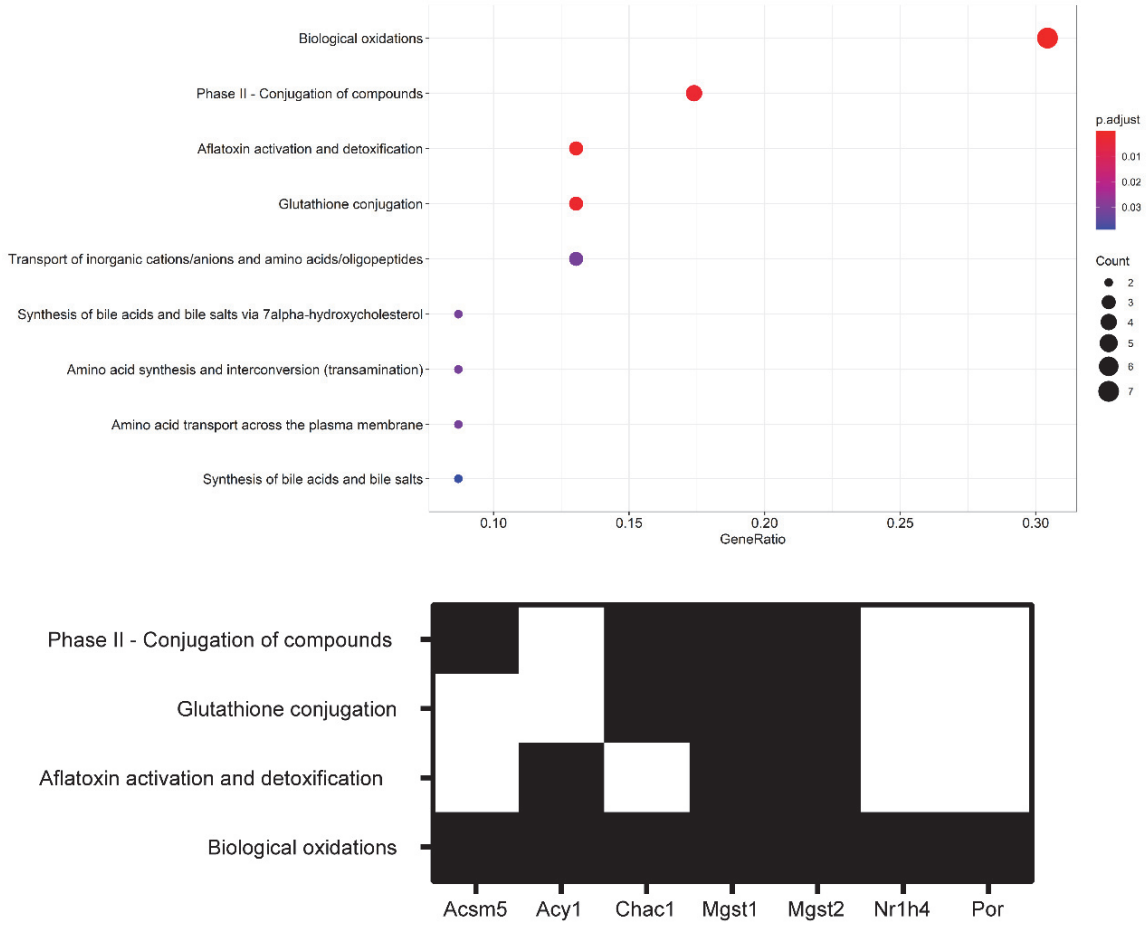

Figure 3-31: Reactome pathways upregulated in *Apc*$^{fl/fl}$; *Pik3ca*$^{H1047R/wt}$ vs Villin-CreER^{T2}; *Apc*$^{fl/fl}$ and genes driving the top four pathways. Significantly upregulated genes were subjected to reactome pathway enrichment analysis. Top: Rows indicate pathways, dot size indicates amount of genes altered, color gradient indicates adjusted p-value (red=more significant, blue=less), and GeneRatio (x-axis) indicates the proportion of genes that are changed in respect to the total number of genes in that pathway. Bottom: Overlapping genes of the top four pathways are indicated in black. Robin Shaw and Kathryn Gilroy contributed to the generation of these data.

Significantly differentially regulated genes give insight into the most drastic changes in a given dataset. Small individual changes in gene expression networks may have biological relevance though, and I therefore used a separate method, gene set enrichment analysis (GSEA), to determine differences between the conditions. Gene set enrichment analysis is a method that determines whether a defined set of genes shows statistically significant difference between two conditions. I conducted GSEA for the "Hallmark" set of gene sets, to get a broad overview of transcriptional changes induced by hyperactive PI3-Kinase signalling. This was done using the full output of the experiment, rather than the list of differentially expressed genes. Using a stringent false discovery parameter (FDR q<0.05), I established enrichments for *Pik3ca* mutants and *Pten* Knock-out (Figure 3-32). Prominent positive enrichment in both PI3-Kinase hyperactive conditions were "mTORC1 signalling" and "cholesterol homeostasis", which indicate increased mTORC1 transcriptional activity. Common negatively enriched pathways were "Downregulated UV response" and "Epithelial to mesenchymal transition".

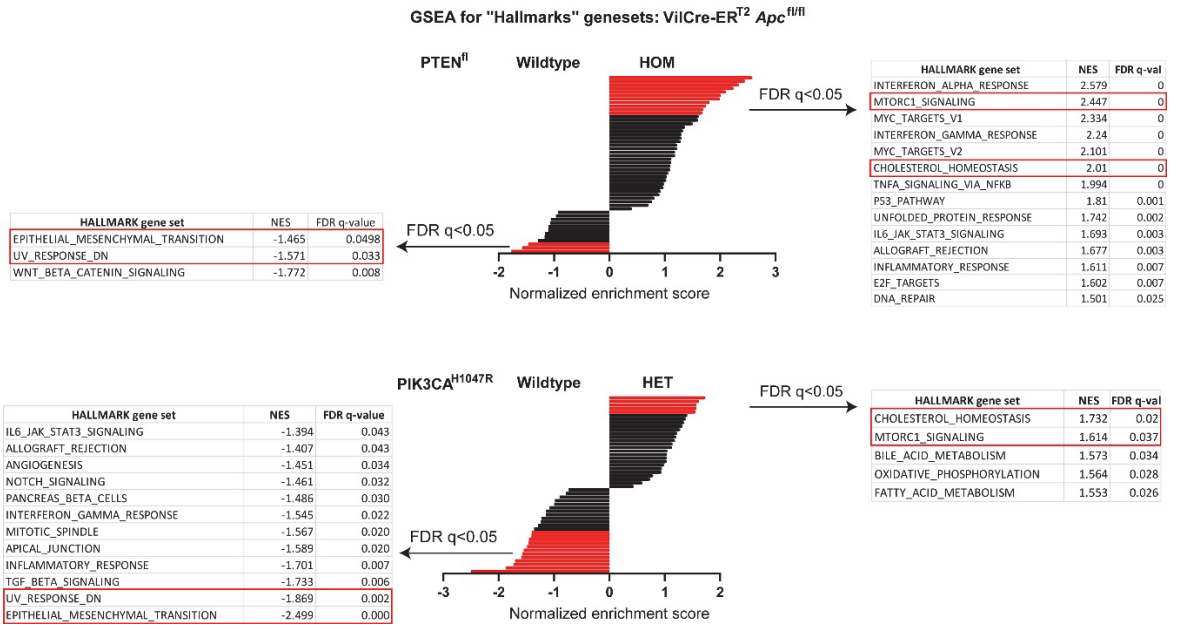

HALLMARK gene set	NES	FDR q-value
EPITHELIAL_MESENCHYMAL_TRANSITION	-1.465	0.0498
UV_RESPONSE_DN	-1.571	0.033
WNT_BETA_CATENIN_SIGNALING	-1.772	0.008

HALLMARK gene set	NES	FDR q-val
INTERFERON_ALPHA_RESPONSE	2.579	0
MTORC1_SIGNALING	2.447	0
MYC_TARGETS_V1	2.334	0
INTERFERON_GAMMA_RESPONSE	2.24	0
MYC_TARGETS_V2	2.101	0
CHOLESTEROL_HOMEOSTASIS	2.01	0
TNFA_SIGNALING_VIA_NFKB	1.994	0
P53_PATHWAY	1.81	0.001
UNFOLDED_PROTEIN_RESPONSE	1.742	0.002
IL6_JAK_STAT3_SIGNALING	1.693	0.003
ALLOGRAFT_REJECTION	1.677	0.003
INFLAMMATORY_RESPONSE	1.611	0.007
E2F_TARGETS	1.602	0.007
DNA_REPAIR	1.501	0.025

HALLMARK gene set	NES	FDR q-value
IL6_JAK_STAT3_SIGNALING	-1.394	0.043
ALLOGRAFT_REJECTION	-1.407	0.043
ANGIOGENESIS	-1.451	0.034
NOTCH_SIGNALING	-1.461	0.032
PANCREAS_BETA_CELLS	-1.486	0.030
INTERFERON_GAMMA_RESPONSE	-1.545	0.022
MITOTIC_SPINDLE	-1.567	0.020
APICAL_JUNCTION	-1.589	0.020
INFLAMMATORY_RESPONSE	-1.701	0.007
TGF_BETA_SIGNALING	-1.733	0.006
UV_RESPONSE_DN	-1.869	0.002
EPITHELIAL_MESENCHYMAL_TRANSITION	-2.499	0.000

HALLMARK gene set	NES	FDR q-val
CHOLESTEROL_HOMEOSTASIS	1.732	0.02
MTORC1_SIGNALING	1.614	0.037
BILE_ACID_METABOLISM	1.573	0.034
OXIDATIVE_PHOSPHORYLATION	1.564	0.028
FATTY_ACID_METABOLISM	1.553	0.026

Figure 3-32: Gene-set enrichment analysis for the Hallmark gene sets. GSEA was conducted on all Hallmark gene sets after RNA sequencing. Gene sets were ranked based on their normalized enrichment score and significantly altered gene sets are depicted as a red bar and listed in the table next to the bar graphs. FRD = False discovery rate. NES = normalized enrichment score. Overlapping gene sets are highlighted in red.

3.3.1 Discussion

In this section, I showed that while *Pten*-KO did not have an effect on proliferation, PI3-Kinase mutation led to an increase in proliferation driven by *Apc* loss. Few genes were significantly differentially regulated between the two mutant conditions and wildtypes. Global gene set enrichment on the HALLMARKS gene sets revealed enrichment for overlapping and unique gene sets.

Given the rapid *Apc*-loss dependent small intestinal tumour initiation phenotype in *Pten* deficient mice, lack of increased proliferation was surprising. The mechanism for the increased tumour initiation may therefore either be independent of increased proliferation or found in the intestinal epithelium before malignant transformation. *Pten* loss is also associated with induction of senescence, potentially leading to a senescence-associated secretory phenotype (SASP) (Jung *et al.*, 2019).

The gene sets “mTORC1 signalling” and “Cholesterol homeostasis” are closely tied to PI3-Kinase and mTORC1 signalling and are enriched in both PI3-Kinase hyperactive conditions. In the *Pten* deficient setting, multiple additional gene sets are enriched, including “p53 pathway”, and “Unfolded protein response”. Taken together, this indicates that cells in *Pten* deficient intestinal tissue may be subject to additional stress. p53 pathway activation indicates genotoxic stress; unfolded protein response indicates proteostatic stress. The enrichment for interferon alpha/gamma response may be more difficult to interpret, although previous publications suggest that PTEN plays a role in escaping immune surveillance. This mechanism in is not fully elucidated yet (Champion, Fisher and Seymour, 2016; Cetintas, Cetintas and Batada, 2020). As mentioned in the introduction, PTEN not only plays a role in de-phosphorylating PIP3 at membranes, but is also a protein phosphatase with a broader spectrum of targets and localisation. Especially cell cycle progression and DNA damage repair seems to be a process it is associated with, where it is able to control cell cycle control and cell fate determination upon cell cycle exit (Brandmaier, Hou and Shen, 2017). Loss of *Pten* is also associated with microsatellite instability (Molinari and Frattini, 2014). Furthermore, occurrence of *Pten* loss is mutually exclusive with p53 mutations in CRC (Danielsen *et al.*, 2008). This indicates that loss of *Pten* might be able promote cell survival in situations of excessive cellular stress, which would be

found immediately upon oncogenic transformation or microsatellite instability. The association with microsatellite instability could therefore be a form of survivorship bias, in which *PTEN* deficient cells are more likely to survive. Further experiments in *Pten*$^{fl/fl}$ mice or organoids would be necessary to determine the exact etiology of *Pten*-loss mediated tumour initiation.

The main overlapping negatively enriched gene set I want to discuss is "epithelial mesenchymal transition". Since tumours in Villin-CreER^{T2}; *Apc*$^{fl/wt}$; *Pik3ca*$^{H1047R/wt}$ tumours were more likely to be invasive adenocarcinomas, this was particularly interesting, as this result would indicate that PI3-Kinase hyperactivation may impact cellular (de-)differentiation. Interestingly, *Pik3ca* mutants were also negatively enriched for TGF beta signalling, which can be a critical determinant of the fate of cancers (Inman, 2011). As mentioned previously, assessment of TGF-beta signalling targets in established tumours would be needed to understand the role of TGF-beta in *Pik3ca* mutant disease better.

Interpreting these hallmark gene sets always needs to done with caution, as these gene set are very much dependent on the cell type one is analysing and may be confounded if multiple cell types are present (Fisher *et al.*, 2022). The most abundant cell type in these experiments are intestinal epithelial cells, but cells of the lamina propria and muscle cells are present, and will be included when preparing samples from intestinal tissue. Single cell RNA sequencing would have to be performed to determine a cell type specific map of the impact of PI3-Kinase hyperactivation.

3.4 Combined *Pten*-KO and *Pik3ca*^{H1047R} mutation in *Apc*-loss dependent intestinal cancer

So far, I have presented the impact of the individual PI3-Kinase hyperactivating alleles in isolation. Human CRC can contain a variety and combinations of mutations, copy number alterations, amplifications, etc. that may have the effect of driving oncogenic pathways such as PI3-Kinase signalling even more robustly. I crossed the *Apc*^{fl}, *Pten*^{fl} and the *Pik3ca*^{H1047R} alleles together and generated ageing cohorts to assess the impact of compound mutations driving PI3-Kinase signalling upon *Apc*-loss dependent cancer initiation and progression.

3.4.1 Heterozygous *Pik3ca*^{H1047R} mutation in Villin-CreER^{T2}; *Apc*$^{fl/wt}$; *Pten*$^{fl/wt}$ accelerates clinical endpoint and progression to invasive adenocarcinoma

To understand co-operation between loss of *Pten* and *Pik3ca*^{H1047R} mutation, I generated Villin-CreER^{T2}; *Apc*$^{fl/wt}$; *Pten*$^{fl/wt}$; *Pik3ca*$^{H1047R/wt}$ mice. I induced genetic recombination as previously described, and went on to age these mice to clinical endpoint, which they reached after a median of 107 days (range: 71 to 140 days). This was significantly earlier than their PI3-Kinase-wildtype counterparts (Figure 3-33). Despite the shortened overall survival observed in these cohorts, intestinal tumour number observed in the PI3-Kinase mutant mice were not significantly higher than in wildtype counterparts (Figure 3-34). 13 of the 17 analysed Villin-CreER^{T2}; *Apc*$^{fl/wt}$; *Pten*$^{fl/wt}$; *Pik3ca*$^{H1047R/wt}$ had invasive adenocarcinomas, most of them large and rich in stromal infiltrate (Figure 3-35). This was not significantly higher than in Villin-CreER^{T2}; *Apc*$^{fl/wt}$; *Pten*$^{fl/wt}$. Finally, I sought to assess the number of PTEN deficient tumours in this setting, and whether *Pik3ca* mutation might result in an increased rate of LOH of *Pten*^{fl}. The number of tumours that had at least partially lost PTEN expression on the protein level was higher in Villin-CreER^{T2}; *Apc*$^{fl/wt}$; *Pten*$^{fl/wt}$; *Pik3ca*$^{H1047R/wt}$ mice than in *Pik3ca* wildtypes, although this was not statistically significant (Figure 3-36).

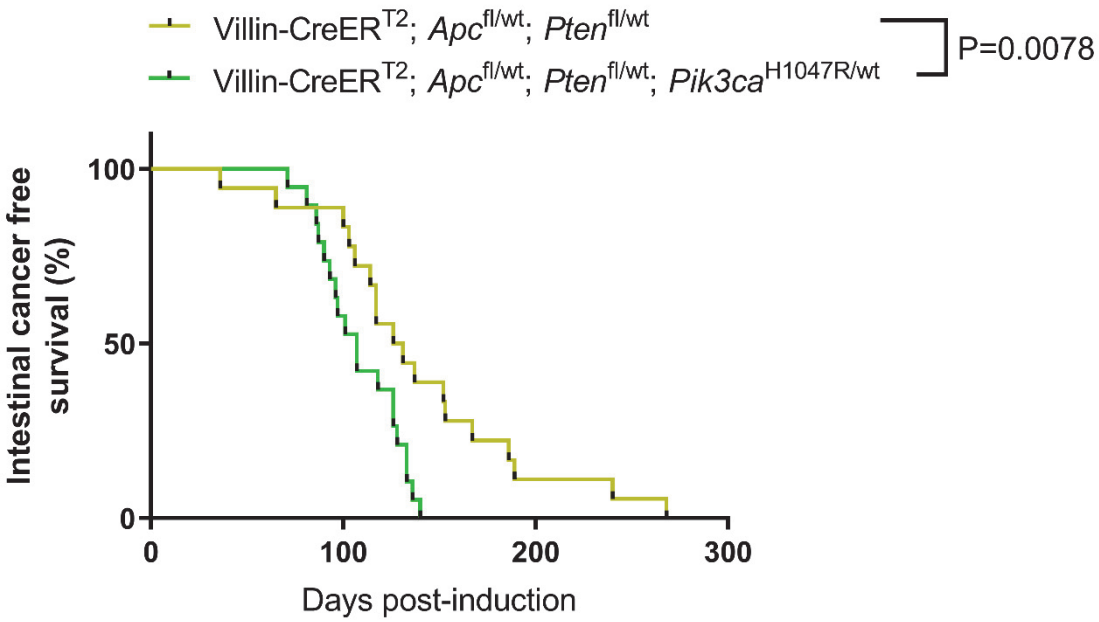

	Villin-CreER^{T2}; *Apc*$^{fl/wt}$; *Pten*$^{fl/wt}$	Villin-CreER^{T2}; *Apc*$^{fl/wt}$; *Pten*$^{fl/wt}$; *Pik3ca*$^{H1047R/wt}$
# censored subjects	0	0
# deaths/events	18	19
Median survival	128.5	107

Figure 3-33: Heterozygous Pik3ca^{H1047R} mutation accellerates the Villin-CreER^{T2}; *Apc*$^{fl/wt}$; *Pten*$^{fl/wt}$ model. Survival curve of Villin-CreER^{T2}; *Apc*$^{fl/wt}$; *Pten*$^{fl/wt}$ mice (yellow), and Villin-CreER^{T2}; *Apc*$^{fl/wt}$; *Pten*$^{fl/wt}$; *Pik3ca*$^{H1047R/wt}$ (green, n=19, median survival=107 days) mice post-induction by administration of 80mg/kg tamoxifen. Log-rank test.

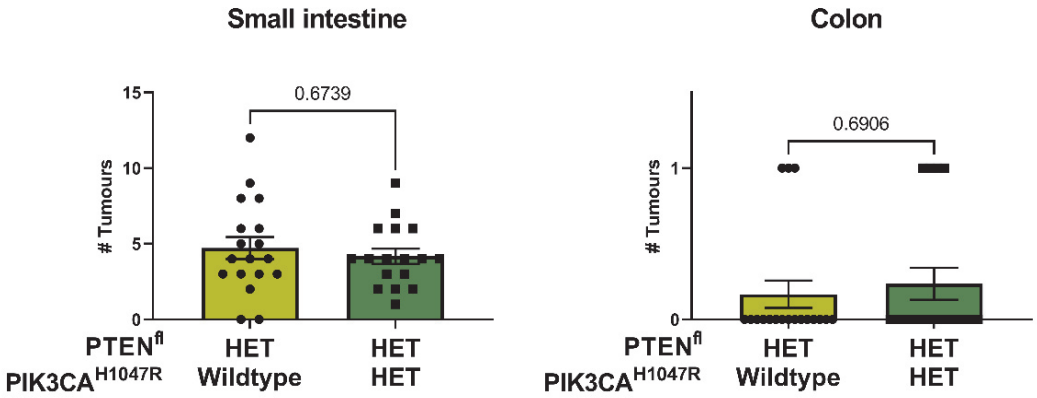

Figure 3-34: Heterozygous *Pik3ca*^{H1047R} mutation does not drive tumour initiation in Villin-CreER^{T2}; *Apc*$^{fl/wt}$; *Pten*$^{fl/wt}$ mice. Villin-CreER^{T2}; *Apc*$^{fl/wt}$; *Pten*$^{fl/wt}$; *Pik3ca*$^{H1047R/wt}$ mice were sampled at endpoint and tumours were scored from the processed H&E stained samples. Mean ± s.e.m. Two-sided Mann-Whitney U test.

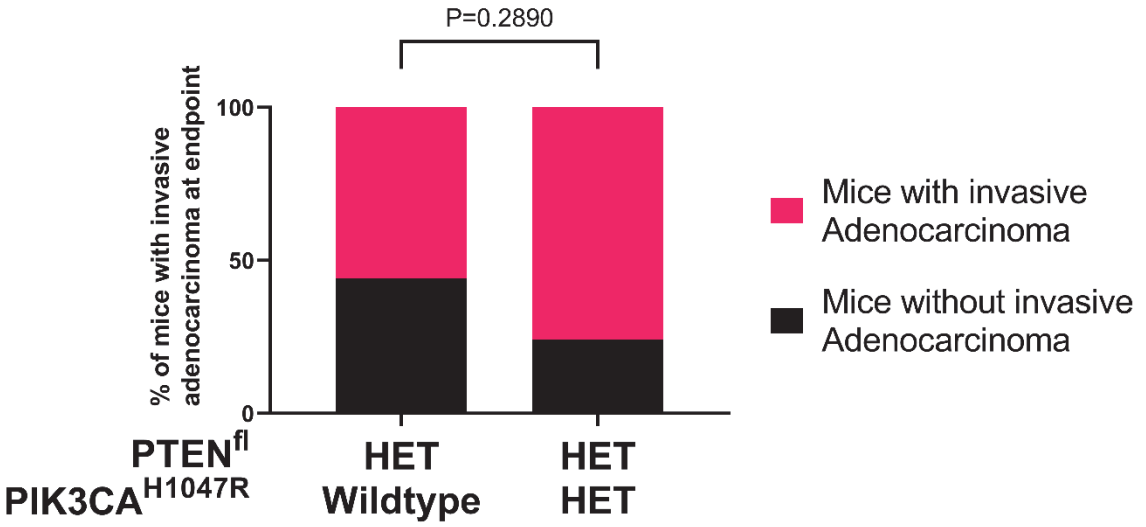

Figure 3-35: Occurrence of invasive adenocarcinoma in Villin-CreER^{T2}; *Apc*$^{fl/wt}$; *Pten*$^{fl/wt}$; *Pik3ca*$^{H1047R/wt}$ mice. Histological assessment of tumours in Villin-CreER^{T2}; *Apc*$^{fl/wt}$; *Pten*$^{fl/wt}$; *Pik3ca*$^{H1047R/wt}$ guts (n=17) at endpoint revealed tumours with adenomatous morphology in 4/17 mice (24%), while 13/17 (76%) developed adenocarcinomas with invasive features. Fisher's exact test.

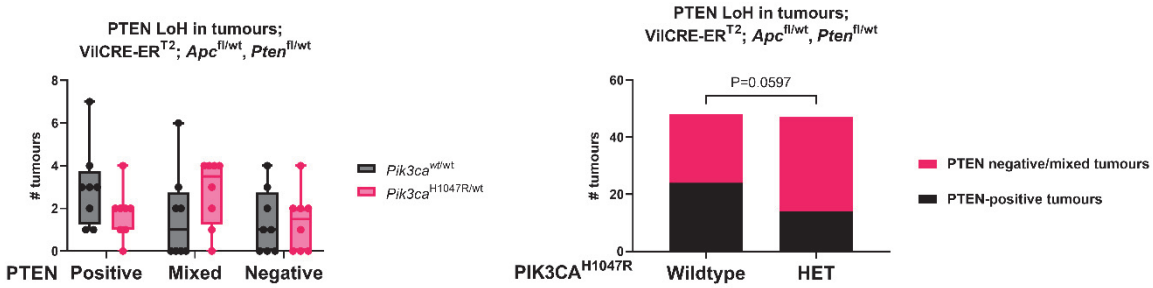

Figure 3-36: Slightly higher frequency of PTEN loss of heterozygosity (LoH) in tumours from PI3-Kinase mutant mice. Villin-CreER^{T2}; *Apc*$^{fl/wt}$; *Pten*$^{fl/wt}$ and Villin-CreER^{T2}; *Apc*$^{fl/wt}$; *Pten*$^{fl/wt}$; *Pik3ca*$^{H1047R/wt}$ mice were sampled at endpoint and histological samples were stained for PTEN. Microscopic analysis revealed frequent loss of PTEN protein in tumours either in a subpopulation or in the complete tumour (left). Mean ± s.e.m. Right: Proportion of tumours being mixed or negative for PTEN was slightly higher in *Pik3ca* mutant mice, although this was not statistically significant. Fisher's exact test.

3.4.2 Homozygous Pik3ca mutation further accelerates the Villin-CreER^{T2}; Apc$^{fl/wt}$; Pten$^{fl/wt}$ model

Given that homozygous mutation of *Pik3ca* drastically accelerated tumorigenesis in the context of heterozygous *Apc* loss (Chapter 3.1.3), I next sought to test whether this acceleration also occurred in Villin-CreER^{T2}; *Apc*$^{fl/wt}$; *Pten*$^{fl/wt}$ animals. To this end, I crossed the mutant *Pik3ca* allele to homozygosity in Villin-CreER^{T2}; *Apc*$^{fl/wt}$; *Pten*$^{fl/wt}$ mice to generate Villin-CreER^{T2}; *Apc*$^{fl/wt}$; *Pten*$^{fl/wt}$; *Pik3ca*$^{H1047R/H1047R}$ mice. These mice reached clinical endpoint at a median of 94

days (range: 37 to 113 days) (Figure 3-37). This was significantly earlier than both *Pik3ca*^{H1047R} heterozygotes and wildtypes. In line with this shortened survival, homozygous *Pik3ca* mutants exhibited more small intestinal tumours at endpoint (Figure 3-38), while 6 out of 15 analysed Villin-CreER^{T2}; *Apc*$^{fl/wt}$; *Pten*$^{fl/wt}$; *Pik3ca*$^{H1047R/H1047R}$ mice developed tumours with features of invasive adenocarcinomas (Figure 3-39).

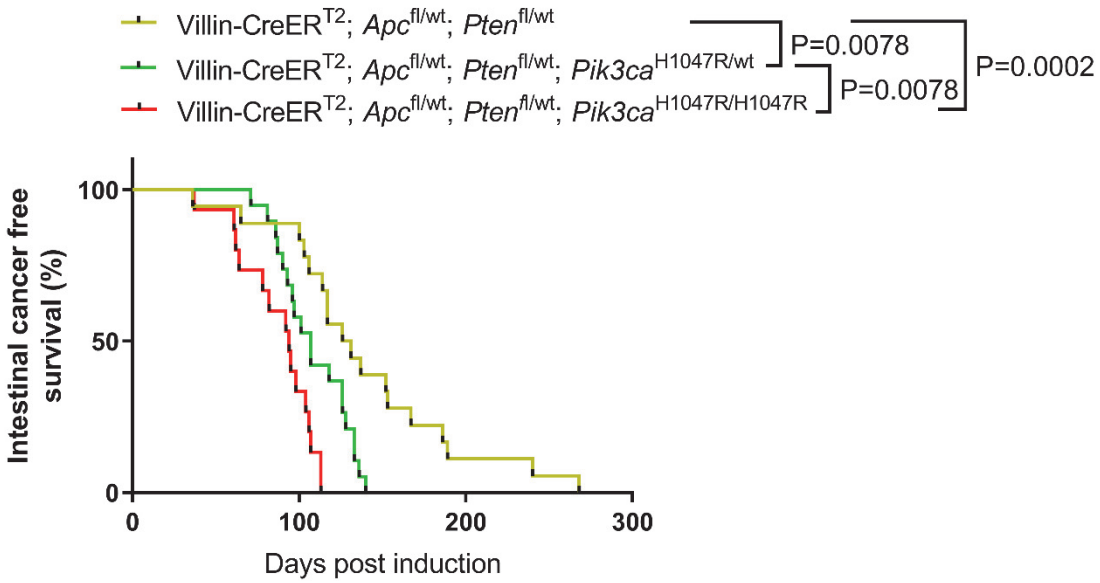

	Villin-CreER^{T2}; Apc$^{fl/wt}$; Pten$^{fl/wt}$	Villin-CreER^{T2}; Apc$^{fl/wt}$; Pten$^{fl/wt}$; Pik3ca$^{H1047R/wt}$	Villin-CreER^{T2}; Apc$^{fl/wt}$; Pten$^{fl/wt}$; Pik3ca$^{H1047R/H1047R}$
# censored su	0	0	0
# deaths/even	18	19	15
Median surviva	128.5	107	94

Figure 3-37: homozygous Pik3ca mutation in Villin-CreER^{T2}; *Apc*$^{fl/wt}$; *Pten*$^{fl/wt}$ mice. Survival curve of Villin-CreER^{T2}; *Apc*$^{fl/wt}$; *PTEN*$^{fl/wt}$ mice (yellow), and Villin-CreER^{T2}; *Apc*$^{fl/wt}$; *Pten*$^{fl/wt}$; *Pik3ca*$^{H1047R/wt}$ (green, n=19, median survival=107 days) post-induction by administration of 80mg/kg tamoxifen. Log-rank test.

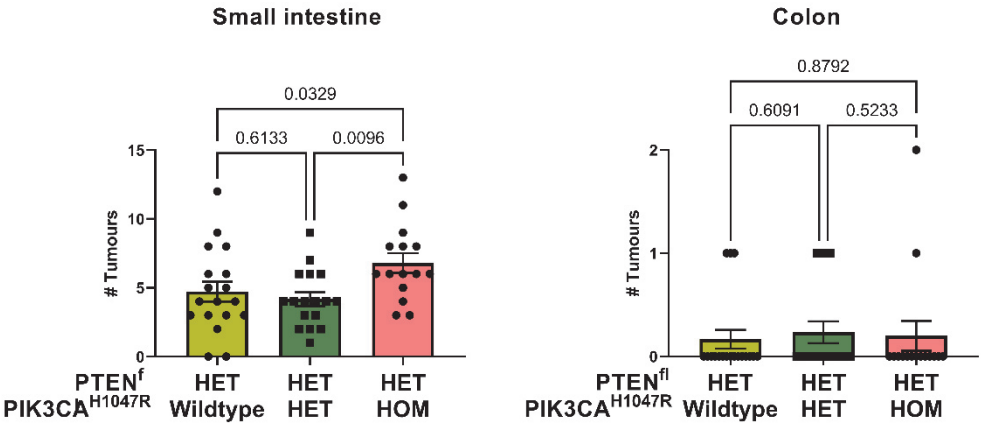

Figure 3-38: Homozygous *Pik3ca*^{H1047R} mutation drives tumour initiation in Villin-CreER^{T2}; *Apc*$^{fl/wt}$; *Pten*$^{fl/wt}$ mice. Mice were sampled at endpoint and tumours were scored from the processed H&E stained samples. Mean ± s.e.m. Kruskal-Wallis test and uncorrected Dunn's multiple comparison test.

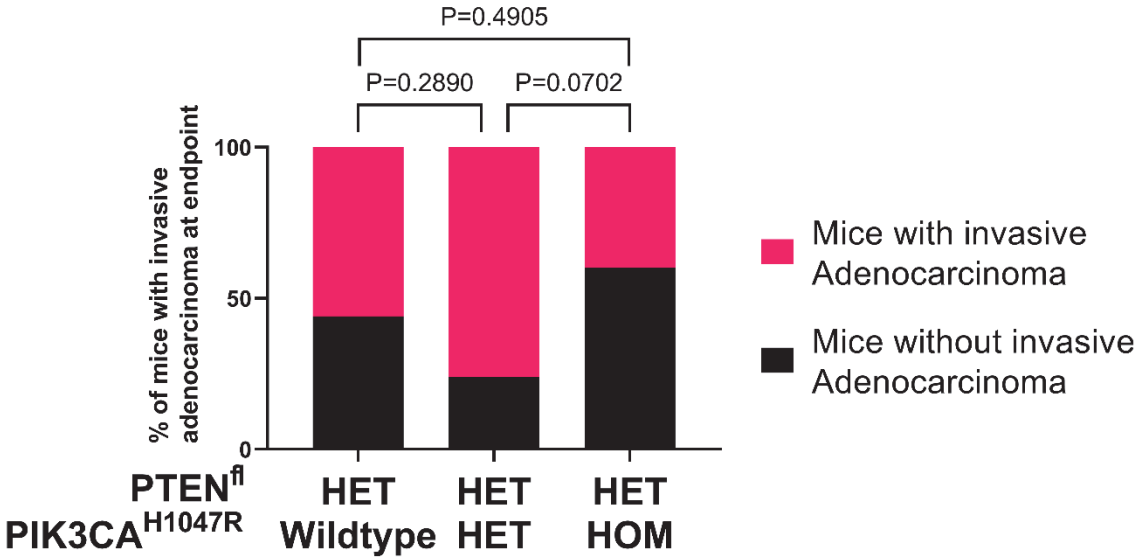

Figure 3-39: Occurrence of invasive adenocarcinoma in Villin-CreER^{T2}; *Apc*$^{fl/wt}$; *Pten*$^{fl/wt}$; *Pik3ca*$^{H1047R/H1047R}$ mice. Histological assessment of tumours in Villin-CreER^{T2}; *Apc*$^{fl/wt}$; *Pten*$^{fl/wt}$; *Pik3ca*$^{H1047R/H1047R}$ guts (n=15) at endpoint revealed tumours with adenomatous morphology in 9/17 mice (60%), while 6/15 (40%) developed adenocarcinomas with invasive features. Fisher's exact tests.

3.4.3 Heterozygous Pik3ca^{H1047} mutation accelerates small intestinal tumour formation in Villin-CreER^{T2}; Apc$^{fl/wt}$; Pten$^{fl/fl}$ mice

Homozygous deletion of *Pten* vastly accelerated *Apc*-loss dependent small intestinal tumour formation. Given that PTEN is commonly thought of as a negative regulator of the PI3-kinase pathway, I sought to determine whether additional activating PI3-Kinase mutations might also have a significant additive effect upon

tumourigenesis in the context of Villin-CreER^{T2}; *Apc*$^{fl/wt}$; *Pten*$^{fl/fl}$ mice. To this end, I generated Villin-CreER^{T2}; *Apc*$^{fl/wt}$; *Pten*$^{fl/fl}$; *Pik3ca*$^{H1047R/wt}$ mice. These mice reached clinical endpoint after a median of 26 days (range: 18 to 28 days), significantly earlier than PI3-Kinase-wildtype counterparts (Figure 3-40). The earlier time to clinical endpoint was associated with a substantially increased number of small intestinal tumours (Figure 3-41).

Moveover, where experiments were carried out in the context of *Pik3ca*^{H1047R} homozygosity, a further robust increase in tumourigenesis was observed. Specifically, Villin-CreER^{T2}; *Apc*$^{fl/wt}$; *Pten*$^{fl/fl}$; *Pik3ca*$^{H1047R/H1047R}$ mice had to be sampled earlier than heterozygous mutants, at a median of 19 days (range: 15 to 28 days) (Figure 3-42), with no further increase in tumour numbers (Figure 3-43). This said, in *Pik3ca*$^{H1047R/H1047R}$ mice, there appeared to be a bimodal distribution of small intestinal tumour number within the experimental cohort (Figure 3-43), which was independent of sex (Figure 3-44).

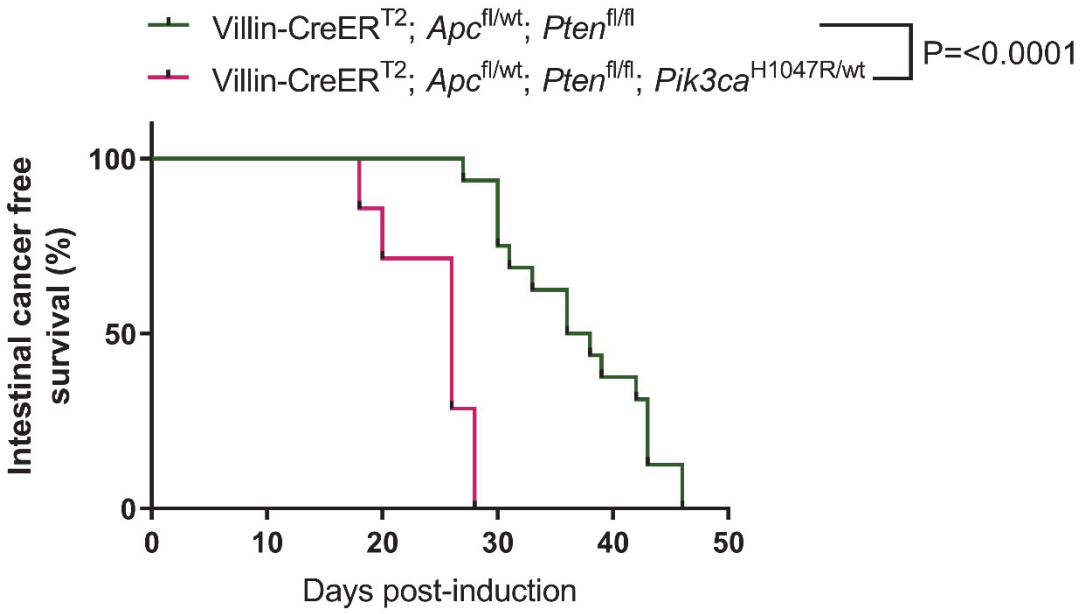

	Villin-CreER^{T2}; Apc$^{fl/wt}$; Pten$^{fl/fl}$	Villin-CreER^{T2}; Apc$^{fl/wt}$; Pten$^{fl/fl}$; Pik3ca$^{H1047R/wt}$
# censored subjects	0	0
# deaths/events	16	7
Median survival	37	26

Figure 3-40: Heterozygous *Pik3ca*^{H1047R} mutation in Villin-CreER^{T2}; *Apc*$^{fl/wt}$; *Pten*$^{fl/fl}$ mice leads to accelerated time to clinical endpoint. Survival curve of Villin-CreER^{T2}; *Apc*$^{fl/wt}$; *Pten*$^{fl/wt}$ mice (green), and Villin-CreER^{T2}; *Apc*$^{fl/wt}$; *Pten*$^{fl/fl}$; *Pik3ca*$^{H1047R/wt}$ (pink, n=7, median survival=26 days) post-induction by administration of 80mg/kg tamoxifen. Log-rank test.

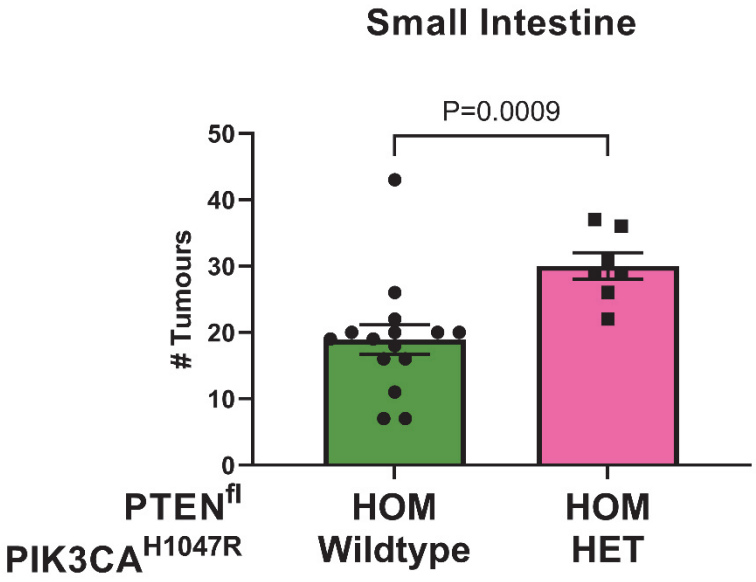

Figure 3-41: Heterozygous *Pik3ca*^{H1047R} mutation drives small intestinal tumour initiation in Villin-CreER^{T2}; *Apc*$^{fl/wt}$; *Pten*$^{fl/fl}$ mice. Villin-CreER^{T2}; *Apc*$^{fl/wt}$; *Pten*$^{fl/fl}$; *Pik3ca*$^{H1047R/wt}$ mice were sampled at endpoint and tumours were scored from the processed H&E stained samples. Mean ± s.e.m. Two-sided Mann-Whitney U test.

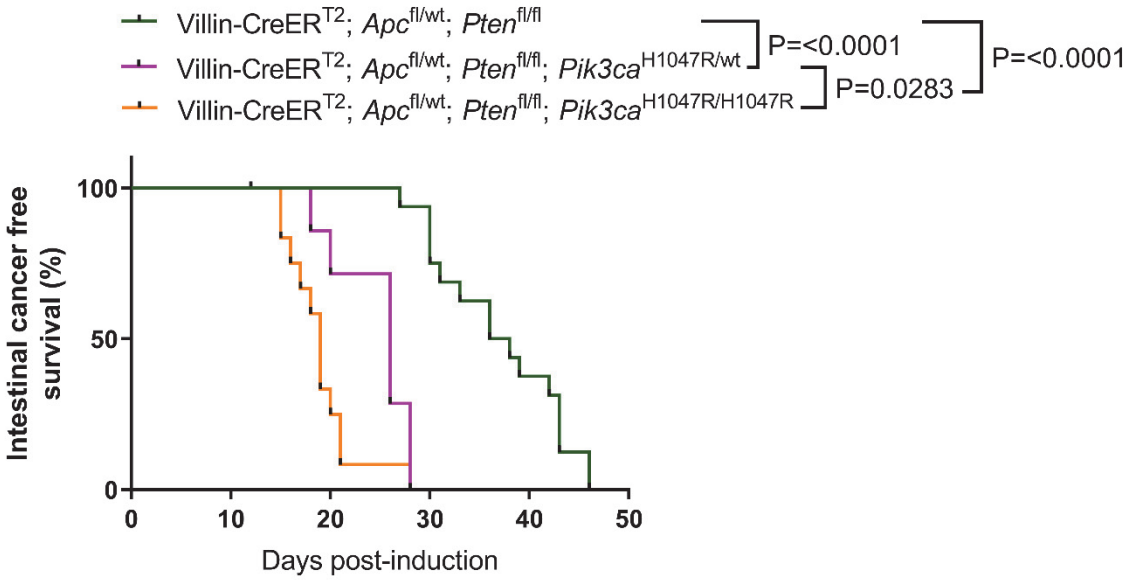

	Villin-CreER^{T2}; *Apc*$^{fl/wt}$; *Pten*$^{fl/fl}$	Villin-CreER^{T2}; *Apc*$^{fl/wt}$; *Pten*$^{fl/fl}$; *Pik3ca*$^{H1047R/wt}$	Villin-CreER^{T2}; *Apc*$^{fl/wt}$; *Pten*$^{fl/fl}$; *Pik3ca*$^{H1047R/H1047R}$
# censored subjects	0	0	1
# deaths/events	16	7	12
Median survival	37	26	19

Figure 3-42: Homozygous PIK3CA mutation accellerates the Villin-CreER^{T2}; *Apc*$^{fl/wt}$; *Pten*$^{fl/fl}$ model even further. Survival curve of Villin-CreER^{T2}; *Apc*$^{fl/wt}$; *PTEN*$^{fl/wt}$ mice (green), Villin-CreER^{T2}; *Apc*$^{fl/wt}$; *Pten*$^{fl/fl}$; *Pik3ca*$^{H1047R/wt}$ (pink), and Villin-CreER^{T2}; *Apc*$^{fl/wt}$; *Pten*$^{fl/fl}$; *Pik3ca*$^{H1047R/H1047R}$ (orange, n=12, median survival=19 days) post-induction by administration of 80mg/kg tamoxifen. Log-rank test.

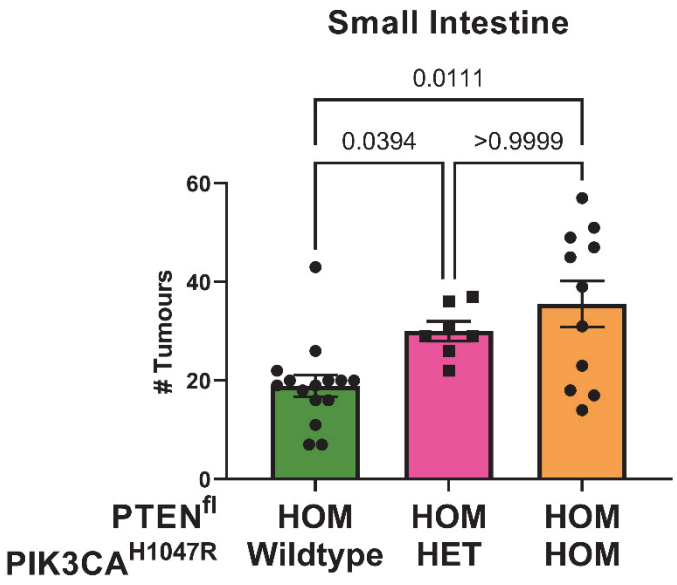

Figure 3-43: Homozygous *PIK3CA*^{H1047R} mutation does not further increase tumour numbers in Villin-CreER^{T2}; *Apc*$^{fl/wt}$; *Pten*$^{fl/fl}$ mice. Villin-CreER^{T2}; *Apc*$^{fl/wt}$; *Pten*$^{fl/fl}$; *Pik3ca*$^{H1047R/wt}$ mice were sampled at endpoint and tumours were scored from the processed H&E stained samples. Mean ± s.e.m. Two-sided Mann-Whitney U test.

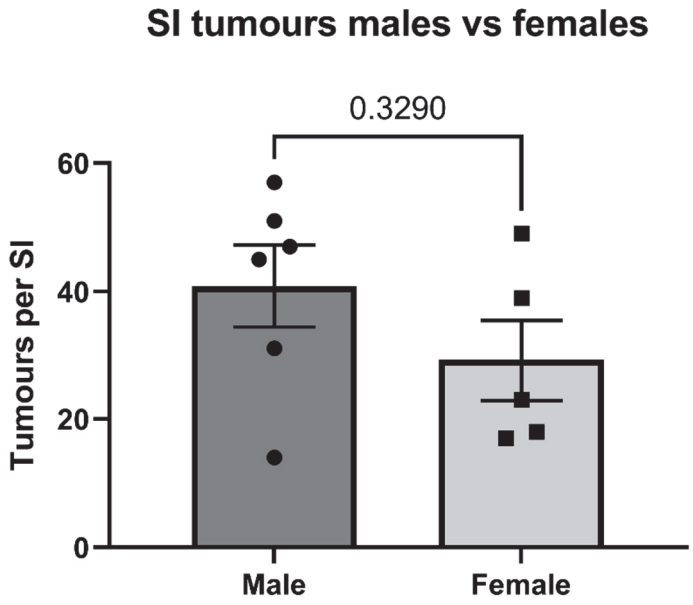

Figure 3-44: Tumour numbers in Villin-CreER^{T2}; *Apc*$^{fl/wt}$; *Pten*$^{fl/fl}$; *Pik3ca*$^{H1047R/H1047R}$ mice at endpoint. Villin-CreERT2; Apcfl/wt; Ptenfl/fl; Pik3caH1047R/H1047R mice were sampled at endpoint and tumours scored from the processed HEs. Two-sided Mann-Whitney U test.

IHC for mTOR targets confirmed drastic PTEN-dependent up-regulation of pAKT-S473, while all tumour tissue was positive for mTORC1 signalling markers. To illustrate this, Figure 3-45 shows a tumour from a Villin-CreER^{T2}; *Apc*$^{fl/wt}$; *Pten*$^{fl/wt}$;

Pik3ca$^{H1047R/wt}$ mouse that is half PTEN positive, and half-negative. The left PTEN positive side has no detectable pAKT-S473, while being positive for pS6 markers and p4E-BP1-T37. This mirrors the situation in Villin-CreER^{T2}; *Apc*$^{fl/wt}$; *Pten*$^{fl/fl}$; *Pik3ca*$^{H1047R/wt}$ mice, although here all tumours are PTEN negative. Expression of pNDRG1-346 was variable. The tumour presented in Figure 3-45 was positive, but I could not make out a clear correlation between pNDRG1-346 and any other markers.

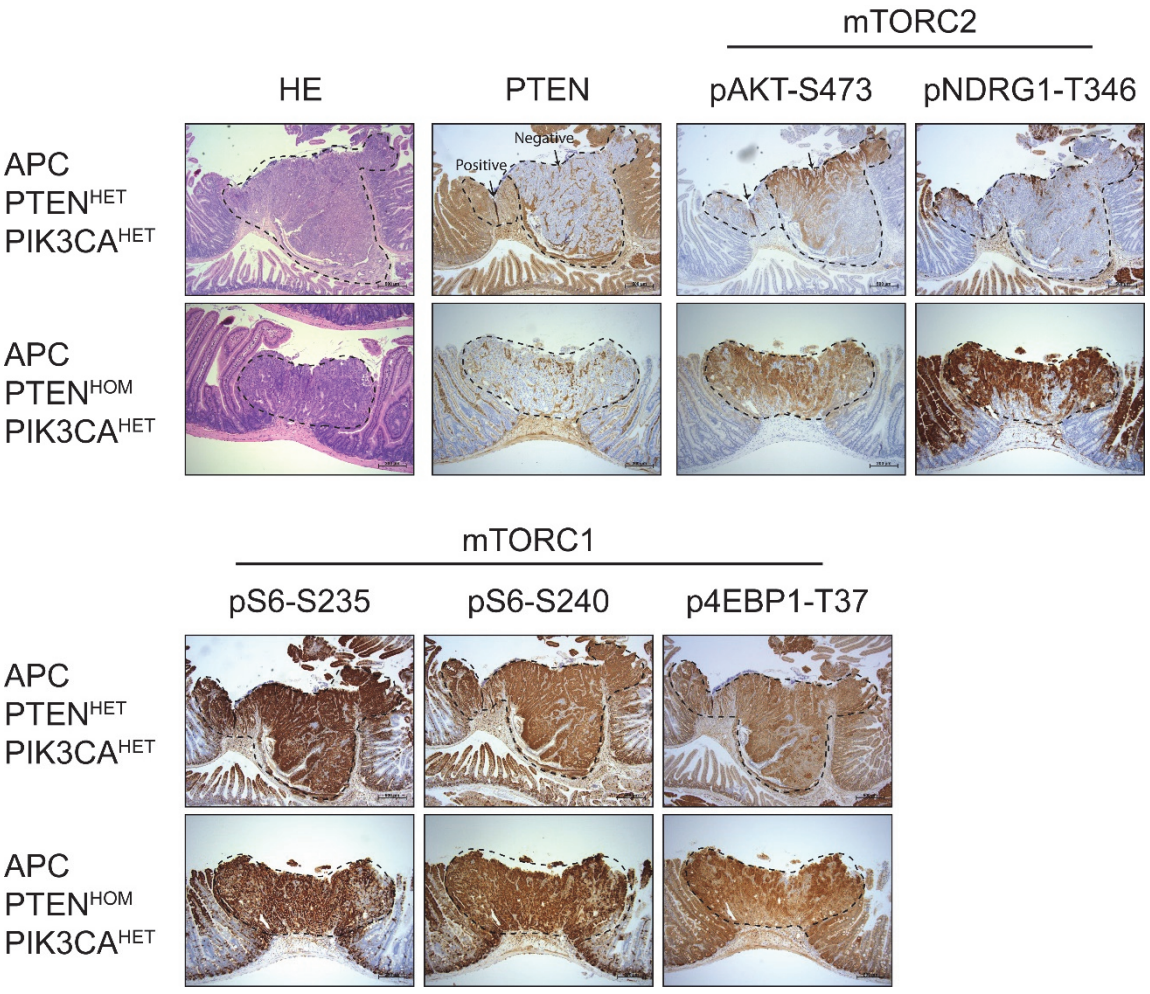

Figure 3-45: *Pik3ca*^{H1047R} mutation does not further modulate mTOR signalling markers in Villin-CreER^{T2}; *Apc*$^{fl/wt}$; *Pten*$^{fl/wt}$ and Villin-CreER^{T2}; *Apc*$^{fl/wt}$; *Pten*$^{fl/fl}$ mice based on IHC. Representative images of immunohistochemistry of tumours from Villin-CreER^{T2}; *Apc*$^{fl/wt}$; *Pten*$^{fl/wt}$; *Pik3ca*$^{H1047R/wt}$ (APC PTEN^{HET} PIK3CA^{HET}) and Villin-CreER^{T2}; *Apc*$^{fl/wt}$; *Pten*$^{fl/fl}$; *Pik3ca*$^{H1047R/wt}$ mice, stained with H&E, or against pAKT-473, pNDRG1-T346, pS6-235, pS6-240, or p4E-BP1-T37. Scale bars 200µm and 500µm. Arrows indicate PTEN positive and negative tumour areas.

3.4.4 Discussion

I previously showed that genetic depletion of *Pten* in a stepwise manner leads to increased SI tumour formation in intestinal cancer models driven by *Apc* deficiency. Further hyperactivation of PI3-Kinase signalling by *Pik3ca* mutation accelerated small intestinal tumour formation and progression to invasive adenocarcinoma in $Pten^{fl/wt}$ mice. Reducing the gene dose at the *Pten* locus therefore drives a tumour permissive phenotype in the intestine, and promotes progression to adenocarcinoma, without a requirement for complete loss of *Pten*. In $Pten^{fl/fl}$ mice, PI3-Kinase mutation led to a further acceleration of the already rapid tumour initiation phenotype, strengthening the notion that PI3-Kinase signal strength can be criticially important in intestinal cancer initiation and subsequent progression.

PI3-Kinase hyperactivating alterations significantly co-occur in human CRC. This is in contrast to MAPK pathway mutations, as e.g. KRas and Braf mutations are mutually exclusive (Table 3-1). This indicates selection for multiple mutations in the human disease is advantageous, although more work will be needed to establish the impact that these multiple mutations have.

Table 3-1: Co-occurrence and Mutual exclusivety between PI3-Kinase and MAPK signalling components. Data from the Metastatic Colorectal Cancer (MSK) cohort, generated using cBioportal.

A	B	Neither	A Not B	B Not A	Both	Log2 Odds Ratio	p-Value	q-Value	Tendency
PIK3CA	**PTEN**	848	199	56	31	1.238	<0.001	**<0.001**	**Co-occurrence**
KRAS	**BRAF**	512	487	115	20	-2.451	<0.001	**<0.001**	**Mutual exclusivity**

Using IHC, I was not able to detect a robust further increase in mTOR signalling in response to additional PI3-Kinase mutation in *Pten* depleted tissue. Pathway activation may be saturated, or there may have been subtle changes to cell signalling undetectable with IHC. $Pik3ca^{H1047R}$ was reported to remain on membranes for longer and have reduced auto-inhibition and could therefore result in an altered dynamics in cells, resulting in prolonged production of PIP3 (Gkeka *et al.*, 2014b). Western blots on lysates from tumours or organoid cultures will be invaluable to determine the impact of *Pik3ca* mutation in *Pten* deficient cells.

3.5 PI3-Kinase hyperactivation in *Apc* wildtype mice

In all ageing experiments described in this study up to this point, tumour initiation was driven by sporadic loss of the remaining wildtype copy of Apc in the context of heterozygous *Apc* deficiency. Given the rapid onset of tumourigenesis in animals in which the PI3-Kinase pathway was hyperactivated (particularly through *Pten* deletion), we next tested whether these mutations were sufficient to drive intestinal tumourigenesis in the absence of heterozygous *Apc* deletion. To this end, we generated Villin-CreER^{T2}; *Pten*$^{fl/fl}$ mice, induced recombination as in previous models, and aged until clinical endpoint. These mice reached clinical endpoint at a median of 595 days (range: 391 to 604 days) (Figure 3-46). These mice were sampled due to progressive weight loss and exhibited few macroscopic small intestinal tumours (Figure 3-47). Having previously seen synergy between Pten KO and Pik3ca mutation in driving Apc-loss dependent intestinal cancer, I generated Villin-CreER^{T2}; *Pten*$^{fl/fl}$ *Pik3ca*$^{H1047R/wt}$ mice. These came down at a median of 485 days (range: 303 to 505 days) (Figure 3-46). This was not significantly shorter than *Pik3ca* wildtypes. At endpoint, Villin-CreER^{T2}; *Pten*$^{fl/fl}$ *Pik3ca*$^{H1047R/wt}$ and control Villin-CreER^{T2}; *Pten*$^{fl/fl}$ control mice had a similar number of SI tumours, but tumour burden was significantly higher in *Pik3ca* mutants than in wildtypes (Figure 3-47). Tumours were concentrated in the proximal half of the SI (Data presented for *Pik3ca*$^{H1047R/wt}$ in Figure 3-48). Despite macroscopically observable tumour burden, upon histological examination, no tumours were observed in the small intestinal samples of Villin-CreER^{T2}; *Pten*$^{fl/fl}$ examined, limiting further analysis. Of the tumours in Villin-CreER^{T2}; *Pten*$^{fl/fl}$; *Pik3ca*$^{H1047R/wt}$ SIs analysed so far, multiple tumours exhibited a polypoid morphology, while one large invasive adenocarcinomas was observed (Figure 3-49).

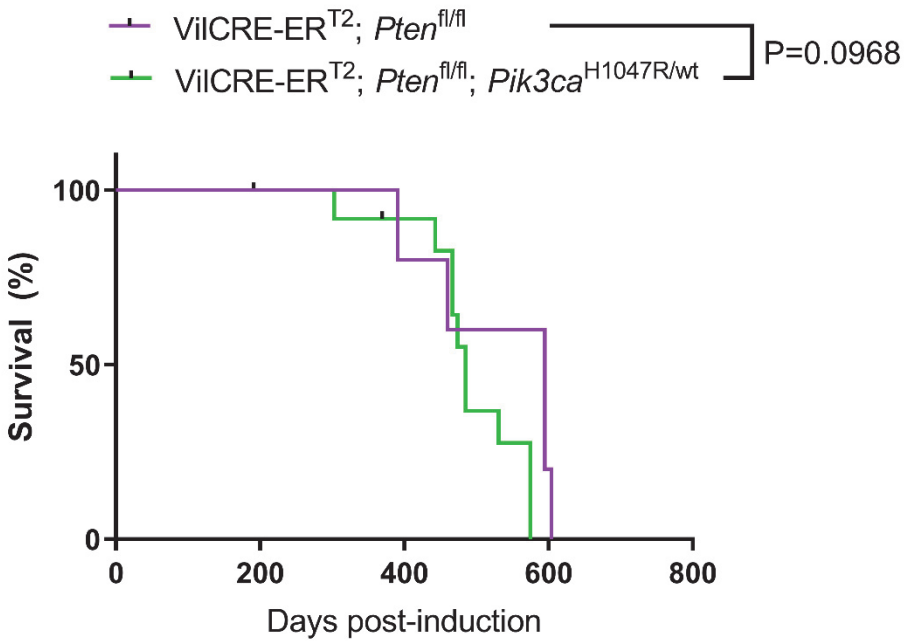

	Villin-Cre^{ERT2}; Pten$^{fl/fl}$	Villin-Cre^{ERT2}; Pten$^{fl/fl}$ PIK3CA$^{H1047R/wt}$
# censored subjects	0	2
# deaths/events	5	11
Median survival	595	485

Figure 3-46: Villin-Cre^{ERT2}; Pten$^{fl/fl}$ and Villin-CreER^{T2}; *Pten*$^{fl/fl}$ Pik3ca$^{H1047R/wt}$ mice develop signs of intestinal cancer with long latency. Survival curve of Villin-Cre^{ERT2}; Pten$^{fl/fl}$; Pik3ca$^{H1047R/wt}$ (n=5, purple) and Villin-Cre^{ERT2}; Pik3ca$^{H1047R/wt}$ (n=13, green) mice post-induction by administration of 80mg/kg tamoxifen. Log-rank test.

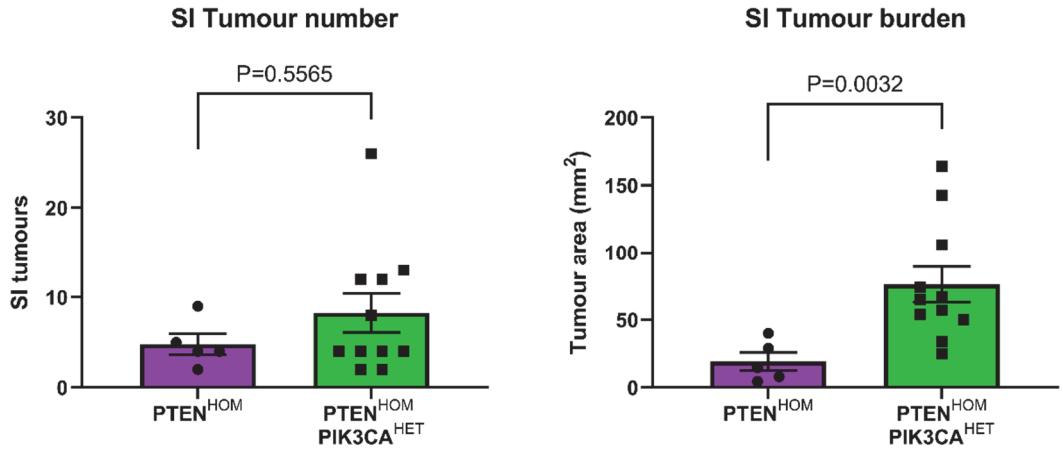

Figure 3-47: Concomittant *Pten* loss and *Pik3ca* mutation results in increased tumour burden in an *Apc*-loss independent model Villin-Cre^{ERT2}; Pten$^{fl/fl}$ and Villin-Cre^{ERT2}; Pten$^{fl/fl}$; Pik3ca$^{H1047R/wt}$ mice were induced and sampled at endpoint. Tumours were counted and measured after fixation in formalin. Mean ± s.e.m. Two-sided Mann-Whitney U test.

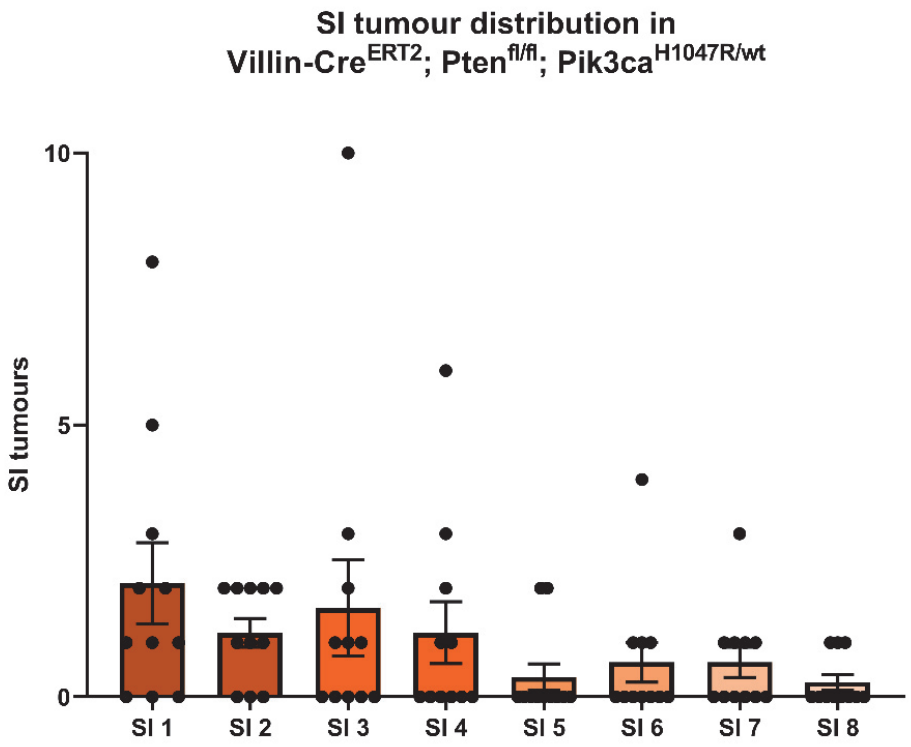

Figure 3-48: Tumour distribution in small intestines of Villin-Cre^{ERT2}; Pten$^{fl/fl}$; Pik3ca$^{H1047R/wt}$ decreases along its axis. Villin-Cre^{ERT2}; Pten$^{fl/fl}$; Pik3ca$^{H1047R/wt}$ mice were induced and sampled at endpoint. Tumours were counted and measured after fixation in formalin. SI 1 is the most proximal 1/8th of the SI, etc. n=11. Mean ± s.e.m.

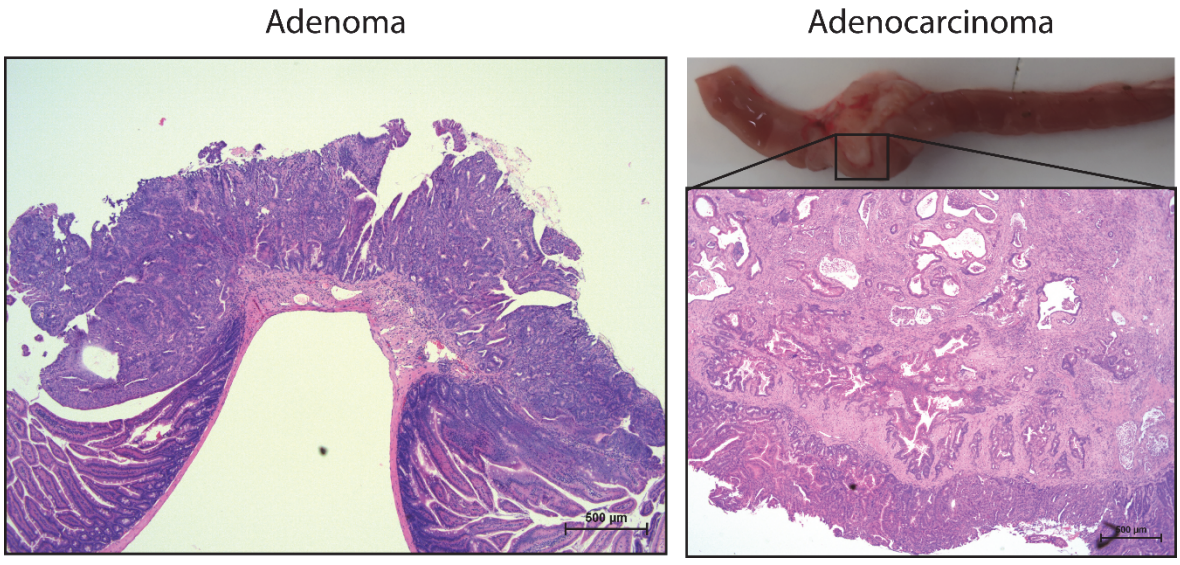

Figure 3-49: Adenoma and adenocarcinoma arising in Villin-CreER^{T2}; *Pten*$^{fl/fl}$; *Pik3ca*$^{H1047R/wt}$ Mice. Villin-CreER^{T2}; *Pten*$^{fl/fl}$; *Pik3ca*$^{H1047R/wt}$ mice were induced and sampled at endpoint. Guts were fixed in formalin and stained with H&E. Macroscopic image was taken at dissection. Scale bars 500µm.

Given that mice were not predisposed to *Apc*-loss, it was then important to establish whether tumours arising exhibited aberrant levels of Wnt signalling. To do so, I again used IHC to stain for ß-catenin on intestinal tumour tissue. ß-catenin

staining in sections from Villin-CreER^{T2}; *Pten*$^{fl/fl}$; *Pik3ca*$^{H1047R/wt}$ mice revealed that cells in adenomas were high for nuclear ß-catenin (Figure 3-50). In the adenocarcinoma, ß-catenin was nuclear at the base of the tumour, but low in the bulk of the extraluminal, stroma-rich part (Figure 3-51), in line with the staining pattern observed in invasive adenomas from the previously described Villin-CreER^{T2}; Apc$^{fl/wt}$; Pik3ca$^{H1047R/wt}$ model. This pattern of nuclear ß-catenin accumulation is suggestive of aberrant Wnt-pathway activation, and hence sporadic mutation of a Wnt pathway component, such as *Apc*, *Rnf43*, or *Ctnnb1* (ß-catenin) itself.

Figure 3-50: Adenoma in Villin-CreER^{T2}; *Pten*$^{fl/fl}$; *Pik3ca*$^{H1047R/wt}$ mouse stained for β-catenin reveals nuclear localisation. Tissue was fixed in formalin and stained for β-catenin. Scale bar is 500µm.

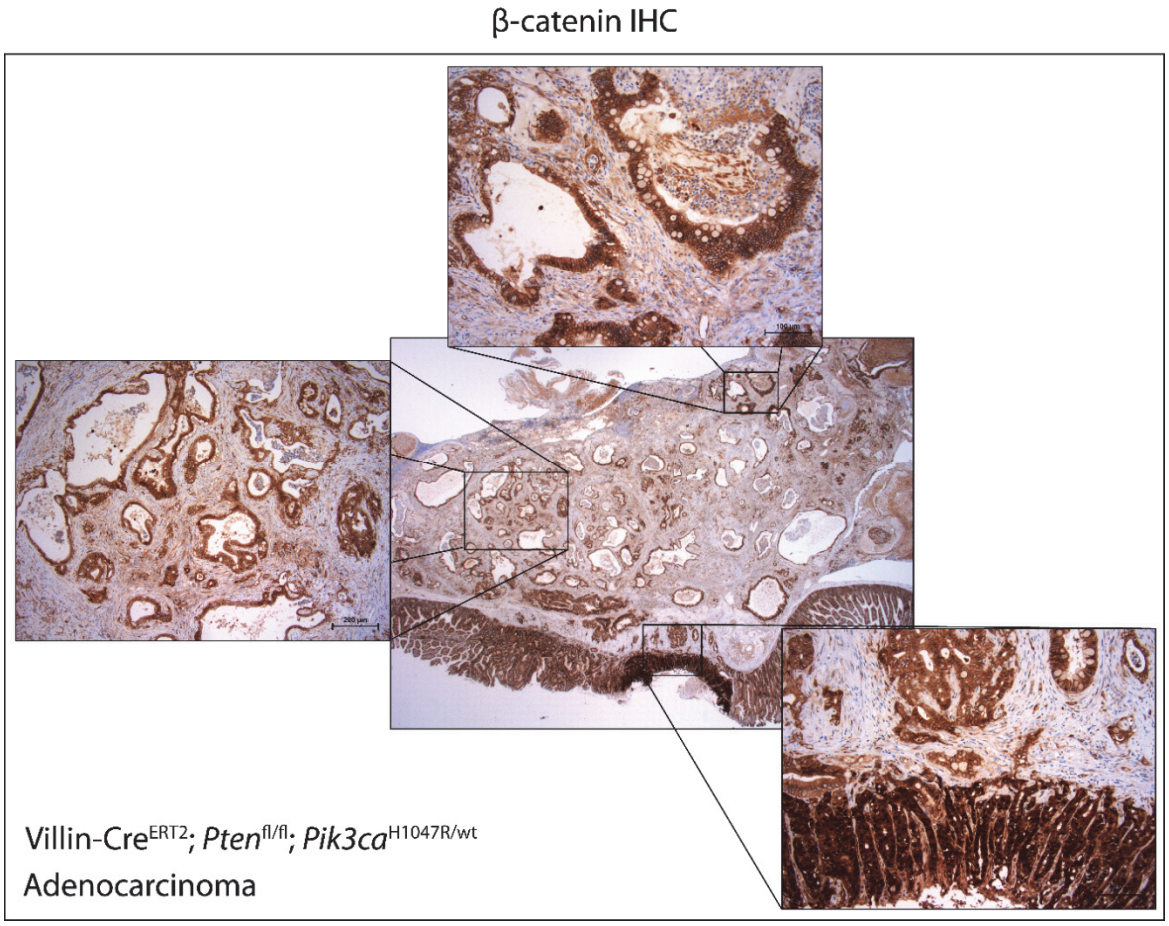

Figure 3-51: Invasive adenocarcinoma of Villin-CreER^{T2}; *Pten*$^{fl/fl}$; *Pik3ca*$^{H1047R/wt}$ mouse stained for β-catenin reveals heterogeneous nuclear localisation. Tissue was fixed in formalin and stained for β-catenin. Scale bars are 100μm and 200μm.

With this in mind, in order to investigate the Wnt-dependence of tumours in Villin-CreER^{T2}; *Pten*$^{fl/fl}$; *Pik3ca*$^{H1047R/wt}$ tumours further, I sought to establish 3D cultures from tumours (tumouroids). In contrast to non-tumour derived intestinal organoids, tumoroid cultures derived from APC-deficient tumours have a reduced dependency upon supply of exogenous Wnt-ligands and related soluble factors for growth, due to the ligand-independent nature of the aberrant Wnt signalling driven by *Apc* loss. Intriguingly, despite the apparent nuclear accumulation of ß-catenin in tumour tissue, tumouroids required complete growth media for efficient growth, most likely due to dependence on Wnt-ligands in the medium, indicative of a Wnt-ligand dependent pathway mutations (e.g. *Rnf43* and/or *Znrf3* loss) (Figure 3-52).

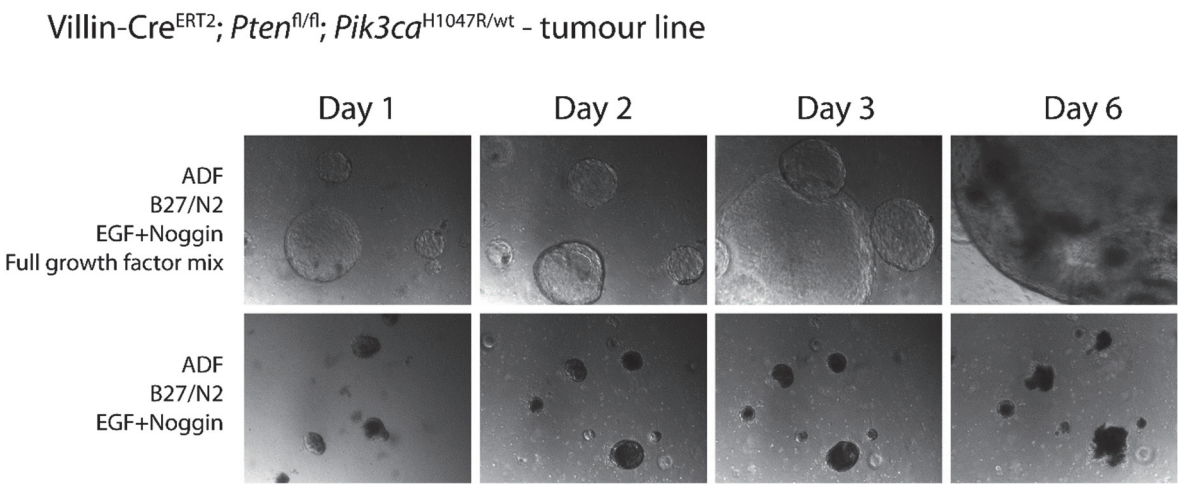

Figure 3-52: Tumouroid culture from Villin-CreER^{T2}; *Pten*$^{fl/fl}$; *Pik3ca*$^{H1047R/wt}$ SI tumour requires full growth factor mix to grow efficiently. SI tumour was excised and grown in matrigel in 3D. ADF = Advanced DMEM F12. B27/N2 = B27 and N2 growth factor supplements. EGF = Epidermal growth factor ligand. Full growth factor mix components described in materials and methods. Representative images from three technical replicates, experiment done twice.

3.5.1 Discussion

In summary, I have shown that PI3-Kinase hyperactivation in the murine gut results in formation of SI tumours, albeit at a very long latency. When expressed in the context of *Pten*-KO, PI3-Kinase mutation resulted in increased tumour burden and occurrence of invasive adenocarcinoma. Preliminary data indicates dependence on Wnt-ligands to grow ex vivo.

The main finding here is that the reason for the rapid tumour initiation in the previously described PI3-Kinase hyperactive models is very likely to be accellerated loss of *Apc*. This raises an important question that I have yet to address: Why exactly is *Apc* lost that frequently in e.g. Villin-CreER^{T2}; *Apc*$^{fl/wt}$; *Pten*$^{fl/fl}$ mice? The mechanism of tumour initiation is loss of heterozygosity of the wildtype allele, as shown by absence of the wildtype allele in tumours. This is the result of repair via the homologous recombination pathway, in which cells use sister chromatids as a template to repair their DNA during cell cycle phases in which this is possible, ie S-Phase, and G2/M phase. This means that the wildtype copy of *Apc* can be lost in cells progressing through the cell cycle. Crypts in the small intestines of Villin-CreER^{T2}; *Pten*$^{fl/fl}$ mice do not obviously contain more BrdU positive cells, and therefore this is not likely to be simply caused by an increase in proliferative cells. It is conceivable that cells lacking *Pten* repair their DNA more, given the previous RNA-sequencing data showing that loss of *Pten* results in

enrichment for a broad spectrum of stress related gene sets including p53 and DNA damage repair. Finally, stem cells could also behave differently in the absence of functional *Pten*. Again, more work would need to be conducted in Villin-CreER^{T2}; *Pten*$^{fl/fl}$ mice or organoid culture to dissect this further.

To ascertain the synergistic effect of *Pten*-KO and *Pik3ca* mutation in *Apc*-wildtype mice, Villin-CreER^{T2}; *Pik3ca*$^{H1047R/wt}$ mice would need to be aged as a control.

Activation of Wnt signalling is a near obligate step in intestinal cancer initiation and outgrowth. The tumours observed in these models displayed nuclear beta-catenin staining, indicating an activated Wnt-signalling pathway. This could be due to mutations in beta-catenin itself, in *Apc*, or other pathway components, such as *Rnf43* or *Znrf3*, leading to Wnt-ligand dependent signalling activation. Growth of the cell line presented in this chapter was Wnt-ligand dependent, indicating that *Apc*-loss was not likely to be the cause for malignant transformation in this particular line.

A limitation in the interpretation of these data so far is that at the time of writing I was only able to stain the guts of four Villin-CreER^{T2}; *Pten*$^{fl/fl}$; *Pik3ca*$^{H1047R/wt}$ mice. I therefore cannot make generalized statements e.g. on the distribution of ß-catenin in tumours. Downstream wnt-targets need to be probed for as well. Furthermore, PI3-Kinase and mTORC signalling markers will be important to assess.

The same limitation applies to the tissue culture experiments: One cell line is not enough to argue for a general wnt-ligand dependent tumour phenotype. The limited amount of tumours I was able to stain for ß-catenin so far showed nuclear localisation, although it was membranous in the large extraluminal part of the adenocarcinoma. Genetic loss of *Apc* or other components of the wnt signalling pathway would have to be probed for to be able to make a more general statement about the cause of high nuclear ß-catenin.

I have already crossed the *Pik3ca*^{H1047R} allele to homozygosity in this colony. Three of those had to be sampled so far and presented with large SI tumours, cultures of which are being established. These will answer whether there is a further gene-

dose dependent effect of *Pik3ca*^{H1047R} in *Apc*-loss dependent intestinal cancer initiation and progression.

3.6 PI3-Kinase-activating mutation in context of KRAS mutation

3.6.1 Kras^{G12D} mutation results in small intestinal, and colonic tumour initiation in Villin-CreER^{T2}; Apc$^{fl/wt}$ mice

Ca. 40-50% of CRC patients present with *KRAS* mutant cancer (Figure 1-4). Furthermore, *KRAS* mutations confer therapeutic resistance to targeted inhibition of EGFR and predict a worse outcome for patients (Siena *et al.*, 2009; Lee *et al.*, 2015). This highlights the need to study this mutation in pre-clinical cancer models. To evaluate impact of MAPK-hyperactivation, I crossed the *Kras*^{G12D} allele to Villin-CreER^{T2}; *Apc*$^{fl/wt}$ mice. This resulted in a profound reduction in survival from a median of 178 days post-induction, down to 78 days (range: 44 to 112 days) (Figure 3-53). This reduced survival was due to increased small intestinal and colonic tumour burden (Figure 3-54). Tumours arising in these mice are high for nuclear ß-catenin and robustly high for pERK in tumours and intestinal epithelium (Figure 3-55, Figure 3-56).

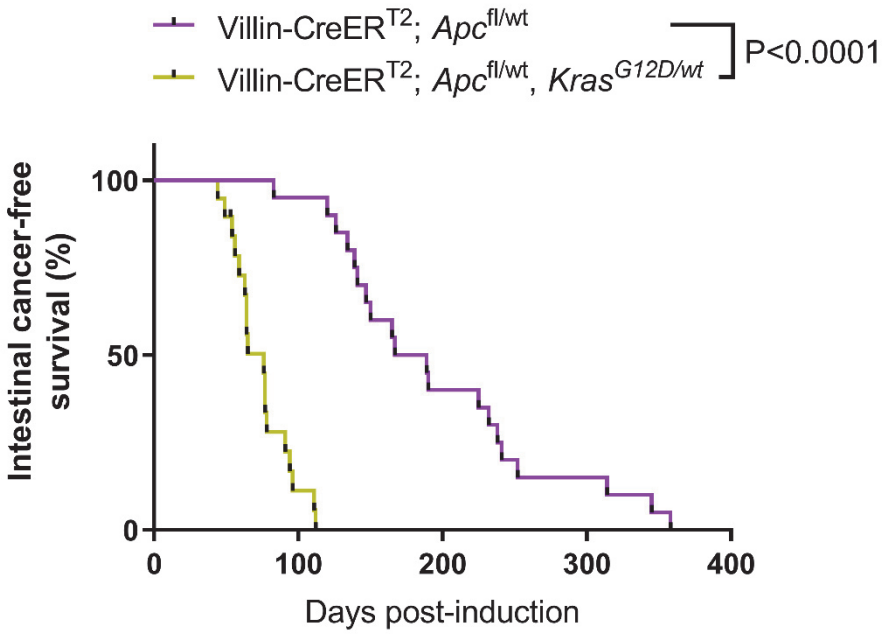

	Villin-CreER^{T2}; *Apc*$^{fl/wt}$	Villin-CreER^{T2}; *Apc*$^{fl/wt}$; *Kras*$^{G12D/wt}$
# censored subjects	0	1
# deaths/events	20	18
Median survival	178	76

Figure 3-53: *Kras*^{G12D} mutation in Villin-CreER^{T2}; *Apc*$^{fl/wt}$ mice results in reduced survival. Survival curve of Villin-CreER^{T2}; *Apc*$^{fl/wt}$ (purple, median survival=178 days), and Villin-CreER^{T2}; *Apc*$^{fl/wt}$; *Kras*$^{G12D/wt}$ (Gold, median survival=76 days, n=18) mice post-induction with tamoxifen. Log-rank test.

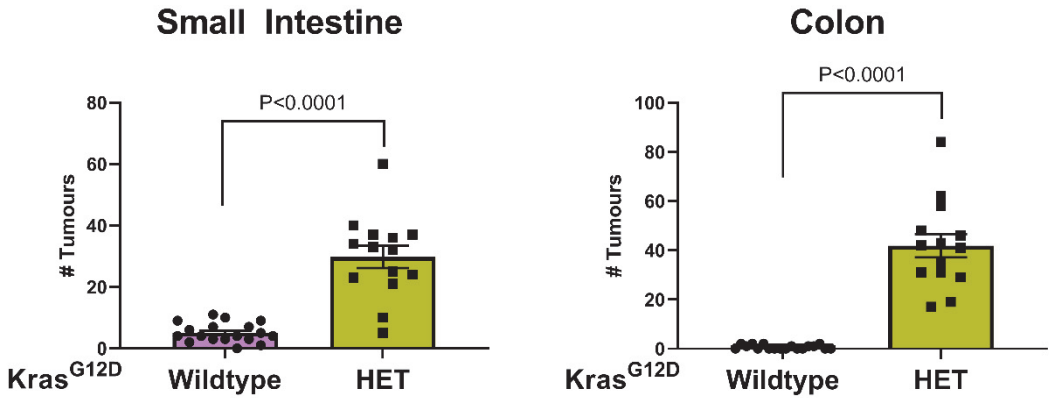

Figure 3-54: *Kras*^{G12D} mutation drives small intestinal and colonic tumour initiation. Tumours of Villin-CreER^{T2}; *Apc*$^{fl/wt}$ and Villin-CreER^{T2}; *Apc*$^{fl/wt}$; *Kras*$^{G12D/wt}$ mice sampled at endpoint were scored from processed H&E stained slides. Mean ± s.e.m. Two-sided Mann-Whitney U test.

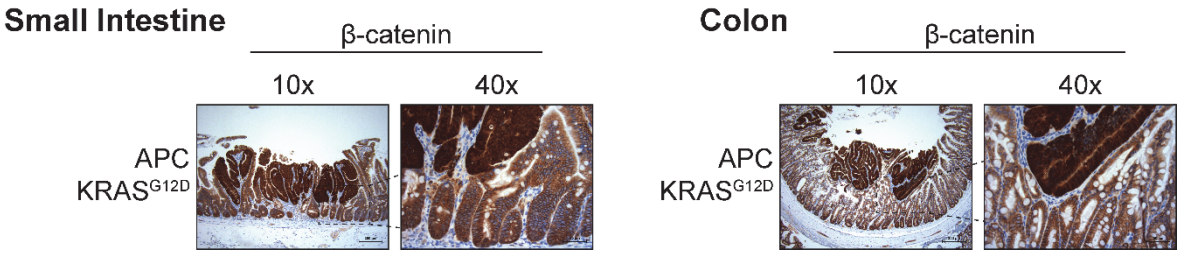

Figure 3-55: Nuclear localisation of β-catenin in Villin-CreER^{T2}; *Apc*$^{fl/wt}$; *Kras*$^{G12D/wt}$ tumour cells. IHC-staining of β-catenin in tumours from Villin-CreER^{T2}; *Apc*$^{fl/wt}$; *Kras*$^{G12D/wt}$ mice taken at endpoint. Scale bars 200μm (10x), and 50μm (40x).

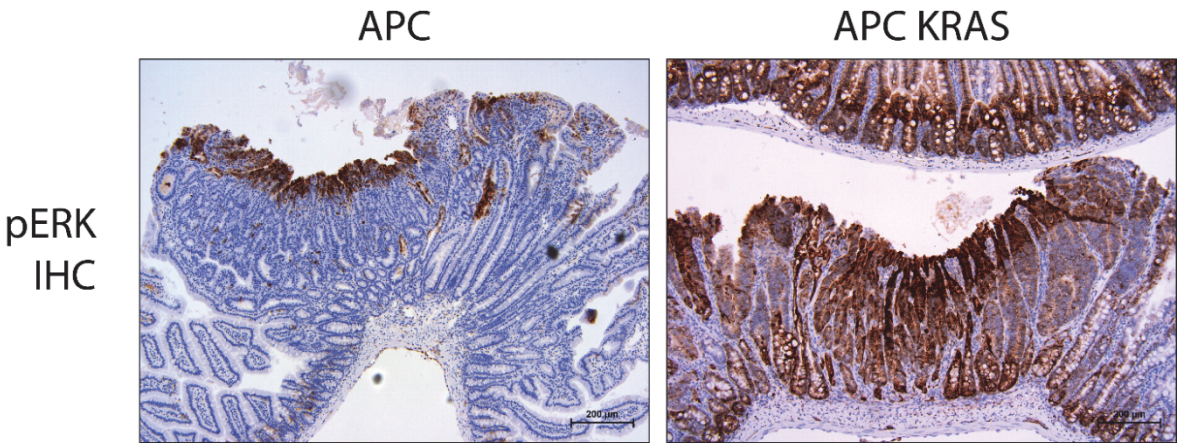

Figure 3-56: Strong pERK staining in *Kras*^{G12D} mutant tumours and surrounding intestinal epithelium. Villin-CreER^{T2}; *Apc*$^{fl/wt}$ and Villin-CreER^{T2}; *Apc*$^{fl/wt}$; *Kras*$^{G12D/wt}$ mice were sampled at endpoint and stained for pERK. Scale bars 200μm.

3.6.2 Heterozygous Pik3ca^{H1047R} mutation further reduces survival in Kras^{G12D} mutant mice by accelerating small intestinal tumour initiation.

KRAS and *PIK3CA* mutations significantly co-occur in human colorectal cancer patients and co-mutation predicts poor prognosis (Table 3-2, (Luo *et al.*, 2020)).

Table 3-2: MSK Metastatic colorectal cancer cohort mutual exclusivety analysis. Input: *KRAS* and *PIK3CA*. Data generated using cBioportal.

A	B	Total	Neither	A Not B	B Not A	Both	p-Value	q-Value	Tendency
KRAS	**PIK3CA**	1134	534	370	93	137	<0.001	**<0.001**	**Co-occurrence**

To assess impact of concomittant *Kras* and *Pik3ca*-mutation, I generated Villin-CreER^{T2}; *Apc*$^{fl/wt}$; *Kras*$^{G12D/wt}$; *Pik3ca*$^{H1047R/wt}$ mice. I induced genetic recombination and aged these mice to clinical endpoint, which they reached at a median of 39 days (range: 27 to 74 days) (Figure 3-57). This was significantly earlier than PI3-Kinase wildtypes (median: 76 days), and likely due to increased small intestinal

tumour burden (Figure 3-58This was surprising, as heterozygous *Pik3ca*^{H1047R} mutation had no effect on tumour initiation in *Kras* wildtype mice. IHC-staining for ß-catenin in tumour revealed nuclear positivity (Figure 3-59).

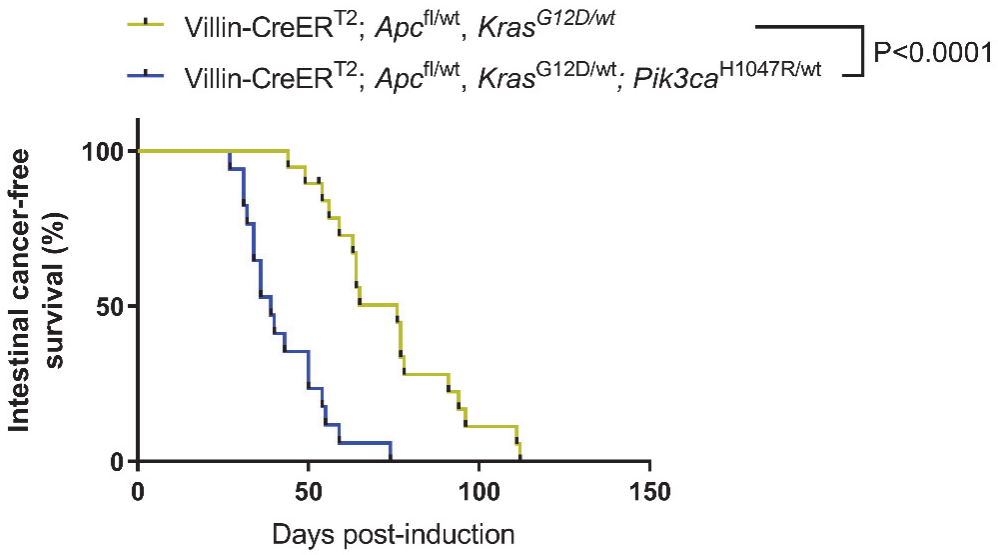

	Villin-CreER^{T2}; *Apc*$^{fl/wt}$, *Kras*$^{G12D/wt}$	Villin-CreER^{T2}; *Apc*$^{fl/wt}$, *Kras*$^{G12D/wt}$; *Pik3ca*$^{H1047R/wt}$
# censored subjects	1	0
# deaths/events	18	17
Median survival	76	39

Figure 3-57: Heterozygous *Pik3ca*^{H1047R} mutation accelerates the Villin-CreER^{T2}; *Apc*$^{fl/wt}$; *Kras*$^{G12D/wt}$ model. Survival curve of Villin-CreER^{T2}; *Apc*$^{fl/wt}$; *Kras*$^{G12D/wt}$ (yellow), and Villin-CreER^{T2}; *Apc*$^{fl/wt}$; *Kras*$^{G12D/wt}$; *Pik3ca*$^{H1047R/wt}$ (blue, n=17, median survival=39 days) mice post-induction with tamoxifen. Log-rank test.

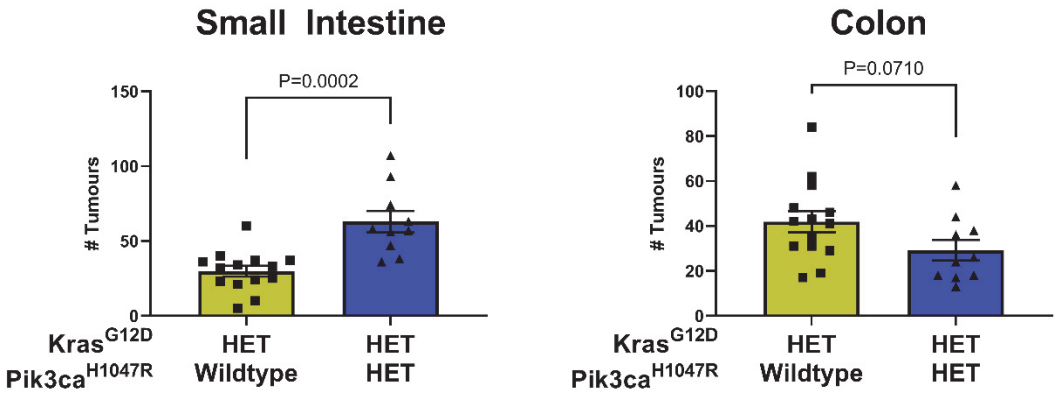

Figure 3-58: PIK3CA^{H1047R} mutation drives small intestinal tumour initiation in Villin-CreER^{T2}; *Apc*$^{fl/wt}$; *Kras*$^{G12D/wt}$ mice. Tumours in the intestinal tract of Villin-CreER^{T2}; *Apc*$^{fl/wt}$; *Kras*$^{G12D/wt}$; *Pik3ca*$^{H1047R/wt}$ mice were scored from H&E stained histological samples. Mean ± s.e.m. Two-sided Mann-Whitney U test.

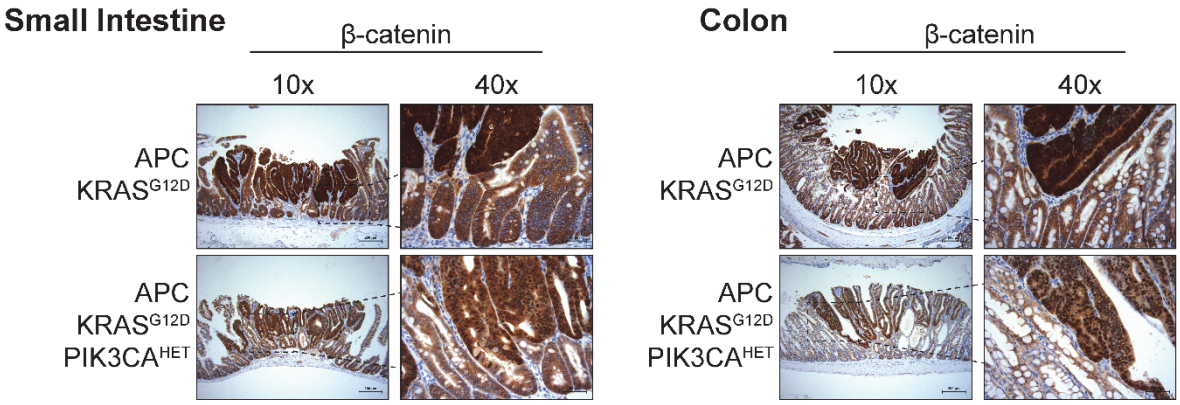

Figure 3-59: Nuclear localisation of β-catenin in Villin-CreER^{T2}; *Apc*$^{fl/wt}$; *Kras*$^{G12D/wt}$; *Pik3ca*$^{H1047R/wt}$ tumour cells. IHC-staining of β-catenin in tumours from Villin-CreER^{T2}; *Apc*$^{fl/wt}$; *Kras*$^{G12D/wt}$; *Pik3ca*$^{H1047R/wt}$ mice taken at endpoint. Scale bars 200µm (10x), and 50µm (40x).

3.6.3 Homozygous Pik3ca^{H1047R} mutation further accelerates the Villin-CreER^{T2}; Apc$^{fl/wt}$; Kras$^{G12D/wt}$ *model*

Heterozygous *Pik3ca*^{H1047R} mutation was not effective in driving intestinal cancer initiation in Villin-CreER^{T2}; *Apc*$^{fl/wt}$ mice, presented at the start of this chapter (Figure 3-7), and required either genetic ablation of *Pten* or homozygous mutation to show significant penetrance. I was therefore interested whether homozygous *Pik3ca*^{H1047R} mutation would further accelerate the Villin-CreER^{T2}; *Apc*$^{fl/wt}$; *Kras*$^{G12D/wt}$ ageing model and crossed the *Pik3ca*^{H1047R} allele to homozygosity. These mice had to be sampled at a median of 28 days (range: 21 to 40 days) (Figure 3-60). This was significantly earlier than wildtypes and heterozygous PI3-Kinase mutant mice. These homozygous PI3-Kinase-mutant mice had even more small intestinal tumours, compared to wildtypes and heterozygotes, and a similar amount of colonic tumours. Given the excessively shorter survival, this indicates increased tumour formation in the small intestine and colon (Figure 3-61).

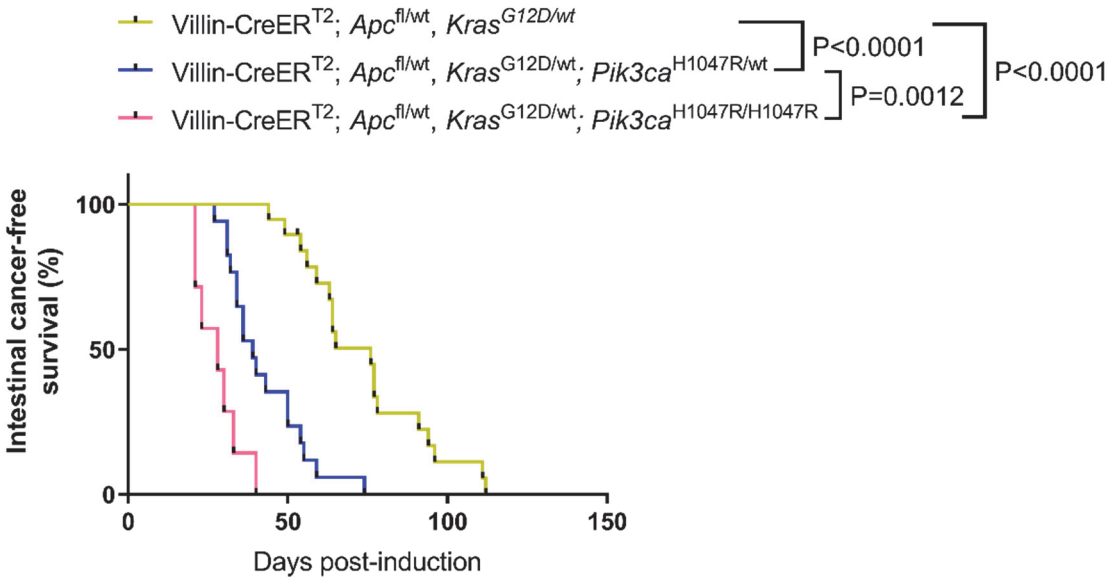

	Villin-CreER^{T2}; *Apc*$^{fl/wt}$, *Kras*$^{G12D/wt}$	Villin-CreER^{T2}; *Apc*$^{fl/wt}$, *Kras*$^{G12D/wt}$; *Pik3ca*$^{H1047R/wt}$	Villin-CreER^{T2}; *Apc*$^{fl/wt}$, *Kras*$^{G12D/wt}$; *Pik3ca*$^{H1047R/H1047R}$
# censored subjects	1	0	0
# deaths/events	18	17	7
Median survival	76	39	28

Figure 3-60: Homozygous *Pik3ca*^{H1047R} mutation further accelerates the Villin-CreER^{T2}; *Apc*$^{fl/wt}$; *Kras*$^{G12D/wt}$ model. Survival curve of Villin-CreER^{T2}; *Apc*$^{fl/wt}$; *Kras*$^{G12D/wt}$ (Gold), Villin-CreER^{T2}; *Apc*$^{fl/wt}$; *Kras*$^{G12D/wt}$; *Pik3ca*$^{H1047R/wt}$ (blue), and Villin-CreER^{T2}; *Apc*$^{fl/wt}$; *Kras*$^{G12D/wt}$; *Pik3ca*$^{H1047R/H1047R}$ (Pink, n=7, median survival=28 days) mice post-induction with tamoxifen. Log-rank test.

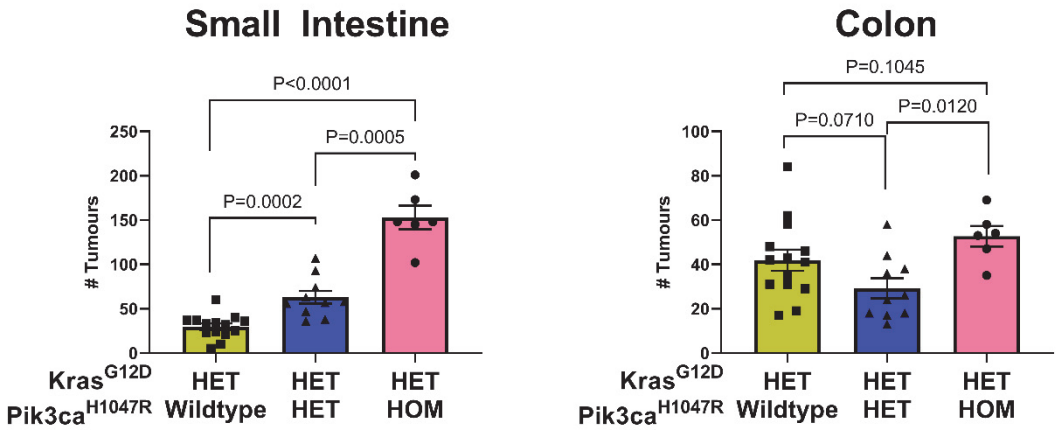

Figure 3-61: Homozygous *Pik3ca*^{H1047R} mutation drives small intestinal and colonic tumour initiation. Tumours in the intestinal tract of Villin-CreER^{T2}; *Apc*$^{fl/wt}$; *Kras*$^{G12D/wt}$; *Pik3ca*$^{H1047R/H1047R}$ mice were scored from H&E stained histological samples. Mean ± s.e.m Two-sided Mann-Whitney U test.

To assess wnt-signalling status in these tumours, I performed ß-catenin IHC, which was nuclear in tumours arising in *Pik3ca*$^{H1047R/H1047R}$ mice, indicating high Wnt

signalling and progression through the classical path to intestinal cancer (Figure 3-62).

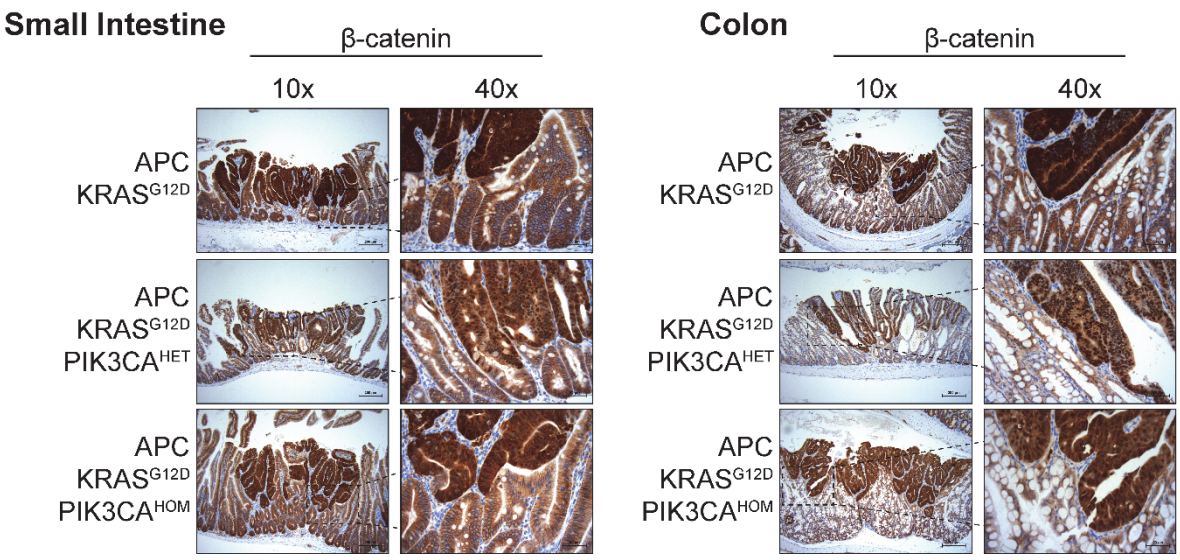

Figure 3-62: Nuclear localisation of β-catenin in Villin-CreER^{T2}; *Apc*$^{fl/wt}$; *Kras*$^{G12D/wt}$; *Pik3ca*$^{H1047R/H1047R}$ tumour cells. IHC-staining of β-catenin in tumours from Villin-CreER^{T2}; *Apc*$^{fl/wt}$; *Kras*$^{G12D/wt}$; *Pik3ca*$^{H1047R/H1047R}$ mice taken at endpoint. Scale bars 200µm (10x), and 50µm (40x).

PTEN may play a direct role in preventing oncogenic PI3-Kinase signalling. I therefore performed PTEN-IHC to establish whether *Kras* or concomitant *Kras* and *Pik3ca* mutations might impact levels of PTEN and contribute to the permissiveness of *Pik3ca* mutation in the context of mutant *Kras*. PTEN levels in normal tissue did not seem to be altered, but *Kras* mutant tumours and especially *Kras*/*Pik3ca* co-mutated tumours displayed a significant reduction of PTEN in tumour tissue vs normal intestinal epithelium (Figure 3-63). This would provide a ready explanation for the increased penetrance of *Pik3ca* in *Kras* mutant models. To further understand the mechanism by which PTEN abundance was decreased, I conducted ISH for Pten mRNA and calculated the amount of probes observed per mm2 of tumour tissue. Results from this experiment indicate that the downregulation of PTEN protein level is not due to decreased transcription (Figure 3-64).

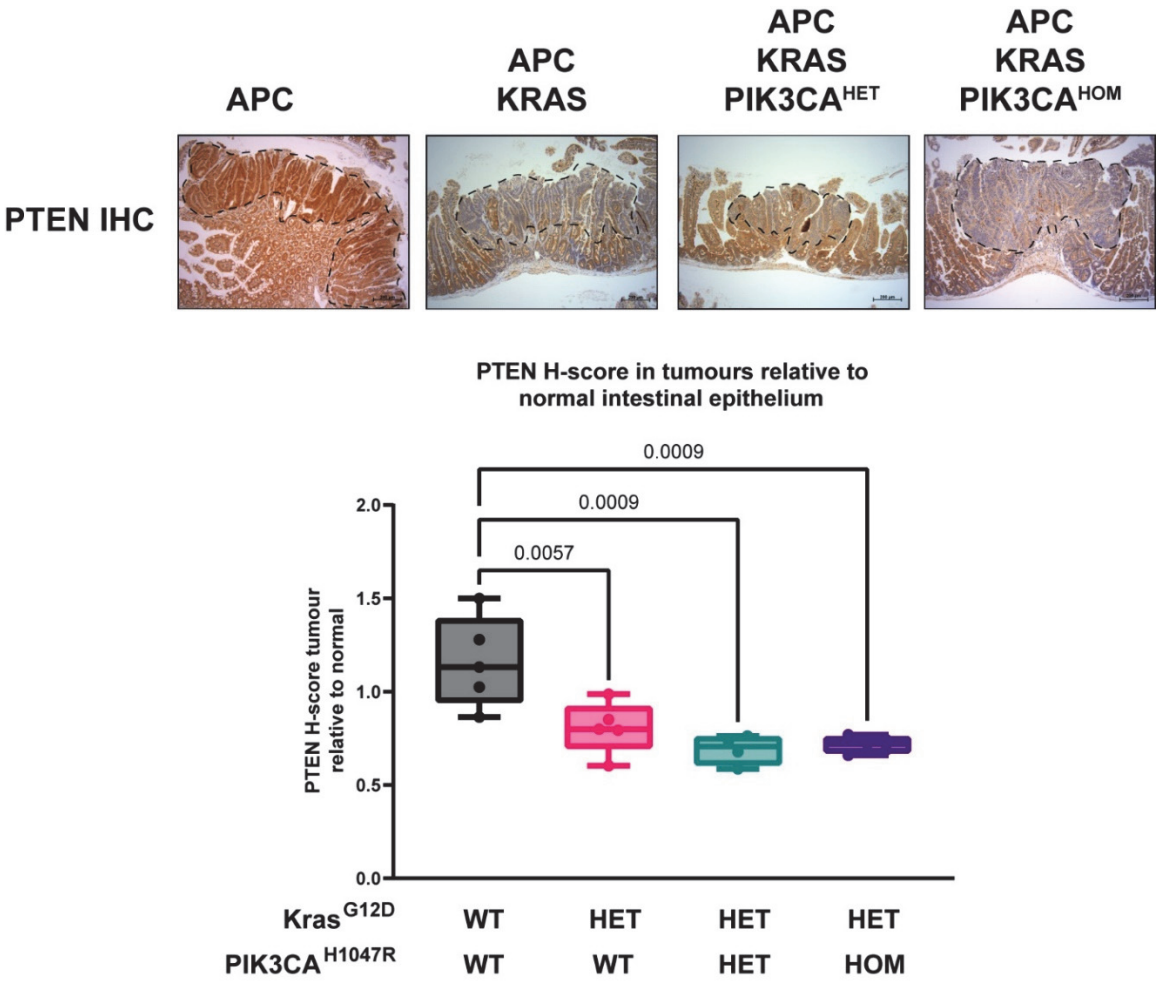

Figure 3-63: Representative images and quatification of PTEN IHC in intestinal tumours from Villin-CreER^{T2}; *Apc*$^{fl/wt}$ (APC), Villin-CreER^{T2}; *Apc*$^{fl/wt}$; *Kras*$^{G12D/wt}$ (APC KRAS), Villin-CreER^{T2}; *Apc*$^{fl/wt}$; *Kras*$^{G12D/wt}$; *Pik3ca*$^{H1047R/wt}$ (APC KRAS PIK3CA^{HET}), and Villin-CreER^{T2}; *Apc*$^{fl/wt}$; *Kras*$^{G12D/wt}$; *Pik3ca*$^{H1047R/H1047R}$ (APC KRAS PIK3CA^{HOM}). Indicated mice were induced and aged to clinical endpoint. Histological samples were stained for PTEN and representative images are shown at the top. PTEN staining intensity was quantified using an adapted version of the CytoNuclear algorithm in Halo software, binned into Negative, Low, Medium, and High. H-Scores were generated from this for normal intestinal epithelium and tumours. H-Scores of tumours were divided by normal tissue H-scores (bottom). Scale bars 200µm and 500µm. Mean ± s.e.m. Ordinary One-Way ANOVA and Dunnet's multiple comparisons test.

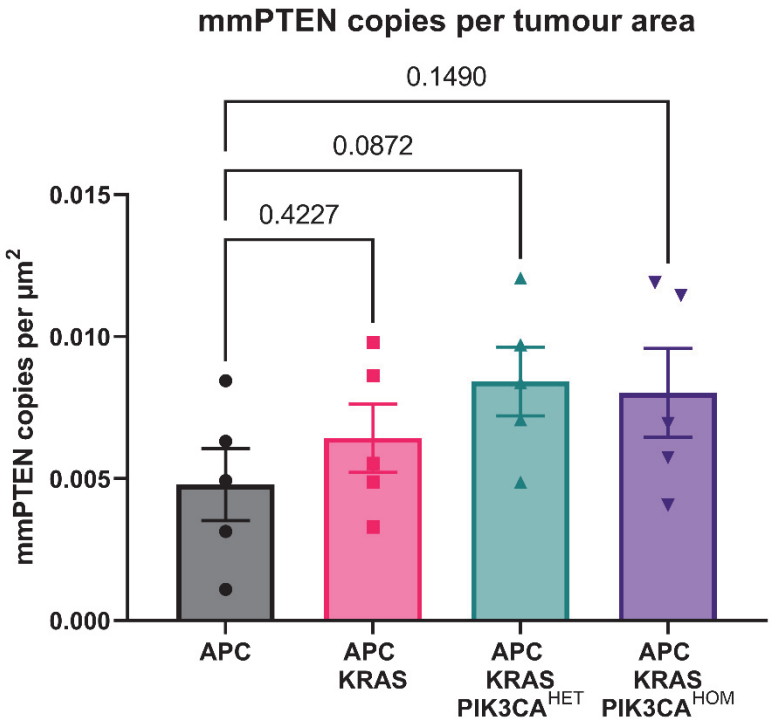

Figure 3-64: Similar abundance of Pten ISH-probe (mmPTEN) in tumours from various mouse models. Villin-CreER^{T2}; *Apc*$^{fl/wt}$ (APC), Villin-CreER^{T2}; *Apc*$^{fl/wt}$; *Kras*$^{G12D/wt}$ (APC KRAS), Villin-CreER^{T2}; *Apc*$^{fl/wt}$; *Kras*$^{G12D/wt}$; *Pik3ca*$^{H1047R/wt}$ (APC KRAS PIK3CA^{HET}) and Villin-CreER^{T2}; *Apc*$^{fl/wt}$; *Kras*$^{G12D/wt}$; *Pik3ca*$^{H1047R/H1047R}$ (APC KRAS PIK3CA^{HOM}) mice were sampled at endpoint and ISH for mouse Pten mRNA was conducted. Probes were detected using halo and normalized to µm^2 of tumour tissue. Mean ± s.e.m. Kruskal-Wallis test and uncorrected Dunn's multiple comparisons test.

3.6.4 Discussion

Increased MAPK activity, driven by mutant Kras led to increased small intestinal and colonic tumour formation. The biological impact of concomitant PI3-Kinase mutation in the *Kras* mutant setting was remarkable, as median survival was halved by introduction of heterozygous PI3-Kinase mutation. The extent of this was surprising, as heterozygous *Pik3ca* mutation did not affect tumour initiation in the *Kras* wildtype setting and indicates that *Kras* mutant tissue may be more permissive to concomitant PI3-Kinase driven tumours initiation. Homozygous *Pik3ca* mutation resulted in an even shorter time to endpoint and increased tumour initiation, indicating that further increase in gene-dosage of *Pik3ca* activating mutations is functionally relevant in *Kras* mutant intestinal cancer.

High nuclear beta catenin suggests these tumours initiate through the classical path to cancer rather than the serrated route. Hadac et al. made a similar observation when inducing focal colonic lesions in *Apc*$^{fl/fl}$; *Kras*^{G12D}; *Pik3ca*^{p110*} mice

(Hadac *et al.*, 2015). Tumours in these mice progressed to advanced adenocarcinoma and even metastasized to the liver in two mice from this cohort. The main criticism of this study is the allele that was used to drive PI3-Kinase hyperactivity, as it escapes regulation by Ras. Furthermore, the expression of the mutant, dominant active PI3-Kinase is expressed on top of the two wildtype *Pik3ca* alleles.

As results in chapter 3.4.3 showed, abundance of PTEN is crucial to suppress PI3-Kinase signalling. PTEN levels in *Kras* mutant tumours were reduced compared to *Kras* wildtypes tumours. The mechanism for this did not seem to be driven by a direct transcriptional downregulation of Pten mRNA. PTEN regulation is known to be dependent on multiple co- and post-translational mechanisms (Brito, Goulielmaki and Papakonstanti, 2015). Potential mechanisms for this downregulation are ubiquitinylation and subsequent proteasomal degradation, or redox dependent regulation, as mutant KRAS is known to alter cellular metabolism (Wang *et al.*, 2007; Huu *et al.*, 2021)

3.7 *Pten*-KO in context of KRAS mutation

Acitvation of the PI3-Kinase pathway through depletion of *Pten* in combination with heterozygous *Apc*–loss led to rapid small intestinal tumour initiation. To determine the effect of concomitant *Kras* mutation and *Pten* loss in the context of *Apc*-loss dependent intestinal cancer, I generated Villin-CreER^{T2}*Apc*$^{fl/wt}$; *Kras*^{G12D}; *Pten*$^{fl/fl}$ mice. I induced recombination of these transgenes and again aged mice to clinical endpoint, which they reached after a median of 16 days, with a range from 16 to 17 days (Figure 3-65). This was significantly faster than *Kras* mutant *Pten* wildtypes and *Kras* wildtype *Pten*-KOs.

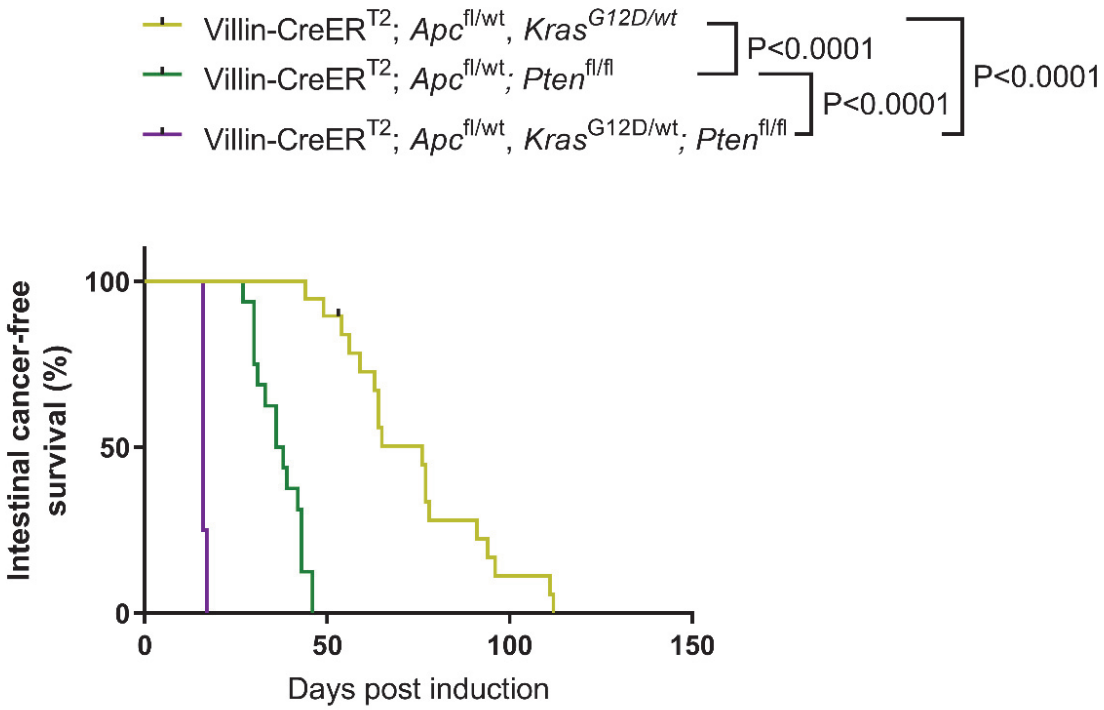

	Villin-CreER^{T2}; *Apc*$^{fl/wt}$, *Kras*$^{G12D/wt}$	Villin-CreER^{T2}; *Apc*$^{fl/wt}$, *Pten*$^{fl/fl}$	Villin-CreER^{T2}; *Apc*$^{fl/wt}$, *Kras*$^{G12D/wt}$; *Pten*$^{fl/fl}$
# censored subjects	1	0	0
# deaths/events	18	16	4
Median survival	76	37	16

Figure 3-65: Villin-CreER^{T2}*Apc*$^{fl/wt}$; *Kras*^{G12D}; *Pten*$^{fl/fl}$ mice develop rapid signs of intestinal cancer. Survival curve of ageing cohorts presented earlier and Villin-CreER^{T2}*Apc*$^{fl/fl}$; *Kras*^{G12D}; *Pten*$^{fl/f}$ (n=4) post-induction by administration of 80mg/kg tamoxifen. Log-rank test.

I quantified tumours in the intestines of these mice. Double mutants presented with a significant increase in small intestinal tumours compared to the two single mutants. They had a similar amount of colonic tumours compared to *Kras* mutants (Figure 3-66). Given the extremely short latency of Villin-CreER^{T2}*Apc*$^{fl/wt}$; *Kras*^{G12D}; *Pten*$^{fl/fl}$ mice, I normalized the amount of tumours to every mouse's time post induction, which was significantly higher in *Kras*/*Pten* co-mutated mice (Figure 3-67).

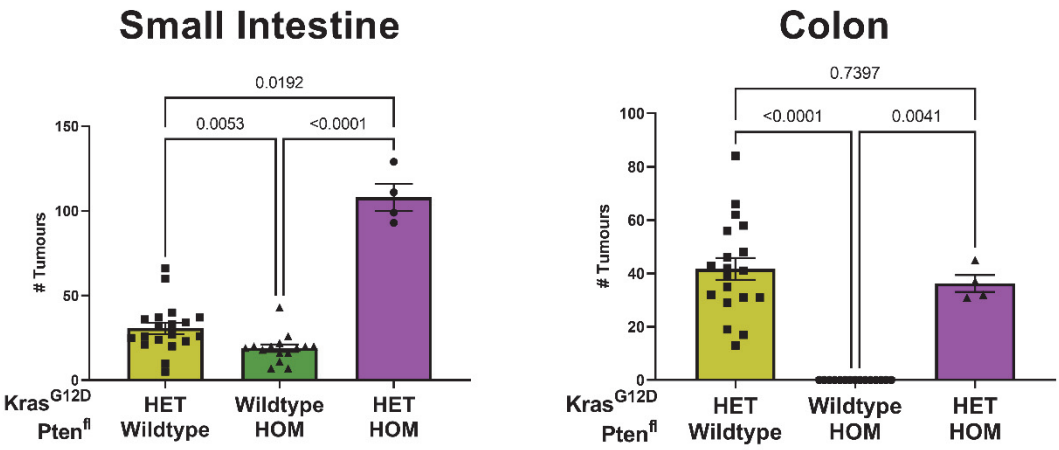

Figure 3-66: *Pten*-KO in the context of *Kras* mutation drives small intestinal and colonic tumour initiation. Tumours of mice sampled at endpoint were scored from processed H&E stained slides. Mean ± s.e.m. Kruskal-Wallis test and uncorrected Dunn's test.

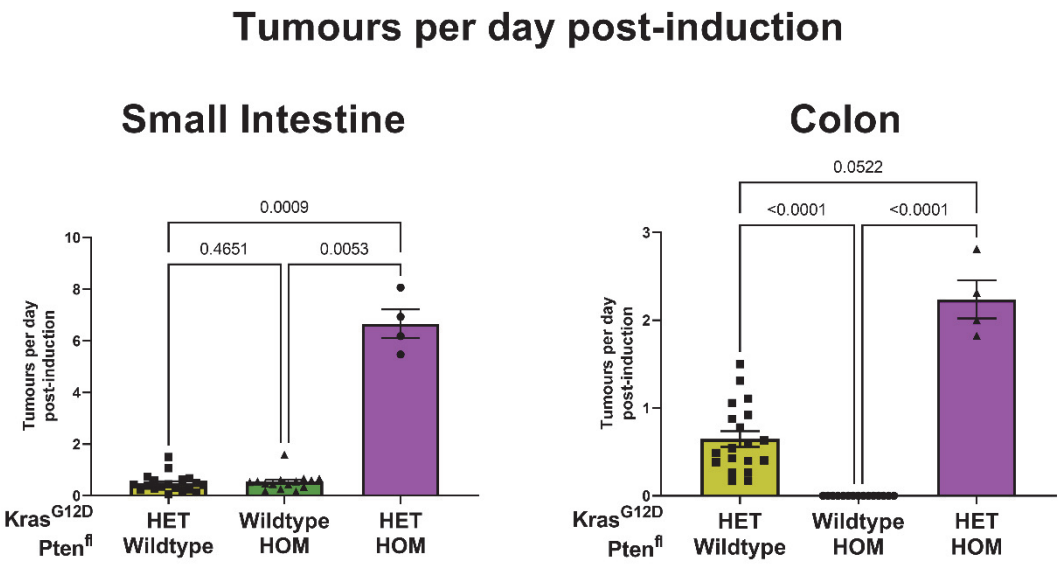

Figure 3-67: Concomitant *Pten*-KO and *Kras* mutation leads to increased small intestinal and colonic tumour initiation. Number of SI and Colon tumours were divided by time to clinical endpoint, normalizing the rate of intestinal tumour initiation to the individual mouse. Mean ± s.e.m. Kruskal-Wallis test and uncorrected Dunn's multiple comparisons test.

3.7.1 Discussion

In summary, I showed that concomitant *Kras* mutation and *Pten*-KO leads to rapid small intestinal and colonic tumour initiation in *Apc*-loss predisposed mice.

While synergy was expected, the extent of tumour initiation was surprising. Adjusted for days post-induction, the increase in SI tumours was more than 10-

fold. This indicates that PTEN is a crucial tumour suppressor in *Kras* mutant intestinal cells, at least in the context of *Apc*-loss.

I have already induced the first cohort of Villin-CreER^{T2}*Apc*$^{fl/wt}$; *Kras*^{G12D}; *Pten*$^{fl/wt}$ ageing mice to determine gene-dose dependent effects of *Pten*.

3.8 PI3-Kinase signalling hyperactivation in *Apc*$^{fl/fl}$; *Kras*^{G12D} mice

Similar to subchapter 3.3, I wanted to determine the effects of PI3-Kinase hyperactivation directly after oncogenic transformation by loss of functional APC, but this time in the context of additional *Kras* mutation.

3.8.1 Kras^{G12D} mutation in Villin-CreER^{T2}; Apc$^{fl/fl}$ mice

To delineate the effects of PI3-Kinase hyperactivation and *Kras* mutation, I first compared Villin-CreER^{T2}; *Apc*$^{fl/fl}$ to Villin-CreER^{T2}; *Apc*$^{fl/fl}$; *Kras*$^{G12D/wt}$ mice. The induction regime for *Kras* mutant mice was one dose of tamoxifen on day 0 and mice were sampled on day three post-induction, as opposed to tamoxifen on days 0 and 1 and sampling on day 4 post-induction for *Kras* wildtypes. Mice were injected BrdU intraperitoneally 2h before sampling and I scored BrdU positive cells per half crypt (Figure 3-68). This was not significantly different. The transcriptome of Kras mutant guts was more profoundly altered than in the previously described PI3-Kinase hyperactive conditions (Figure 3-69). Using this list of significantly differentially regulated genes, I determined Ractome pathway enrichment, depicted in Figure 3-70. Multiple metabolic pathways were enriched in the *Kras*^{G12D} mutant condition, including metabolism of carbohydrates, steroids, and glucose. Additionally, SLC mediated transmembrane transport was upregulated. Wnt signalling was downregulated upon introduction of mutant *Kras*.

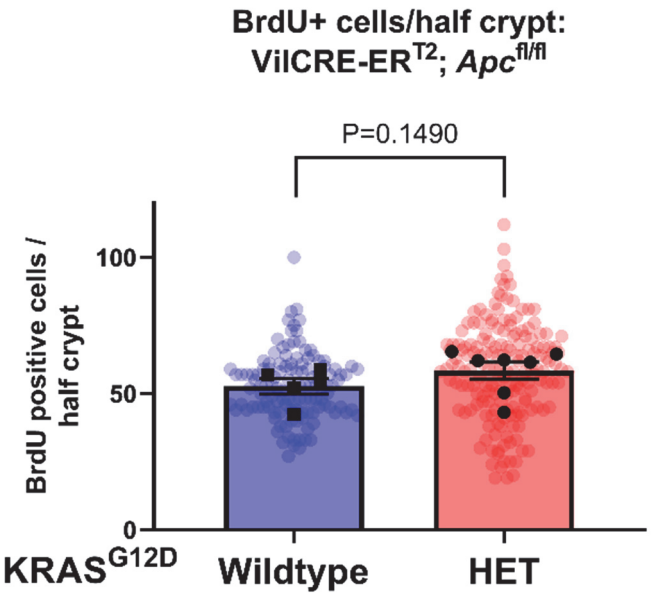

Figure 3-68: Similar amounts of proliferations upon *Kras* mutation in the short term model. Mice were administered 80mg/kg tamoxifen once. BrdU was administered IP on day 3 post-induction, 2h before sampling. BrdU positive cells per half crypt (n=25) were quantified off histological samples. Pale coloured dots represent single half-crypts, black dots are means of biological replicates. Mean ± s.e.m. Two-sided Mann-Whitney U test.

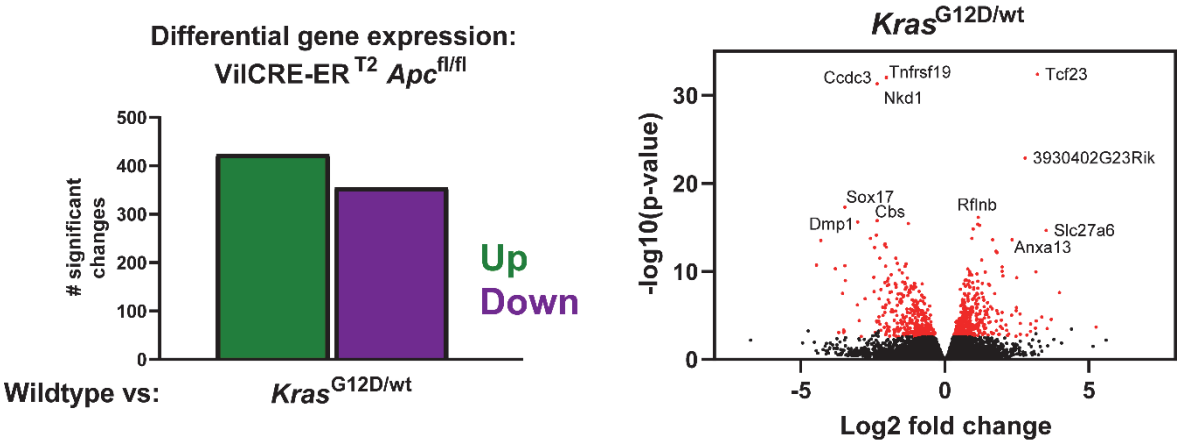

Figure 3-69: Number of significantly altered genes and volcano plot visualization in wildtype vs *Kras* mutant RNA-sequencing experiment. Bar graph showing number of differentially regulated genes (adjusted p-value <0.05) following RNA-sequencing of small intestinal samples from Villin-CreER^{T2}; *Apc*$^{fl/fl}$ and Villin-CreER^{T2}; *Apc*$^{fl/fl}$; *Kras*^{G12D}. Volcano plot: p-value was –log10 transformed and fold change was Log2 transformed. Red dot indicates p-value <0.05 and individual genes are highlighted next to their position. n=4 mice used per experimental condition. Robin Shaw and Kathryn Gilroy contributed to the generation of these data.

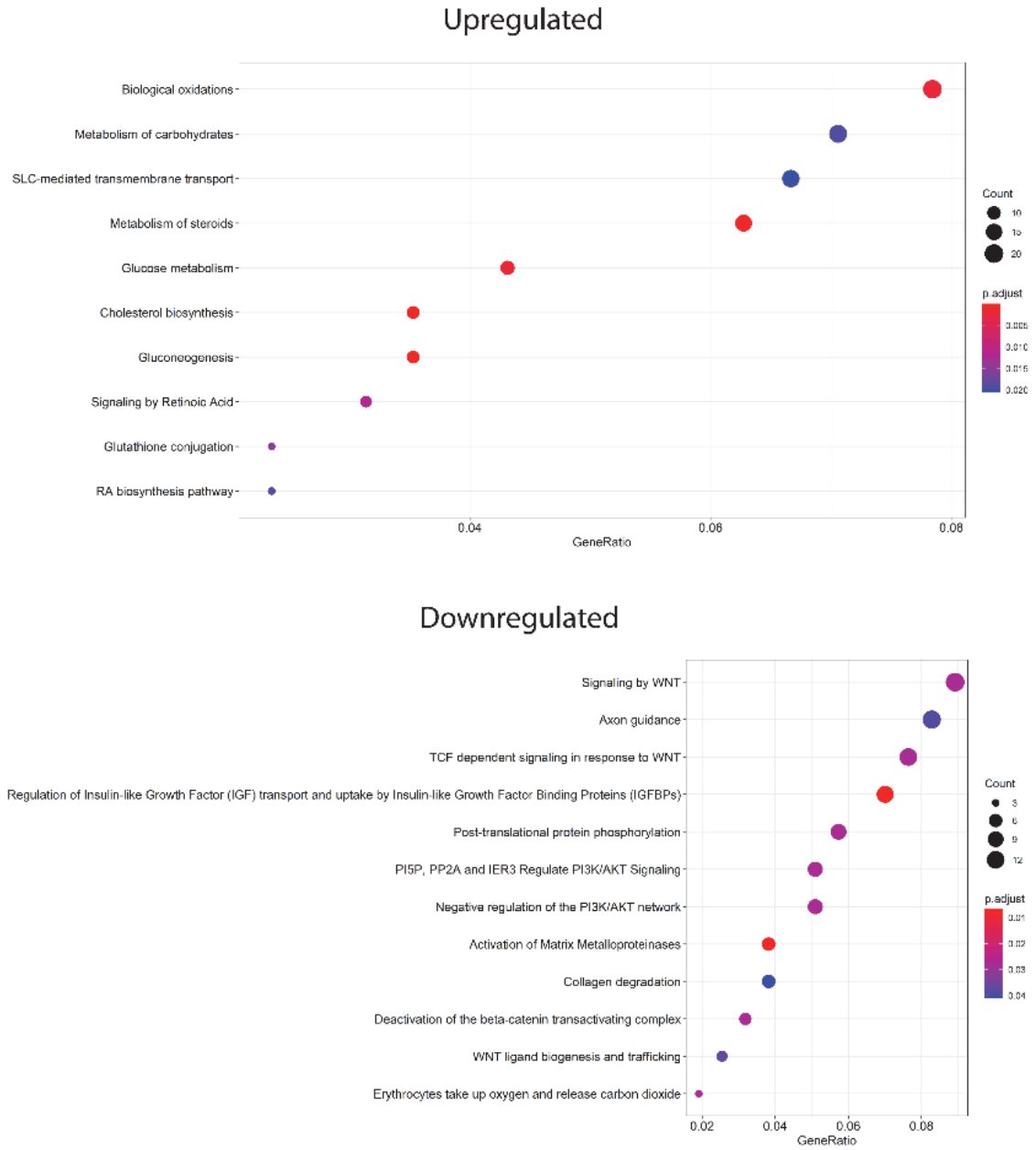

Figure 3-70: Significantly altered Reactome pathways in wildtype vs *Kras* mutant RNA-sequencing experiment. RNA sequencing of Villin-CreER^{T2}; *Apc*$^{fl/fl}$ and Villin-CreER^{T2}; *Apc*$^{fl/fl}$; *Kras*$^{G12D/wt}$ SI samples and differential gene expression were performed. Reactome pathway analysis was performed to determine most significantly up- and downregulated pathways. Kathryn Gilroy contributed to the generation of these data.

Using the global output of the RNA-sequencing experiment, I performed GSEA on the "Hallmarks" genesets, which revealed positive and negative enrichment of pathways depicted in Figure 3-71.

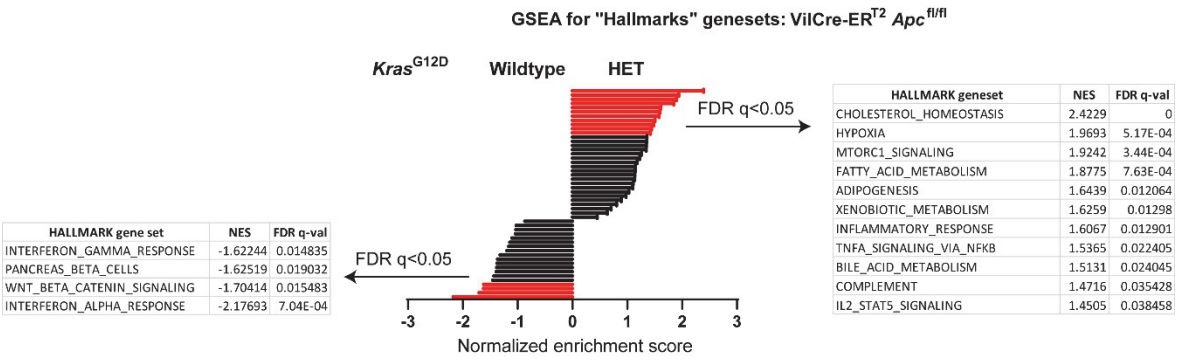

HALLMARK gene set	NES	FDR q-val
INTERFERON_GAMMA_RESPONSE	-1.62244	0.014835
PANCREAS_BETA_CELLS	-1.62519	0.019032
WNT_BETA_CATENIN_SIGNALING	-1.70414	0.015483
INTERFERON_ALPHA_RESPONSE	-2.17693	7.04E-04

HALLMARK geneset	NES	FDR q-val
CHOLESTEROL_HOMEOSTASIS	2.4229	0
HYPOXIA	1.9693	5.17E-04
MTORC1_SIGNALING	1.9242	3.44E-04
FATTY_ACID_METABOLISM	1.8775	7.63E-04
ADIPOGENESIS	1.6439	0.012064
XENOBIOTIC_METABOLISM	1.6259	0.01298
INFLAMMATORY_RESPONSE	1.6067	0.012901
TNFA_SIGNALING_VIA_NFKB	1.5365	0.022405
BILE_ACID_METABOLISM	1.5131	0.024045
COMPLEMENT	1.4716	0.035428
IL2_STAT5_SIGNALING	1.4505	0.038458

Figure 3-71: Gene-set enrichment analysis for the hallmark gene sets. GSEA was conducted on all hallmark gene sets after RNA sequencing. Gene sets were ranked based on their normalized enrichment score and significantly altered gene sets are depicted as a red bar and listed in the table next to the bar graphs. FRD = False discovery rate. NES = normalized enrichment score.

3.8.2 PI3-Kinase hyperactivation in Villin-CreER^{T2}; Apc$^{fl/fl}$; Kras$^{G12D/wt}$ mice

Having established a baseline for the effects of mutant *Kras* upon homozygous KO of *Apc*, I next sought to determine the impact of additional PI3-Kinase hyperactivation in the Villin-CreER^{T2}; *Apc*$^{fl/fl}$; *Kras*$^{G12D/wt}$ "short term" experimental setting. To this end, I generated Villin-CreER^{T2}*Apc*$^{fl/fl}$; *Kras*^{G12D}; *Pten*$^{fl/fl}$ and Villin-CreER^{T2}; *Apc*$^{fl/fl}$; *Kras*$^{G12D/wt}$; *Pik3ca*$^{H1047R/wt}$ mice and induced genetic recombination with tamoxifen. I assessed impact on intestinal epithelial proliferation by injecting BrdU 2h before sampling and staining for the labelled nucleotide analogue. Mirroring results in *Kras* wildtype mice, *Pten*-KO did not influence proliferation, while *Pik3ca*^{H1047R} mutation increased BrdU positive cells per half-crypt (Figure 3-72).

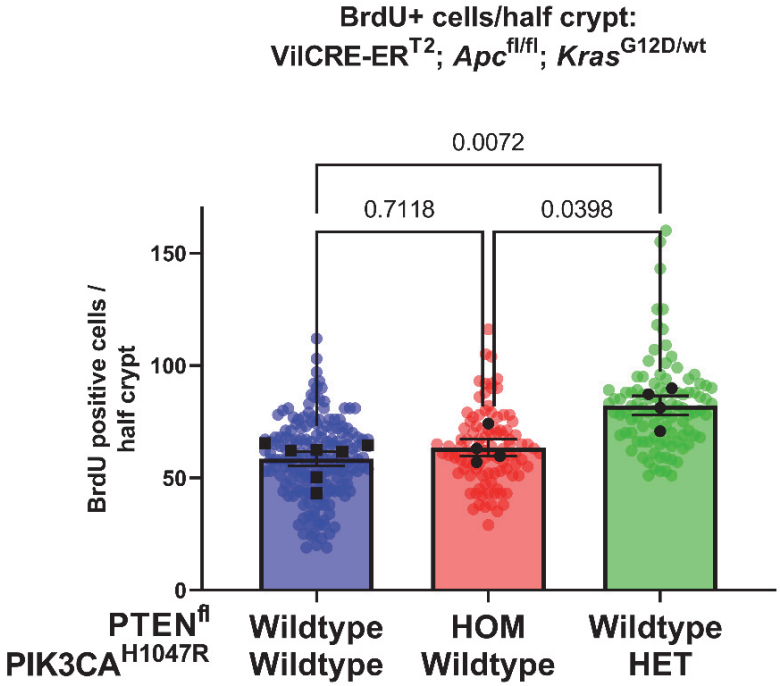

Figure 3-72: Impact of PI3-Kinase-hyperactivation on proliferation immediately post *Apc*-loss in the context of *Kras* mutation. Mice were administered 80mg/kg tamoxifen once. BrdU was administered IP on day 3 post-induction, 2h before sampling. BrdU positive cells per half crypt (n=25) were quantified off histological samples. Pale coloured dots represent single half-crypts, black dots are means of biological replicates. Mean ± s.e.m. Kruskal-Wallis test, uncorrected Dunn's multiple comparison test.

Differential gene expression analysis revealed an abundance of significant changes (Figure 3-73). Here, and remarkably contrasting to the studies carried out in the absence of *Kras*^{G12D} mutation, both *Pik3ca* mutation and *Pten* deletion resulted in significant enrichment for Reactome pathways. *Pten*-KO dependent pathway enrichments are presented in Figure 3-74 and Figure 3-75, while PIK3CA mutation dependent up- and downregulated reactome pathways pathways are depicted in Figure 3-76 and Figure 3-77. Regulation of transamination was the only upregulated reactome pathway upon KO of *Pten*, while *Pik3ca* mutation most notably induced upregulation of pathways governing the metabolism of RNA. Both Pi3-Kinase hyperactivating mutations led to downregulation of extracellular matrix organisation.

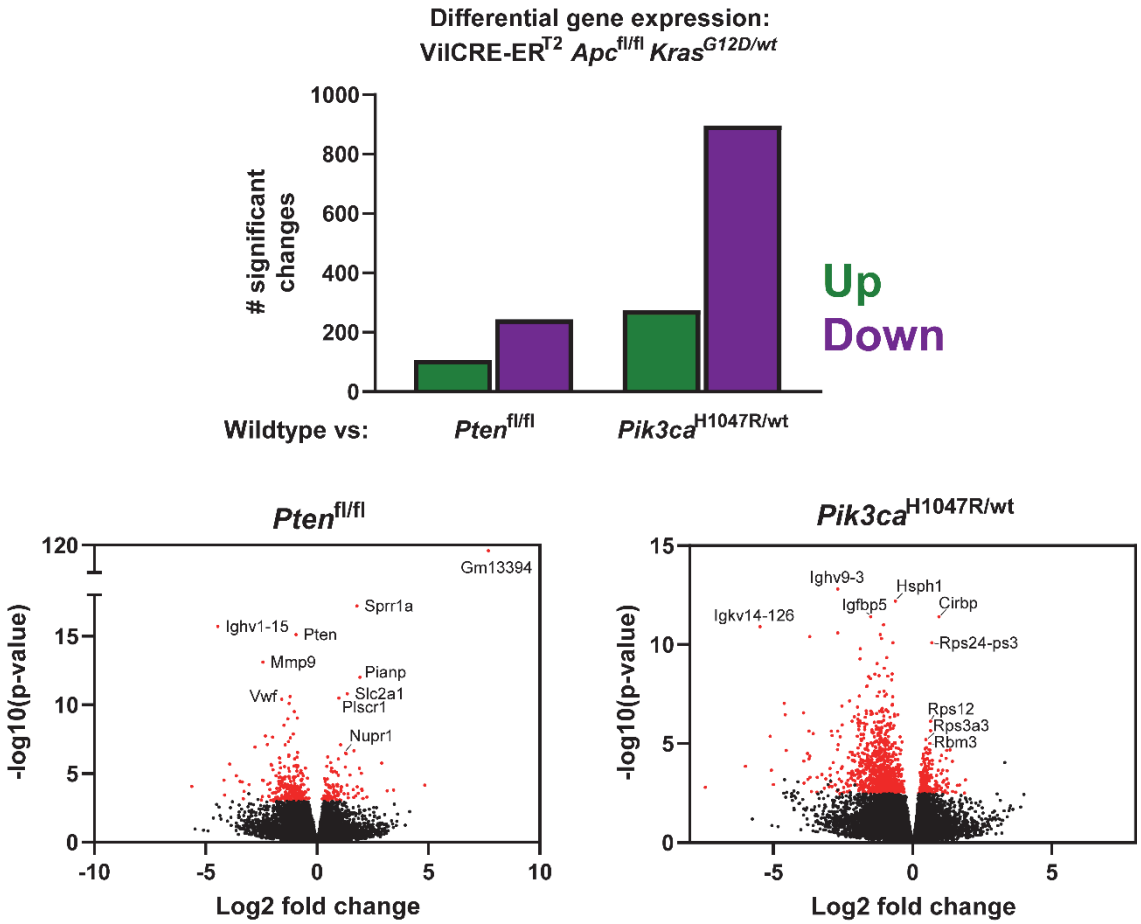

Figure 3-73: Number of significantly altered genes and volcano plot visualization in wildtype vs PI3-Kinase hyperactive models from RNA-sequencing experiment in the context of *Kras* mutation. Bar graph showing number of differentially regulated genes (adjusted p-value <0.05) following RNA-sequencing of small intestinal samples from Villin-CreER^{T2}; *Apc*$^{fl/fl}$; Kras^{G12D}; *Pten*$^{fl/fl}$ and Villin-CreER^{T2}; *Apc*$^{fl/wt}$; *Kras*^{G12D}; *Pik3ca*^{H1047R} compared to non-PI3-Kinase hyperactivated. Volcano plot: p-value was –log10 transformed and fold change was Log2 transformed. Red dot indicates p-value <0.05 and individual genes are highlighted next to their position. n=4 mice used per experimental condition. Robin Shaw and Kathryn Gilroy contributed to the generation of these data.

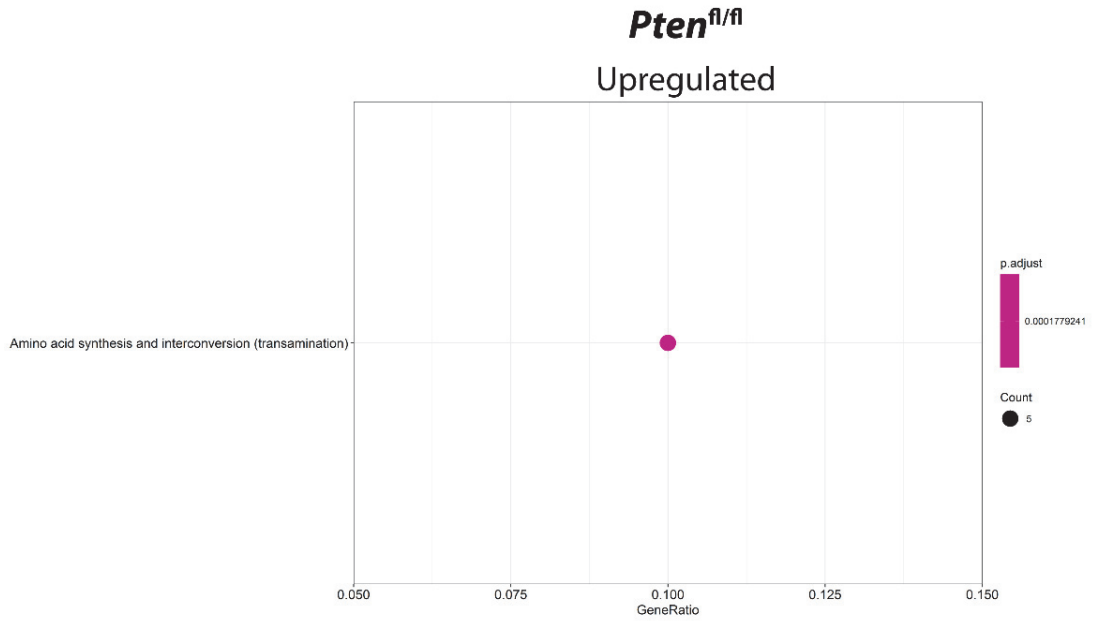

Figure 3-74: Reactome pathways upregulated in Villin-CreER^{T2}; *Apc*$^{fl/fl}$; Kras^{G12D} vs Villin-CreER^{T2}; *Apc*$^{fl/fl}$; Kras^{G12D}; *Pten*$^{fl/fl}$. RNA sequencing of Villin-CreER^{T2}; *Apc*$^{fl/fl}$ and Villin-CreER^{T2}; *Apc*$^{fl/fl}$; *Kras*$^{G12D/wt}$ SI samples and differential gene expression were performed. Reactome pathway analysis was performed to determine most significantly up- and downregulated pathways. Kathryn Gilroy contributed to the generation of these data.

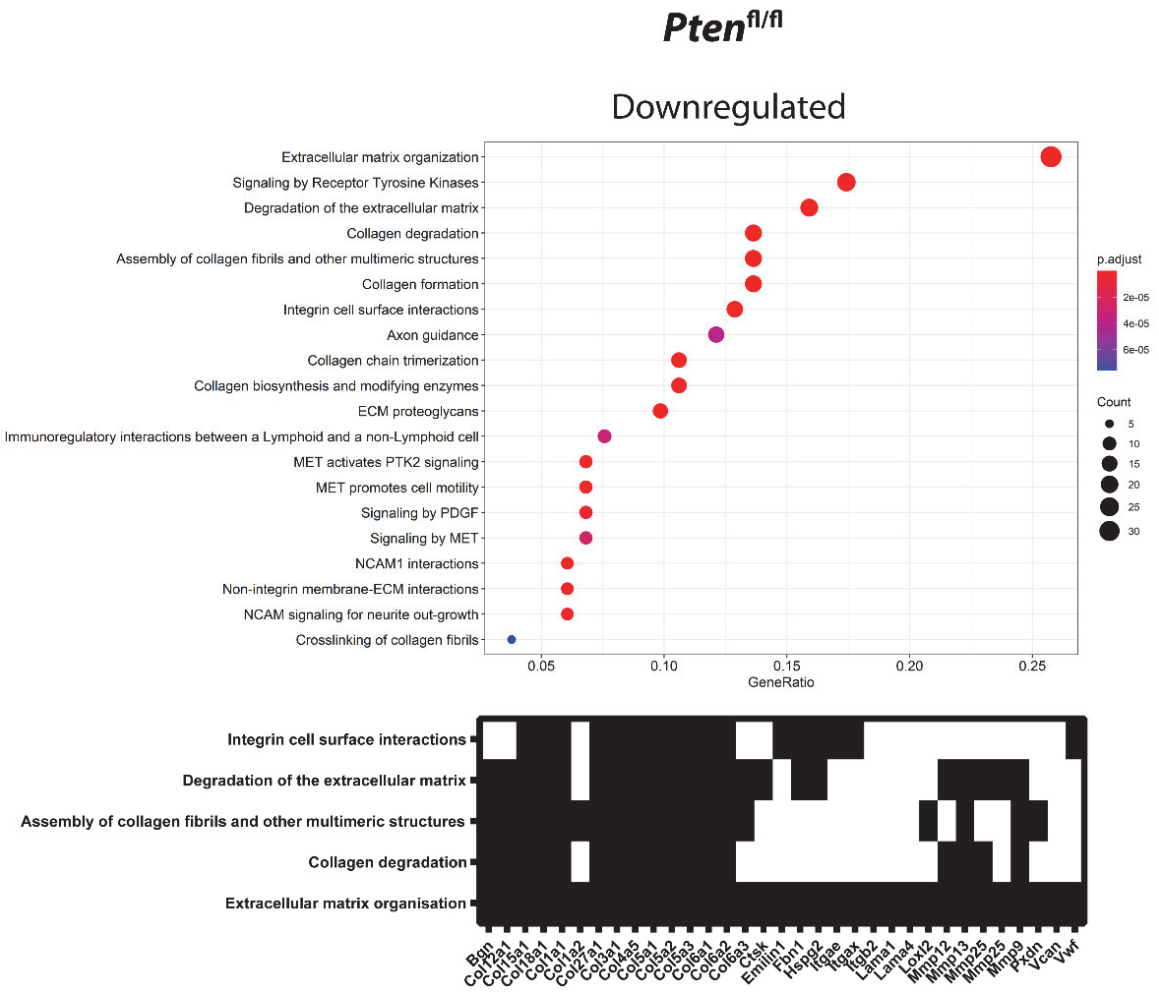

Figure 3-75: Reactome pathways downregulated in Villin-CreER^{T2}; *Apc*$^{fl/fl}$; Kras^{G12D} vs Villin-CreER^{T2}; *Apc*$^{fl/fl}$; Kras^{G12D}; *Pten*$^{fl/fl}$ and genes driving enrichment for the extracellular matrix organisation pathway. Significantly downregulated genes were subjected to Reactome pathway enrichment analysis (top). Individual genes of overlapping pathways centred around extracellular matrix organisation are depicted in black (bottom). Kathryn Gilroy contributed to the generation of these data.

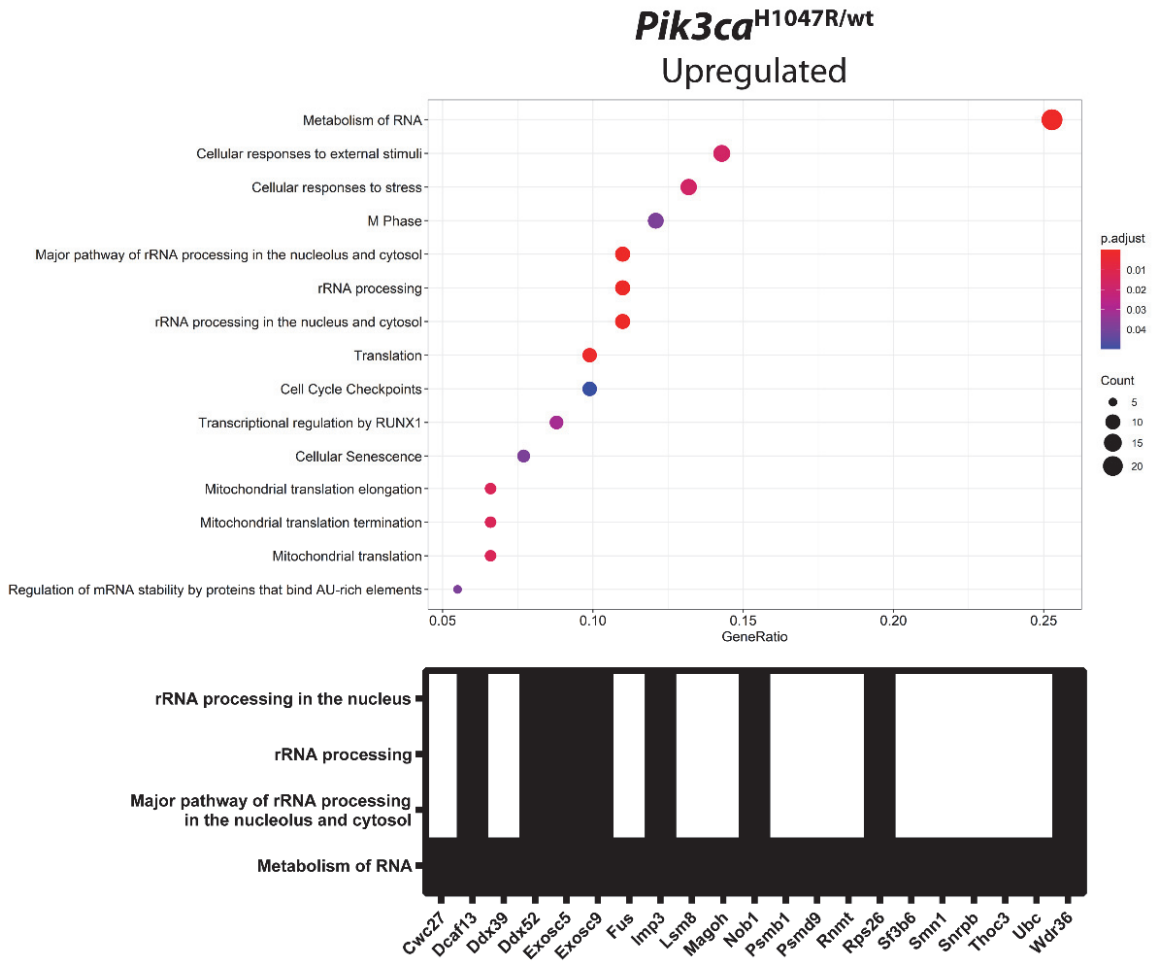

Figure 3-76: Reactome pathways upregulated in Villin-CreER^{T2}; *Apc*$^{fl/fl}$; Kras^{G12D} vs Villin-CreER^{T2}; *Apc*$^{fl/fl}$; Kras^{G12D}; *Pik3ca*$^{H1047R/wt}$. Significantly upregulated genes were subjected to reactome pathway enrichment analysis (top). Individual genes of overlapping pathways centred around metabolism of RNA are depicted in black (bottom). Kathryn Gilroy contributed to the generation of these data.

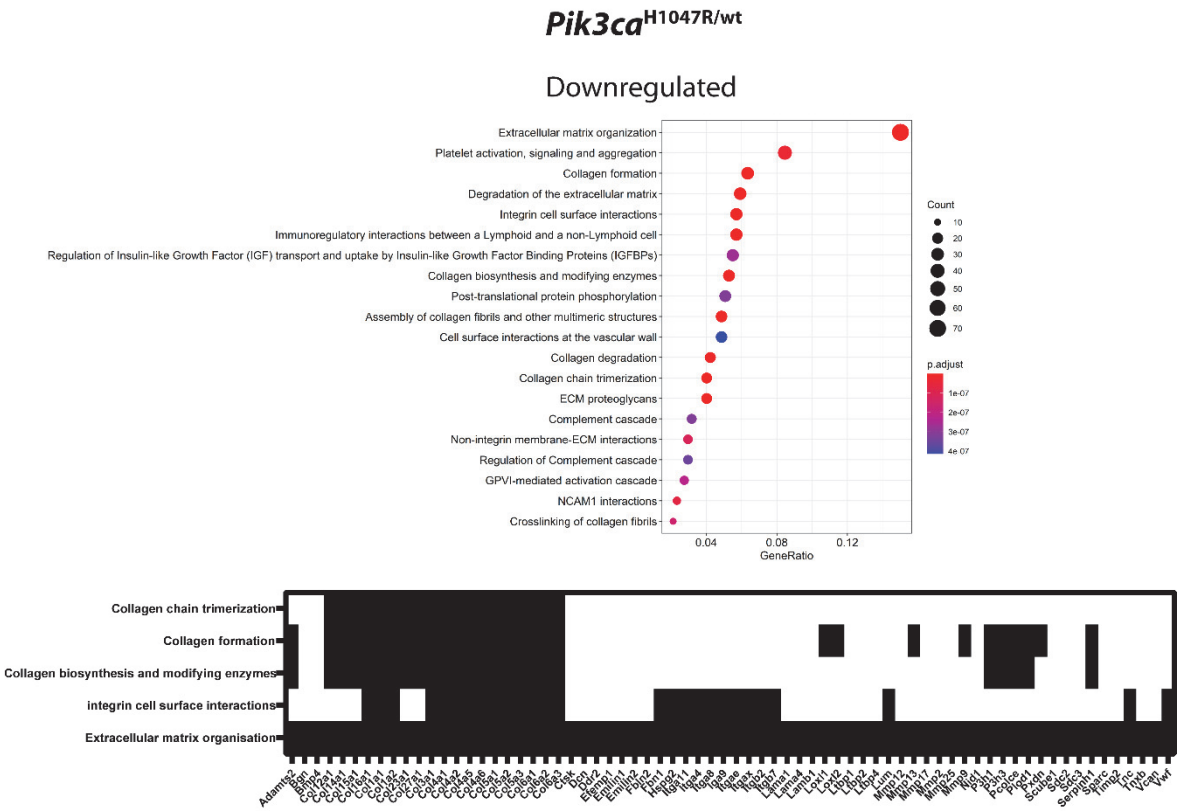

Figure 3-77: Reactome pathways downregulated in Villin-CreER^{T2}; *Apc*$^{fl/fl}$; Kras^{G12D} vs Villin-CreER^{T2}; *Apc*$^{fl/fl}$; Kras^{G12D}; *Pik3ca*$^{H1047R/wt}$. Significantly upregulated genes were subjected to reactome pathway enrichment analysis (top). Individual genes of overlapping pathways centred around extracellular matrix organisation are depicted in black (bottom). Kathryn Gilroy contributed to the generation of these data.

Again, using the full transcriptional output from these experiments, I conducted GSEA on the Hallmarks gene sets to gain a broad overview on expression networks that were altered upon introduction of PI3-Kinase hyperactivation (Figure 3-78). Commoly regulated gene sets were highlighted in red. Both, *Pten*-KO and *Pik3ca* mutation led to enrichment for Myc targets, E2F targets and mTORC1 signalling. Furthermore, unfolded protein response, DNA-damage repair, cholesterol homeostasis and G2M checkpoint were upregulated in both. *Pten*-KO resulted in enrichment for uniquely upregulation of hypoxia, glycolysis, p53 pathway, and androgen response, again indicating potential additional functions of PTEN. Downregulated gene sets were mostly overlapping between the two conditions. Epithelial to mesenchymal transition was again one of the strongest negatively enriched gene sets in both conditions.

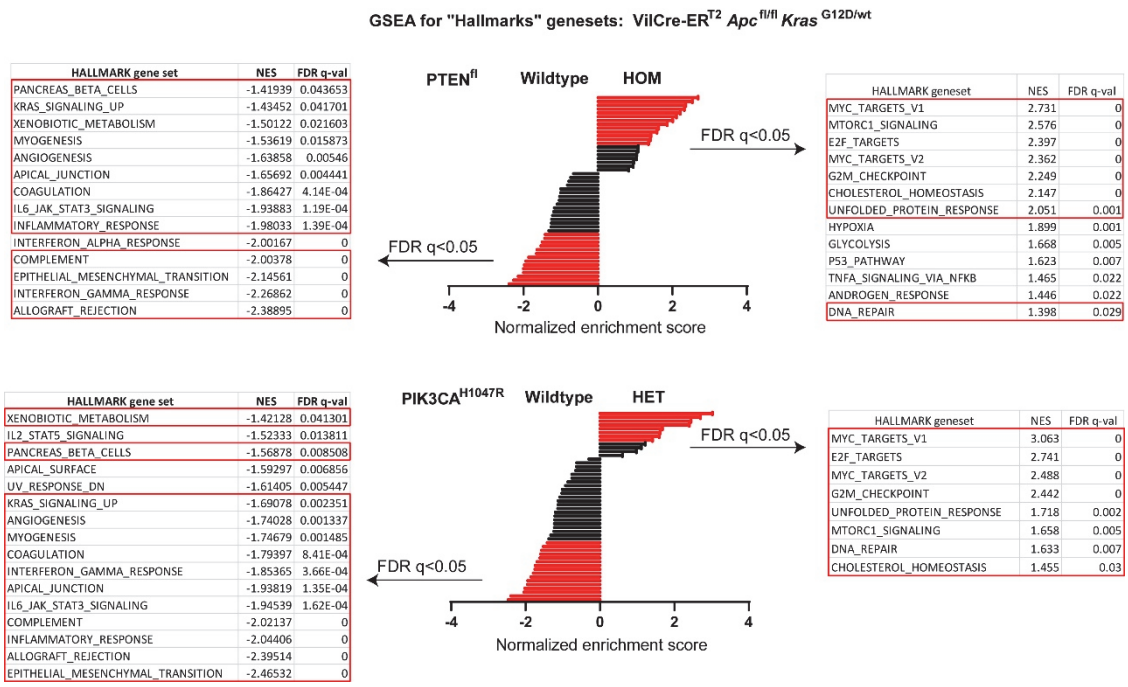

HALLMARK gene set	NES	FDR q-val
PANCREAS_BETA_CELLS	-1.41939	0.043653
KRAS_SIGNALING_UP	-1.43452	0.041701
XENOBIOTIC_METABOLISM	-1.50122	0.021603
MYOGENESIS	-1.53619	0.015873
ANGIOGENESIS	-1.63858	0.00546
APICAL_JUNCTION	-1.65692	0.004441
COAGULATION	-1.86427	4.14E-04
IL6_JAK_STAT3_SIGNALING	-1.93883	1.19E-04
INFLAMMATORY_RESPONSE	-1.98033	1.39E-04
INTERFERON_ALPHA_RESPONSE	-2.00167	0
COMPLEMENT	-2.00378	0
EPITHELIAL_MESENCHYMAL_TRANSITION	-2.14561	0
INTERFERON_GAMMA_RESPONSE	-2.26862	0
ALLOGRAFT_REJECTION	-2.38895	0

HALLMARK geneset	NES	FDR q-val
MYC_TARGETS_V1	2.731	0
MTORC1_SIGNALING	2.576	0
E2F_TARGETS	2.397	0
MYC_TARGETS_V2	2.362	0
G2M_CHECKPOINT	2.249	0
CHOLESTEROL_HOMEOSTASIS	2.147	0
UNFOLDED_PROTEIN_RESPONSE	2.051	0.001
HYPOXIA	1.899	0.001
GLYCOLYSIS	1.668	0.005
P53_PATHWAY	1.623	0.007
TNFA_SIGNALING_VIA_NFKB	1.465	0.022
ANDROGEN_RESPONSE	1.446	0.022
DNA_REPAIR	1.398	0.029

HALLMARK gene set	NES	FDR q-val
XENOBIOTIC_METABOLISM	-1.42128	0.041301
IL2_STAT5_SIGNALING	-1.52333	0.013811
PANCREAS_BETA_CELLS	-1.56878	0.008508
APICAL_SURFACE	-1.59297	0.006856
UV_RESPONSE_DN	-1.61405	0.005447
KRAS_SIGNALING_UP	-1.69078	0.002351
ANGIOGENESIS	-1.74028	0.001337
MYOGENESIS	-1.74679	0.001485
COAGULATION	-1.79397	8.41E-04
INTERFERON_GAMMA_RESPONSE	-1.85365	3.66E-04
APICAL_JUNCTION	-1.93819	1.35E-04
IL6_JAK_STAT3_SIGNALING	-1.94539	1.62E-04
COMPLEMENT	-2.02137	0
INFLAMMATORY_RESPONSE	-2.04406	0
ALLOGRAFT_REJECTION	-2.39514	0
EPITHELIAL_MESENCHYMAL_TRANSITION	-2.46532	0

HALLMARK geneset	NES	FDR q-val
MYC_TARGETS_V1	3.063	0
E2F_TARGETS	2.741	0
MYC_TARGETS_V2	2.488	0
G2M_CHECKPOINT	2.442	0
UNFOLDED_PROTEIN_RESPONSE	1.718	0.002
MTORC1_SIGNALING	1.658	0.005
DNA_REPAIR	1.633	0.007
CHOLESTEROL_HOMEOSTASIS	1.455	0.03

Figure 3-78: Gene-set enrichment analysis for the hallmark gene sets. GSEA was conducted on all hallmark gene sets after RNA sequencing. Gene sets were ranked based on their normalized enrichment score and significantly altered gene sets are depicted as a red bar and listed in the table next to the bar graphs FRD = False discovery rate. NES = normalized enrichment score. Overlapping gene sets are highlighted in red.

3.8.3 Discussion

In summary, I have shown that while *Kras* mutation did not cause hyperproliferation, it had a profound impact on the transcriptome of the *Apc* deficient intestinal epithelium. In the *Kras* mutant context, additional *Pten*-KO did not increase proliferation, while *Pik3ca* mutation did. The transcriptional profiles were significantly altered upon PI3-Kinase hyperactivation which was in contrast to the *Kras* wildtype context.

Lack of increased proliferation in the *Kras* mutant vs wildtype SI was unexpected, as previous data from the lab suggests that *Kras* mutation would lead to an increase (Cammareri *et al.*, 2017; Knight *et al.*, 2021; Najumudeen *et al.*, 2021). Crypts in Villin-CreER^{T2}; *Apc*$^{fl/fl}$ controls in this experiment contained more proliferative cells compared to previous experiments in the lab, which might have masked the impact of *Kras* mutation on proliferation. “Short term” experiments are designed to capture the phenotype at the peak of hyperproliferation. From previous experience, this is reached after three days post-induction in *Kras* mutant guts, and four days post-induction in *Kras* wildtype. Additionally, *Kras* mutants

only received one dose of tamoxifen, while *Kras* wildtypes received two. Under equal conditions, *Kras* mutant mice may have more proliferative guts.

Mirroring the previous experiments in *Kras* wildtype *Apc*$^{fl/fl}$ mice, *Pten*-KO did not increase the amount of proliferative cells, while PI3-Kinase mutation did. This was surprising given both alleles synergize with *Kras*^{G12D} to drive tumour initiation. The key to the tumour initiation phenotype may therefore again lie in the untransformed epithelium, which is either more permissive to transformation or is more prone to lose the wildtype copy of *Apc*.

The impact of *Kras* mutation on the transcriptional landscape of *Apc*$^{fl/fl}$ "short term" mice was published previously and I could recapitulate the key findings, especially upregulation of metabolic pathways and SLC mediated transmembrane transport (Najumudeen *et al.*, 2021).

Multiple gene sets were enriched in both PI3-Kinase hyperactive conditions. The transcription factors Myc and E2F seem to be engaged more. mTORC1 signalling and cholesterol homeostasis were enriched for, indicating PI3-Kinase hyperactivation in the gut indeed culminates in increased transcription of known mTORC1 effectors. Unfolded protein response, G2M checkpoint, and DNA repair were enriched in both conditions, indicating activation of additional stress response mechanisms. Overall, this highlights the overall pro-survival and proliferative outputs of PI3-Kinase signalling, especially when combined with oncogenic *Kras*. While all gene sets of the *Pik3ca* mutants were enriched in the *Pten*-KOs, five unique gene sets were enriched in *Pten*-KOs: Hypoxia, glycolysis, p53 pathway, TNF-α signalling via NFKB, and androgen response. This again indicates more ubiquitous roles of *Pten,* which might be responsible for these additional effects and lack of hyperproliferation, similarly to data on *Kras* wildtype mice presented in chapter 3.3.

Most negatively enriched gene sets were overlapping for the PI3-Kinase hyperactive conditions. Epithelial to mesenchymal transition was strongly negatively enriched, mirroring the previous experiment in the *Kras* wildtype setting. The functional relevance of this will still have to be determined, as it could impact stromal reaction, invasion and metastasis. Orthotopic injection of organoids could yield valuable information in this context.

Cholesterol homeostasis and mTORC1 signalling were first upregulated upon *Kras* mutation and then further upregulated upon introduction of PI3-Kinase hyperactivation. This indicates PI3-Kinase signalling dependent potentiation of mTORC1 activity, a mechanism known to be crucially important for the outgrowth of *Apc* deficient cells. Functionally, this may in part be the reason for the excessive tumour initiation phenotypes observed in *Kras* and PI3-Kinase signalling co-mutated models. Furthermore, these cells might be particularly difficult to target, as mTORC1 activity seems to be stimulated from two angles and might confer these cells resistance to specific inhibitors.

These experiments were conducted on SI tissue. Given the regional differences in tumour initiation upon MAPK and PI3-Kinase mutation it would be interesting to investigate the transcriptional impact e.g. on colon tissue or in Organoids under different cell culture conditions.

3.9 Discussion

In this chapter, I presented the characterisation of multiple new PI3-Kinase signalling hyperactive mouse models of intestinal cancer.

Since all mice are of the same genetic background, I can make statements about the transformative capacity of the alleles. *Pik3ca*^{H1047R} is a weak allele in terms of impact on cell signalling and *Apc*-loss mediated oncogenic transformation, certainly when introduced heterozygously. *Pik3ca*^{H1047R} synergizes with mutations both within, and outwith the same pathway to drive intestinal cancer, as shown by concomitant KO of *Pten* and co-expression with *Kras*^{G12D}. There seems to be a “just right” level of PI3-Kinase signalling that leads tumours down an aggressive path.

Figure 3-79 shows that the addition of the alleles has non-linear effects in driving small intestinal cancer, indicating strong biological synergy. Especially crossing the *Pten*^{fl} and *Pik3ca*^{H1047R} alleles to homozygosity in the mutant *Kras* context vastly increased small intestinal tumour initiation – far outscaling the effect of the individual alleles.

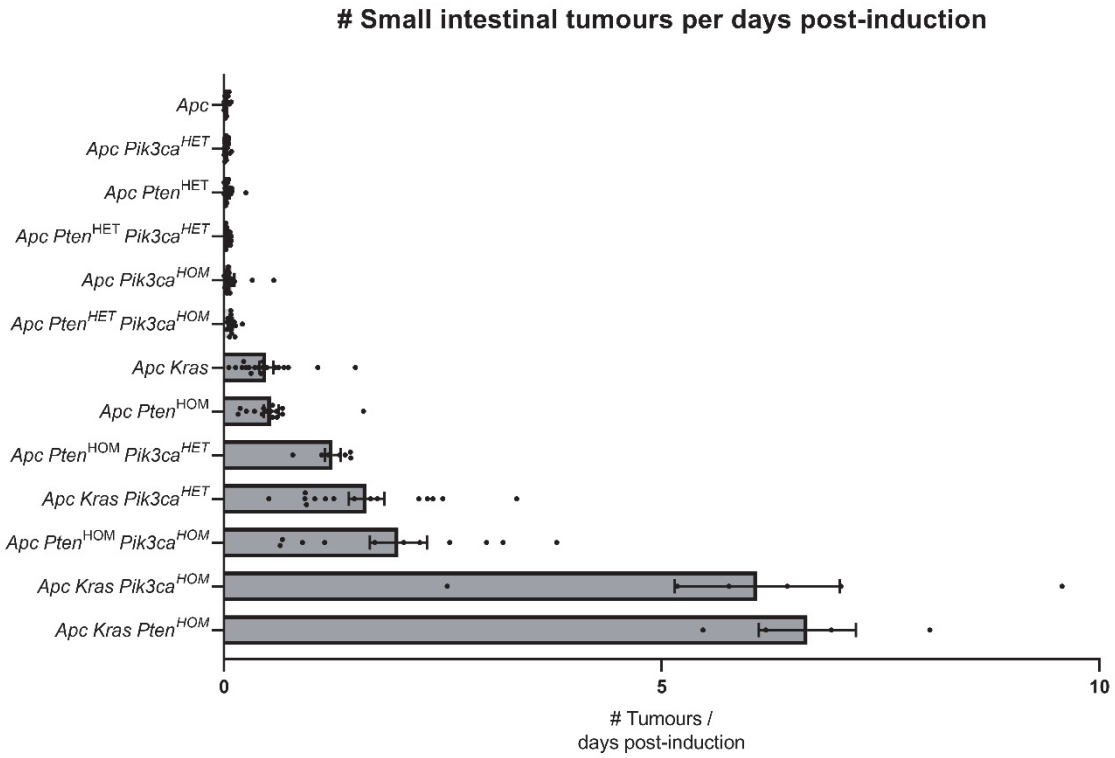

Figure 3-79: Occurrence of SI tumours per day survival post-induction in the models presented in this results chapter. Mice were sampled at endpoint and tumours scored from the processed slides. The amount of tumours was divided by days sampled post-induction with tamoxifen. All mice were Villin-CreER^{T2} positive. *Apc* = *Apc*$^{fl/wt}$ *Kras* = *Kras*^{G12D}. Mean ± s.e.m.

While PI3-Kinase hyperactivation has a profound small intestinal tumour initiation, Figure 3-80 demonstrates that *Kras* mutation is necessary for colonic tumour initiation through loss of *Apc*. Indeed, Kras mutation alone is sufficient to drive this process, but is further potentiated by concomitant PI3-Kinase hyperactivation. This indicates that even within the same organ, there is tissue specificity dictating the oncogenic capacity of the described mutations. Decline of Wnt-ligand abundance from proximal SI to distal colon is a potential reason for this. MAPK signalling may be necessary to induce a phenotype in colonic cells in which they are prone to lose *Apc* and can grow out as tumours. Furthermore, there is an increased abundance of luminal nutrients in the SI, which might aid PI3-Kinase signalling dependent tumour initiation through e.g. additional mTORC1 activation by nutrient sensing.

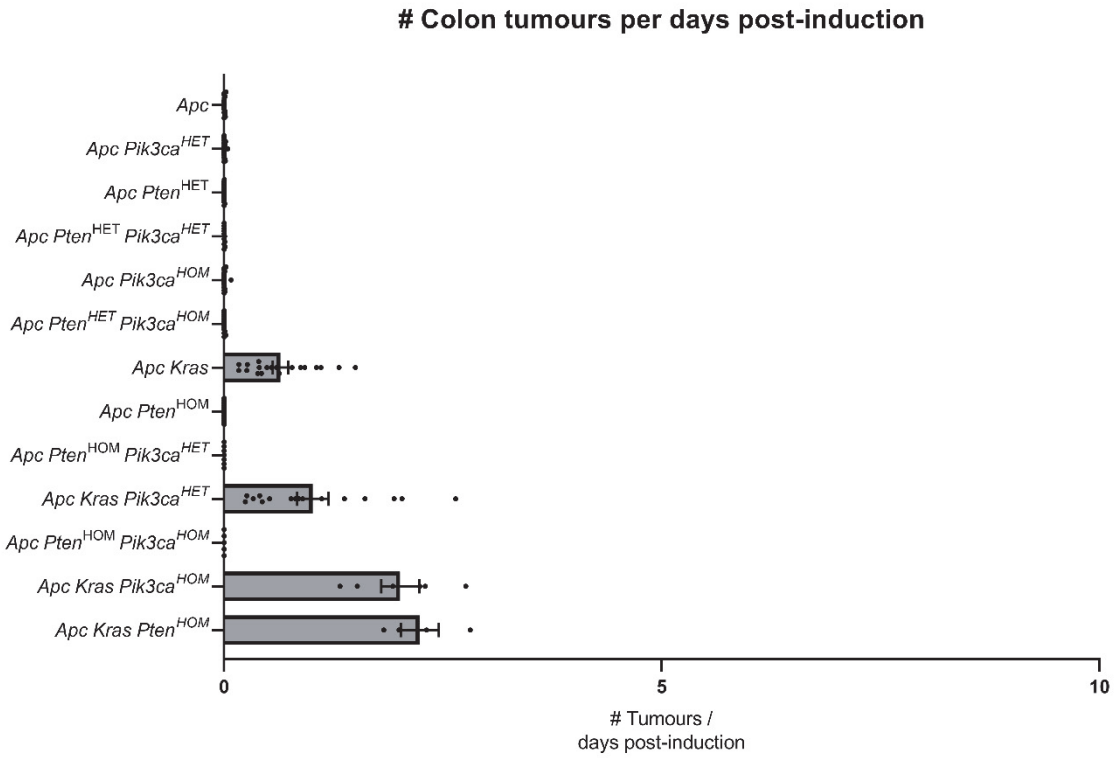

Figure 3-80: Occurrence of SI tumours per day survival post-induction in the models presented in this results chapter. Mice were sampled at endpoint and tumours scored from the processed slides. The amount of tumours was divided by days sampled post-induction with tamoxifen. All mice were Villin-CreER^{T2} positive. *Apc* = *Apc*$^{fl/wt}$. Mean ± s.e.m

There are still multiple open questions: What is the cell-type specific response to PI3-Kinase hyperactivation and why does it lead to such excessive loss of wildtype *Apc* e.g. in the context of *Pten*-KO? What is the mechanism of invasive adenocarcinoma formation, and at what stage are tumours destined to turn bad? Is there a threshold for too high PI3-Kinase signalling in the formation of advanced cancer (and/or is there a specific role for wildtype PI3-Kinase)? What is the full extent of synergy on cell physiology of Kras and PI3-Kinase co-mutation? Is the synergy of PI3-Kinase hyperactivation specific to Kras, or more generically MAPK signalling? Is there a role for PI3-Kinase signalling in metastasis? Is there a role for physiological PI3-Kinase pathway activation by e.g. insulin, especially in Kras mutant cells?

While it will take more time to answer some of the previous questions, the second half of this thesis will deal with the following: Are tumours in the newly described models sensitive to targeted inhibition of the PI3-Kinase/MAPK/mTOR signalling network?

Chapter 4 Targeted inhibition of the PI3K/MAPK/MTOR signalling network in PI3-Kinase signalling hyperactive intestinal cancer GEMMs

In the previous results chapter I have shown that hyperactive PI3-Kinase signalling, either driven by *Pik3ca*^{H1047R} mutation, or genetic ablation of *Pten*, can vastly accelerate *Apc*-loss dependent SI tumour formation, depending on the gene dose of these alleles. Introduction of oncogenic *Kras*^{G12D} induced formation of SI and colonic tumours and was synergistic with PI3-Kinase pathway hyperactivation. In this chapter, I will present data on my effort to dissect the PI3-K/MAPK/mTOR signalling network using genetic models and small molecule inhibitors (Table 4-1, Figure 4-1). Understanding tumour cell intrinsic dependence of on particular signalling nodes would be highly advantageous to inform on therapy in the clinics. Since PI3-Kinase pathway hyperactivating mutations synergized within the same pathway, but also with *Kras* mutation, I sought to investigate the roles of individual signalling molecules in PI3-Kinase signalling hyperactive models in the *Kras* wildtype, and mutant settings. In this chapter, I will address the following concepts:

- Is class 1A PI3-Kinase isoform specific inhibition effective at treating Intestinal cancer?
- What is the role of mTOR signalling in intestinal cancer models?
- Can MAPK inhibition prevent cancer initiation and outgrowth?
- What is the most effective combination therapy?

Table 4-1: Small molecule inhibitors used in this thesis

Drug	Target
AZD6244	MEK1/2
AZD2014	mTOR-Kinase
AZD5363	AKT
AZD8186	PI3-Kinase beta/delta
AZD8835	PI3-Kinase alpha/delta

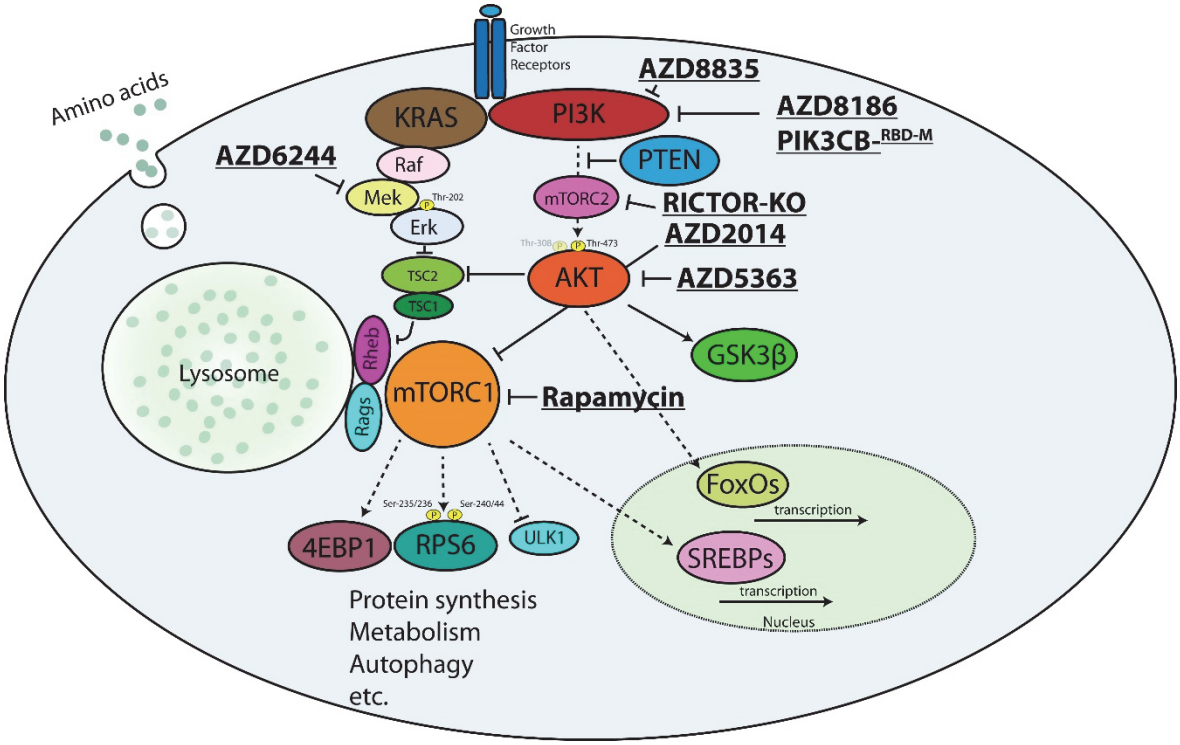

Figure 4-1: Targeted PI3-Kinase/MAPK/mTOR pathway inhibition by genetics and small molecule inhibitors. Summary of targeted inhibition utilized in this thesis in the context of PI3-Kinase/MAPK/mTOR signalling. Drugs used were AZD8835 to target PI3-Kinase alpha, AZD8186 to target PI3-Kinase beta, AZD6244 to target MEK1/2, AZD2014 to target mTOR kinase, AZD5363 to target AKT, and Rapamycin to target mTORC1. Genetic models: KO of *Rictor* to prevent mTORC2 formation and *Pik3cb-RBD* mutation to prevent Rac1/PI3-Kinase beta interaction.

4.1 Targeting PI3-Kinase isoforms in intestinal cancer GEMMs

As mentioned in the introduction, two class 1A PI3-Kinases are expressed in intestinal epithelial cells: PI3-Kinase alpha and beta. The impact of isoform-specific PI3-Kinase inhibitors in autochthonous models of intestinal cancer has not been fully explored so far. In this sub-chapter, I will describe the impact of the PI3-Kinase beta/delta inhibitor AZD8186 and the PI3-Kinase alpha/delta inhibitor AZD8835 on intestinal cancer initiation and outgrowth. Finally, I also used a PI3-Kinase beta Ras-binding domain mutant (*Pik3cb-RBD*^{mut}) mouse to dissect the impact of PI3-Kinase beta inhibition further. I will first present data on purely PI3-Kinase signalling driven models, and then describe the impact of *Kras* mutation on the response to treatment.

4.1.1 PI3-Kinase beta/delta inhibition does not prevent outgrowth of Pten deficient intestinal cancer models

In the absence of *Pten*, negative regulation of PI3-Kinase signalling is reduced. This gave me the opportunity to identify functional roles for either PI3-Kinase isoform in driving intestinal cancer by treating mice with isoform-specific inhibitors from an early stage post-induction. To this end, Villin-CreER^{T2}; *Apc*$^{fl/wt}$; *Pten*$^{fl/fl}$ mice were treated with the PI3-Kinase beta/delta specific inhibitor AZD8186 from day 5 post-induction. Drug-treated mice had to sampled after a median of 44 days (range: 38 to 56 days), compared to 42 days (range: 35 to 55 days) in vehicle treated controls (Figure 4-2). While there was a trend towards less tumours in mice treated with the PI3-Kinase beta inhibitors, this was not significantly different from vehicle controls (Figure 4-3). No colonic tumours were observed.

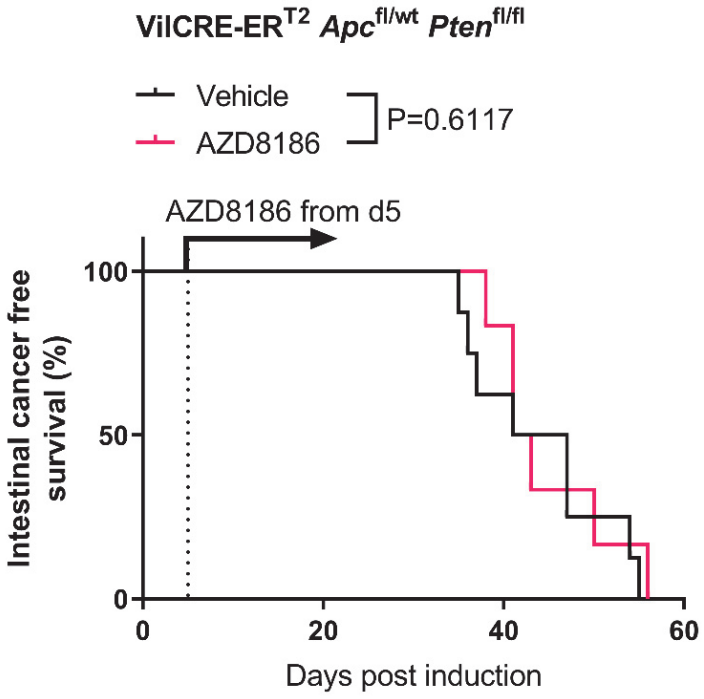

	Vehicle	AZD8186 from d5
# censored subjects	0	0
# deaths/events	8	6
Median survival	44	42

Figure 4-2: PI3-Kinase beta/delta inhibition does not extend survival of Villin-CreER^{T2}; *Apc*$^{fl/wt}$; *Pten*$^{fl/fl}$ ageing mice. Villin-CreER^{T2}; *Apc*$^{fl/wt}$; *Pten*$^{fl/fl}$ mice were dosed 2x daily with 50mg/kg AZD8186 from day 5 post-induction. Vehicle controls were dosed 0.5% HPMC + 0.1% tween 1x daily. Mice were sampled at clinical endpoint. Log-rank test.

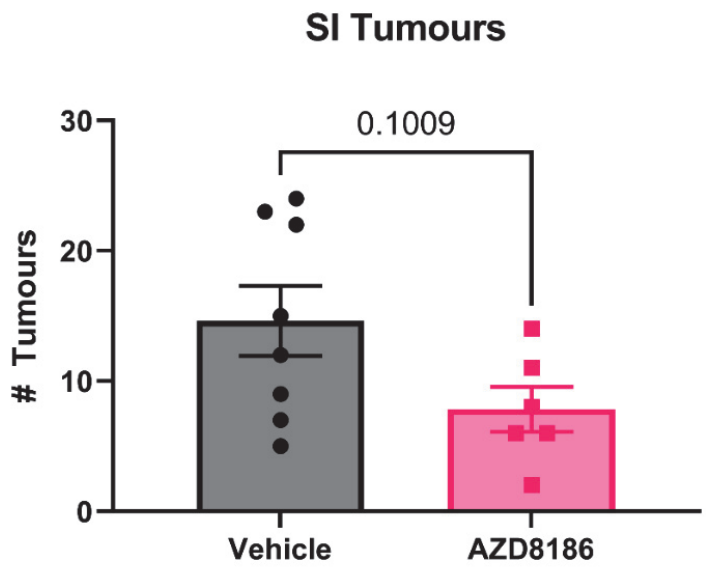

Figure 4-3: Similar amount of tumours at endpoint after AZD8186 treatment from day 5 post-induction in Villin-CreER^{T2}; *Apc*$^{fl/wt}$; *Pten*$^{fl/fl}$. Mice were sampled at endpoint and tumours were scored from processed H&E stained samples. Mean ± s.e.m. Two-sided Mann-Whitney U test.

PI3-Kinase beta/delta inhibition is therefore not sufficient to prevent intestinal cancer outgrowth in absence of *Pten*. If PI3-Kinase beta or delta signalling is important for the initiation and outgrowth of intestinal cancers, it could therefore be insufficiently inhibited, or it could be compensated for by the alpha isoform. To test involvement of PI3-Kinase alpha in this context, I proceeded to treat mice of this genotype with AZD8835.

4.1.2 PI3-Kinase alpha inhibition delays tumour formation in Villin-CreER^{T2}; Apc$^{fl/wt}$; Pten$^{fl/fl}$ ageing mice

PIK3CA mutations are more common than PIK3CB, indicating that alpha may be functionally more important in driving cancer in humans, or more prone to mutation for other reasons. Since PI3-Kinase beta/delta inhibition had limited effect in *Pten* deficient mice, I hypothesized that alpha may be a better target when it comes to PI3-Kinase inhibition. To test this, Villin-CreER^{T2}; *Apc*$^{fl/wt}$; *Pten*$^{fl/fl}$ mice were treated with the PI3-Kinase alpha/delta specific inhibitor AZD8835 from day five post-induction. They reached clinical endpoint at a median of 59 days, which was significantly later than vehicle-treated controls (Figure 4-4). Tumour number at endpoint was not significantly different (Figure 4-5). This indicates that PI3-Kinase alpha inhibition delays, but does not prevent tumour initiation and outgrowth in the *Pten*-KO setting.

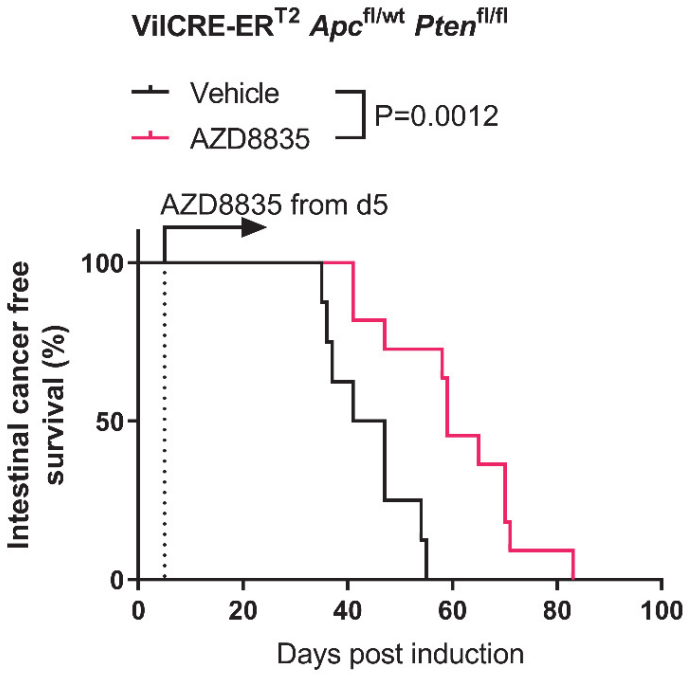

	Vehicle	AZD8835 from d5
# censored subjects	0	0
# deaths/events	8	11
Median survival	44	59

Figure 4-4: AZD8835 prolongs survival of Villin-CreER^{T2}; *Apc*$^{fl/wt}$; *Pten*$^{fl/fl}$ mice. Villin-CreER^{T2}; *Apc*$^{fl/wt}$; *Pten*$^{fl/fl}$ mice were dosed 2x daily with 25mg/kg AZD8835 from day 5 post-induction. Vehicle controls were dosed 0.5% HPMC + 0.1% tween 1x daily. Mice were sampled at clinical endpoint. David Gay contributed to these data. Log-rank test.

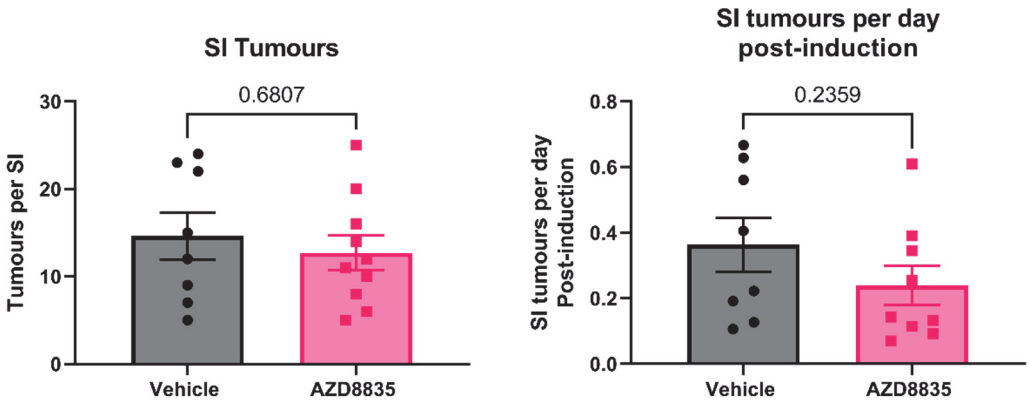

Figure 4-5: Similar amount of tumours at endpoint after AZD8835 treatment from day 5 post-induction in Villin-CreER^{T2}; *Apc*$^{fl/wt}$; *Pten*$^{fl/fl}$. Mice were sampled at endpoint and tumours were scored from the processed H&E samples. SI tumour numbers were divided by days sampled post-induction. David Gay from the lab contributed to these data. Mean ± SEM. Two-sided Mann-Whitney U test.

I have previously demonstrated marked synergy between *Pten*-KO and *Pik3ca*^{H1047R} mutation and wanted to establish whether additional PI3-Kinase mutation affects the efficacy of the PI3-Kinase alpha inhibitor.

4.1.3 *Pik3ca*^{H1047R} mutant mice still respond to PI3-Kinase alpha inhibition

In vitro, AZD8835 inhibits H1047R mutant PI3-Kinase alpha (Hudson *et al.*, 2016). To test whether the mutation would result in a differential response to the inhibitor *in vivo*, I induced Villin-CreER^{T2}; *Apc*$^{fl/wt}$; *Pten*$^{fl/fl}$; Pik3ca$^{H1047R/wt}$ mice and treated them from day 5 post-induction until they reached clinical endpoint. AZD8835 treatment resulted in a significant survival benefit (Figure 4-6). Furthermore, it resulted in a slight reduction in SI tumour number, which was significant when adjusted for time post-induction (Figure 4-7). No colonic tumours were observed.

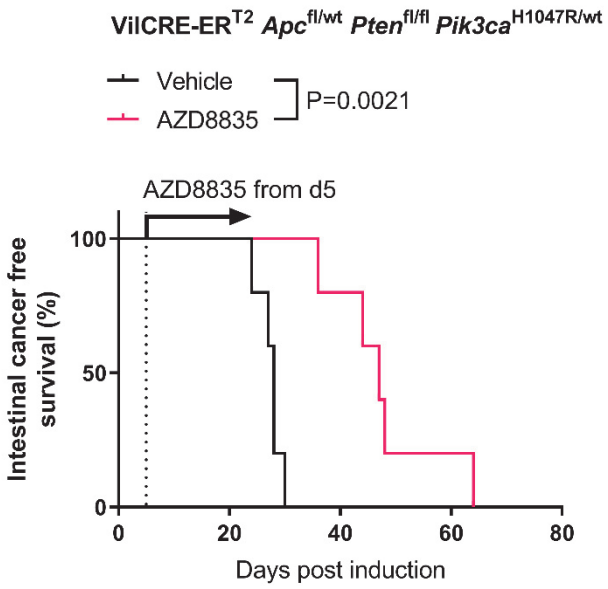

	Vehicle	AZD8835
# censored subjects	0	0
# deaths/events	5	5
Median survival	28	47

Figure 4-6: AZD8835 prolongs survival of Villin-CreER^{T2}; *Apc*$^{fl/wt}$; *Pten*$^{fl/fl}$; *Pik3ca*$^{H1047R/wt}$ mice. Villin-CreER^{T2}; *Apc*$^{fl/wt}$; *Pten*$^{fl/fl}$; *Pik3ca*$^{H1047R/wt}$ mice were dosed 2x daily with 25mg/kg AZD8835 from day 5 post-induction. Vehicle controls were dosed 0.5% HPMC + 0.1% tween 2x daily. Mice were sampled at clinical endpoint. Log-rank test.

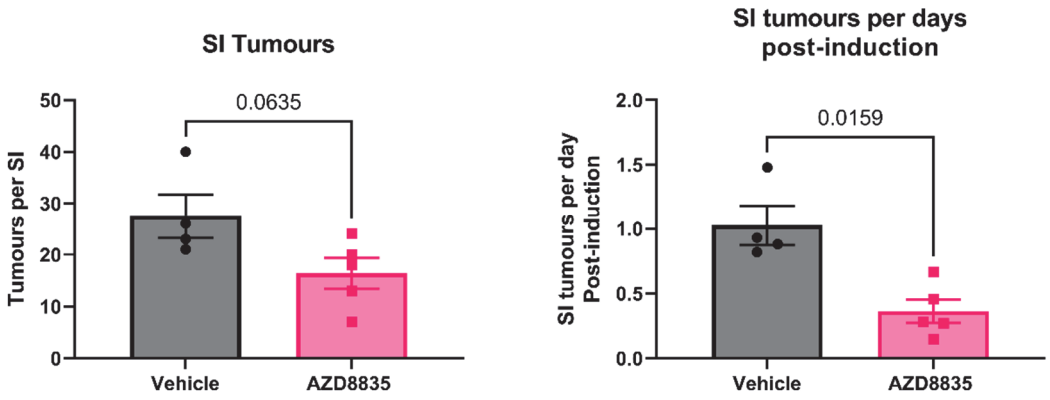

Figure 4-7: Similar amount of tumours at endpoint, less when adjusted for longer survival after AZD8835 treatment from day 5 post-induction in Villin-CreER^{T2}; *Apc*$^{fl/wt}$; *Pten*$^{fl/fl}$; *Pik3ca*$^{H1047R/wt}$ Mice were sampled at endpoint and tumours were scored from the processed H&E samples. Tumours per days post-induction ratio was calculated. Mean ± SEM. Two-sided Mann-Whitney U test.

Data presented in the previous chapter revealed further synergy between *Pten*-loss and bi-allelic *Pik3ca* mutation to drive small intestinal cancer, compared to mono-allelic *Pik3ca* mutation. To test whether bi-allelic *Pik3ca* mutation burden would induce greater dependence on PI3-Kinase alpha inhibition, I induced Villin-CreER^{T2}; *Apc*$^{fl/wt}$; *Pten*$^{fl/fl}$; *Pik3ca*$^{H1047R/H1047R}$ mice and treated them with AZD8835 from day 5 post-induction. PI3-Kinase alpha inhibition also prolonged survival in these mice (Figure 4-8) and led to reduced SI tumour number (Figure 4-9).

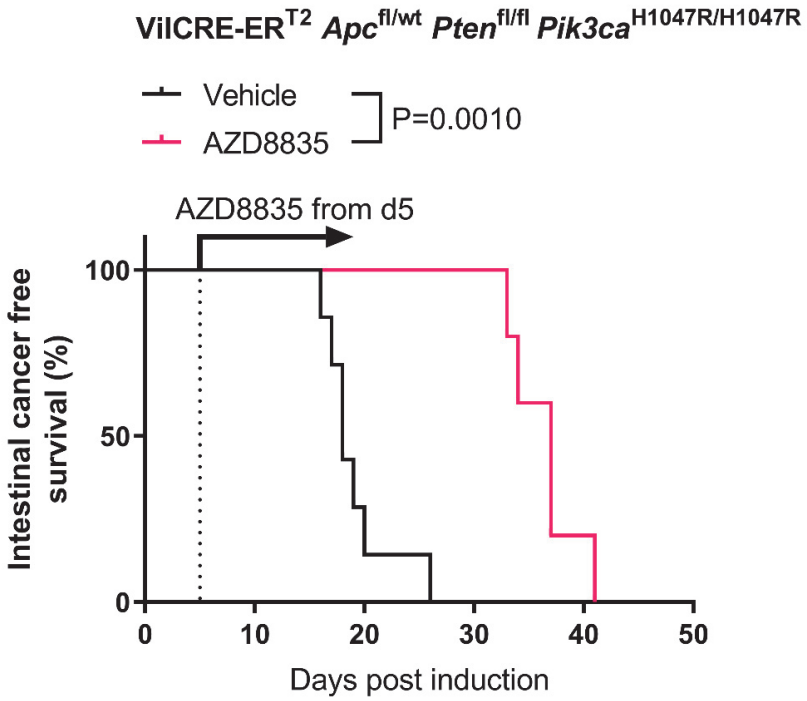

	Vehicle	AZD8835
# censored subjects	0	0
# deaths/events	7	5
Median survival	18	37

Figure 4-8: AZD8835 prolongs survival of Villin-CreER^{T2}; *Apc*$^{fl/wt}$; *Pten*$^{fl/fl}$; *Pik3ca*$^{H1047R/H1047R}$ mice. Villin-CreER^{T2}; *Apc*$^{fl/wt}$; *Pten*$^{fl/fl}$; *Pik3ca*$^{H1047R/H1047R}$ mice were dosed 2x daily with 25mg/kg AZD8835 from day 5 post-induction. Vehicle controls were dosed 0.5% HPMC + 0.1% tween 2x daily. Mice were sampled at clinical endpoint. Log-rank test.

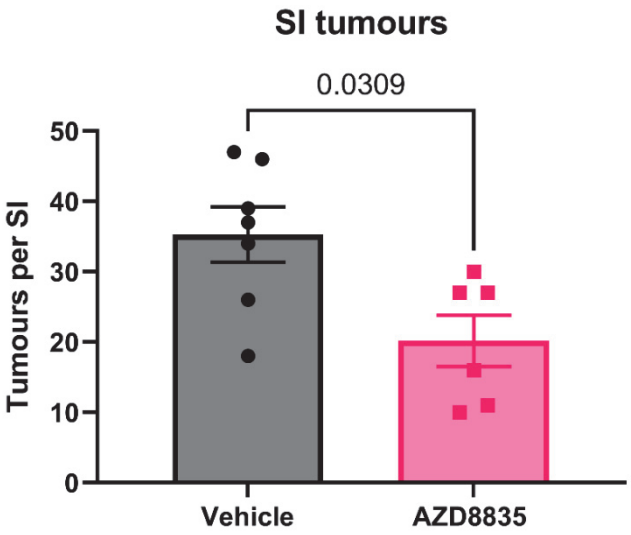

Figure 4-9: Reduced amount of tumours at endpoint after AZD8835 treatment from day 5 post-induction in Villin-CreER^{T2}; *Apc*$^{fl/wt}$; *Pten*$^{fl/fl}$; *Pik3ca*$^{H1047R/wt}$ Mice were sampled at endpoint and tumours were scored from the processed H&E samples. Mean ± SEM. Two-sided Mann-Whitney U test.

The decreased tumour number indicates that PI3-Kinase inhibition prevents tumour initiation in these models. To gain insight into the effect of the PI3-Kinase alpha inhibitor on the tumours that grew out, I conducted immunohistochemistry for PI3-Kinase- and mTOR signalling markers (Figure 4-10). These revealed no changes in vehicle treated vs AZD8835 treated mice, indicating that these tumours are resistant to the inhibitor.

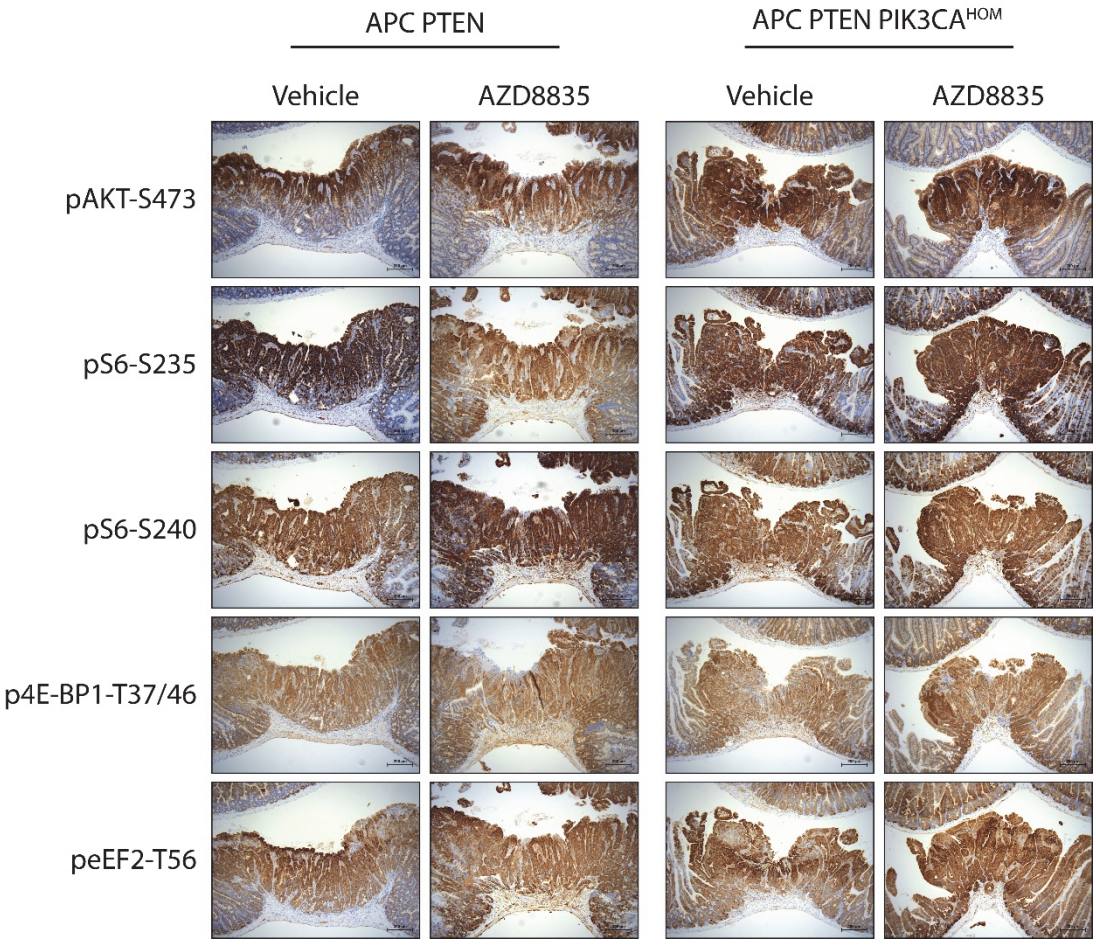

Figure 4-10: No signalling changes in AZD8835 treated small intestinal tumours in PI3-K high models.Villin-CreER^{T2}; *Apc*$^{fl/wt}$; *Pten*$^{fl/fl}$ and Villin-CreER^{T2}; *Apc*$^{fl/wt}$; *Pten*$^{fl/fl}$; *Pik3ca*$^{H1047R/H1047R}$ mice were treated with Vehicle/AZD8835 from day 5 post-induction to endpoint. Sections were stained for the indicated markers. Representative images from n=5 per condition.

4.1.4 Discussion

Using isoform-specific PI3-Kinase inhibitors, I could show that PI3-Kinase beta/delta inhibition does not prevent initiation or outgrowth of PI3-Kinase hyperactive intestinal tumours. PI3-Kinase alpha inhibition on the other hand resulted in extended survival and reduced number of tumours in PI3-Kinase hyperactive intestinal cancer GEMMs.

Previous publications, including a study from AstraZeneca, showed a dependence on PI3-Kinase beta signalling in *Pten* deficient cell lines (Hancox *et al.*, 2015). This finding does not seem to hold true in the context of *Apc*-loss mediated, *Pten*-deficient intestinal cancer as PI3-Kinase beta inhibition was not effective at preventing the initiation and outgrowth of tumours. This indicates either insufficient PI3-Kinase beta inhibition or dominance of PI3-Kinase alpha over beta in this context. Furthermore, *Apc*-loss and subsequent high Wnt signalling might overrule the dependence on PI3-Kinase signalling as a whole. Further experiments in a purely Wnt driven model, e.g. Lgr5-Cre *Apc*$^{fl/fl}$, could shed light on Wnt-signalling mediated resistance.

PI3-Kinase alpha and beta were shown to an extent to be functionally redundant, but one is usually dominant depending on the context (Al-Qassab *et al.*, 2009; Thorpe, Yuzugullu and Zhao, 2015). PI3-Kinase alpha seems to be the dominant isoform in intestinal cancer initiation and progression. This makes sense given that PIK3CA mutations far outweigh the abundance of PIK3CB mutations in humans. Investigating differential impact of PIK3CA and PIK3CB mutations in cancers may be interesting though, as their functional output may differ.

Vasan et al. showed that breast cancer patients can harbour double *PIK3CA* mutations in cis (Vasan *et al.*, 2019). This resulted in increased oncogenicity and, important for this context, increased sensitivity to PI3-Kinase inhibitors. Here I could show that survival benefit and reduction of tumour number at endpoint was more robust in *Pik3ca* mutants than wildtypes. While the setting is not exactly the same, this indicates that higher PI3-Kinase pathway activity may lead to increased sensitivity to pathway inhibitors. Given the lack of change in biomarker abundance in tumours at endpoint, even PI3-Kinase double mutant tumours eventually seem to be resistant to the PI3-Kinase alpha inhibitor. Lack of change in biomarkers at endpoint could be explained by insufficient pathway inhibition, redundancy between PI3-Kinase isoforms upon inhibition, or activation of mTOR through other stimuli such as MAPK or lysosomal nutrient signalling. To firm up these observations, and to determine whether tumours possess intrinsic or acquired resistance, treatment at a later stage would be needed. Furthermore, short-term treatment at a late stage would give more insight into the dynamics of resistance. Finally, PI3-Kinase alpha and beta co-inhibition could be trialled, although this would be predicted to be toxic.

As this work is still on going, tumour scores have not been available for all mice presented in the survival plots as the histological samples are still being processed. Tumours displayed adenomatous morphology.

Given the marked synergy between PI3-Kinase alpha and *Kras* mutation in intestinal cancer GEMMs and co-occurrence in human CRC, I next wanted to establish whether isoform specific PI3-Kinase inhibition had an impact in this setting.

4.1.5 *Kras* mutation drives resistance to PI3-Kinase alpha inhibition

I have previously shown that models driven by aberrant PI3-Kinase signalling gain a survival benefit from treatment with the PI3-Kinase alpha inhibitor AZD8835, but tumours grow out eventually showing fully activated signalling pathways. Given the role of PI3-Kinase signalling as a key downstream effector of KRAS, it is conceivable that KRAS mutation might result in potentiated PI3-Kinase signalling and an acquired sensitivity to PI3-Kinase alpha inhibition. For this reason, I sought to establish whether therapeutic resistance to AZD8835 was maintained or modified by introduction of oncogenic *Kras*. To achieve this, I used the Villin-CreER^{T2}; *Apc*$^{fl/wt}$; *Kras*$^{G12D/wt}$ model described in the previous chapter. Mice were induced as previously described, and subsequently treated from an early timepoint at five days post-induction. As opposed to their *Kras* wildtype counterparts, these mice did not experience a survival benefit following AZD8835 treatment (Figure 4-11). Interestingly, they presented with an increase in SI tumour number, but decrease in colonic tumours (Figure 4-12). The altered

location of tumours could be due to tissue specific impact on tumour initiation or differential impact upon growth of one population vs another.

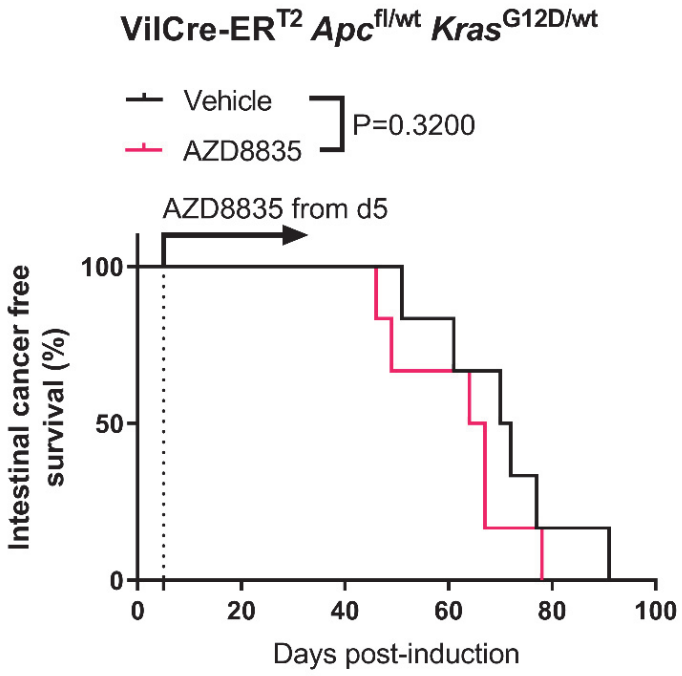

	Vehicle - d5 PI	AZD8835 - d5 PI
# censored subjects	0	0
# deaths/events	6	6
Median survival	71	65.5

Figure 4-11: PI3-Kinase alpha inhibition does not extend survival of Villin-CreER^{T2}; *Apc*$^{fl/wt}$; *Kras*$^{G12D/wt}$ ageing mice. Villin-CreER^{T2}; *Apc*$^{fl/wt}$; *Kras*$^{G12D/wt}$ mice were dosed 2x daily with 25mg/kg AZD8835 from day 5 post-induction. Vehicle controls were dosed 0.5% HPMC + 0.1% tween 2x daily. Mice were sampled at clinical endpoint. Log-rank test.

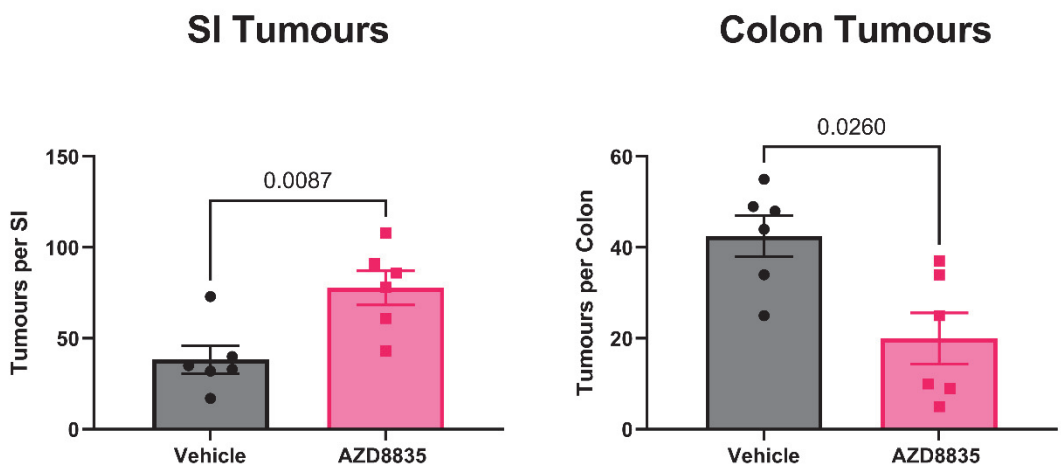

Figure 4-12: Increased SI tumour, decreased colon tumour number in AZD8835-treated Villin-CreER^{T2}; *Apc*$^{fl/wt}$; *Kras*$^{G12D/wt}$ mice at endpoint. Mice were sampled at endpoint and tumours were scored from the processed H&E samples. Mean ± SEM. Two-sided Mann-Whitney U test.

Having observed a lack of therapeutic impact in the Villin-CreER^{T2}; *Apc*$^{fl/wt}$; *Kras*$^{G12D/wt}$ model, I reasoned that PI3-Kinase inhibition may be more likely to exhibit benefit in the context of PI3-Kinase activating mutations. Given the known co-occurrence of KRAS and PIK3CA mutation in human disease, and the observed synergy between *Kras* and *Pik3ca* mutation in potentiating tumour initiation *in vivo*, I was keen to test whether this synergy could be reverted by PI3-Kinase inhibition. AZD8835 treatment from day 5 post-induction did not result in a prolonged survival compared to the untreated ageing cohort (Figure 4-13). The distribution of tumours in response to the PI3-Kinase inhibitor again shifted from

colon to SI, as observed in the Villin-CreER^{T2}; *Apc*$^{fl/wt}$; *Kras*$^{G12D/wt}$ model described previously (Figure 4-14).

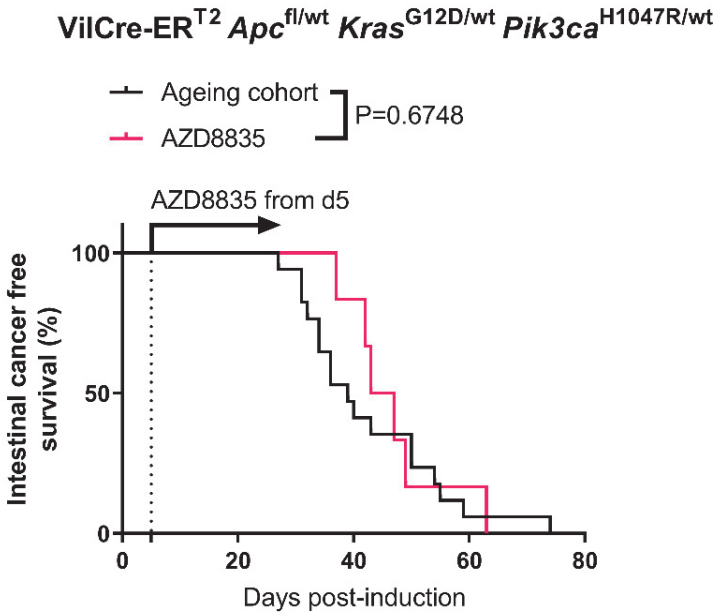

	ageing cohort	AZD8835 d5 PI
# censored subjects	0	0
# deaths/events	17	6
Median survival	39	45

Figure 4-13: PI3-Kinase alpha inhibition does not extend survival of Villin-CreER^{T2}; *Apc*$^{fl/wt}$; *Kras*$^{G12D/wt}$; *Pik3ca*$^{H1047R/wt}$ ageing mice. Villin-CreER^{T2}; *Apc*$^{fl/wt}$; *Kras*$^{G12D/wt}$; *Pik3ca*$^{H1047R/wt}$ mice were dosed 2x daily with 25mg/kg AZD8835 from day 5 post-induction. Mice were sampled at clinical endpoint. Log-rank test.

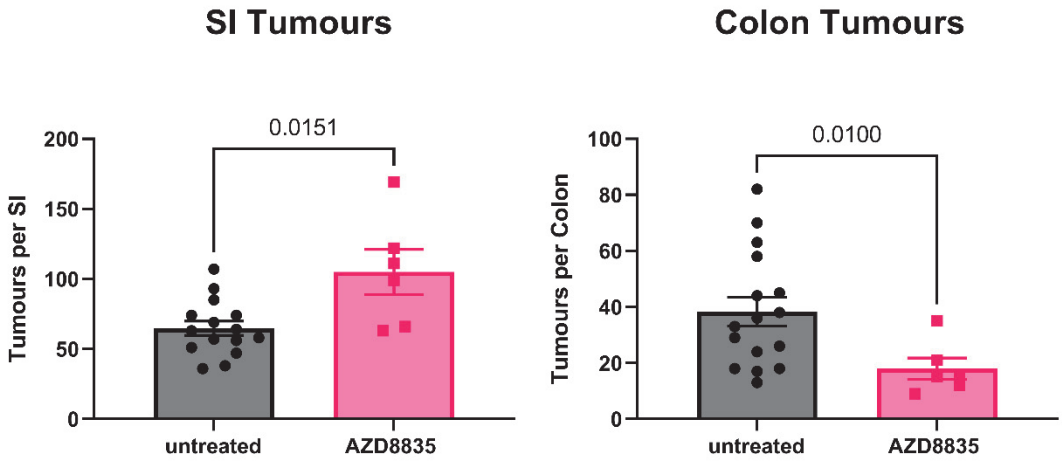

Figure 4-14: Increased SI tumour, decreased colon tumour number in AZD8835-treated Villin-CreER^{T2}; *Apc*$^{fl/wt}$; *Kras*$^{G12D/wt}$; *Pik3ca*$^{H1047R/wt}$ mice at endpoint Mice were sampled at endpoint and tumours were scored from the processed H&E samples. Mean ± SEM. Two-sided Mann-Whitney U test.

This indicates that *Kras* mutation bestows broad resistance to PI3-Kinase alpha targeting, and overcomes sensitivity to PI3-Kinase alpha inhibition identified in *Pik3ca* wild-type models in the previous section. Since homozygous *Pik3ca* mutation drove further tumour initiation in the *Kras* mutant context and resulted in a robust response to PI3-Kinase alpha inhibition, I then aimed to test whether these mice are also resistant to the PI3-Kinase alpha inhibitor. The further potentiation of PI3-Kinase activity did not drive sensitivity to AZD8835, although this is preliminary data at this stage (Figure 4-15).

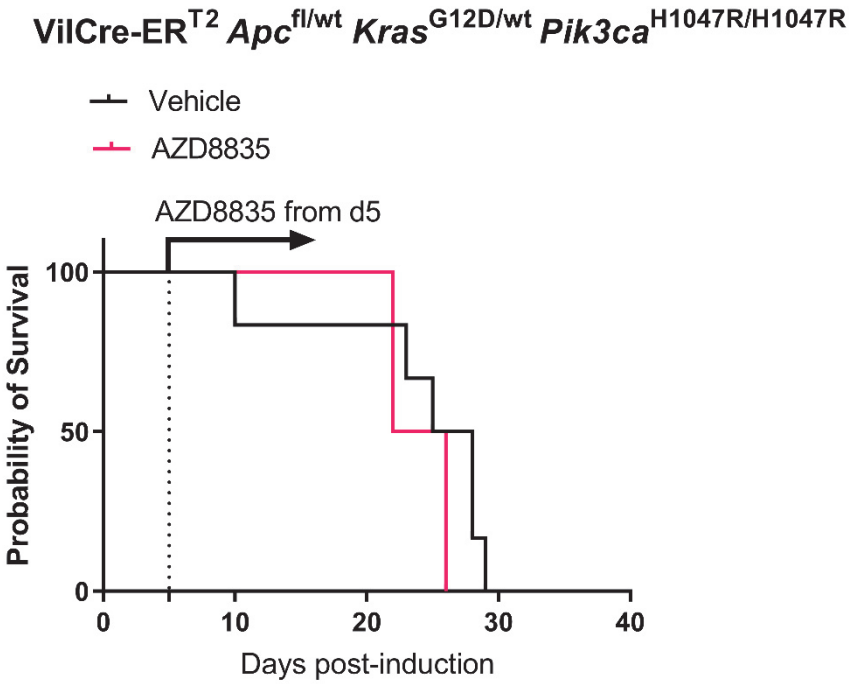

	Vehicle	AZD8835 - d5
# censored subjects	0	0
# deaths/events	6	2
Median survival	24	26.5

Figure 4-15: PI3-Kinase alpha inhibition does not extend survival of Villin-CreER^{T2}; *Apc*$^{fl/wt}$; *Kras*$^{G12D/wt}$; *Pik3ca*$^{H1047R/H1047R}$ ageing mice. Villin-CreER^{T2}; *Apc*$^{fl/wt}$; *Kras*$^{G12D/wt}$; *Pik3ca*$^{H1047R/H0147R}$ mice were dosed 2x daily with 25mg/kg AZD8835 from day 5 post-induction. Vehicle controls were dosed 0.5% HPMC + 0.1% tween 2x daily. Mice were sampled at clinical endpoint. Log-rank test.

Previous results in PI3-Kinase hyperactive, *Kras* wildtype mice indicate that tumours growing out under PI3-Kinase alpha inhibitor are phenotypically equivalent to vehicle treated mice. It is important to note that these comparisons are made at a single point, following long-term administration of the therapeutic agent, and as a result, the tumour may have overcome and outgrown any initial

sensitivity, for example any anti-proliferative effect. To test whether PI3-Kinase inhibition has an effect on proliferation in the short term in *Kras* mutant models, I turned to the Villin-CreER^{T2}; *Apc*$^{fl/fl}$ *Kras*$^{G12D/wt}$ and Villin-CreER^{T2}; *Apc*$^{fl/fl}$; *Kras*$^{G12D/wt}$; *Pik3ca*$^{H1047R/wt}$ models. AZD8835 treatment reduced amount of BrdU positive cells per half-crypt in both PI3-Kinase wildtype and PI3-Kinase mutant small intestines, indicating that the treatment has an initial growth-reducing effect, but is met with resistance following longer term treatment (Figure 4-16).

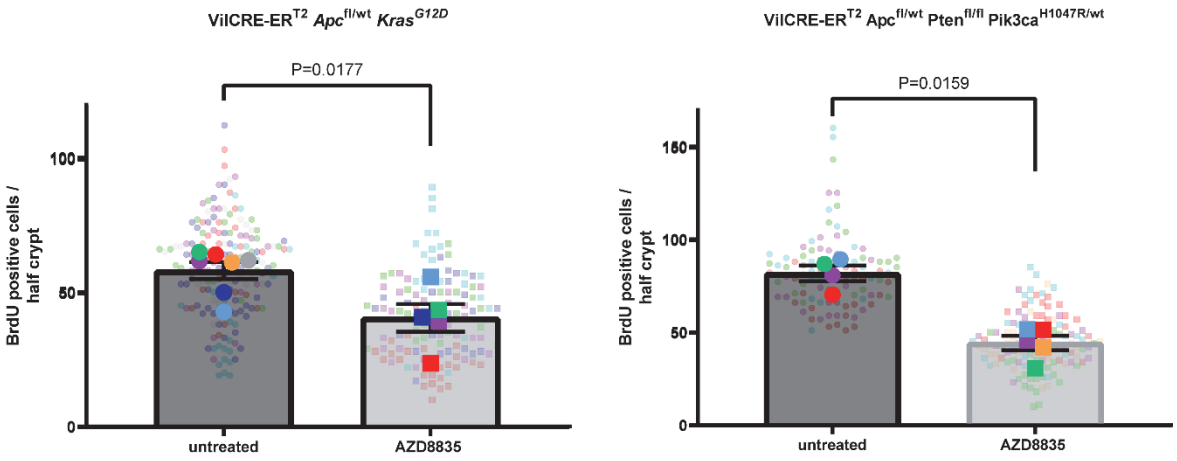

Figure 4-16: Less BrdU positive cells per half crypt in AZD8835 treated CreER^{T2}; *Apc*$^{fl/fl}$ *Kras*$^{G12D/wt}$ and Villin-CreER^{T2}; *Apc*$^{fl/fl}$; *Kras*$^{G12D/wt}$; *Pik3ca*$^{H1047R/wt}$ mice, compared to untreated control. Mice were administered 80mg/kg tamoxifen once and AZD8835 treated mice were treated with 25mg/kg AZD8835 from day 1 to 3 post-induction. BrdU was administered IP on day 3 post-induction, 2h before sampling. BrdU positive cells per half crypt (n=25) were quantified off histological samples. Pale coloured dots represent single half-crypts, large colored dots are means of biological replicates. Two-sided Mann-Whitney U test.

In summary, *Kras* mutant intestinal cancer models did not gain a survival benefit from PI3-Kinase alpha inhibition, irrespective of presence of *Pik3ca* mutation. The pattern of tumour occurrence was altered, leading to an increased number of small intestinal tumours, while reducing number of colonic tumours. Short-term treatment resulted in a reduction of proliferative cells in the SI, indicating that there is an initial anti-proliferative effect.

The aforementioned rewiring of signalling in *Kras* mutant tissue could mean that tumours in these mice are now dependent on PI3-Kinase beta rather than alpha, which was a possibility I wanted to test.

4.1.6 PI3-Kinase beta/delta inhibition prolongs survival in Villin-CreER^{T2}; *Apc*$^{fl/wt}$; *Kras*$^{G12D/wt}$ mice, likely not through the Rac1/CDC42 axis

Active KRAS has a broad effector network, including activation of PI3-Kinase beta signalling through direct activation of the Rac1-GEF TIAM1 (Lambert *et al.*, 2002). To test the functional relevance of this axis in intestinal cancer, two approaches were employed: 1) AZD8186-mediated inhibition of PI3-Kinase beta/delta, and 2) a genetically engineered mouse model in which the Ras-binding domain of PI3-Kinase beta is mutated, preventing Rac1 and CDC42 binding.

Previously generated data from the lab indicates that Villin-CreER^{T2}; *Apc*$^{fl/wt}$; *Kras*$^{G12D/wt}$ mice experienced a small, but significant a survival benefit when treated with AZD8186 from day 21 post-induction (Figure 4-17).

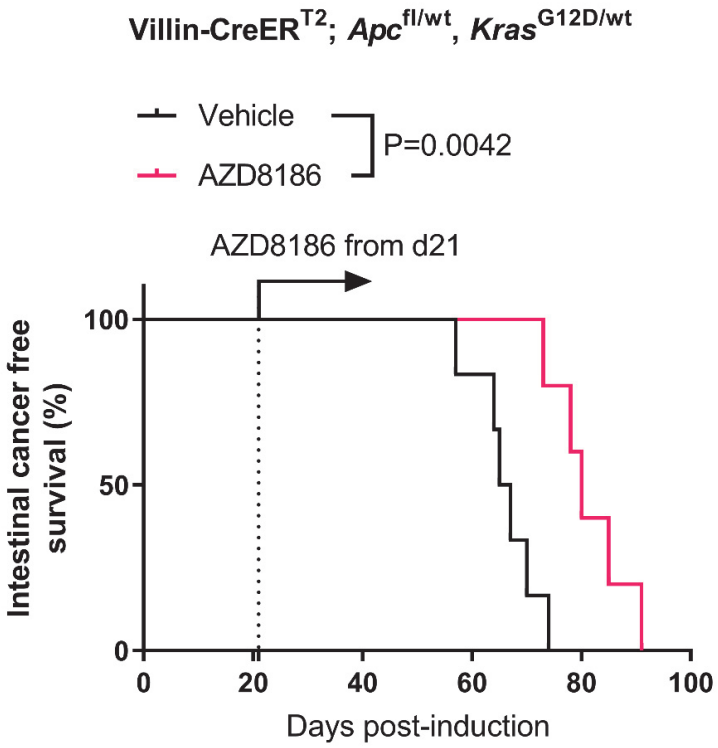

	Vehicle	AZD8186
# censored subjects	0	0
# deaths/events	6	5
Median survival	66	80

Figure 4-17: PI3-Kinase beta/delta inhibition extended survival of Villin-CreER^{T2}; *Apc*$^{fl/wt}$; *Kras*$^{G12D/wt}$ ageing mice. Villin-CreER^{T2}; *Apc*$^{fl/wt}$; *Kras*$^{G12D/wt}$ mice were dosed 2x daily with 50mg/kg AZD8186 from day 5 post-induction. Vehicle controls were dosed 0.5% HPMC + 0.1% tween 2x daily from d21 PI (n=4) or day 1 PI (n=2). Log-rank test. Mice were sampled at clinical endpoint. This data was generated by Andrew Campbell in the Sansom laboratory.

This was surprising, given the previous data showing that PI3-Kinase beta/delta inhibition had limited effect in *Kras* wildtype models. To shed light on the mechanism of the survival benefit I crossed the aforementioned PI3-Kinase beta Ras-binding domain mutant allele (*Pik3cb-RBD*^{mut}) to Villin-CreER^{T2}; *Apc*$^{fl/wt}$; *Kras*$^{G12D/wt}$ mice to generate Villin-CreER^{T2}; *Apc*$^{fl/wt}$; *Kras*$^{G12D/wt}$; *Pik3cb-RBD*$^{mut/wt}$ and Villin-CreER^{T2}; *Apc*$^{fl/wt}$; *Kras*$^{G12D/wt}$; *Pik3cb-RBD*$^{mut/mut}$ mice. This had no significant effect on survival (Figure 4-18) or tumour number and distribution (Figure 4-19).

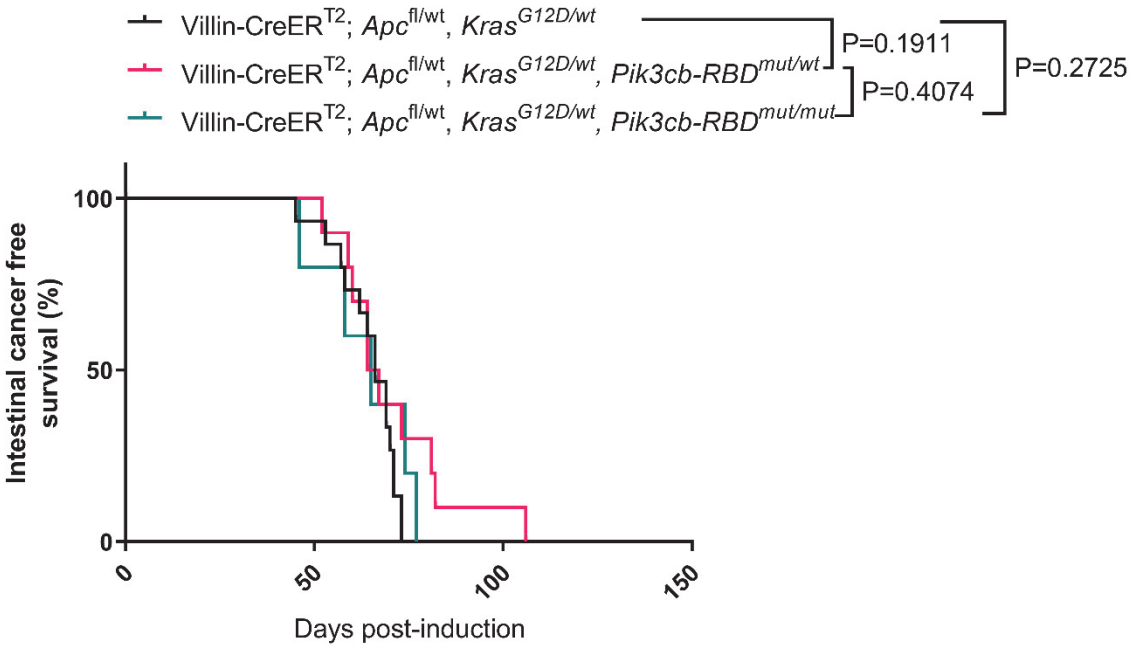

	APC KRAS	APC KRAS PIK3CB-RBDmut HET	APC KRAS PIK3CB-RBDmut HOM
# censored subjects	0	0	0
# deaths/events	15	10	5
Median survival	66	65.5	65

Figure 4-18: PI3-Kinase beta Ras-binding domain mutation did not confer a survival benefit to Villin-CreER^{T2}; *Apc*$^{fl/wt}$; *Kras*$^{G12D/wt}$ ageing mice Villin-CreER^{T2}; *Apc*$^{fl/wt}$; *Kras*$^{G12D/wt}$, Villin-CreER^{T2}; *Apc*$^{fl/wt}$; *Kras*$^{G12D/wt}$; *Pik3cb-RBD*$^{mut/wt}$, and Villin-CreER^{T2}; *Apc*$^{fl/wt}$; *Kras*$^{G12D/wt}$; *Pik3cb-RBD*$^{mut/mut}$ mice were induced with tamoxifen and aged to clinical endpoint. Log-rank test.

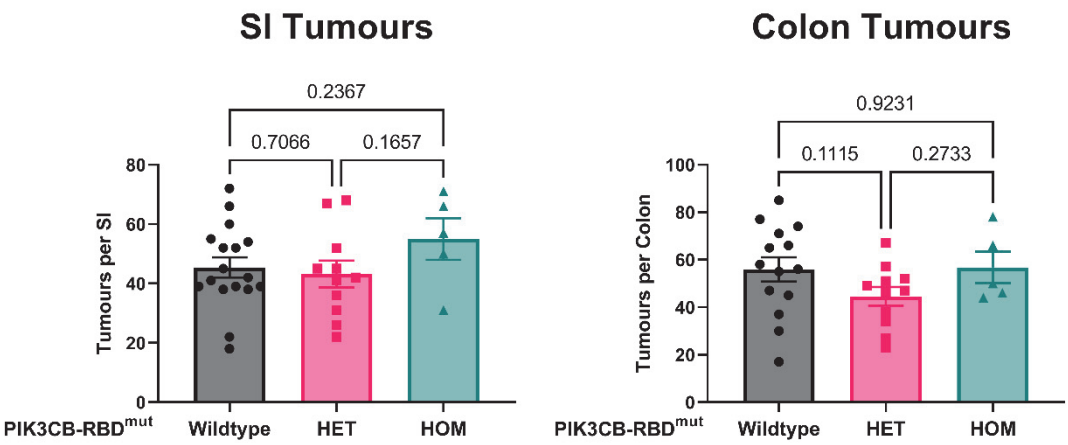

Figure 4-19: Similar tumour numbers in Villin-CreER^{T2}; *Apc*$^{fl/wt}$; *Kras*$^{G12D/wt}$; *Pik3cb-RBD*^{Mut} models. Mice were induced and aged to clinical endpoint. Tumours were scored from H&E stained histological slides. Mean ± SEM. Kruskal-Wallis test and uncorrected Dunn's multiple comparisons test.

This indicates that the survival benefit observed in AZD8186 treated Villin-CreER^{T2}; *Apc*$^{fl/wt}$; *Kras*$^{G12D/wt}$ mice was likely not due to activation of PI3-Kinase beta by the RAS effectors Rac1/CDC42.

4.1.7 Discussion

In the previous section, I showed that unlike in *Kras* wildtype models, PI3-Kinase alpha inhibition did not result in a survival benefit in *Kras* mutant mice. Tumour distribution was altered, resulting in more SI tumours but less colonic tumours. In the *Apc*$^{fl/fl}$ short-term model, PI3-Kinase inhibition reduced number of proliferative cells in the SI, indicating initial efficacy before resistance. PI3-Kinase beta/delta inhibition extended survival in Villin-CreER^{T2}; *Apc*$^{fl/wt}$; *Kras*$^{G12D/wt}$ mice, likely by a Rac1/CDC42 independent mechanism.

The observed resistance to PI3-Kinase alpha inhibition following *Kras* mutation, as has been reported for EGFR inhibitor treatment, was not entirely surprising. Lack of effect in *Kras* and *Pik3ca* co-mutated mice was unexpected though. KRAS, and by extension MAPK signalling, may therefore have functional dominance over PI3-Kinase signalling in the initiation and outgrowth of intestinal cancers. Data from *Kras*^{G12D}-driven lung cancer mouse-models indicates that PI3-Kinase mutation strongly synergizes with *Kras* mutation to drive tumorigenesis. Importantly, PI3-Kinase alpha inhibition reverted this synergy, proposing a PIP3 specific role in driving cell cycle progression in this context (Green, Trejo and McMahon, 2015).

Other factors, such as Wnt signalling, may therefore drive progression through the cell cycle in intestinal cancer, even under PI3-Kinase inhibition. Increase in SI tumours, but decrease in colonic tumours is in favour of that hypothesis, as there is a proximal to distal Wnt signalling gradient in the intestine (Leedham *et al.*, 2012). Furthermore, PI3-Kinase alpha inhibition has a well-described effect on organism-scale glucose homeostasis. PI3-Kinase inhibitors were shown to result in systemic hyperglycaemia, followed by insulin secretion. In a mouse model of pancreatic cancer, this was functionally relevant, and could be suppressed with a ketogenic diet that prevents this insulin feedback (Hopkins *et al.*, 2018). Therefore, in addition to cell-intrinsic resistance, this could provide intestinal cancer cells a proliferative signal.

PI3-Kinase beta is a downstream effector of RAS signalling. Canonically, this is described as occurring through direct binding of Ras-GTP to the Rac1 GEF TIAM1 (Lambert *et al.*, 2002), although a PIP3 dependent pathway through P-Rex1 and 2 also exists (Welch *et al.*, 2002). By utilizing a *Pik3cb* Ras-binding domain mutant I could show that Rac1 dependent activation of PI3-Kinase beta is likely not an important factor in *Kras* driven intestinal cancer. This was surprising, as Rac1 has an important role in intestinal epithelial homeostasis (Sumigray, Terwilliger and Lechler, 2018). PI3-Kinase beta has a Rac1-independent role in KRas driven intestinal cancer, since AZD8186 treated mice gained a survival benefit. Redundancy between PI3-Kinase alpha and beta in the local production of PIP3 and activation of Rac1 could explain lack of an effect. Furthermore, AZD8186 also inhibits PI3-Kinase delta, which could either result in an immune cell phenotype, relevant for tumour outgrowth in mutant *Kras* models, or inhibit tumour cell-intrinsic PI3-Kδ signalling.

Villin-CreER^{T2}; *Apc*$^{fl/wt}$; *Kras*$^{G12D/wt}$; *Pik3ca*$^{H1047R/wt}$ mice were compared to untreated mice, as the vehicle treated cohort was still underway at the time of writing and it was thought to provide better insight than an - at the time being - underpowered comparison. As this work is still on going, tumour scores have not been available for all mice presented in the survival plots as the histological samples are still being processed.

Taken together, there seems to be a stark difference between *Kras* mutant and wildtype models in their response to PI3-Kinase inhibitor treatment. Considering

these data, it would advised not to treat *KRAS* mutant CRC patients with PI3-Kinase alpha inhibitors, irrespective of existing PIK3CA mutation. While PI3-Kinase beta/delta inhibition extended survival in the *Kras* mutant model, single agent treatment would also be predicted to be ineffective in the clinic.

Given the apparent role for PI3-Kinase signalling in driving *Apc*-loss mediated intestinal cancer, I sought to determine which downstream effectors in the PI3-K/mTOR signalling network are crucial for tumour initiation and growth. Again, this was done in *Kras* wildtype and subsequently in *Kras* mutant, PI3-Kinase signalling hyperactive models.

4.2 Targeting mTOR in PI3-Kinase hyperactive GEMMs

In chapter III, I have shown that PI3-Kinase signalling can efficiently drive initiation of *Apc*-loss dependent intestinal tumours. PI3-Kinase and mTOR signalling are closely linked, as described in the introduction to this thesis. In summary, PI3-Kinase promotes mTOR kinase activity when present in both mTORC1 and mTORC2. Following this activation, AKT is thought to convey information from mTORC2 to activate mTORC1. mTORC2 has multiple apparent roles in cellular physiology, mostly attributed to its phosphorylation of AGC-family kinases such as AKT and SGK1. Its role in intestinal cancer initiation and progression is not well understood at all, since no specific inhibitors have been available. Rapamycin-mediated mTORC1 inhibition on the other hand was shown to be effective in the treatment of *Apc* deficient cells by inhibition of translation elongation (Faller *et al.*, 2015). *Kras* mutation drove resistance to Rapamycin in the intestinal cancer setting (Knight *et al.*, 2021). It is not known whether hyperactive PI3-Kinase signalling would lead to Rapamycin resistance as well, and how *Kras* and PI3-Kinase signalling co-activation would affect response to mTOR signalling inhibition.

To shed light on the importance of these individual mTOR signalling components in intestinal cancer initiation and progression I made use of specific inhibitors and genetic KOs:

1) Inducible genetic knockout of *Rictor* was used to prevent mTORC2 formation.

2) The AKT inhibitor AZD5363 was used to prevent crosstalk between mTORC2 and mTORC1 (although AKT inhibition may have multiple additional effects).

3) mTORC1 was inhibited using Rapamycin. Rapamycin inhibits translation elongation via S6-kinase, but not 4E-BP1 dependent translation initiation.

4) AZD2014 was used to inhibit mTOR-kinase, which targets mTOR independently of the complex in which it is incorporated.

4.2.1 Rictor KO does not prevent outgrowth of tumours in Villin-CreER^{T2}; Apc$^{fl/wt}$; Pten$^{fl/fl}$ mice

Since mTORC2 is one of the immediate downstream effectors of PI3-Kinase signalling, I hypothesized that genetic depletion of *Rictor* would lead to an extension of survival in PI3-Kinase hyperactive intestinal cancer models. To test this, I crossed the *Rictor*^{fl} allele to Villin-CreER^{T2}; *Apc*$^{fl/wt}$; *Pten*$^{fl/fl}$ mice.

Surprisingly, Villin-CreER^{T2}; *Apc*$^{fl/wt}$; *Pten*$^{fl/fl}$; *Rictor*$^{fl/fl}$ reached clinical endpoint at a similar timepoint as *Rictor* wildtypes (Figure 4-20). Furthermore, *Rictor*-KO mice had an increased number of small intestinal tumours (Figure 4-21).

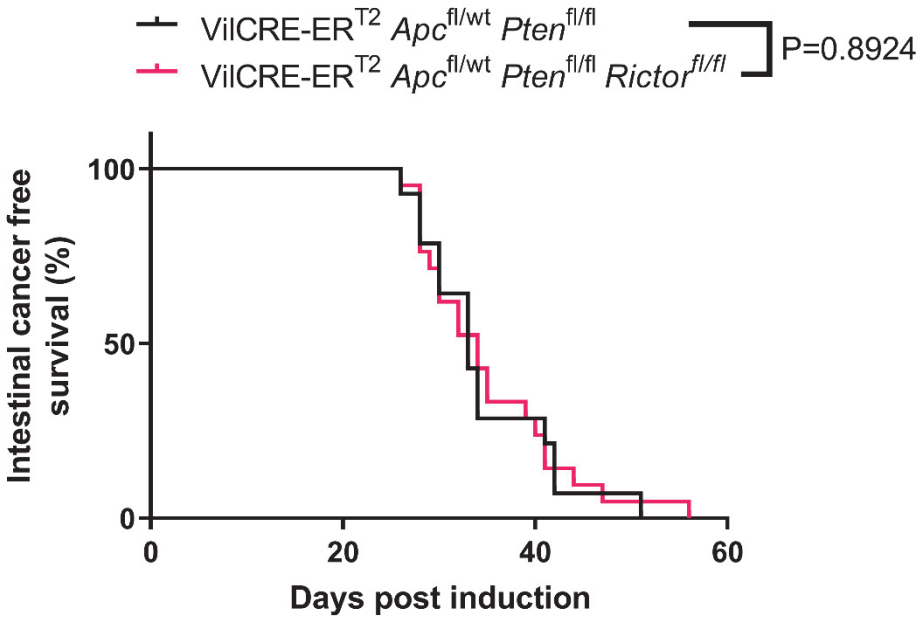

	Apc$^{fl/fl}$ *Pten*$^{fl/fl}$	*Apc*$^{fl/fl}$ *Pten*$^{fl/fl}$ *Rictor*$^{fl/fl}$
# censored subjects	0	0
# deaths/events	14	21
Median survival	33	34

Figure 4-20: Genetic depletion of *Rictor* does not alter time to clinical endpoint in the Villin-CreER^{T2}; *Apc*$^{fl/wt}$; *Pten*$^{fl/fl}$ ageing model. Villin-CreER^{T2}; *Apc*$^{fl/wt}$; *Pten*$^{fl/fl}$; and Villin-CreER^{T2}; *Apc*$^{fl/wt}$; *Pten*$^{fl/fl}$; *Rictor*$^{fl/fl}$ mice were induced and aged until clinical endpoint. Log-rank test. David Gay (ex-Sansom lab member) contributed to these data.

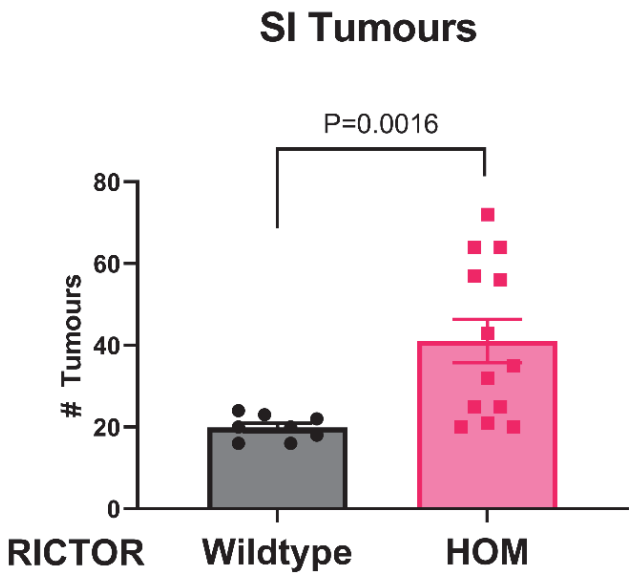

Figure 4-21: Increased amount of SI tumours at endpoint after *Rictor*-KO in the Villin-CreER^{T2}; *Apc*$^{fl/wt}$; *Pten*$^{fl/fl}$ model Mice were sampled at endpoint and tumours were scored from the processed H&E samples. Mean ± SEM. Two-sided Mann-Whitney U test. David Gay (ex-Sansom lab member) contributed to these data.

I did not manage to optimize a staining protocol to detect RICTOR via IHC. To ensure that RICTOR was indeed depleted I performed PCR to amplify the recombined allele and confirmed loss of protein via western blot. As a caveat, the recombined allele PCR was done using small intestinal and colonic 3D-cultures established from Villin-CreER^{T2}; *Apc*$^{fl/fl}$; *Kras*$^{G12D/wt}$; *Rictor*$^{fl/fl}$ mice, and cultures from Villin-CreER^{T2}; *Apc*$^{fl/fl}$; *Kras*$^{G12D/wt}$ mice were used as a control alongside DNA extracted from tails of the mice used to generate cell lines. I harvested cells, generated genomic DNA and used a previously published set of primers to amplify the recombined allele, which would only yield a product if the recombination has taken place. This confirmed presence of the recombined allele specifically in cultures established from *Rictor*$^{fl/fl}$ mice (Figure 4-22).

To ensure protein levels of RICTOR were sufficiently depleted in tumours arising in the inducible KO mice, I generated five independent tumour organoid/spheroid cultures from Villin-CreER^{T2}; *Apc*$^{fl/wt}$; *Pten*$^{fl/fl}$ and Villin-CreER^{T2}; *Apc*$^{fl/wt}$; *Pten*$^{fl/fl}$; *Rictor*$^{fl/fl}$ mice and probed for RICTOR via Western blot. Cultures generated from Villin-CreER^{T2}; *Apc*$^{fl/fl}$ mice were used as an additional control. RICTOR was not detectable in cultures generated from *Rictor*$^{fl/fl}$ mice (Figure 4-23).

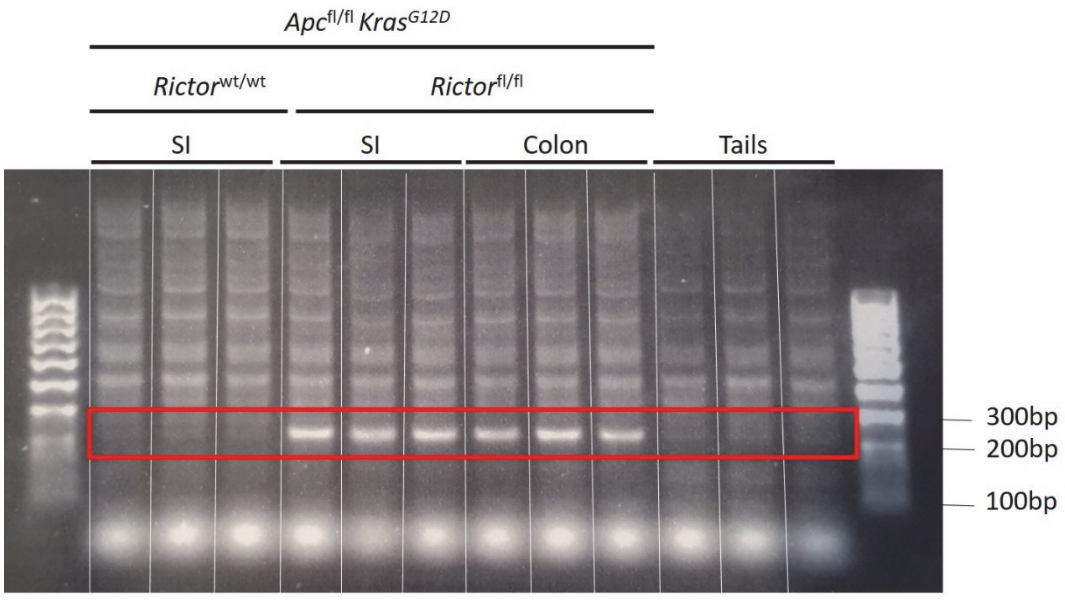

Figure 4-22: PCR amplification of recombined *Rictor*^{fl} allele Genomic DNA was generated from 3D cultures established from Villin-CreER^{T2}; *Apc*$^{fl/fl}$; *Kras*$^{G12D/wt}$ controls and Villin-CreER^{T2}; *Apc*$^{fl/fl}$; *Kras*$^{G12D/wt}$; *Rictor*$^{fl/fl}$, and the corresponding tails. Primers designed to amplify the recombined *Rictor* allele were used, products were run on a 1% agarose, EtBr containing gel, and detected via UV light. Lines indicate marker sizes. Red box indicates expected area of amplicon at 280bp.

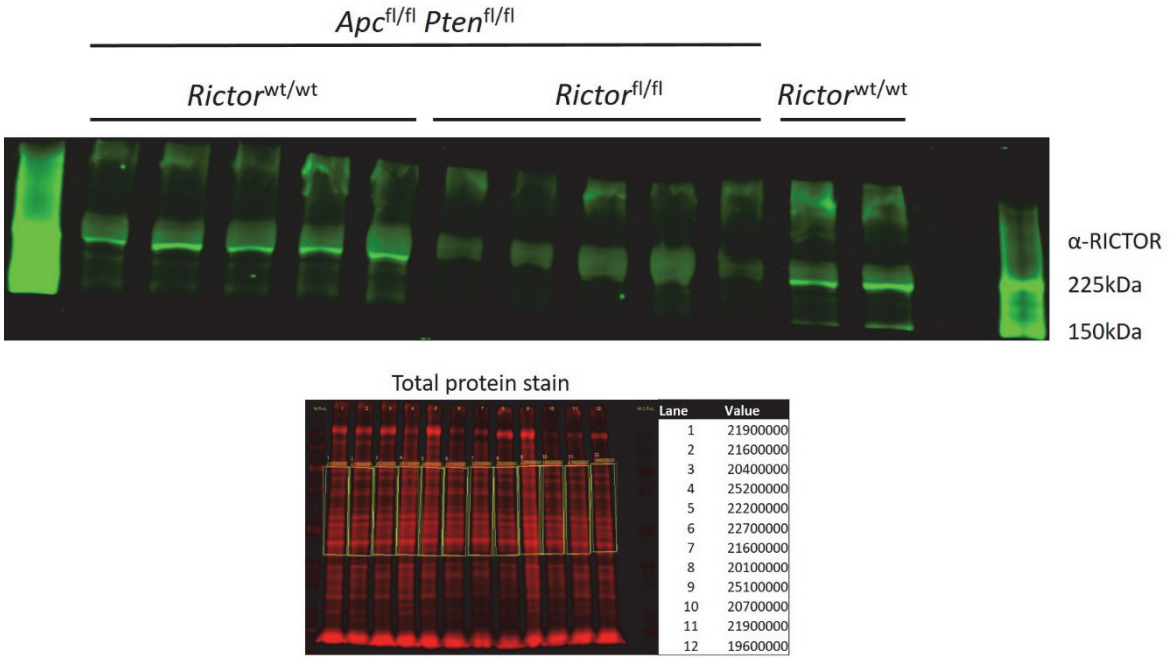

Figure 4-23: Western blot against RICTOR reveals absence of RICTOR protein in organoids/spheroids generated from tumours arising in Villin-CreER^{T2}; *Apc*$^{fl/wt}$; *Pten*$^{fl/fl}$; *Rictor*$^{fl/fl}$ mice. At clinical endpoint of ageing mice, tumours were harvested and cultured as organoids/spheroids. Cultures were harvested 3 days after seeding and protein lysates generated: Villin-CreER^{T2}; *Apc*$^{fl/wt}$; *Pten*$^{fl/fl}$ (lanes 1-5); Villin-CreER^{T2}; *Apc*$^{fl/wt}$; *Pten*$^{fl/fl}$; *Rictor*$^{fl/fl}$ (lanes 6-10). Lanes 11 and 12 are lysates from crypt cultures established from Villin-CreER^{T2}; *Apc*$^{fl/fl}$ small intestines as an additional control. Anti-RICTOR (α-RICTOR) antibody was used to detect RICTOR at an expected size of ca 200kD. Total protein was stained for and quantified to ensure similar amount of loaded protein.

Physiologically, mTORC2 may therefore have a tumour suppressive role, as indicated by the increase in small intestinal tumours upon KO of *Rictor*. Since PTEN could have PI3-Kinase pathway independent functions, I wanted to determine whether this phenotype is PI3-Kinase pathway specific and depleted *Rictor* in the context of *Pik3ca*^{H1047R} mutation.

4.2.2 *Rictor* KO is dispensable for PI3-Kinase mutant intestinal cancer outgrowth, but limits occurrence of invasive adenocarcinoma

Canonical PI3-Kinase signalling, initiated by the alpha isoform, seems to contribute to intestinal cancer initiation and progression to invasive cancer. The role of mTORC2 downstream of PI3-Kinase has not been fully established. I therefore crossed the *Rictor*^{fl} allele to Villin-CreER^{T2}; *Apc*$^{fl/wt}$; *Pik3ca*$^{H1047R/wt}$ mice to generate Villin-CreER^{T2}; *Apc*$^{fl/wt}$; *Pik3ca*$^{H1047R/wt}$; *Rictor*$^{fl/fl}$ mice. Mirroring the results presented in the *Pten* deficient background, *Rictor* KO did not result in an

altered survival (Figure 4-24), but resulted in increased small intestinal and colonic tumour numbers (Figure 4-25).

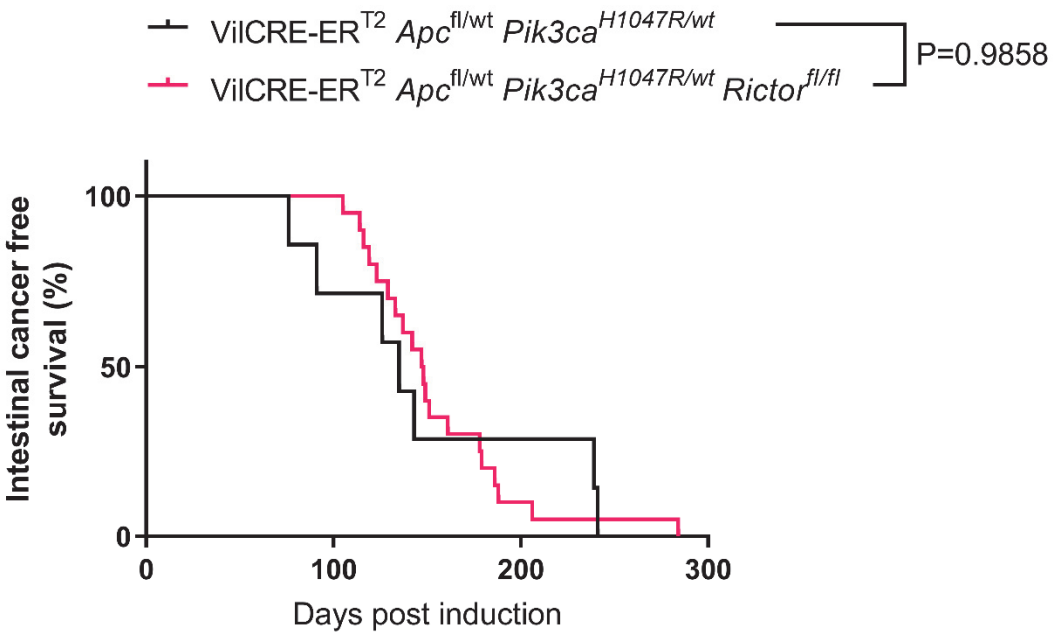

	APC PIK3CA^{HET}	APC RICTOR^{HOM} PIK3CA^{HET}
# censored subjects	0	0
# deaths/events	7	20
Median survival	135	147.5

Figure 4-24: Genetic depletion of *Rictor* does not alter time to clinical endpoint in the Villin-CreER^{T2}; *Apc*$^{fl/wt}$; *Pik3ca*$^{H1047R/wt}$ ageing model. Villin-CreER^{T2}; *Apc*$^{fl/wt}$; *Pik3ca*$^{H1047R/wt}$ and Villin-CreER^{T2}; *Apc*$^{fl/wt}$; *Pik3ca*$^{H1047R/wt}$; *Rictor*$^{fl/fl}$ mice were induced and aged until clinical endpoint. Log-rank test.

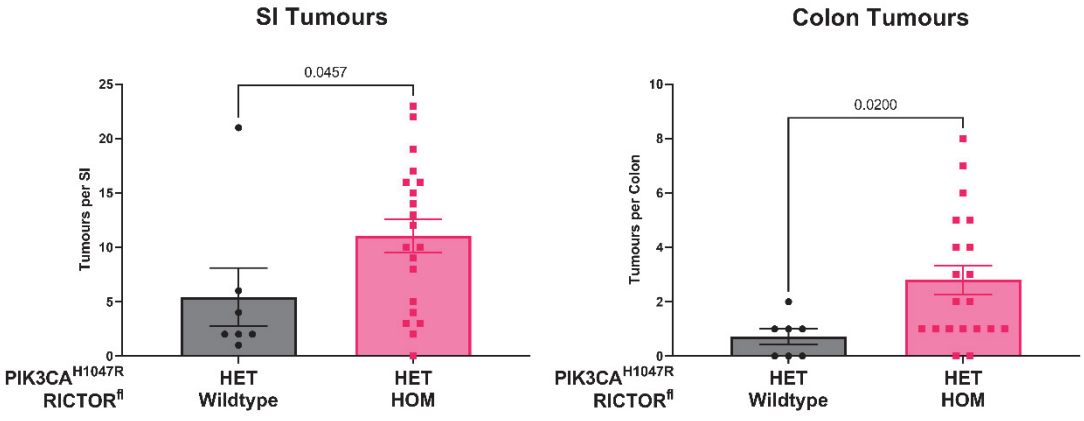

Figure 4-25: Increased amount of SI tumours at endpoint after *Rictor*-KO in the Villin-CreER^{T2}; *Apc*$^{fl/wt}$; *Pik3ca*$^{H1047R/wt}$ model Mice were sampled at endpoint and tumours were scored from the processed H&E samples. Mean ± SEM. Two-sided Mann-Whitney U test.

The previously observed phenotype is therefore likely to be directly dependent upon PI3-Kinase signalling. I have previously shown that the gene-dosage of the *Pik3ca*^{H1047R} allele has functional relevance in intestinal cancer initiation and progression. To establish the importance of mTORC2 under increasing gene-dosage of the mutant *Pik3ca* allele, I generated Villin-CreER^{T2}; *Apc*$^{fl/wt}$; *Rictor*$^{fl/fl}$ mice and further crossed the *Pik3ca*^{H1047R} allele to homozygosity in the *Rictor* deficient context.

Using Villin-CreER^{T2}; *Apc*$^{fl/wt}$; *Rictor*$^{fl/fl}$ as a baseline, both heterozygous and homozygous PI3-Kinase mutants had a significantly shorter lifespan (Figure 4-26). Importantly, this is in contrast to data presented in chapter III, as heterozygous mutation of *Pik3ca* did not result in a reduced lifespan in *Rictor* wildtype mice. This indicates that functional mTORC2 can suppress PI3-Kinase mediated intestinal cancer formation, although SI tumour numbers were only increased when Pik3ca^{H1047R} was expressed homozygously (Figure 4-27). Interestingly, unlike in *Rictor*-wildtype mice, heterozygous *Pik3ca* mutation was not associated with increased occurrence of invasive adenocarcinomas in *Rictor*-KOs (Figure 4-28). *Villin-CreER^{T2}; Apc$^{fl/wt}$; Rictor$^{fl/fl}$* mice had similar rates of invasive adenocarcinoma to Villin-CreER^{T2}; *Apc*$^{fl/wt}$ controls presented earlier.

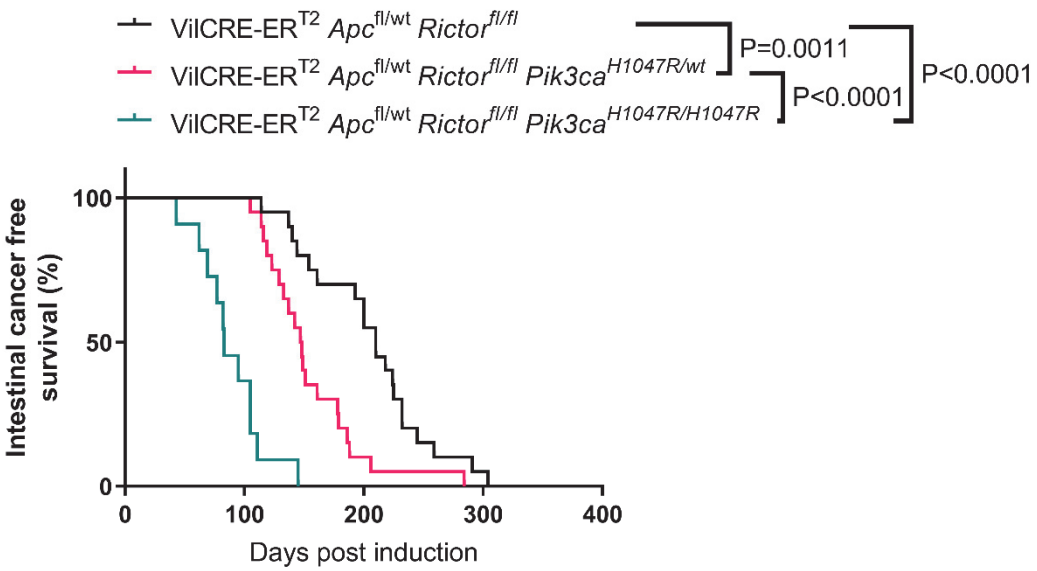

	Apc$^{fl/wt}$ *Rictor*$^{fl/fl}$	*Apc*$^{fl/wt}$ *Rictor*$^{fl/fl}$ *Pik3ca*$^{H1047R/wt}$	*Apc*$^{fl/wt}$ *Rictor*$^{fl/fl}$ *Pik3ca*$^{H1047R/H1047R}$
# censored subjects	0	0	0
# deaths/events	20	20	11
Median survival	210	147.5	95

Figure 4-26: Increased gene-dosage of *Pik3ca*^{H1047R} reduces survival of Villin-CreER^{T2}; *Apc*$^{fl/wt}$; *Rictor*$^{fl/fl}$ mice. Villin-CreER^{T2}; *Apc*$^{fl/wt}$; *Rictor*$^{fl/fl}$, and *Pik3ca*^{H1047R} mutant mice were induced with tamoxifen and aged to clinical endpoint. Log-rank test.

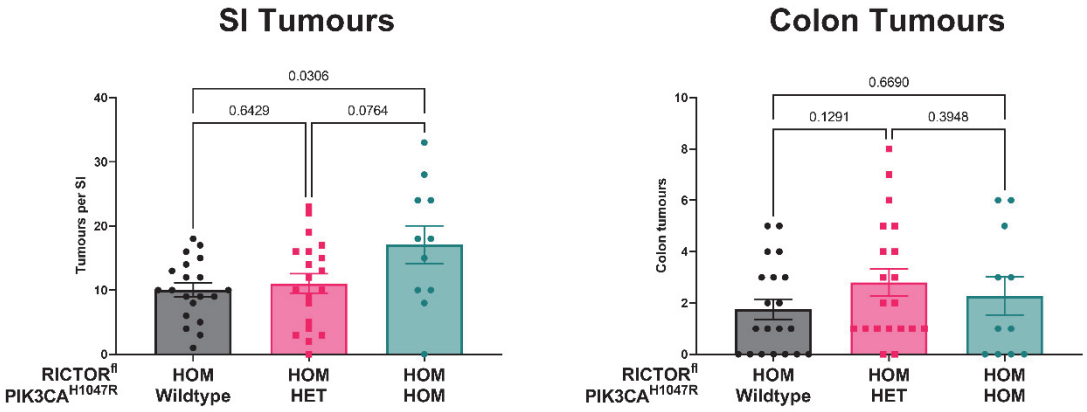

Figure 4-27: *Pik3ca*^{H1047R} mutation dependent small intestinal tumour initiation in *Rictor* deficient mice. Mice were sampled at endpoint and tumours were scored from the processed H&E samples. Mean ± SEM. Kruskal-Wallis test and uncorrected Dunn'd multiple comparisons test.

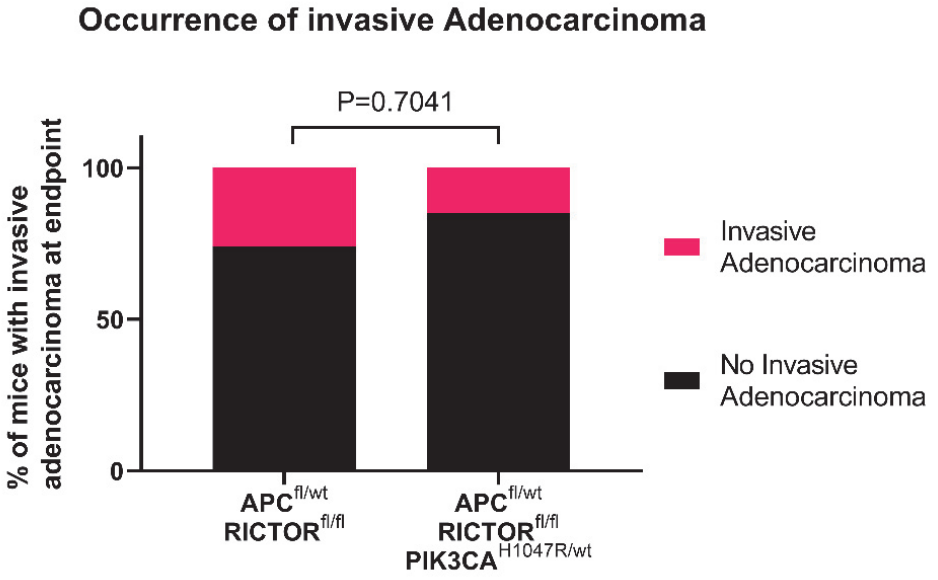

	No Invasive Adenocarcinoma	Invasive Adenocarcinoma
APC$^{fl/wt}$ RICTOR$^{fl/fl}$	13	5
APC$^{fl/wt}$ PIK3CA $^{H1047R/wt}$ RICTOR$^{fl/fl}$	17	3

Figure 4-28: *Rictor*-KO limits *Pik3ca*^{H1047R} dependent occurrence of invasive adenocarcinoma. Mice were sampled at endpoint and tumours were evaluated from the processed H&E stained slides as described in the materials and methods section.

In summary, loss of functional mTORC2 did not prevent PI3-Kinase signalling driven intestinal cancers, but physiologically might have a tumour suppressive role.

AKT, downstream of PI3-Kinase and mTORC2, has been shown to activate mTORC1 through inhibition of TSC2. The previously presented data suggests that AKT inhibition would be ineffective at preventing PI3-Kinase signalling mediated tumours and I wanted to test this hypothesis.

4.2.3 AKT inhibition does not prevent outgrowth of Pten deficient intestinal tumours

To establish whether AKT inhibition can prevent initiation or outgrowth of intestinal cancers driven by PI3-Kinase signalling, I turned to the Villin-CreER^{T2}; *Apc*$^{fl/wt}$; *Pten*$^{fl/fl}$ model. Inhibition of AKT from an early timepoint was not sufficient to prevent intestinal cancer (Figure 4-29). The AKT inhibitor-treated mice presented with an increased number of SI tumours, phenocopying the effect of *Rictor*-KO (Figure 4-30)

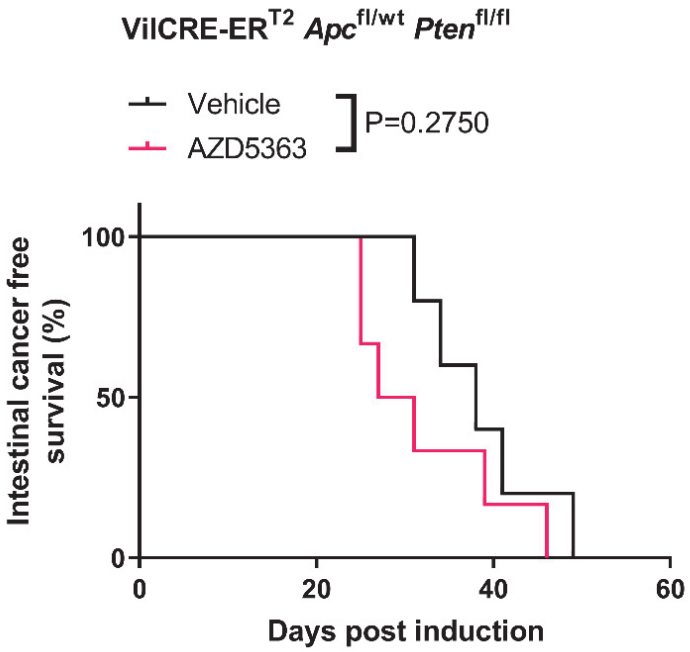

	Vehicle	AZD5363
# censored subjects	0	0
# deaths/events	5	6
Median survival	38	29

Figure 4-29: Villin-CreER^{T2}; *Apc*$^{fl/wt}$; *Pten*$^{fl/fl}$ mice did not get a survival benefit from AZD5363 mediated AKT inhibition. Villin-CreER^{T2}; *Apc*$^{fl/wt}$; *Pten*$^{fl/fl}$ mice were dosed 2x daily with 200mg/kg AZD5363 from day 5 post-induction. Vehicle controls were dosed 100µl of 10% DMSO, 25% Kleptose HPB 2x daily. Mice were sampled at clinical endpoint. Log-rank test.

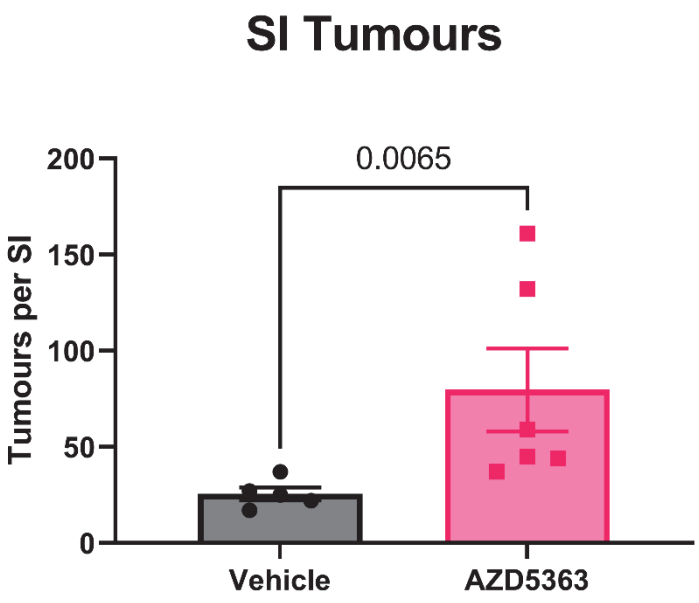

Figure 4-30: Increased amount of SI tumours at endpoint, after AZD5363 treatment from day 5 post-induction in the Villin-CreER^{T2}; *Apc*$^{fl/wt}$; *Pten*$^{fl/fl}$ model Mice were sampled at endpoint and tumours were scored from the processed H&E samples. Mean ± SEM. Two-sided Mann-Whitney U test.

AKT has multiple roles in cell physiology. It can drive anti-apoptosis, glucose metabolism, cell cycle progression, DNA-damage response, and more. The AKT dependent activation of mTORC1 is commonly assumed to be physiologically relevant, although dependent on the context (Dibble and Cantley, 2015). Lack of effect in these mice suggests that the PI3-K→mTORC2→AKT→mTORC1 axis is not crucial to drive and sustain intestinal tumour growth in the absence of *Pten*. In fact, inhibition of this axis leads to a counter-intuitive tumour initiation phenotype.

To test whether seemingly AKT-independent mTORC1 activity has relevance in PI3-Kinase high models I proceeded to treat mice with Rapamycin.

4.2.4 Rapamycin rescues late stage PI3-Kinase driven intestinal cancer models

Rapamycin is a potent mTORC1 inhibitor, with propensity to inhibit the eEF2K-mediated elongation arm of mRNA translation. Our lab has previously shown that *Apc*-deficient cells are sensitive to inhibition of this process by administration of Rapamycin (Faller *et al.*, 2015). I wanted to establish whether PI3-Kinase high models are still sensitive to Rapamycin, or whether high PI3-Kinase signalling causes resistance. To this end, I aged Villin-CreER^{T2}; *Apc*$^{fl/wt}$; *Pten*$^{fl/fl}$ to 25 days – an age at which mice would be expected to bear tumours – and commenced treatment with Rapamycin. These mice did not reach clinical endpoint within 10 weeks of treatment (Figure 4-31). Upon dissection, Rapamycin treated mice had similar number of SI tumours as the untreated cohort, although when adjusted for the time of sampling post-induction, this was significantly lower (Figure 4-32).

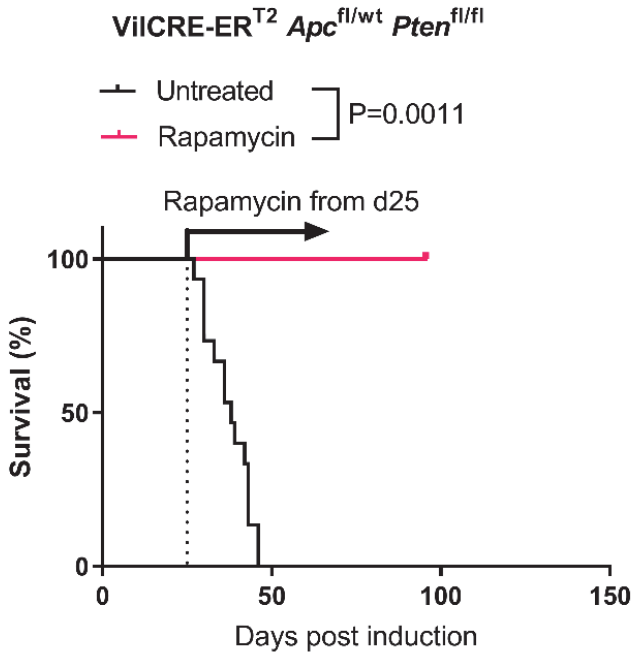

	Untreated	Rapamycin from d25
# censored subjects	0	4
# deaths/events	15	0
Median survival	38	Undefined

Figure 4-31: Rapamycin treatment rescues late stage survival of Villin-CreER^{T2}; *Apc*$^{fl/wt}$; *Pten*$^{fl/fl}$ ageing mice. Villin-CreER^{T2}; *Apc*$^{fl/wt}$; *Pten*$^{fl/fl}$ mice were dosed 1x daily with 10mg/kg Rapamycin from day 25 post-induction. Untreated mice were sampled at clinical endpoint, Rapamycin treated mice after 10 weeks of treatment. Log-rank test.

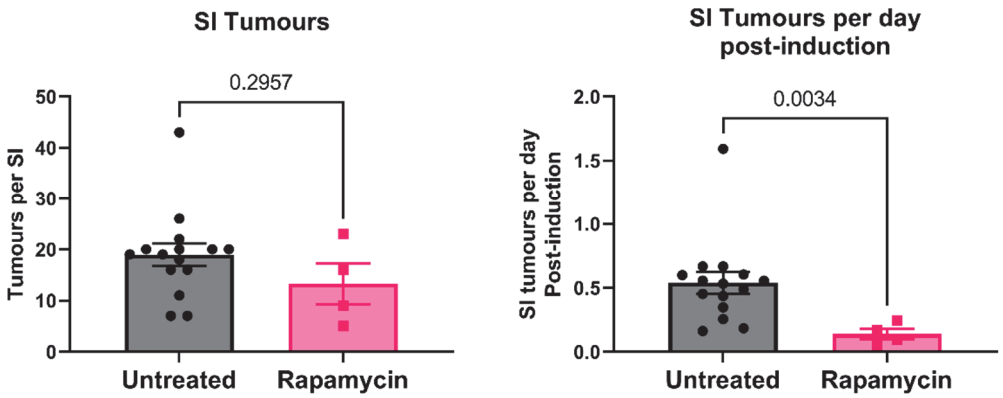

Figure 4-32: Similar number of tumours in Rapamycin treated Villin-CreER^{T2}; *Apc*$^{fl/wt}$; *Pten*$^{fl/fl}$ mice, less when adjusted for the time of sampling. Untreated mice were sampled at endpoint, Rapamycin treated mice were sampled after 10 weeks of treatment. Tumours were scored from the processed H&E samples. SI tumour numbers were divided by day of sampling post-induction. Mean ± SEM. Two-sided Mann-Whitney U test.

mTORC1 inhibition in this context therefore seems to halt the initiation of new tumours, while preventing outgrowth of the existing ones to the point at which mice have to be sampled.

I have previously shown an additive effect of PI3-Kinase mutation and loss of *Pten*. To establish whether this would have a functional relevance in the sensitivity to Rapamycin, I treated Villin-CreER^{T2}; *Apc*$^{fl/wt}$; *Pten*$^{fl/fl}$; *Pik3ca*$^{H1047R/wt}$ mice at a late stage. These mice also did not reach clinical endpoint before they were sampled after 8 weeks of treatment (Figure 4-33). After 8 weeks of treatment, Rapamycin treated mice had a similar amount of SI tumours, which was again lower when adjusted to their time of sampling (Figure 4-34).

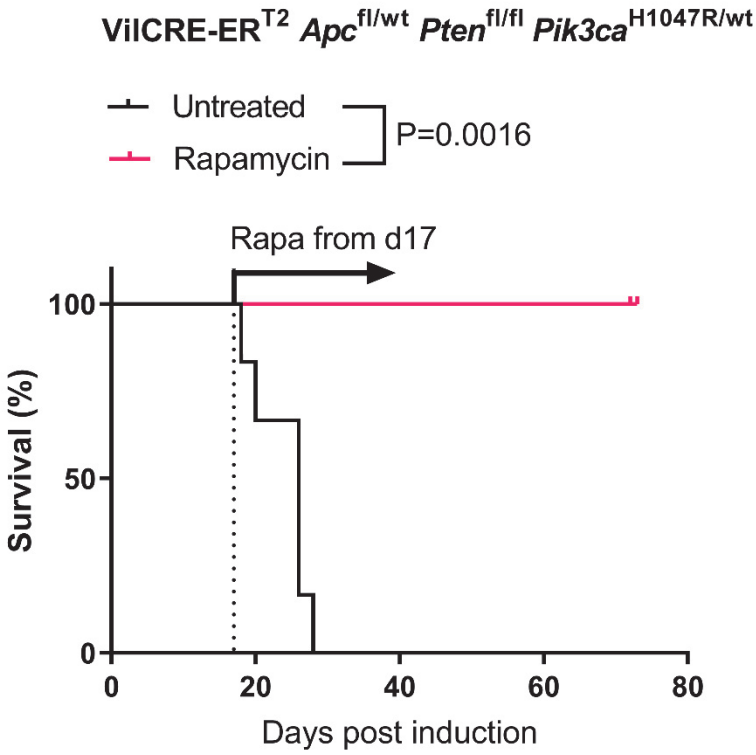

	Untreated	Rapamycin - d17
# censored subjects	0	5
# deaths/events	6	0
Median survival	26	Undefined

Figure 4-33: Rapamycin treatment rescues late stage survival of Villin-CreER^{T2}; *Apc*$^{fl/wt}$; *Pten*$^{fl/fl}$; *Pik3ca*$^{H1047R/wt}$ ageing mice. Villin-CreER^{T2}; *Apc*$^{fl/wt}$; *Pten*$^{fl/fl}$; *Pik3ca*$^{H1047R/wt}$ mice were dosed 1x daily with 10mg/kg Rapamycin from day 17 post-induction. Untreated mice were sampled at clinical endpoint, Rapamycin treated mice after 8 weeks of treatment. Log-rank test.

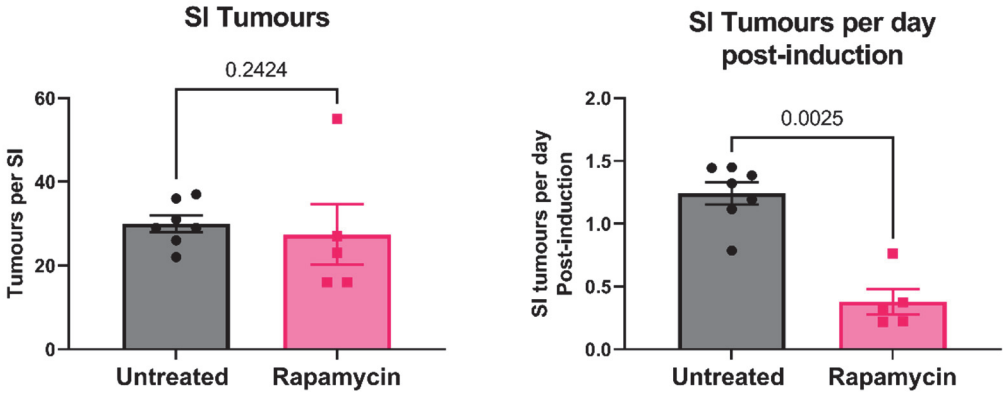

Figure 4-34: Similar number of tumours in Rapamycin treated Villin-CreER^{T2}; *Apc*$^{fl/wt}$; *Pten*$^{fl/fl}$; *Pik3ca*$^{H1047R/wt}$ mice, less when adjusted for the time of sampling. Untreated mice were sampled at endpoint, Rapamycin treated mice were sampled after 8 weeks of treatment. Tumours were scored from the processed H&E samples. SI tumour numbers were divided by day of sampling post-induction. Mean ± SEM. Two-sided Mann-Whitney U test.

Villin-CreER^{T2}; *Apc*$^{fl/wt}$; *Pten*$^{fl/fl}$; *Pik3ca*$^{H1047R/wt}$ mice, when treated from a late stage, did not show further tumour initiation and the existing tumours seemed to be thwarted in their growth. To gain insight into the effect of Rapamycin on biomarkers of PI3-Kinase and mTOR signalling I used IHC to stain for pAKT-473, pS6-S235 and S240, p4E-BP1-T37/46, and pEEF2-T56 (Figure 4-35). Morphologically, Rapamycin treated tumours looked similar, albeit somewhat more compact. pAKT was uniformly high in tumour tissue, indicating that PI3-Kinase signalling was still active. Importantly, the strong inhibition of S6-kinase by rapamycin was upheld even after weeks of constant treatment, as shown by absence of the markers pS6-S235 and pS6-S240 in tumour-epithelial cells. p4E-BP1-T37/46 levels were high and seemingly not affected by Rapamycin treatment. This indicates that efficient translation elongation still seems to be the crucial factor for tumour initiation and growth. eEF2K, a negative regulator of eEF2, is a known target of S6K. This enables mTORC1 to control levels of translation elongation (Browne and Proud, 2004). In previously published data, peEF2 levels increased upon Rapamycin treatment in short term experiments, resulting in decreased translation (Knight *et al.*, 2021). Unexpectedly, peEF2 levels were high in PI3-Kinase signalling hyperactive tumours the first place, and not altered upon Rapamycin treatment, indicating adaptation to long-term Rapamycin treatment.

To assess the effect of Rapamycin on proliferation in tumours, I stained for BrdU and quantified the proportion of positive cells per total tumour cells. These preliminary data suggest that while there might be a decrease, there is still a

population of proliferative cells in Rapamycin treated tumours (Figure 4-36). A differentiation marker, e.g. lysozyme, could be used to determine whether cells in these tumours show a more differentiated phenotype.

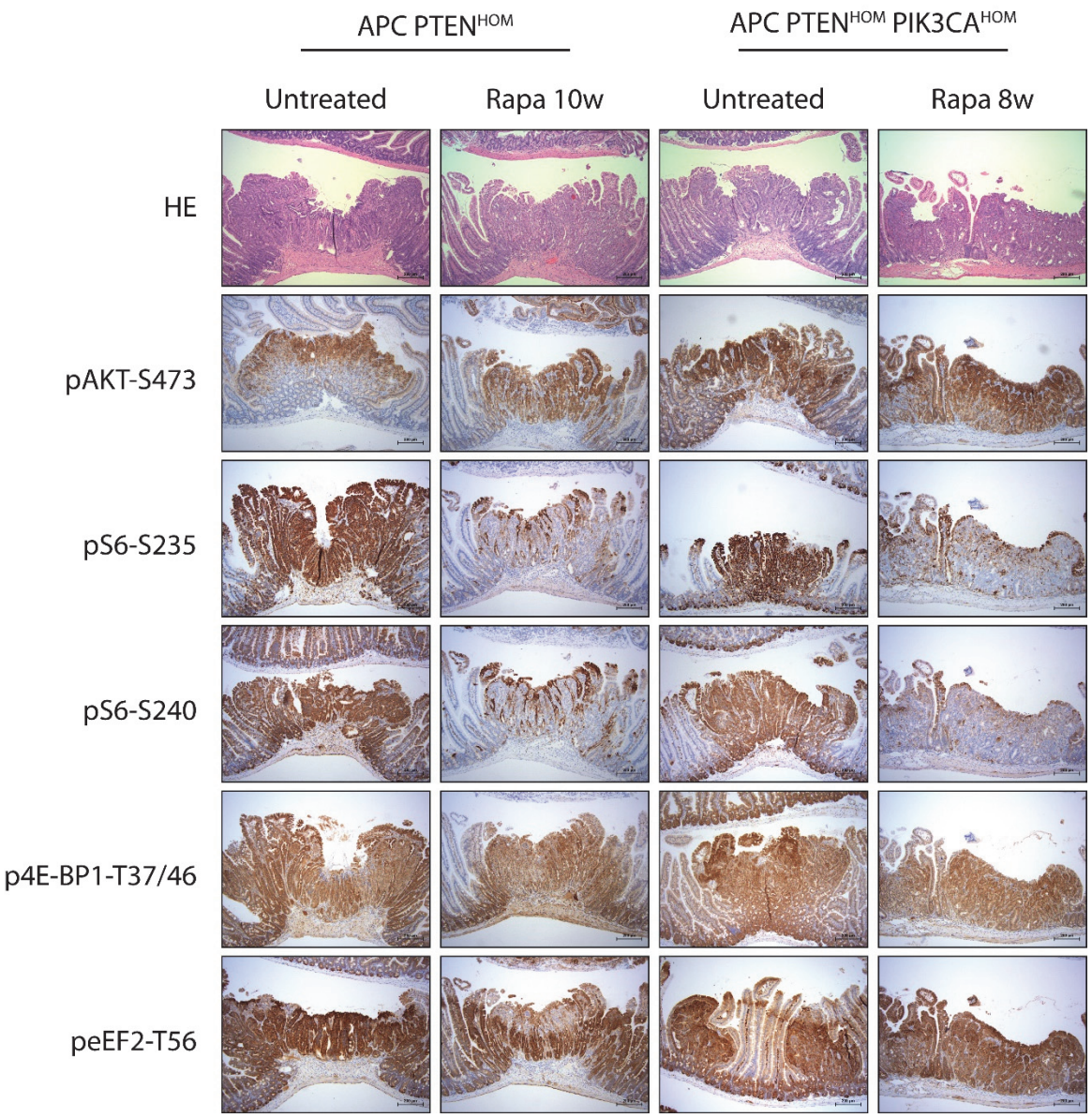

Figure 4-35: Immunohistochemical analysis of PI3-K/mTOR signalling targets reveal Rapamycin dependent signalling changes. Villin-CreER^{T2}; *Apc*$^{fl/wt}$; *Pten*$^{fl/fl}$ and Villin-CreER^{T2}; *Apc*$^{fl/wt}$; *Pten*$^{fl/fl}$; *Pik3ca*$^{H1047R/wt}$ mice were treated with Rapamycin from d25 for 10 weeks and from d17 for 8 weeks respectively. Biological samples were processed and stained with H&E, or against pAKT-473, pS6-235, pS6-240, p4E-BP1-T37/46, or peEF2-T56. Representative images from n=3 for each condition. Scale bars 200µm.

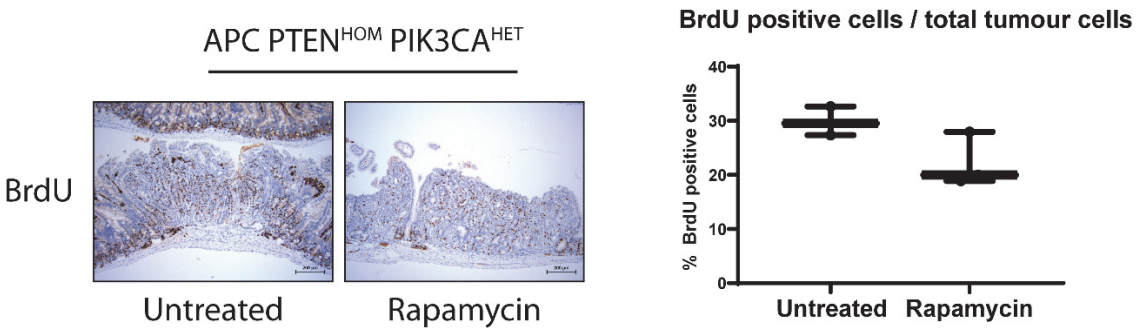

Figure 4-36: A BrdU positive cell population remains in tumours under Rapamycin treatment. Mice were injected with BrdU two hours before sampling. Sections were stained for BrdU using IHC. Stained slides were scanned and BrdU positive cells/total tumour cells were quantified using image analysis software (Halo). Representative image from n=3 mice for each condition (left) and quantification on the right. Mean ± s.e.m.

In summary, Rapamycin-mediated inhibition of mTORC1 prevents tumour initiation and further outgrowth of established tumours, likely through an eEF2K-mediated mechanism. Tumours still have a proliferative cell population.

Rapamycin has a well-established mechanism of action by binding FKBP12 and thereby strongly inhibiting some aspects of mTORC1 signalling, including translation elongation. As previously mentioned, Rapamycin effectively blocks S6K-mediated translation elongation to efficiently drive intestinal cancer. The mTOR-kinase inhibitor AZD2014 inhibits this process as well, but not as deeply (Guichard *et al.*, 2015). It can be seen as blunting overall mTOR signalling, without specificity for a particular process. This was an opportunity to characterize the dependence of PI3-Kinase hyperactive models further, and shed light on the most crucial mechanism for mTOR-dependent tumour growth.

4.2.5 mTOR kinase inhibition extends survival in late stage Pten-KO models

As an ATP-competitive kinase inhibitor, unlike rapamycin, AZD2014 can inhibit mTOR regardless of the signalling complex that it is associated with. I was particularly interested to compare AZD2014 to Rapamycin, which seemed to halt tumour initiation and outgrowth in Villin-CreER^{T2}; *Apc*$^{fl/wt}$; *Pten*$^{fl/fl}$ mice. I therefore treated those mice with the mTOR-Kinase inhibitor from day 25 post-induction, which was again a late-stage intervention. I let those mice age to clinical endpoint, which they reached at 59 days post-induction (range: 42 to 64 days), compared to 39 days (range: 35 to 53 days) in vehicle controls (Figure 4-37).

This was a significant survival benefit, although not as impressive as Rapamycin. Tumour scores were not significantly different in AZD2014 treated mice vs vehicle (Figure 4-38).

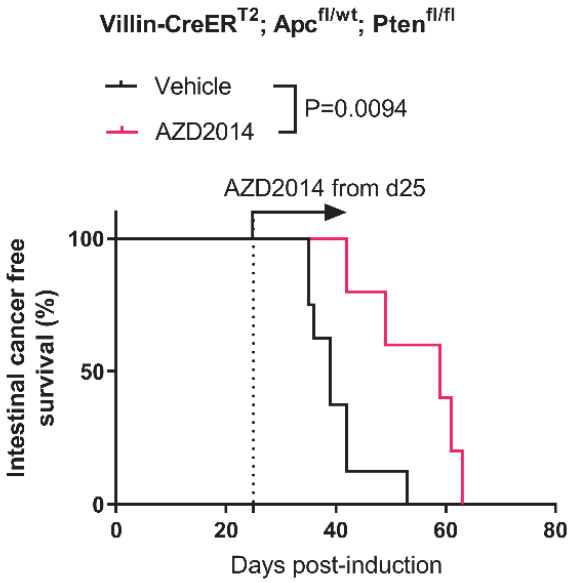

	Vehicle	AZD2014
# censored subjects	0	0
# deaths/events	8	5
Median survival	39	59

Figure 4-37: Rapamycin treatment extends survival of Villin-CreER^{T2}; *Apc*$^{fl/wt}$; *Pten*$^{fl/fl}$ ageing mice. Villin-CreER^{T2}; *Apc*$^{fl/wt}$; *Pten*$^{fl/fl}$ mice were dosed 1x daily with 15mg/kg AZD2014, or 1x daily 0.5% HPMC + 0.1% tween from day 25 post-induction. Mice were sampled at clinical endpoint. Log-rank test.

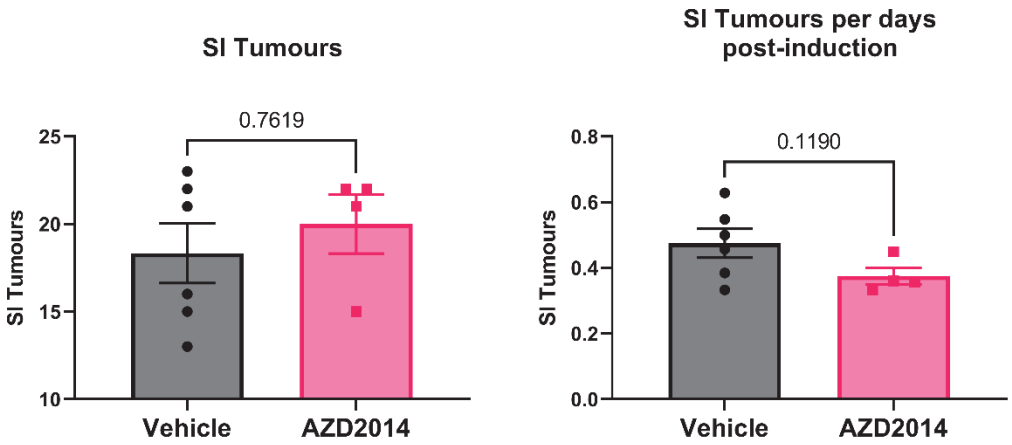

Figure 4-38: Similar number of tumours in AZD2014 treated Villin-CreER^{T2}; *Apc*$^{fl/wt}$; *Pten*$^{fl/fl}$ mice, also when adjusted for the time of sampling. Mice were sampled at endpoint and tumours were scored from the processed H&E samples. SI tumour numbers were divided by day of sampling post-induction. Mean ± SEM. Two-sided Mann-Whitney U test.

This indicates that while AZD2014 has a growth-suppressive effect in the *Pten* deficient model, it is not robust enough to prevent further tumour initiation and outgrowth of existing tumours. Immunohistochemical characterisation of mTOR targets will be important to identify differences between Rapamycin and AZD2014 treatments.

4.2.6 Discussion

In the previous section, I attempted to shed light on the functional relevance of mTOR signalling components in the context of PI3-Kinase driven intestinal cancer. mTORC2-KO and AKT inhibition did not show promising anti-cancer effects in the PI3-Kinase hyperactive setting. mTOR-Kinase inhibition had a modest effect on survival, while mTORC1 inhibition effectively prevented tumour initiation and thwarted outgrowth of existing lesions.

Lack of resistance to Rapamycin in the PI3-Kinase high setting was surprising, as PI3-Kinase signalling is thought to have a broad range of effectors. Rapamycin treatment not only prevented existing tumours from growing out and causing mice to reach clinical endpoint, but also prevented tumour initiation. This indicates that the *Pten*-loss and *Pik3ca*^{H1047R} driven tumour initiation phenotypes presented earlier are crucially dependent on functional mTORC1 signalling. This effect is likely due to inhibition of translation elongation, as Rapamycin is known to be a strong inhibitor of this process mediated by eEF2K, while AZD2014 dampens overall mTOR signalling (the extent of which remains to be determined in this setting). Furthermore, it is likely that the previously described PI3-Kinase inhibition did not sufficiently block mTORC1 activity, and was therefore far less effective. This further expands the potential clinical application of mTORC1, or specific inhibition of translation elongation, to *KRAS* wildtype, PI3-Kinase high intestinal cancers.

As this work is still on going, tumour scores have not been available for all mice presented in the survival plots as the histological samples are still being processed.

The mTORC2-loss driven tumour initiation phenotype was unexpected. While I could show that this was likely to be AKT-mediated, I was not able to explain its exact aetiology. Since genetic KO of *Pten* drastically increased small intestinal

tumour initiation, I was expecting inhibition of two major downstream signalling nodes to reduce this effect. Similar to the previous tumour-initiation phenotypes I have presented, the answer might lie in the untransformed tissue. *Rictor*-KO and AKT-inhibition might result in a different behaviour in proliferating cells, making them more prone to loss of wildtype *Apc*. Furthermore, genetic KO of *Rictor* in the murine gut was recently shown to cause a mild barrier defect, which could cause accelerated tumour initiation (Castro-Martinez *et al.*, 2021). Regardless of the increased tumour initiation, tumours still grew out and caused mice to reach clinical endpoint, indicating resistance to mTORC2 and AKT inhibition. Treatment for a shorter time may shed light on the resistance mechanism. Preliminary data from the lab indicates that *Pten* wildtype intestinal tumours are sensitive to AKT inhibition, which would point towards *Pten*-loss driving resistance to AKT-inhibition.

Lack of efficacy in mTORC2 and AKT-inhibitor treated mice indicates that while mTORC1 activity is crucial for the initiation and progression of intestinal tumours, what is thought to be canonical activation through the PI3K→mTORC2→AKT→mTORC1 axis may not be as relevant as anticipated in this setting. This raises the question how mTORC1 signalling is activated here. AKT-inhibition was either not strong enough to shut down this process, or other factors such as lysosomal nutrient sensing or MAPK signalling can uphold mTORC1 activation. Since MAPK signalling is activated by *Kras* mutation, I wanted to establish whether *Kras* and *Kras* and *Pik3ca*/*Pten* co-mutated cancers respond to perturbation of mTOR signalling.

4.3 Targeting mTOR signalling in *Kras* mutant intestinal cancer models

I have previously shown absolute requirement for functional mTORC1 signalling in PI3-Kinase high, Kras wildtype intestinal tumours, while mTORC2 and AKT inhibition was insufficient in preventing tumour initiation and outgrowth. Recent publications indicate that different intracellular pools of mTORC2 may be activated by PI3-Kinase and Ras signalling in a context dependent manner (Smith, Collins and Charest, 2020). The mTORC2 subunit mSIN1 can be activated directly by Ras-GTP (Lone *et al.*, 2019), but also by PIP3 (Liu *et al.*, 2015). This hints at a differential role for the two pathways in their activation of mTORC2, but

experimental evidence in the context of intestinal cancer is lacking. As a previous publication from the lab indicates, *Kras* mutation drives resistance to mTORC1 inhibition through upregulation of signalling through MNKs (Knight *et al.*, 2021).

4.3.1 *Rictor*-KO dependent survival benefit in Villin-CreER^{T2}; *Apc*$^{fl/wt}$; *Kras*$^{G12D/wt}$ mice

To test whether mTORC2 has a role in the initiation and outgrowth of intestinal cancers driven by mutant *Kras* and loss of *Apc*, I crossed the *Rictor*^{fl} allele to the Villin-CreER^{T2}; *Apc*$^{fl/wt}$; *Kras*$^{G12D/wt}$ model to generate Villin-CreER^{T2}; *Apc*$^{fl/wt}$; *Kras*$^{G12D/wt}$; *Rictor*$^{fl/wt}$ and Villin-CreER^{T2}; *Apc*$^{fl/wt}$; *Kras*$^{G12D/wt}$; *Rictor*$^{fl/fl}$ mice. Homozygous *Rictor*-KO mice reached clinical endpoint at a median of 92 days post-induction (range: 67 to 120 days), compared to 80 days in heterozygotes and 72 days in *Rictor* wildtypes (Figure 4-39). The difference between *Rictor* homozygotes and wildtypes was statistically significant. Tumour scoring revealed no differences in SI or Colonic tumour numbers between any of the conditions (Figure 4-40).

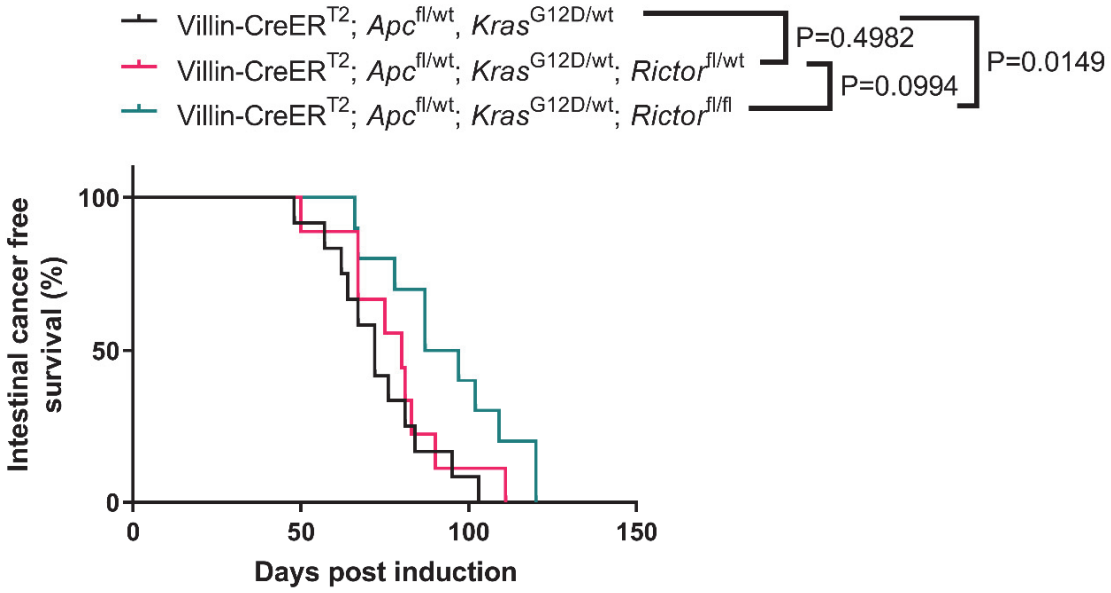

	APC KRAS^{G12D}	APC KRAS^{G12D} RICTOR^{HET}	APC KRAS^{G12D} RICTOR^{HOM}
# censored subjects	0	0	0
# deaths/events	12	9	10
Median survival	72	80	92

Figure 4-39: Genetic depletion of Rictor delays time to clinical endpoint in Villin-CreER^{T2}; *Apc*$^{fl/wt}$; *Kras*$^{G12D/wt}$ mice. Villin-CreER^{T2}; *Apc*$^{fl/wt}$; *Kras*$^{G12D/wt}$, Villin-CreER^{T2}; *Apc*$^{fl/wt}$; *Kras*$^{G12D/wt}$; *Rictor*$^{fl/wt}$, and Villin-CreER^{T2}; *Apc*$^{fl/wt}$; *Kras*$^{G12D/wt}$; *Rictor*$^{fl/fl}$ mice were induced and aged to clinical endpoint. Log-rank test.

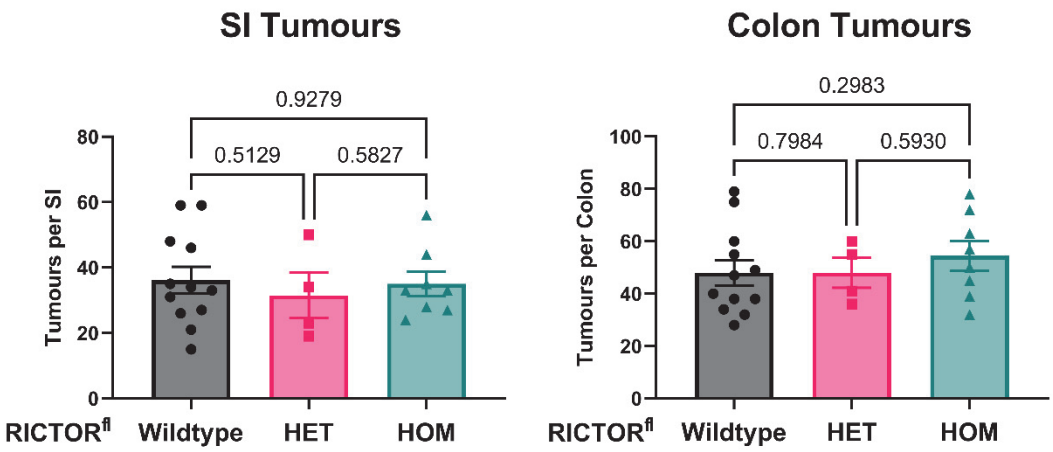

Figure 4-40: No impact on tumour numbers upon *Rictor*-KO in Villin-CreER^{T2}; *Apc*$^{fl/wt}$; *Kras*$^{G12D/wt}$ mice. Mice were sampled at clinical endpoint and tumours were scored from the processed H&E stained sections. Mean ± SEM. Kruskal-Wallis test and uncorrected Dunn's multiple comparisons test.

Kras^{G12D} mutation therefore rendered mice sensitive to *Rictor*-KO, unlike the previously presented purely PI3-Kinase driven models. While this was a modest effect, and tumour number or distribution was not altered, it suggested differential dependence on mTORC2 activity.

Given the absolute requirement of PI3-Kinase driven models on mTORC1, I wanted to establish whether concomitant *Kras* and PI3-Kinase signalling activation would lead to sensitivity to Rapamycin.

4.3.2 Kras mutant/PI3-Kinase signalling high models are resistant to Rapamycin treatment

Kras mutation synergized with both *Pik3ca* mutation and *Pten*-KO to drive intestinal tumours. mTORC1 signalling was still absolutely required for PI3-Kinase signalling hyperactive models, while published data from our lab suggests that *Kras* mutation drives resistance. It is not known whether *Kras*^{G12D} mutation-mediated resistance is still upheld when both MAPK and PI3-Kinase pathways are hyperactivated. To test this, I treated Villin-CreER^{T2}; *Apc*$^{fl/wt}$; *Kras*$^{G12D/wt}$; *Pik3ca*$^{H1047R/wt}$ and Villin-CreER^{T2}*Apc*$^{fl/wt}$; *Kras*^{G12D}; *Pten*$^{fl/fl}$ mice with Rapamycin from an early stage – day 5 post-induction - until clinical endpoint. Villin-CreER^{T2}; *Apc*$^{fl/wt}$; *Kras*$^{G12D/wt}$; *Pik3ca*$^{H1047R/wt}$ mice had to be sampled at a median of 22 days post-induction (range: 11 to 32 days), while mice without intervention had to be sampled at a median of 39 days post-induction (range: 27 to 74 days) (Figure 4-41). This was significantly shorter and likely due to tumour burden, as Rapamycin-

treated mice presented with multiple small intestinal and colonic tumours. Albeit less than untreated controls, they were similar when adjusted for the earlier clinical endpoint (Figure 4-42).

Preliminary data in Villin-CreER^{T2}*Apc*$^{fl/wt}$; *Kras*^{G12D}; *Pten*$^{fl/fl}$ suggests that these mice also do not gain a survival benefit when treated with Rapamycin from day 5 post-induction (Figure 4-43). This indicates that Kras mutation dependent Rapamycin resistance is still upheld under additional PI3-Kinase hyperactivation.

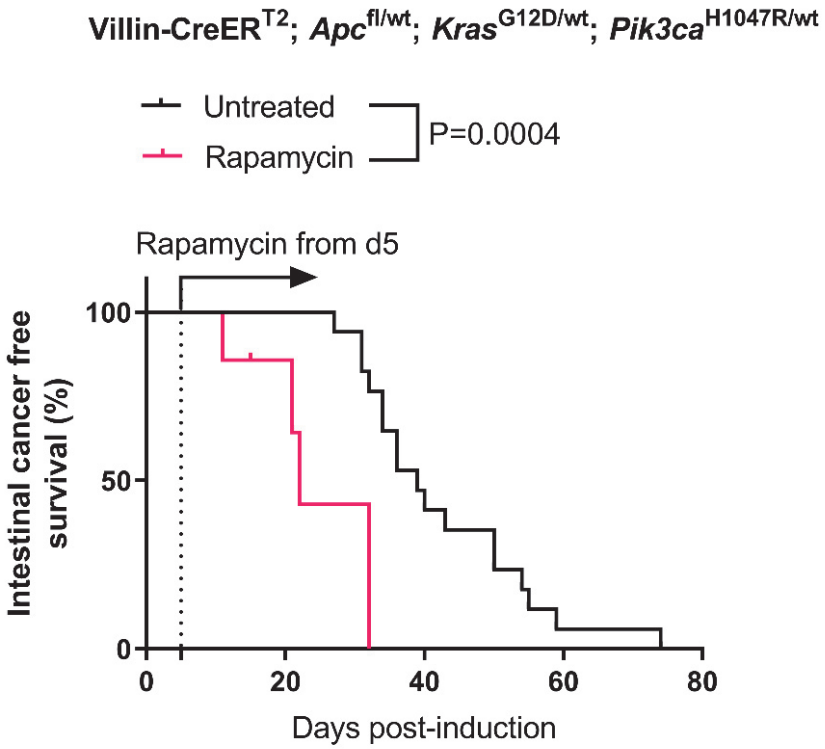

	Untreated	Rapamycin
# censored subjects	0	2
# deaths/events	17	5
Median survival	39	22

Figure 4-41: Shorter time to clinical endpoint in Rapamycin-treated Villin-CreER^{T2}; *Apc*$^{fl/wt}$; *Kras*$^{G12D/wt}$; *Pik3ca*$^{H1047R/wt}$ ageing mice, compared to untreated controls. Villin-CreER^{T2}; *Apc*$^{fl/wt}$; *Kras*$^{G12D/wt}$; *Pik3ca*$^{H1047R/wt}$ mice were dosed 1x daily with 10mg/kg Rapamycin from day 5 post-induction. Mice were sampled at clinical endpoint. Log-rank test.

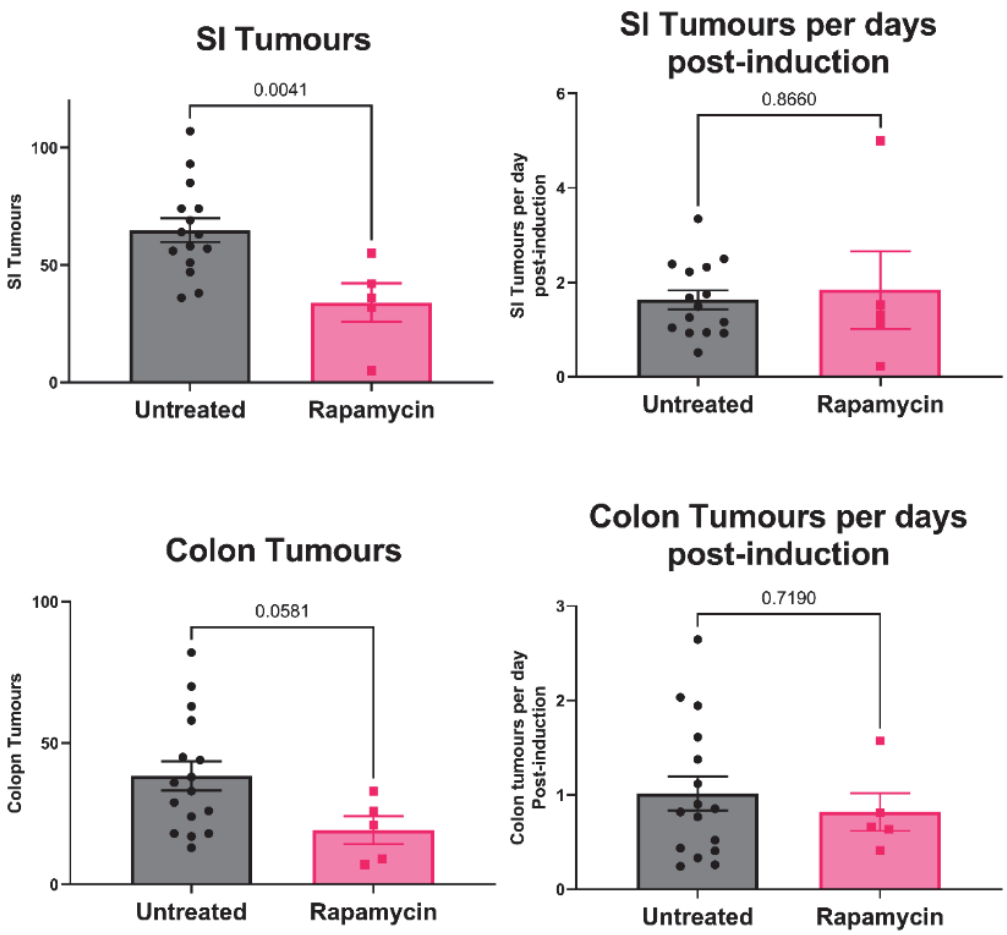

Figure 4-42: Less tumours at endpoint, but similar tumour number adjusted for time to endpoint in Rapamycin vs untreated Villin-CreER^{T2}; *Apc*$^{fl/wt}$; *Kras*$^{G12D/wt}$; *Pik3ca*$^{H1047R/wt}$ mice. Mice were sampled at clinical endpoint and tumours were scored from the processed H&E stained sections. Mean ± SEM. Two-sided Mann-Whitney U test.

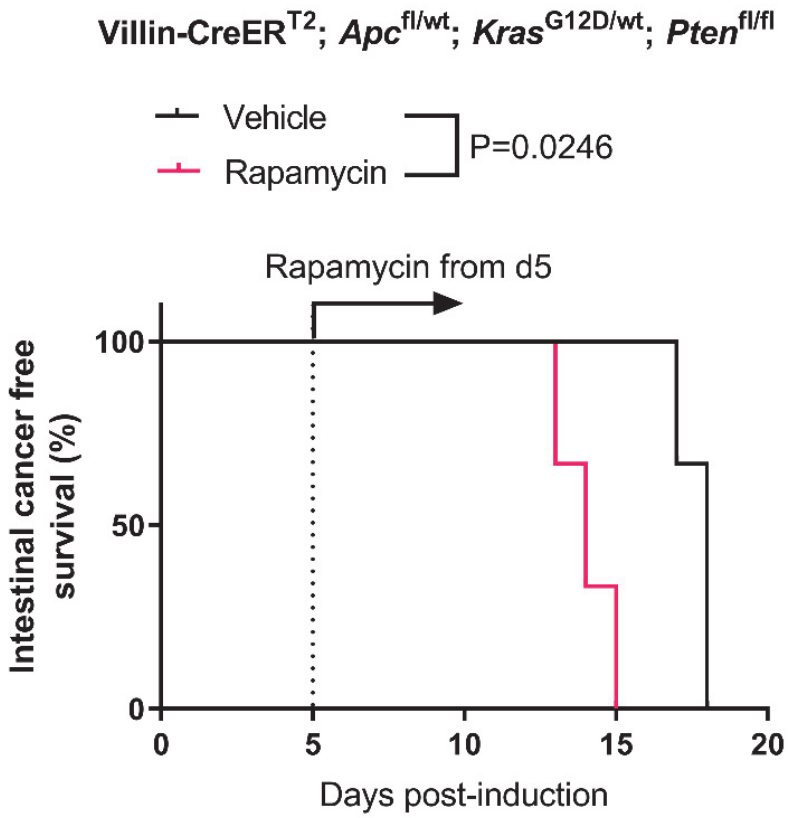

	Vehicle	Rapamycin
# censored subjects	0	0
# deaths/events	3	3
Median survival	18	14

Figure 4-43: Shorter time to clinical endpoint in Rapamycin-treated Villin-CreER^{T2}; *Apc*$^{fl/wt}$; *Kras*$^{G12D/wt}$; *Pten*$^{fl/fl}$ ageing mice, compared to vehicle-treated controls. Villin-CreER^{T2}; *Apc*$^{fl/wt}$; *Kras*$^{G12D/wt}$; *Pten*$^{fl/fl}$ mice were dosed 1x daily with 10mg/kg Rapamycin from day 5 post-induction. Vehicle treated mice were treated 1x daily with Rapamycin vehicle. Mice were sampled at clinical endpoint. Log-rank test.

4.3.3 Discussion

In this section, I showed that unlike in PI3-Kinase hyperactive models, *Rictor*-KO resulted in a significantly later time to clinical endpoint in *Kras* mutant mice. mTORC1 inhibition was ineffective in *Kras* mutant, PI3-Kinase hyperactive models.

Given the results presented in PI3-Kinase driven models, a *Kras* mutation-dependent response to mTORC2 depletion was unexpected. Studies conducted in cancers of other tissues have generally proposed tumour-promoting roles for mTORC2: In the liver, mTORC2 signalling promoted cancer by upregulating de-novo fatty acid synthesis, leading to steatosis (Guri *et al.*, 2017). In prostate

cancer, mTORC2 was required for the development of cancer, induced by *Pten*-loss in mice (Guertin *et al.*, 2009). In the pancreas, mTORC2 drives development and progression of cancer (Driscoll *et al.*, 2016; Schmidt *et al.*, 2017). Given the striking effect of *Rictor*-KO in pancreatic cancer models driven by *Kras* mutation, together with recent data indicating the mTORC2 is a direct effector of active KRAS, one could speculate that *Kras* mutant cancers generally rely on mTORC2 more than wildtypes. Treatment with an AKT-inhibitor may provide insight into this process in the first instance, but the exact mechanism behind this will still have to be elucidated.

mTORC1 inhibition showed by far the strongest effect in *Kras* wildtype, PI3-Kinase hyperactive models. Lack of sensitivity in *Kras* mutant, PI3-Kinase signalling high models was anticipated, but still had to be verified experimentally. Kras mutation seems to override the dependence on mTORC1→S6K mediated translation elongation, even in the presence of a strong PI3-Kinase signalling drive. Published data from our lab would suggest this occurs, at least in part, through a MNK-mediated process (Knight *et al.*, 2021).

Additional immunohistochemistry and treatment for short periods will be invaluable in characterizing the effects of targeted inhibition further and may shed light on the impact of mTOR inhibition in these settings. As this work is still on going, tumour scores have not been available for all mice presented in the survival plots as the histological samples are still being processed.

Multiple cell signalling pathways converge on mTOR, including the aforementioned PI3-Kinase signalling, but also MAPK signalling. I previously showed strong synergy between PI3-Kinase and MAPK signalling in driving cancer. For these reasons I next aimed to delineate the role of MEK1/2-inhibition in PI3-Kinase signalling high models in the context of wildtype and mutant *Kras*.

4.4 Targeting MEK1/2 in intestinal cancer models

MEK is a crucial part of MAPK signalling, physiologically initiated at growth-factor receptors or at mutated proto-oncogenes, such as *Kras*. MAPK signalling has roles in intestinal homeostasis and cancer (Ternet and Kiel, 2021). While MEK inhibitors have so far not performed well clinically, they are good tools to study the role of

MAPK signalling in cancer biology. Here, I wanted to establish the importance of MEK1/2 signalling in PI3-Kinase high intestinal cancer GEMMs in *Kras*-wildtype and mutant context.

4.4.1 MEK1/2 inhibition does not provide a clear benefit in late stage Villin-CreER^{T2}; Apc$^{fl/wt}$; Pten$^{fl/fl}$ mice

Given the fundamental role of MAPK signalling in developmental biology and intestinal homeostasis, MAPK signalling might have a role in intestinal cancer initiation and growth, irrespective of MAPK-activating mutation. To test this in the *Pten*-deficient setting, I treated Villin-CreER^{T2}; *Apc*$^{fl/wt}$; *Pten*$^{fl/fl}$ mice from day 25 post-induction with the MEK1/2 inhibitor AZD6244. Mice had to be sampled at a median of 49.5 days (range: 35 to 64 days), compared to 39 days (range: 35 to 53 days) in vehicle treated controls (Figure 4-44). This was a trend towards a benefit, but not statistically significant. Tumour number at endpoint was similar, although significantly lower when adjusted to days post-induction (Figure 4-45). This hints at a role for MAPK signalling in tumour initiation, even in the absence of activating mutations. Outgrowth of existing tumours did not seem to be affected though, which still resulted in Villin-CreER^{T2}; *Apc*$^{fl/wt}$; *Pten*$^{fl/fl}$ mice reaching clinical endpoint.

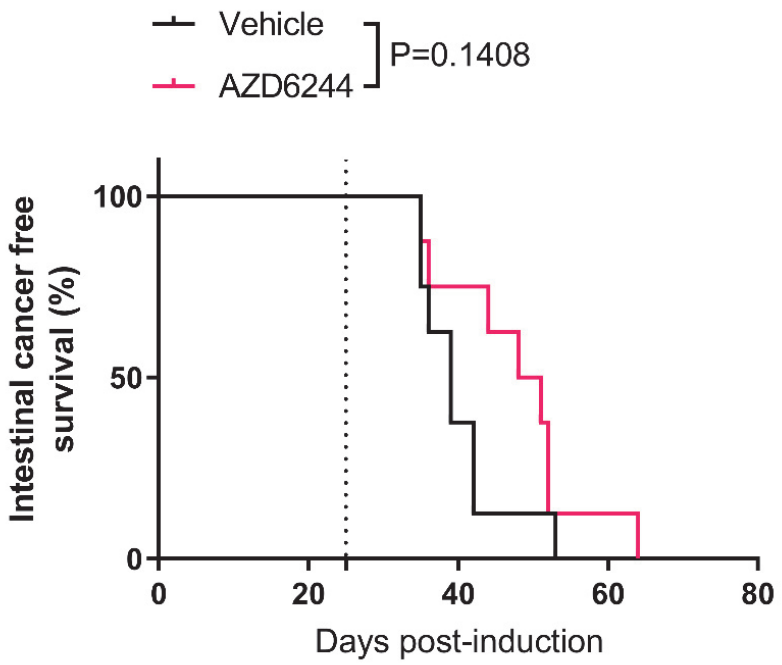

	Vehicle	AZD6244
# censored subjects	0	0
# deaths/events	8	8
Median survival	39	49.5

Figure 4-44: Mek inhibition does not extend survival of Villin-CreER^{T2}; *Apc*$^{fl/wt}$; *Pten*$^{fl/fl}$ ageing mice. Villin-CreER^{T2}; *Apc*$^{fl/wt}$; *Pten*$^{fl/fl}$ mice were dosed 2x daily with 25mg/kg AZD6244 from day 5 post-induction. Vehicle controls were dosed 0.5% HPMC + 0.1% tween 2x daily. Mice were sampled at clinical endpoint. Log-rank test.

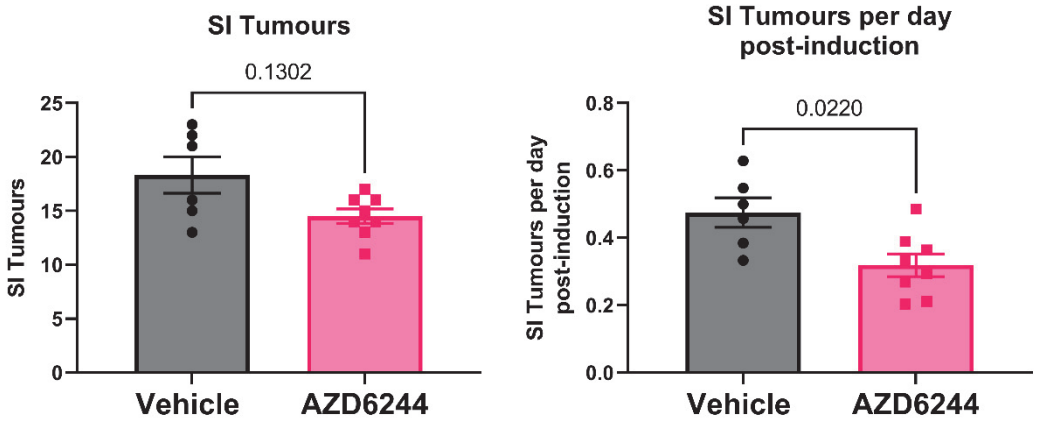

Figure 4-45: Similar number of tumours in AZD6244 treated Villin-CreER^{T2}; *Apc*$^{fl/wt}$; *Pten*$^{fl/fl}$; mice, lower when adjusted for days post-induction. Mice were sampled at endpoint and tumours were scored from the processed H&E samples. SI tumour numbers were divided by day of sampling post-induction. Mean ± SEM. Two-sided Mann-Whitney U test.

It is not known whether combined *Pten-KO* and *Pik3ca*-mutant models would have a greater dependency on MEK, but this would be interesting to follow up on.

While MEK1/2-inhibition may have a slight effect in Kras-wildtype, PI3-Kinase signalling high models, the obvious application for MAPK-inhibition is in the *Kras* mutant setting. Since KRAS has been exceedingly difficult to inhibit directly, targeting the downstream effector network has been a long-standing goal in oncology.

4.4.2 MEK1/2 inhibition is effective when treated from early, but not from late in Kras and PI3-Kinase pathway co-mutated models

MAPK inhibition is a rational treatment approach for *Kras* mutant cancers, although it has not been very effective in the clinics. To evaluate the effect of MEK1/2 inhibition in $Kras^{G12D}$ and $Kras^{G12D}$/PI3-Kinase high intestinal cancer models, I made use of Villin-$CreER^{T2}$; $Apc^{fl/wt}$; $Kras^{G12D/wt}$ mice with additional hetero-and homozygous $Pik3ca^{H1047R}$ mutation. The two aspects I was interested in were whether MEK1/2 inhibition was effective in the early setting from day five post-induction, and in a later stage setting at day 21, where tumours were already expected to be present. To this end, Villin-$CreER^{T2}$; $Apc^{fl/wt}$; $Kras^{G12D/wt}$; $Pik3ca^{H1047R/wt}$ mice were induced and treated with AZD6244 from day 5 post-induction. These mice had to be sampled after a median of 89 days (range: 80 to 147 days), compared to 39 days (range: 27 to 74 days) in untreated controls, which was statistically significant (Figure 4-46). The treatment resulted in reduced SI and Colon tumour number (Figure 4-27).

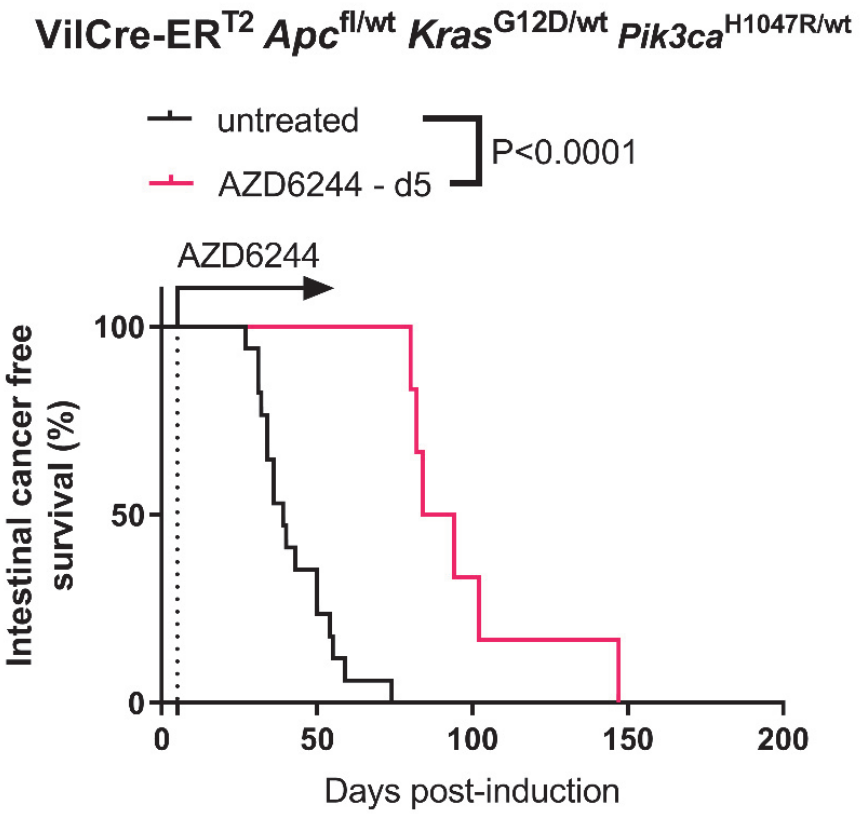

	untreated	AZD6244 - d5
# censored subjects	0	0
# deaths/events	17	6
Median survival	39	89

Figure 4-46: MEK1/2 inhibition extended survival of Villin-CreER^{T2}; *Apc*$^{fl/wt}$; *Kras*$^{G12D/wt}$; *Pik3ca*$^{H1047R/wt}$ ageing mice when treated from day 5 post-induction. Villin-CreER^{T2}; *Apc*$^{fl/wt}$; *Kras*$^{G12D/wt}$; *Pik3ca*$^{H1047R/wt}$ mice were dosed 2x daily with 25mg/kg AZD6244 from day 5 post-induction. Mice were sampled at clinical endpoint. Log-rank test.

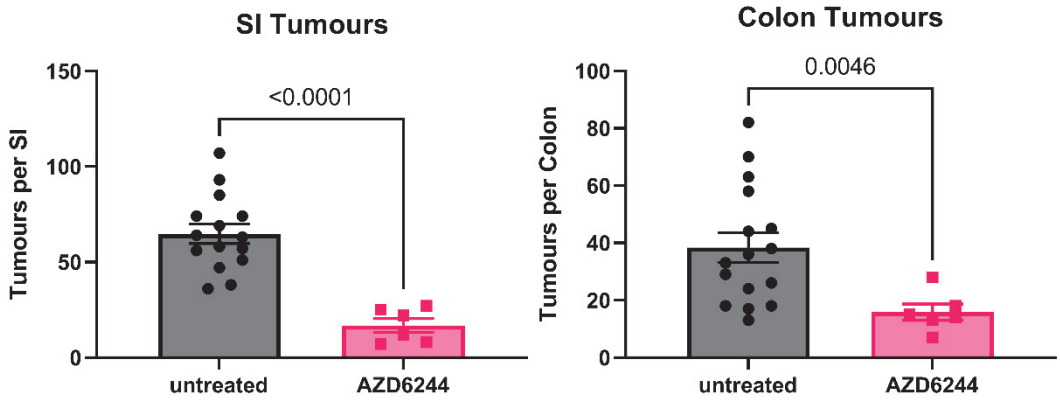

Figure 4-47: Reduced tumour number in AZD6244 treated Villin-CreER^{T2}; *Apc*$^{fl/wt}$; *Kras*$^{G12D/wt}$; *Pik3ca*$^{H1047R/wt}$ mice. Mice were induced and treated with AZD6244 from day 5 post-induction. Tumours were scored from H&E stained slides. Mean ± SEM. Two-sided Mann-Whitney U test.

Since homozygous mutation further exacerbated tumour initiation in Villin-CreER^{T2}; *Apc*$^{fl/wt}$; *Kras*$^{G12D/wt}$ mice, I performed the same experiment in Villin-CreER^{T2}; *Apc*$^{fl/wt}$; *Kras*$^{G12D/wt}$; *Pik3ca*$^{H1047R/H1047R}$ mice. AZD6244 treatment from day 5 post-induction again led to a significant extension of survival, with mice reaching endpoint at a median of day 70 post-induction (range: 25 to 97 days) compared to vehicle controls at 26.5 days (range: 10 to 29 days) (Figure 4-48). Again, treatment with AZD6244 significantly reduced occurrence of SI and colonic tumours (Figure 4-49).

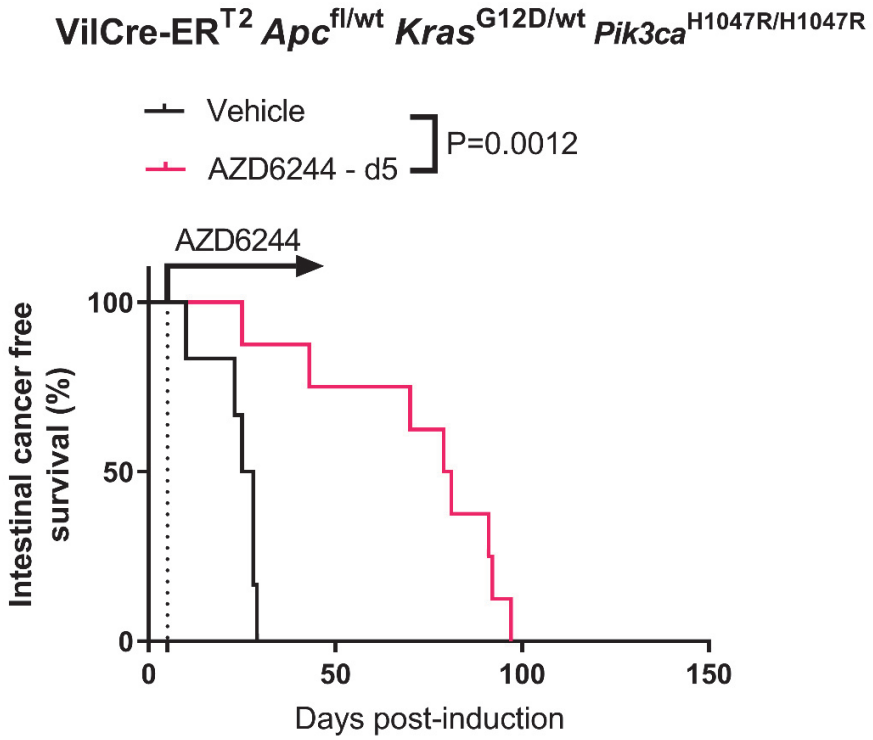

	Vehicle	AZD6244 - d5
# censored subjects	0	0
# deaths/events	6	8
Median survival	26.5	70

Figure 4-48: MEK1/2 inhibition extended survival of Villin-CreER^{T2}; *Apc*$^{fl/wt}$; *Kras*$^{G12D/wt}$; *Pik3ca*$^{H1047R/H1047R}$ ageing mice when treated from day 5 post-induction. Villin-CreER^{T2}; *Apc*$^{fl/wt}$; *Kras*$^{G12D/wt}$; *Pik3ca*$^{H1047R/H1047R}$ mice were dosed 2x daily with 25mg/kg AZD6244 from day 5 post-induction. Vehicle controls were dosed 0.5% HPMC + 0.1% tween 2x daily. Mice were sampled at clinical endpoint. Log-rank test.

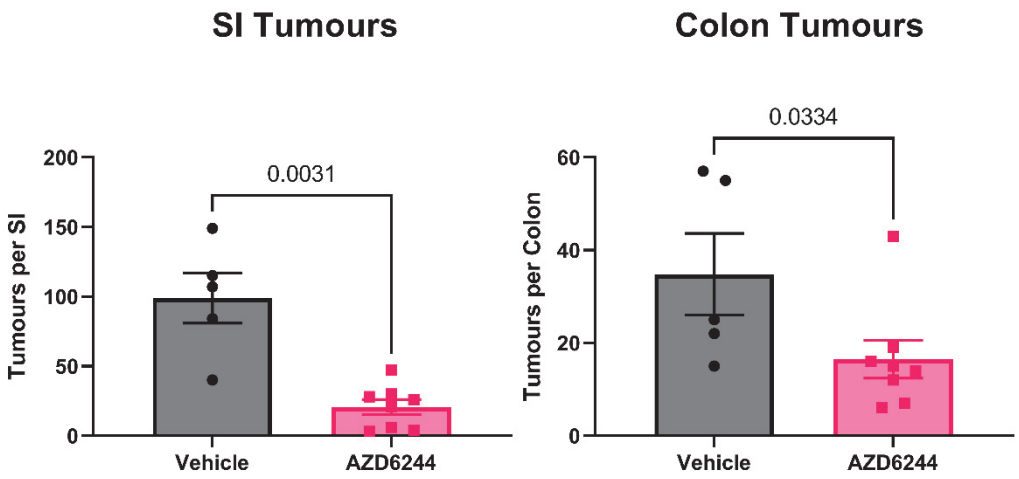

Figure 4-49: Reduced tumour number in AZD6244 treated Villin-CreER^{T2}; *Apc*$^{fl/wt}$; *Kras*$^{G12D/wt}$; *Pik3ca*$^{H1047R/H1047R}$ mice. Mice were induced and treated with AZD6244 from day 5 post-induction. Tumours were scored from H&E stained slides. Mean ± SEM. Two-sided Mann-Whitney U test.

MEK1/2 inhibition therefore ameliorated the tumour initiation phenotype driven by *Kras* and PI3-Kinase co-mutation when treated from an early stage, indicating a strong dependency on MAPK signalling even in a PI3-Kinase hyperactive setting. To evaluate efficacy of the drug on established tumours, I induced Villin-CreER^{T2}; *Apc*$^{fl/wt}$; *Kras*$^{G12D/wt}$; *Pik3ca*$^{H1047R/wt}$ mice and commenced AZD6244 treatment at day 21 post-induction. The effect of AZD6244 was diminished when treating from this timepoint, as drug treated mice reached clinical endpoint at a median of 37 days post-induction (range: 31 to 117 days) compared to 39 days in the untreated control cohort (range: 27 to 74 days). Tumour numbers were reduced in the AZD6244 treated mice (Figure 4-51).

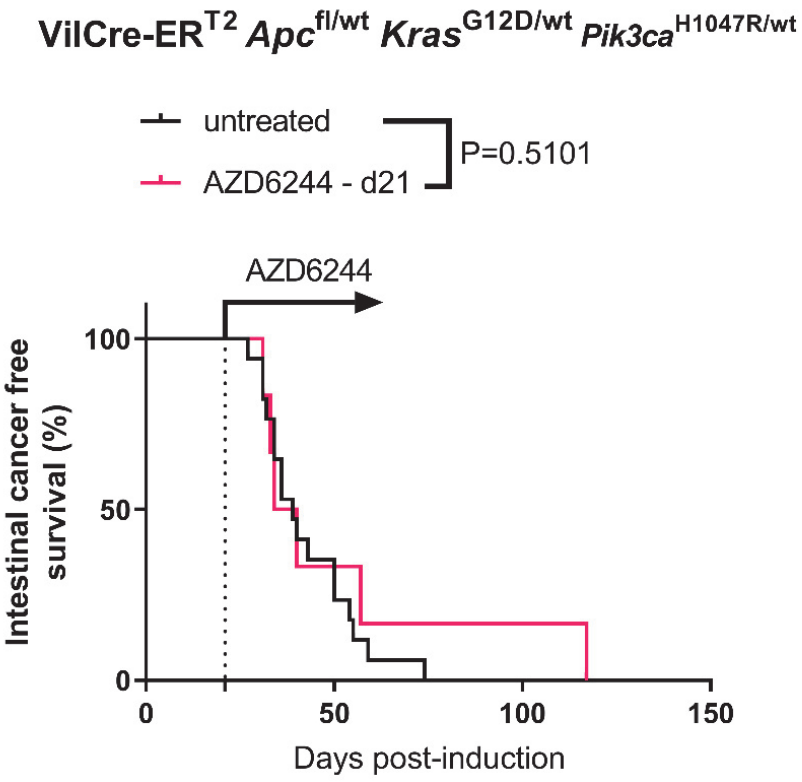

	untreated	AZD6244 - d21
# censored subjects	0	0
# deaths/events	17	6
Median survival	39	37

Figure 4-50: Diminished effect of MEK1/2 inhibition on survival of Villin-CreER^{T2}; *Apc*$^{fl/wt}$; *Kras*$^{G12D/wt}$; *Pik3ca*$^{H1047R/wt}$ ageing mice when treated from day 21 post-induction. Villin-CreER^{T2}; *Apc*$^{fl/wt}$; *Kras*$^{G12D/wt}$; *Pik3ca*$^{H1047R/wt}$ mice were dosed 2x daily with 25mg/kg AZD6244 from day 21 post-induction. Mice were sampled at clinical endpoint. Log-rank test.

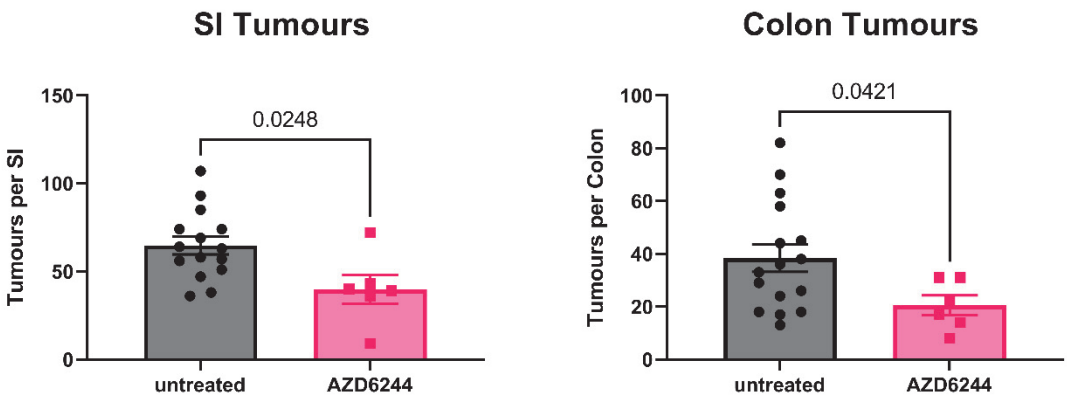

Figure 4-51: Reduced tumour number in AZD6244 treated Villin-CreER^{T2}; *Apc*$^{fl/wt}$; *Kras*$^{G12D/wt}$; *Pik3ca*$^{H1047R/wt}$ mice from d21 post-induction. Mice were induced and treated with AZD6244 from day 21 post-induction. Tumours were scored from H&E stained slides. Mean ± SEM. Two-sided Mann-Whitney U test.

This indicates that at a later stage, established tumours are resistant to MEK1/2 inhibition. Work presented in the previous chapter indicates that *Pten*-KO and *Pik3ca* mutation may affect *Kras*-mutant models somewhat differently. To establish whether MEK1/2 inhibition was also effective in the *Pten*-KO setting, I treated Villin-CreER^{T2}*Apc*$^{fl/wt}$; *Kras*^{G12D}; *Pten*$^{fl/fl}$ mice with AZD6244. *Pten*-KO in this context leads to rapid tumour formation and mice usually have to be sampled at around day 19 post-induction. I decided to treat Villin-CreER^{T2}*Apc*$^{fl/wt}$; *Kras*^{G12D}; *Pten*$^{fl/fl}$ mice from day 10 post-induction, serving as an intermediate timepoint. This resulted in a significant survival benefit, as AZD6244 treated mice were sampled at a median of 23 days (range 21 to 44 days), compared to vehicle treated controls at 19 days (range 16 to 24 days).

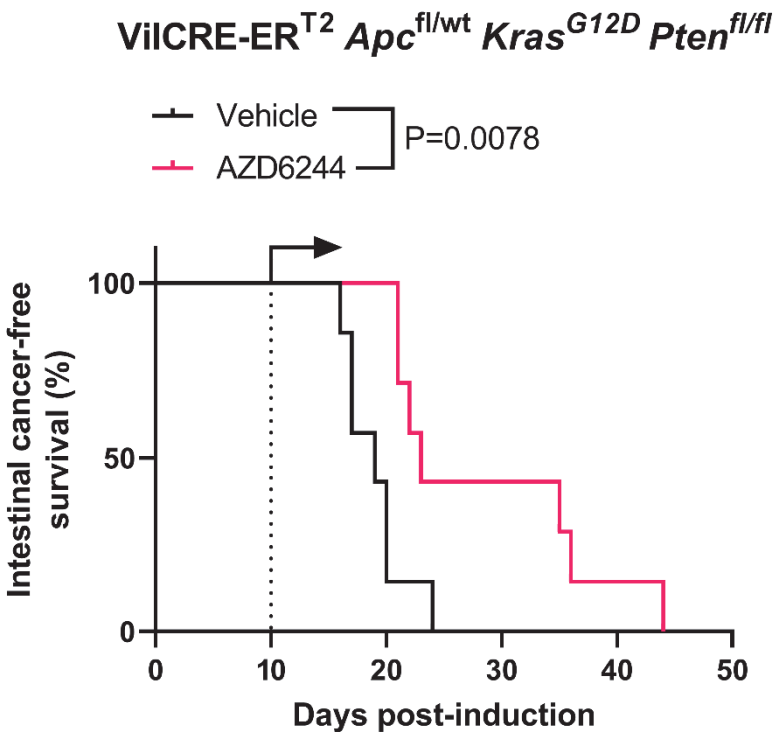

	Vehicle	AZD6244
# censored subjects	0	0
# deaths/events	7	7
Median survival	19	23

Figure 4-52: MEK1/2 inhibition extended survival of Villin-CreER^{T2}; *Apc*$^{fl/wt}$; *Kras*$^{G12D/wt}$; *Pten*$^{fl/fl}$ ageing mice when treated from day 10 post-induction. Villin-CreER^{T2}; *Apc*$^{fl/wt}$; *Kras*$^{G12D/wt}$; *Pten*$^{fl/fl}$ mice were dosed 2x daily with 25mg/kg AZD6244 from day 10 post-induction. Vehicle controls were dosed 0.5% HPMC + 0.1% tween 2x daily. Mice were sampled at clinical endpoint. Log-rank test.

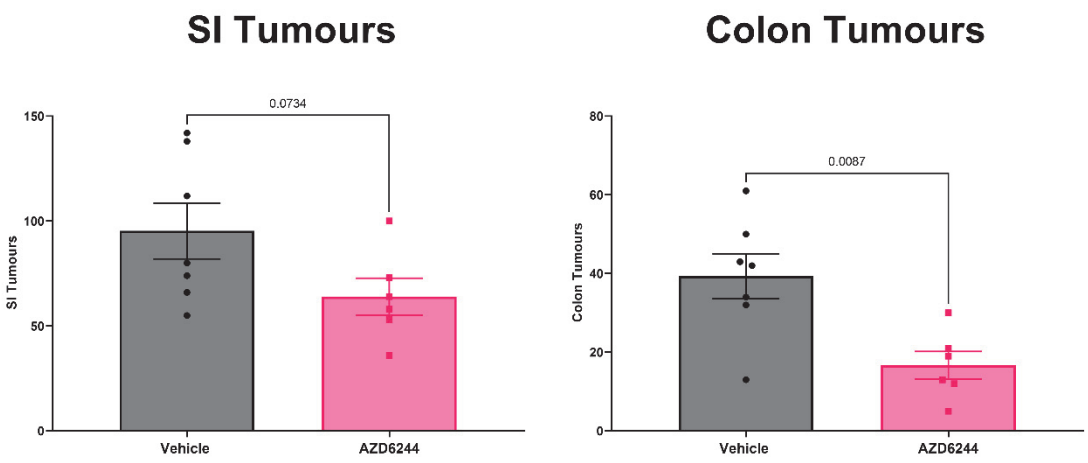

Figure 4-53: Reduced tumour number in AZD6244 treated Villin-CreER^{T2}; *Apc*$^{fl/wt}$; *Kras*$^{G12D/wt}$; *Pten*$^{fl/fl}$ mice from d10 post-induction. Mice were induced and treated with AZD6244 from day 10 post-induction. Tumours were scored from H&E stained slides. Mean ± SEM. Two-sided Mann-Whitney U test.

4.4.3 Discussion

In this section, I showed that the tumour-initiation effect of *Kras*/*Pik3ca* co-mutation heavily relies on functional MEK signalling. MEK1/2-inhibitor treated mice gained a survival benefit and had significantly less tumours at endpoint when treated from day 5 post-induction. When treated at a stage at which multiple tumours were likely already established, MEK1/2 inhibition did not result in a survival benefit, although tumour number at endpoint was lower.

Inhibition of tumour initiation in both SI and Colon was expected, although the extent to which this occurred was impressive. Since PI3-Kinase alpha inhibition was not sufficient to inhibit formation or outgrowth of tumours in *Kras*/*Pik3ca* co-mutated models, it suggests that MAPK signalling is functionally more important than PI3-Kinase signalling in this process. Alternatively, MAPK and PI3-Kinase signalling could be two separately redundant pathways to drive tumour initiation. If this is the case, either PI3-Kinase inhibitors do not inhibit the pathway deeply enough, or there could be PI3-Kinase isoform or downstream pathway component compensation that drives resistance.

While the effect on tumour initiation was striking, AZD6244 did not seem to stop tumour outgrowth in Villin-CreER^{T2}; *Apc*$^{fl/wt}$; *Kras*$^{G12D/wt}$; *Pik3ca*$^{H1047R/wt}$ mice when treated from late, since time to endpoint was the same. As this would be closer to mimicking the clinical situation, this indicates that *Kras*/*Pik3ca* co-mutant

tumours are resistant to MEK1/2 inhibition. Clinically, Selumetinib in combination with classical chemotherapy has not shown a beneficial effect in Solid cancers, including colorectal cancer (Deming *et al.*, 2016; Jänne *et al.*, 2017). In cell lines, resistance to Selumetinib in colorectal cancer cell lines seems to be mediated by activation of the PI3-Kinase/mTOR signalling effectors p70S6K and RPS6 (Grasso *et al.*, 2014). It is therefore reasonable to speculate that mTOR activity can overcome the documented cell cycle arrest induced by AZD6244. In established tumours, this could be occurring either through mutations/amplifications of PI3-Kinase signalling components or physiological activation of the pathway through e.g. insulin-receptor signalling or lysosomal nutrient sensing of mTOR. PI3-Kinase independent pathways, especially wnt signalling, may also confer resistance.

Since the Villin-CreER^{T2}*Apc*$^{fl/wt}$; *Kras*^{G12D}; *Pten*$^{fl/fl}$ model is fast and mice need to be sampled at a median of 19 days post-induction, it was difficult to choose the right experimental setup. I decided to start treatment at day 10 post-induction in the first place, and this can be seen as an intermediate timepoint between early and late stage treatment. There was a somewhat bimodal distribution in the survival curve. Four mice had to be sampled at d21, 22, and 23, while the remaining three were sampled at d35, 36, and 44. Lower tumour numbers indicate that MEK1/2 inhibition had an effect on tumour initiation. Already initiated tumours seemed to grow out under MEK1/2 inhibition, although it is not clear whether they grow out at the same rate. If MEK1/2 inhibition mostly prevented tumour initiation, it would be less effective in mice in which tumours initiated slightly earlier by chance. Treatment from an earlier timepoint, and for a short period to avoid adaptation, would be needed to strengthen the notion that AZD6244 is inhibiting mostly tumour initiation in this setting.

As this work is still on going, tumour scores have not been available for all mice presented in the survival plots as the histological samples are still being processed. Tumours displayed adenomatous morphology.

So far, I have focused on single drug treatment studies. While these can shed light on the most important signalling nodes, experience from the clinic and the previously described treatment studies have shown that tumours usually become resistant. As previously mentioned, co-inhibition of MAPK and PI3-Kinase/mTOR

signalling components may be necessary to be effective in these models, and this will be the topic of the final sub-chapter.

4.5 Combination treatment approaches in intestinal cancer models

I have so far presented single agent treatment in many of the newly characterized models. Three of the previously presented drugs were designed to be combined in the clinical setting: 1) The MEK1/2 inhibitor AZD6244; 2) The PI3-Kinase beta/delta inhibitor AZD8186; 3) The mTOR kinase inhibitor AZD2014 (Schmid *et al.*, 2017; Marques *et al.*, 2020; Choudhury *et al.*, 2022). All three of those drugs have been met with resistance, when used as single agent treatments. To potentially overcome this and reveal synergies between those drugs, I wanted to establish the effect of combination treatments in PI3-Kinase signalling high-, and *Kras* mutant, PI3-Kinase signalling high settings.

4.5.1 PI3-Kinase beta/delta inhibition does not synergize with MEK1/2 or mTOR kinase inhibition in Villin-CreER^{T2}; Apc$^{fl/wt}$; Pten$^{fl/fl}$ mice

PI3-Kinase beta/delta inhibition did not prevent tumour initiation and outgrowth of *Pten* deficient tumours as a single agent. It is not known though, whether combinatory inhibition with other pathway components would reveal a role for PI3-Kinase beta or delta in a potentially rewired pathway. To this end, I treated Villin-CreER^{T2}; *Apc*$^{fl/wt}$; *Pten*$^{fl/fl}$ mice with combinations of both AZD6244/AZD8186 and AZD2014/AZD8186 to inhibit PI3-Kinase beta/delta alongside MEK1/2 and mTOR kinase, respectively. There was no added benefit in survival in either of those drug combinations (Figure 4-54). Combination treatment did not further reduce tumour numbers (Figure 4-55).

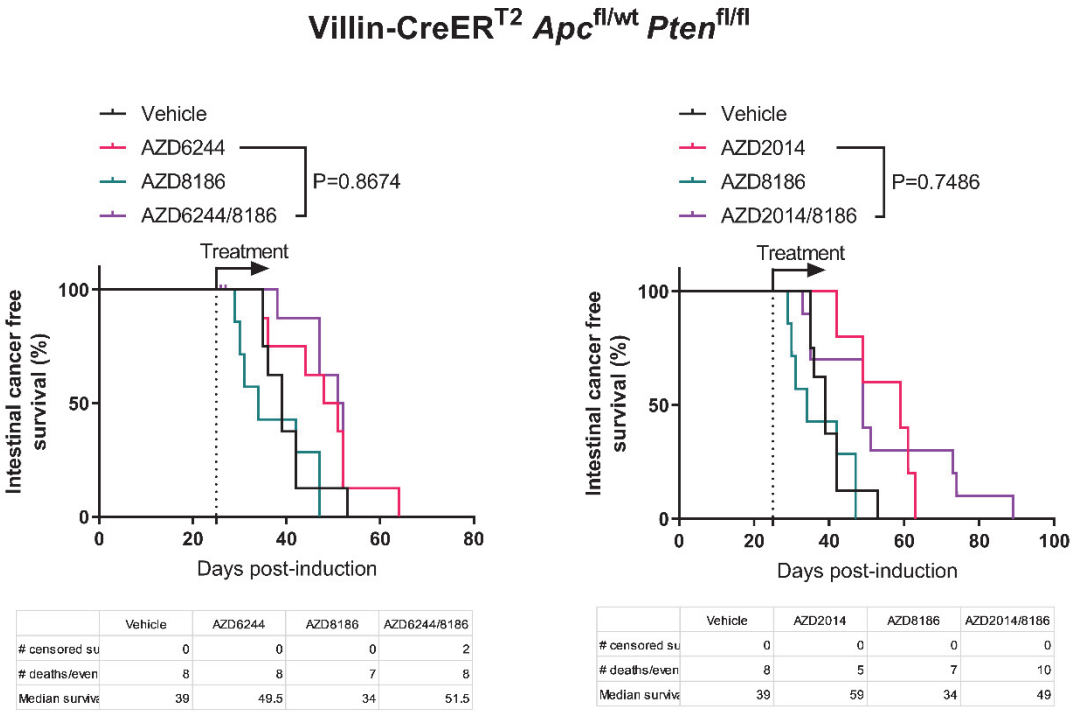

	Vehicle	AZD6244	AZD8186	AZD6244/8186
# censored su	0	0	0	2
# deaths/even	8	8	7	8
Median surviva	39	49.5	34	51.5

	Vehicle	AZD2014	AZD8186	AZD2014/8186
# censored su	0	0	0	0
# deaths/even	8	5	7	10
Median surviva	39	59	34	49

Figure 4-54: MEK1/2 and mTOR kinase inhibition did not synergize with AZD8186 in Villin-CreER^{T2}; *Apc*$^{fl/wt}$; *Pten*$^{fl/fl}$ mice from day 25. Villin-CreER^{T2}; *Apc*$^{fl/wt}$; *Pten*$^{fl/fl}$ mice were dosed 2x daily with 25mg/kg AZD6244 from day 5 post-induction; 2x daily with 50mg/kg AZD8186; 1x daily with 15mg/kg AZD2014, or combinations thereof. Vehicle controls were dosed 0.5% HPMC + 0.1% tween 2x daily. Log-Rank test. Mice were sampled at clinical endpoint. Andrew Campbell and Catriona Ford from the Sansom laboratory have contributed to this data.

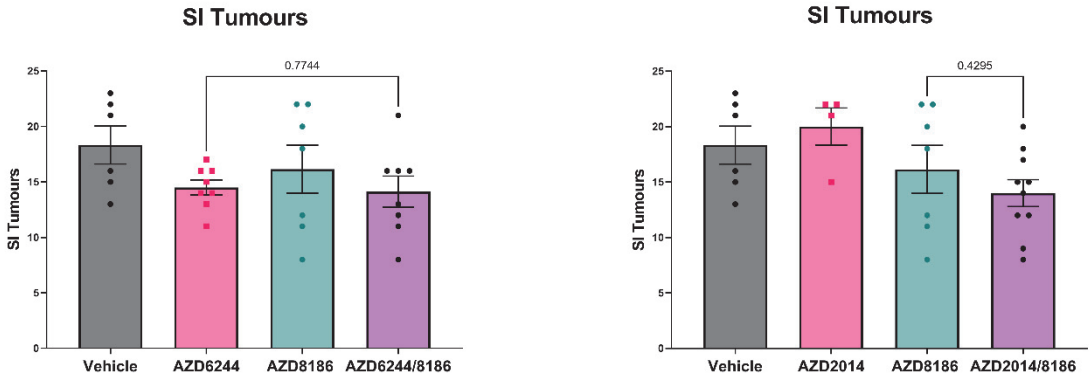

Figure 4-55: No further reduction in combination treatments driven by AZD8186 in Villin-CreER^{T2}; *Apc*$^{fl/wt}$; *Pten*$^{fl/fl}$; mice. Mice were sampled at endpoint and tumours were scored from the processed H&E samples. Mean ± SEM. Two-sided Mann-Whitney U test. Andrew Campbell and Catriona Ford from the Sansom laboratory have contributed to this data.

This further strengthens the notion that PI3-Kinase beta/delta is not essential for tumour initiation and outgrowth in Villin-CreER^{T2}; *Apc*$^{fl/wt}$; *Pten*$^{fl/fl}$ model, even in the context of concomitant inhibition of other pathway components. Given that both MEK1/2 and mTOR kinase inhibition showed some efficacy in the Villin-

CreER^{T2}; *Apc*$^{fl/wt}$; *Pten*$^{fl/fl}$ model, I was eager to test whether combination of those two drugs might show synergy.

4.5.2 Combined MEK1/2 and mTOR kinase inhibition shows synergy in Villin-CreER^{T2}; *Apc*$^{fl/wt}$; *Pten*$^{fl/fl}$ mice

Literature suggests that MAPK and PI3-Kinase/mTOR signalling co-inhibition can result in synergistic effects (Jaaks, Elizabeth A. Coker, *et al.*, 2022). To test this *in vivo*, I induced and aged Villin-CreER^{T2}; *Apc*$^{fl/wt}$; *Pten*$^{fl/fl}$ mice to day 25 post-induction, after which I treated them with the AZD6244/2014 combination. This resulted in a significant survival benefit, as mice reached clinical endpoint at a median of 71 days post-induction (range: 60 to 95 days) compared to the best single-arm treatment AZD2014 (median: 59 days; range: 42 to 63 days) (Figure 4-56). AZD6244/2014-combination treated mice had similar tumour numbers as AZD6244 treated mice, although this was reduced when adjusted for their prolonged survival (Figure 4-57).

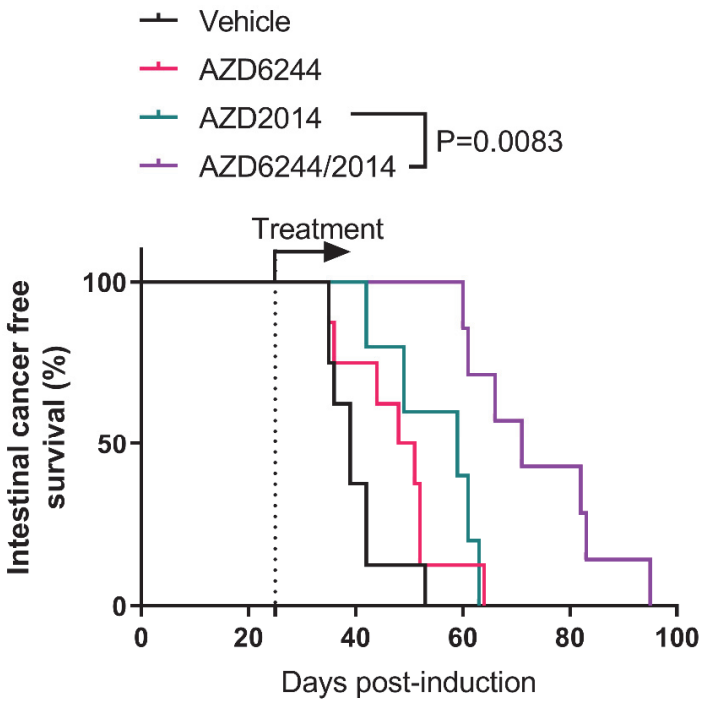

	Vehicle	AZD6244	AZD2014	AZD6244/2014
# censored subjects	0	0	0	0
# deaths/events	8	8	5	7
Median survival	39	49.5	59	71

Figure 4-56: MEK1/2 and mTOR kinase inhibitor co-treatment results in a further survival benefit in Villin-CreER^{T2}; *Apc*$^{fl/wt}$; *Pten*$^{fl/fl}$ mice when treated from day 25 post-induction. Villin-

CreER^{T2}; *Apc*$^{fl/wt}$; *Pten*$^{fl/fl}$ mice were dosed 2x daily with 25mg/kg AZD6244 from day 5 post-induction; 1x daily with 15mg/kg AZD2014, or a combination of both. Vehicle controls were dosed 0.5% HPMC + 0.1% tween 2x daily. Log-rank test. Mice were sampled at clinical endpoint. Andrew Campbell and Catriona Ford from the Sansom laboratory have contributed to this data.

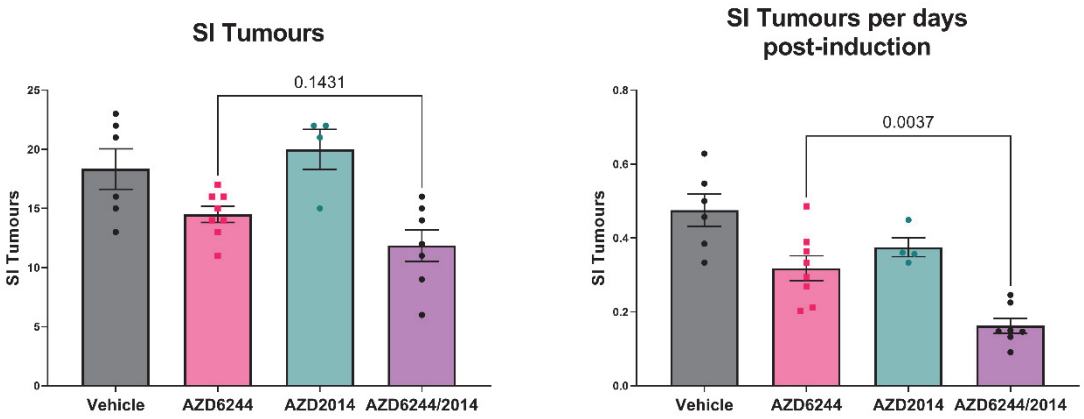

Figure 4-57: Similar total tumour number, reduction in tumour number per day post-induction in AZD6244/2014 combination treated Villin-CreER^{T2}; *Apc*$^{fl/wt}$; *Pten*$^{fl/fl}$ mice
Mice were sampled at endpoint and tumours were scored from the processed H&E samples. Tumour number was divided by days post-induction. Mean ± SEM. Two-sided Mann-Whitney U test. Andrew Campbell and Catriona Ford from the Sansom laboratory have contributed to this data.

Co-inhibition of MEK1/2 and mTOR-kinase was therefore the most promising of the tested combinations in Villin-CreER^{T2}; *Apc*$^{fl/wt}$; *Pten*$^{fl/fl}$ mice.

I have previously shown differential response to treatment upon *Kras* mutation and therefore the next step was to treat Villin-CreER^{T2}*Apc*$^{fl/wt}$; *Kras*^{G12D}; *Pten*$^{fl/fl}$ mice with the drug combinations to assess if the response to combination treatment is altered.

4.5.3 MEK1/2 inhibition is needed to achieve synergy in drug combinations in Kras mutant models

To address the impact of *Kras*^{G12D} mutation on the response to combination treatments, Villin-CreER^{T2}*Apc*$^{fl/wt}$; *Kras*^{G12D}; *Pten*$^{fl/fl}$ mice were induced and treated at day 10 post-induction with the aforementioned combinations of MEK1/2, mTOR-kinase and PI3-Kinase beta/delta inhibitors.

Combination of AZD8186 and AZD2014 did not have a synergistic effect (Figure 4-58). Colonic tumour number at endpoint was similar for all conditions, while SI

tumour number was slightly elevated in the small intestines of AZD2014 treated mice, compared to AZD8186 single arm (Figure 4-59).

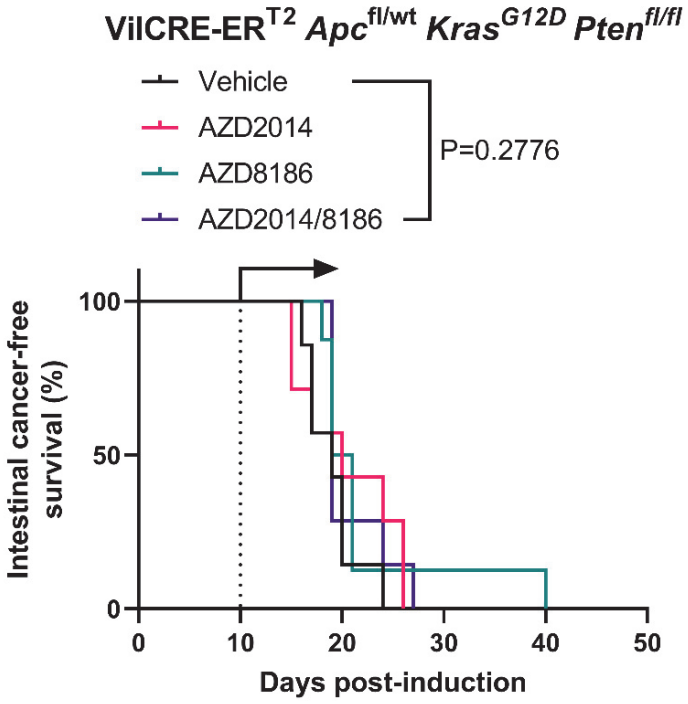

	Vehicle	AZD2014	AZD8186	AZD2014/8186
# censored subjects	0	0	0	0
# deaths/events	7	7	8	7
Median survival	19	20	20	19

Figure 4-58: No added benefit of PI3-Kinase beta/delta (AZD8186) and mTOR-Kinase (AZD2014) inhibitors in Villin-CreER^{T2}*Apc*$^{fl/wt}$; *Kras*^{G12D}; *Pten*$^{fl/fl}$ mice from day 10 post-induction. Villin-CreER^{T2}; *Apc*$^{fl/wt}$; *Kras*$^{G12D/wt}$; *Pik3ca*$^{H1047R/wt}$ mice were dosed from day 10 post-induction with 2x daily with 50mg/kg AZD8186; 1x daily with 15mg/kg AZD2014, or combinations thereof. Vehicle controls were dosed 0.5% HPMC + 0.1% tween 2x daily. Mice were sampled at clinical endpoint. Log-rank test. Andrew Campbell and Catriona Ford from the Sansom laboratory have contributed to this data.

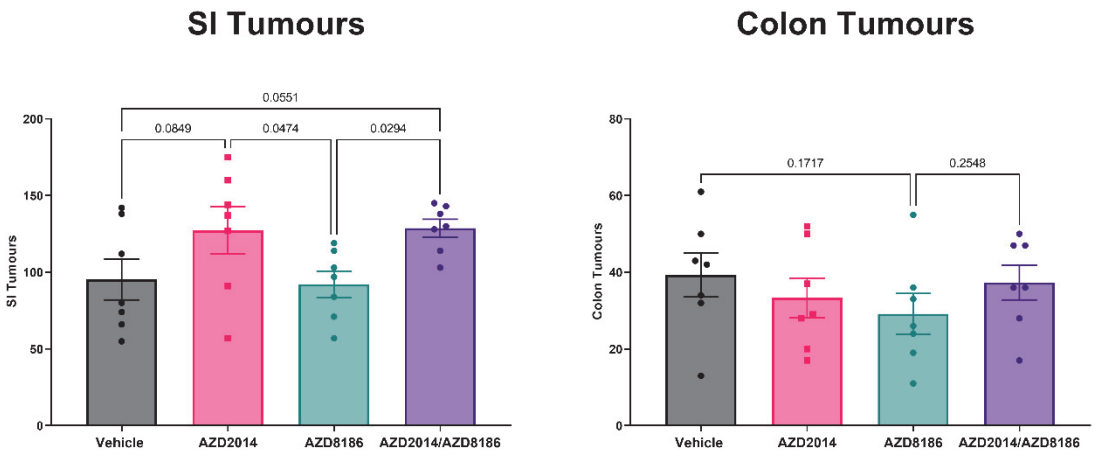

Figure 4-59: Increased SI tumour number in AZD2014 and AZD2014/AZD8186 treated Villin-CreER^{T2}*Apc*$^{fl/wt}$; *Kras*^{G12D}; *Pten*$^{fl/fl}$ mice, similar colon tumour number. Villin-CreER^{T2}*Apc*$^{fl/wt}$; *Kras*^{G12D}; *Pten*$^{fl/fl}$ mice were induced and treated from day 10 post-induction until clinical endpoint with the indicated drugs. Tumours were scored from histological sections. Mean ± SEM. Kruskal-Wallis test and uncorrected Dunn's multiple comparison test. Andrew Campbell and Catriona Ford from the Sansom laboratory have contributed to this data.

While treatment with AZD6244 extended survival of Villin-CreER^{T2}*Apc*$^{fl/wt}$; *Kras*^{G12D}; *Pten*$^{fl/fl}$ mice, AZD8186 did not. To test whether combination of those compounds would result in a synergistic effect, mice were subjected to AZD6244/AZD8186 combination treatment. This resulted in a robust survival benefit compared to vehicle treated mice, although it was not significantly different from AZD6244 single agent (Figure 4-60). Increased sample size would likely show an added benefit. Tumour number was also robustly decreased in combination treated mice compared to vehicles, although again not lower than in the AZD6244 treatment arm (Figure 4-61).

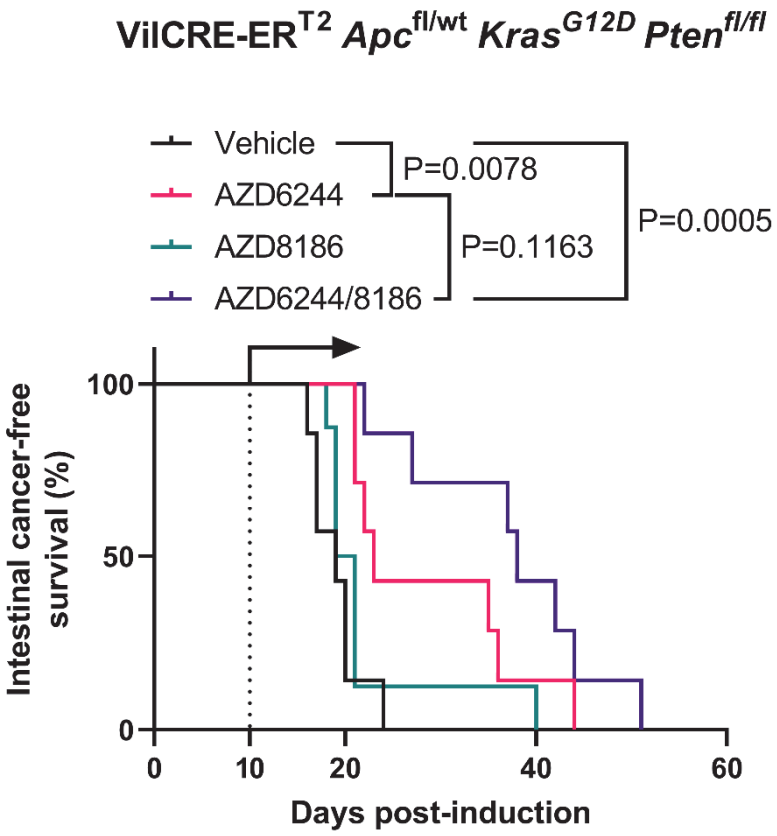

	Vehicle	AZD6244	AZD8186	AZD6244/8186
# censored subjects	0	0	0	0
# deaths/events	7	7	8	7
Median survival	19	23	20	38

Figure 4-60: PI3-Kinase beta/delta (AZD8186) and MEK1/2 (AZD6244) inhibitor combination robustly extends survival in Villin-CreER^{T2}*Apc*$^{fl/wt}$; *Kras*^{G12D}; *Pten*$^{fl/fl}$ mice from day 10 post-induction. Villin-CreER^{T2}; *Apc*$^{fl/wt}$; *Kras*$^{G12D/wt}$; *Pten*$^{fl/fl}$ mice were dosed from day 10 post-induction 2x daily with 50mg/kg AZD8186; 2x daily with 25mg/kg AZD6244, or combinations thereof. Vehicle controls were dosed 0.5% HPMC + 0.1% tween 2x daily. Mice were sampled at clinical endpoint. Log-rank test. Andrew Campbell and Catriona Ford from the Sansom laboratory have contributed to this data.

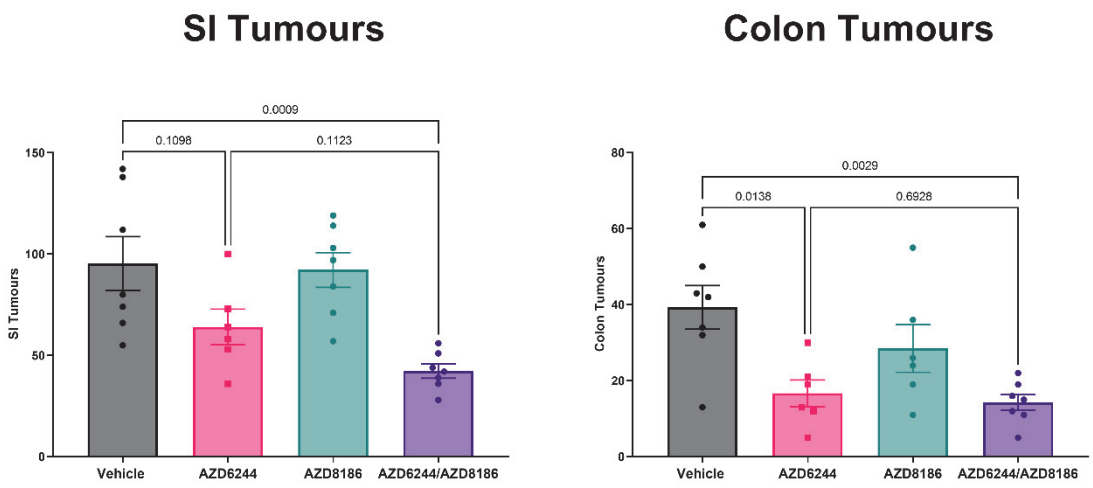

Figure 4-61: AZD6244 dependent reduction in SI and Colon in Villin-CreER^{T2}*Apc*$^{fl/wt}$; *Kras*^{G12D}; *Pten*$^{fl/fl}$ mice treated from day 10 post-induction. Villin-CreER^{T2}*Apc*$^{fl/wt}$; *Kras*^{G12D}; *Pten*$^{fl/fl}$ mice were induced and treated from day 10 post-induction until clinical endpoint with the indicated drugs. Tumours were scored from histological sections. Mean ± SEM. Kruskal-Wallis test and uncorrected Dunn's multiple comparison test. Andrew Campbell and Catriona Ford from the Sansom laboratory have contributed to this data.

This was surprising, as AZD8186 did not have an effect in *Kras* wildtype, *Pten* mutants. *Kras* mutation therefore might alter this dependence.

Since PI3-Kinase beta could potentially be downstream of PI3-Kinase alpha signalling, I next wanted to test whether *Kras*/*Pik3ca* co-mutated mice would exhibit a response to AZD6244/AZD8186 combination. I treated Villin-CreER^{T2}; *Apc*$^{fl/wt}$; *Kras*$^{G12D/wt}$; *Pik3ca*$^{H1047R/H1047R}$ mice from day 5 post-induction to clinical endpoint. AZD8186 did not provide an additional benefit, compared to AZD6244 single agent (Figure 4-62), indicating that the effect observed in Villin-CreER^{T2}*Apc*$^{fl/wt}$; *Kras*^{G12D}; *Pten*$^{fl/fl}$ is not dependent on PI3-Kinase alpha signalling.

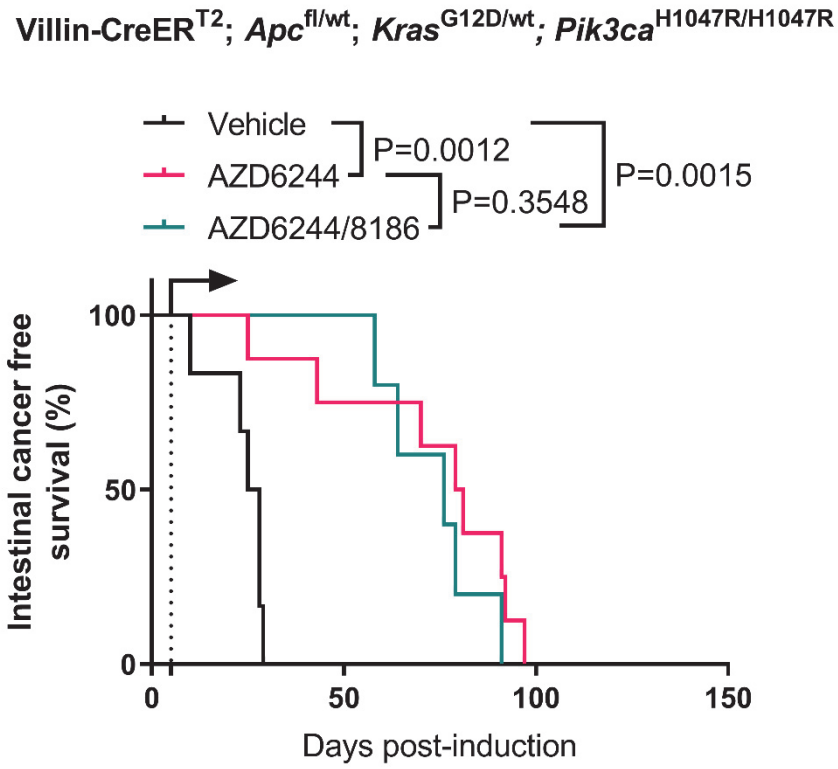

	Vehicle	AZD6244	AZD6244/8186
# censored subjects	0	0	0
# deaths/events	6	8	5
Median survival	26.5	80	76

Figure 4-62: PI3-Kinase beta/delta (AZD8186) inhibitor does not add benefit to MEK1/2 (AZD6244) inhibitor treatment in Villin-CreER^{T2}*Apc*$^{fl/wt}$; *Kras*^{G12D}; *Pik3ca*$^{H1047R/H1047R}$ mice from day 10 post-induction. Villin-CreER^{T2}; *Apc*$^{fl/wt}$; *Kras*$^{G12D/wt}$; *Pik3ca*$^{H1047R/H1047R}$ mice were dosed from day 5 post-induction 2x daily with 50mg/kg AZD8186; 2x daily with 25mg/kg AZD6244, or combinations thereof. Vehicle controls were dosed 0.5% HPMC + 0.1% tween 2x daily. Mice were sampled at clinical endpoint. Log-rank test. Andrew Campbell and Catriona Ford from the Sansom laboratory have contributed to this data.

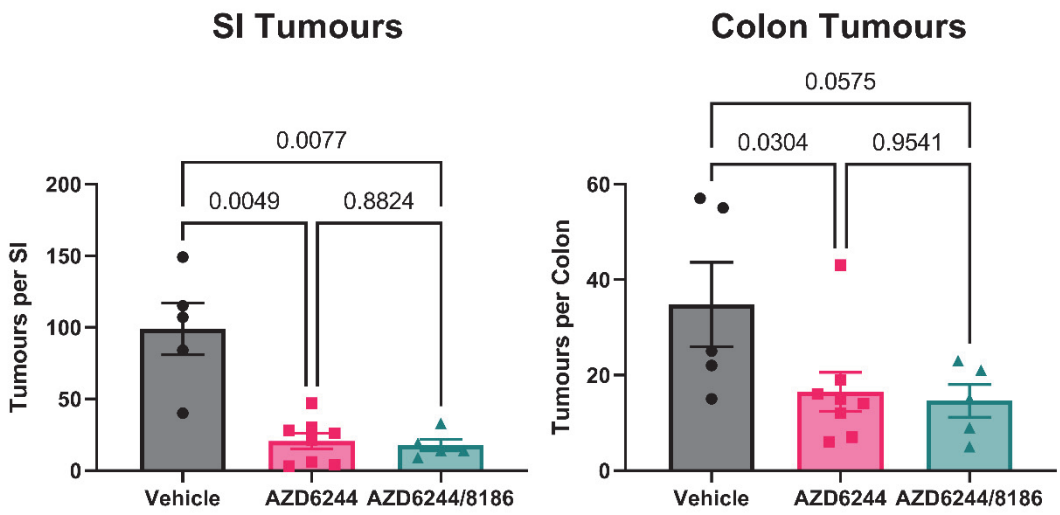

Figure 4-63: AZD6244 dependent reduction in SI and Colon in Villin-CreER^{T2}*Apc*$^{fl/wt}$; *Kras*^{G12D}; *Pik3ca*$^{H1047R/H1047R}$ mice treated from day 10 post-induction. Villin-CreER^{T2}*Apc*$^{fl/wt}$; *Kras*^{G12D}; *Pik3ca*$^{H1047R/H1047R}$ mice were induced and treated from day 10 post-induction until clinical endpoint with the indicated drugs. Tumours were scored from histological sections. Mean ± SEM. Kruskal-Wallis test and uncorrected Dunn's multiple comparison test. Andrew Campbell and Catriona Ford from the Sansom laboratory have contributed to this data.

Previous results indicated that co-formulation of AZD6244 and AZD2014 was the only combination that strongly synergized to drive a survival benefit in Villin-CreER^{T2}*Apc*$^{fl/wt}$; *Pten*$^{fl/fl}$ mice. To establish whether *Kras* mutation alters this phenotype, Villin-CreER^{T2}*Apc*$^{fl/wt}$; *Kras*^{G12D}; *Pten*$^{fl/fl}$ mice were induced and treated from day 10 post-induction. This resulted in a significant survival benefit in AZD6244/AZD2014 combination treated mice (Figure 4-64). Total SI and colonic tumours were not reduced beyond the previously described AZD6244 treatment in AZD6244/AZD2014 treated mice (Figure 4-65).

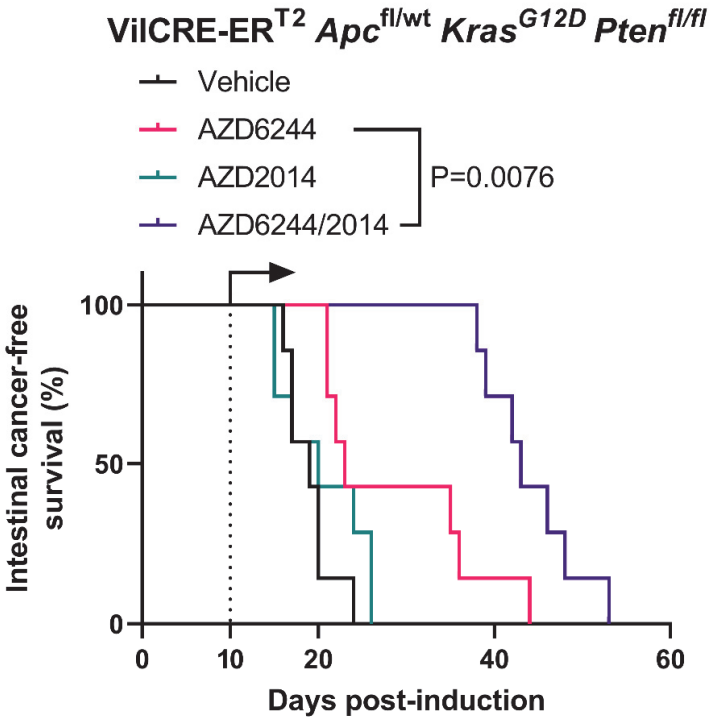

	Vehicle	AZD6244	AZD2014	AZD6244/2014
# censored subjects	0	0	0	0
# deaths/events	7	7	7	7
Median survival	19	23	20	43

Figure 4-64: MEK1/2 (AZD6244) and mTOR (AZD2014) inhibitors synergize to extend survival in Villin-CreER^{T2}*Apc*$^{fl/wt}$; *Kras*^{G12D}; *Pten*$^{fl/fl}$ mice from day 10 post-induction. Villin-CreER^{T2}; *Apc*$^{fl/wt}$; *Kras*$^{G12D/wt}$; *Pten*$^{fl/fl}$ mice were dosed from day 10 post-induction 1x daily with 15mg/kg AZD2014; 2x daily with 25mg/kg AZD6244, or combinations thereof. Vehicle controls were dosed 0.5% HPMC + 0.1% tween 2x daily. Mice were sampled at clinical endpoint. Log-rank test. Andrew Campbell and Catriona Ford from the Sansom laboratory have contributed to this data.

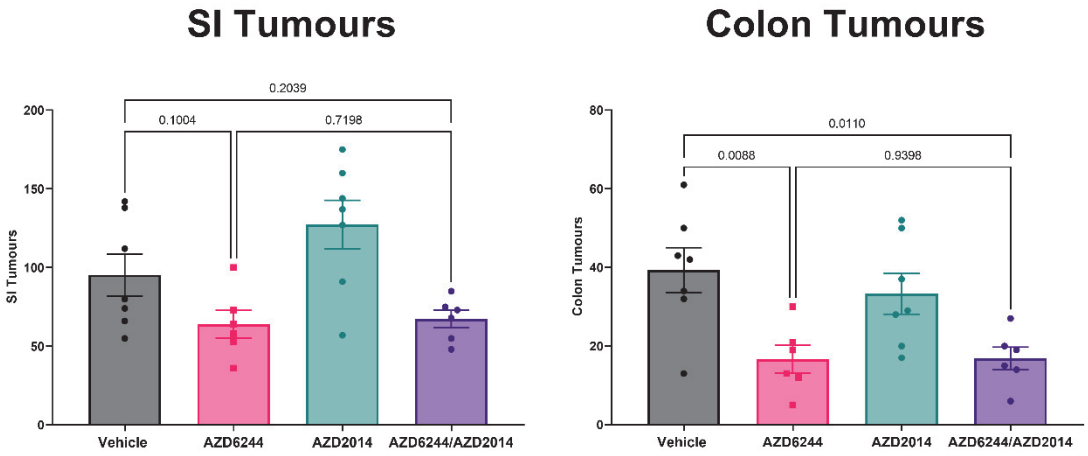

Figure 4-65: AZD6244 dependent reduction in SI and Colon in Villin-CreER^{T2}*Apc*$^{fl/wt}$; *Kras*^{G12D}; *Pten*$^{fl/fl}$ mice treated from day 10 post-induction. Villin-CreER^{T2}*Apc*$^{fl/wt}$; *Kras*^{G12D}; *Pten*$^{fl/fl}$ mice were induced and treated from day 10 post-induction until clinical endpoint with the indicated drugs. Tumours were scored from histological sections. Mean ± SEM. Kruskal-Wallis test and uncorrected Dunn's multiple comparison test. Andrew Campbell and Catriona Ford from the Sansom laboratory have contributed to this data.

4.5.4 Discussion

In this section I showed that the PI3-Kinase beta/delta inhibitor AZD8186 did not synergize with inhibition of either MEK1/2 or mTOR kinase in Villin-CreER^{T2}; *Apc*$^{fl/wt}$; *Pten*$^{fl/fl}$ mice. Combination of MEK1/2 and mTOR kinase inhibitor on the other hand demonstrated synergy and resulted in prolonged survival and reduction in tumour numbers when adjusted for this. Added Kras mutation rendered mice slightly more sensitive to AZD6244/AZD8186 combination, likely in a PI3-Kinase alpha independent manner. AZD2014 did not synergize with AZD8186, while co-treatment with AZD6244 resulted in a robust, additional survival benefit.

Lack of synergy between the PI3-Kinase beta/delta inhibitor and MEK1/2/mTOR kinase inhibitors in Villin-CreER^{T2}; *Apc*$^{fl/wt}$; *Pten*$^{fl/fl}$ mice was partly expected, given the earlier presented irrelevance of PI3-Kinase beta and delta in initiation and sustainment tumour growth in this setting. It was still somewhat surprising though, since there are multiple publications claiming a general dependence of *Pten* deficient cancers on PI3-Kinase beta to sustain proliferation (Wee *et al.*, 2008; Hancox *et al.*, 2015). Interestingly, upon introduction of a *Kras* mutation, PI3-Kinase beta inhibition seemingly became more relevant, as the combination resulted in a survival benefit. This again points towards tissue/cancer type specificity and confirms the previously presented results using AZD8186 as a single agent being more relevant in *Kras* mutant models. Lack of additional efficacy between AZD6244/AZD8186 in Villin-CreER^{T2}; *Apc*$^{fl/wt}$; *Kras*$^{G12D/wt}$; *Pik3ca*$^{H1047R/wt}$ mice demonstrated that PI3-Kinase alpha signalling does not result in a dependence on beta upon *Kras*/*Pik3ca* co-mutation. As mentioned earlier, PI3-Kinase beta has a potential role downstream of PI3-Kinase alpha, but this does not seem to be a vulnerability in this setting.

Combining mTOR kinase and MEK1/2 inhibition had the greatest effect of the trialled combination therapies in both *Kras* wildtype and mutant models. Pre-clinical studies, including large screening efforts in cell lines, have pointed towards the necessity to inhibit both MAPK and PI3-Kinase/mTOR signalling to achieve efficacy (Jaaks, Elizabeth A. Coker, *et al.*, 2022). To this end, combining the MEK1/2 inhibitor with the PI3-Kinase alpha inhibitor would also be an appropriate experiment as I have shown that mice gain a survival benefit from PI3-Kinase alpha inhibition. Unfortunately, this combination is toxic when treated

systemically, presumable due to on-target effects on various cell population throughout the organism.

As this work is still on going, tumour scores have not been available for all mice presented in the survival plots as the histological samples are still being processed.

It is important to highlight that in Villin-CreER^{T2}; *Apc*$^{fl/wt}$; *Pten*$^{fl/fl}$ mice, neither of these combination treatments were as effective as Rapamycin. Further immunohistochemical and western blot analysis will be needed to determine why the combination treatments were not as potent. I would expect sustained mTORC1 signalling markers in tumours under combination treatment. One could speculate that drugs (or combinations) in this context may not be effective unless they can shut down mTORC1 driven translation elongation. Since mTORC2 seems to have a role in the outgrowth of tumours in *Kras* mutant models, and AZD2014 is expected to hit both mTORC1 and mTORC2, there is a rationale to use this drug in the *Kras* mutant setting. Especially the combination of AZD6244/AZD2014 showed marked synergy in this model. Characterisation of the tumours that grew out eventually may shed light on the resistance mechanism.

4.6 Discussion

In this chapter, I presented my effort in dissecting the PI3K/MAPK/mTOR signalling network using genetic models and small molecule inhibitors in the previously characterized PI3-Kinase hyperactive GEMMs of intestinal cancer.

In *Kras* wildtype, *Pten* deficient models I showed that PI3-Kinase alpha was dominant over the beta isoform. Targeting mTORC1 directly, rather than through mTORC2 or AKT, was most effective at preventing initiation and outgrowth of tumours. Translation elongation still seemed to be the rate-limiting factor in this setting, as mTOR-Kinase inhibition was not as effective as Rapamycin. Single agent MEK1/2 inhibition did not show a clear benefit, but synergized with mTOR-Kinase inhibition to drive a survival benefit (Figure 4-66).

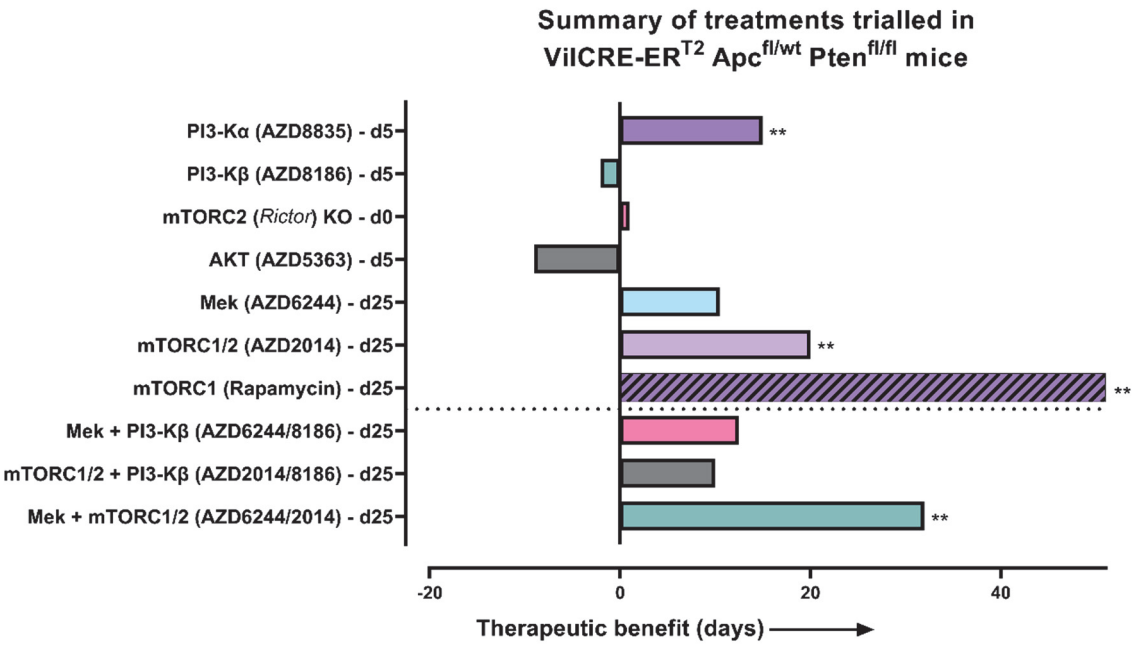

Figure 4-66: Summary of treatments trialled in Villin-CreER^{T2}; *Apc*$^{fl/wt}$; *Pten*$^{fl/fl}$ mice. Data generated for this graph were presented in chapter 4 of this thesis.Therapeutic benefit was defined as change in median survival in treated vs vehicle/untreated cohorts. Fill pattern in mTORC1 treatment indicates that these mice did not reach clinical endpoint and were sampled at timepoint. Dashed line separates single from combination therapies. Two stars (**) represent P-value <0.01.

Overall, *Kras* mutation had a profound impact on treatment response. PI3-Kinase alpha was ineffective in *Kras* mutant models, regardless of *Pik3ca* mutation. *Kras* mutation led to a slightly increased dependence on PI3-Kinase beta/delta, which was still upheld after *Pten*-KO. While MEK1/2 inhibition was effective at preventing tumour formation, tumour outgrowth seemed to be unaffected. Combination therapy revealed that while combination of MEK1/2 and PI3-Kinase beta/delta inhibition resulted in a slight benefit, MEK1/2 and mTOR-kinase co-inhibition remained the most promising of the trialled combinations.

Characterizing the response of tumours to the targeted inhibitors initially, vs after they have adapted to the treatment would be beneficial to understand the dynamics of resistance. For instance, treating mice with drugs for two days might reveal an initial response, followed by adaptation after some time. IHC on biomarkers in tandem with additional methods could then shed light on the exact resistance mechanism.

All models presented in this chapter are fast models with rapid tumour initiation, with endpoint characterised by accumulation of large numbers of pathologically

“early” tumours. While this enables relatively high throughput and predictable time to endpoint, it fails to capture true late-stage disease, including treatment response in advanced adenocarcinomas. A stroma might lead to differential response in tumours. On the flipside, it is difficult to imagine a drug eliciting a relevant response in human CRC if it does not show any efficacy in these rather simple models.

Targeted therapy in the PI3-Kinase pathway has on-target toxicity on an organismal level, causing adverse effects in the clinic. Combining multiple targeted inhibitors in this space has proven to be difficult, as e.g. combined PI3-Kinase alpha and MEK12 inhibition is toxic in mice when treated for more than a few days (unpublished data from the lab). This is a limitation sometimes forgotten, or not taken into account in cell culture experiments. While combined PI3-Kinase and MEK1/2 inhibition may be effective *in vitro*, systemic treatment may be too challenging for many patients.

Presumably, all of the drug treatments presented so far have some effect on cellular physiology, and therefore in vitro drug screening efforts might reveal unexpectedly promising combination treatment approaches that can be trialled and compared to the ones presented in this thesis.

Chapter 5 Discussion and Outlook

In this thesis I presented a characterisation of multiple new GEMMs of intestinal cancer, driven by hyperactive PI3-Kinase and KRAS signalling. I made use of inducible genetics to introduce human disease-relevant alterations to the murine intestine. Most experiments were performed in the context of intestinal tumorigenesis driven by predisposition to *Apc*-loss, resulting in aberrant wnt signalling. Furthermore, most experiments were performed in the same genetic background, which enabled direct comparison of the oncogenic mutations and their impact on intestinal cancer initiation and progression, and treatment response *in vivo*. Expression of the *Pik3ca*^{H1047R} point-mutation resulted in a gene-dosage dependent effect on tumour initiation and progression to advanced cancer. Heterozygous mutation did not affect the rate of tumour initiation, but promoted progression to invasive adenocarcinoma. Homozygous mutation drove tumour initiation, but did not lead to increased occurrence of advanced cancer. Genetic KO of the main negative regulator of PI3-Kinase signalling *Pten* had a similar gene-dosage effect, although the tumour initiating phenotype was more profound in bi-allelic *Pten*-KO mice than in *Pik3ca*$^{H1047R/H1047R}$ mutant mice. I could show marked synergy between the two alleles, indicating that there is functional relevance of multiple pathway activating mutations in intestinal cancer initiation and progression to invasive adenocarcinoma. The tumour initiation phenotypes were acutely dependent on *Apc*-loss predisposition, as tumours only formed after a very long latency in the guts of *Apc* wildtype mice. Synergy to drive tumour initiation was not only observed within the PI3-Kinase signalling pathway, but also with *Kras*^{G12D}. In *Kras*^{G12D} mutant mice, heterozygous *Pik3ca* mutation already resulted in additional tumour formation, which was further exacerbated upon homozygous *Pik3ca*^{H1047R} mutation. This was in contrast to *Kras* wildtype models and indicates biological synergy between those two pathways.

Following characterisation of these models, I used further genetic and pharmacological targeting of key nodes in the PI3-K/MAPK/mTOR signalling network to understand dependence upon individual components. Overall I could show that *Kras* mutation had a profound impact on the response to targeted inhibition of PI3-K/MAPK/mTOR signalling components. While *Kras* wildtype models responded to PI3-Kinase alpha inhibition, *Kras* mutants were resistant, regardless of concomitant *Pik3ca*^{H1047R} mutation. PI3-Kinase beta inhibition on the

other hand was not effective in *Kras* wildtype models, but resulted in a survival benefit in the *Kras* mutant context, likely in a RAC1/PI3-Kinase beta -interaction independent manner. By targeting mTOR signalling, I could show that PI3-Kinase driven models are not sensitive to *Rictor*/mTORC2 KO and presented with a counter-intuitive tumour initiation phenotype. In *Kras* mutant mice, *Rictor*/mTORC2 KO resulted in a delayed outgrowth of tumours, indicating increased dependency on this aspect of mTOR signalling. mTORC1 inhibition was extremely effective at preventing initiation and outgrowth of PI3-Kinase hyperactive intestinal tumours. This vulnerability was overridden by *Kras* co-mutation, which drove acute resistance to mTORC1 inhibition. Targeting MAPK signalling in *Kras* wildtype, *Pten* deficient mice yielded no clear benefit, while the tumour initiation phenotype in *Kras*/*Pik3ca* co-mutated mice was dependent on functional MAPK signalling. Established tumours were not sensitive to MEK1/2 inhibition though, indicated by a lack of efficacy in *Kras*/*Pik3ca* co-mutant mice treated from a later timepoint. In search for the best co-treatment, combined MEK1/2 and mTOR-kinase inhibition outperformed MEK1/2/PI3-Kinase beta and mTOR-kinase/PI3-Kinase beta inhibitor combinations.

GEMMs of intestinal cancer have undergone multiple iterations of development, (Jackstadt and Sansom, 2016; Lannagan *et al.*, 2021). Complex genetic models have been developed to capture important aspects of human disease, such as recently describing the role of NOTCH signalling in driving metastasis (Jackstadt *et al.*, 2019). While the exact role of PI3-Kinase signalling is not fully understood yet, data presented in this thesis would indicate that strong PI3-Kinase hyperactivation, e.g. bi-allelic *Pten*-loss, may facilitate tumour formation, while more subtle increases can promote adenoma to adenocarcinoma progression. Involvement of PI3-Kinase signalling in metastasis would certainly be interesting to investigate further and could be addressed by orthotopic transplantation of cell lines generated in the context of this project. Increased tumour formation could be due to increased pro-survival signalling directly upon oncogenic transformation, or different behaviour in cells leading to transformation. Finally, PI3-Kinase signalling might become relevant in treatment response, although clinically there is no clear signal indicating resistance to standard of care treatment.

The set of treatments, presented in the second results chapter, were done in a hypothesis driven manner to determine reliance on individual pathway components. Screening for drugs *in vitro*, using organoid lines generated from these genotypes, could be a useful way to discover unexpected synergies. Ultimately, this should facilitate the progression of drugs to the clinic and inform on resistances to avoid treatments in patients that were going to fail from the start. Association of e.g. PI3-Kinase hyperactivating mutations or functional markers such as high pAKT could help to guide patient stratification and guide clinical trial design.

Given the data presented in the second results chapter, some predictions on treatment response in human CRC can be made:

1) *KRAS* mutant cancers are likely going to be acutely resistant to PI3-Kinase alpha inhibitors, irrespective of concomitant PI3-Kinase activating mutations. Especially since even *KRAS* wildtype, PI3-Kinase signalling high tumours did not respond well to targeted PI3-Kinase inhibition.

2) MAPK wildtype, PI3-Kinase signalling-biomarker high tumours could still be sensitive to mTORC1 inhibition or targeted inhibition of translation elongation.

3) MEK1/2 inhibition as a single agent may not be effective, regardless of MAPK mutation, but combination with mTOR-kinase inhibition might be a promising combination approach.

While treatment from an early stage may inform on important processes in tumour formation and outgrowth, the most clinically relevant setting is treatment of established tumours at a late stage. In this setting, tumours were resistant to most of the trialled treatments. More short-term treatments at a late stage will be necessary to elucidate the exact mechanism of resistance, i.e. whether tumour cells are intrinsically resistant, or acquire resistance to the targeted inhibitors over time.

PI3-Kinase inhibitors have entered the clinics, but despite initial optimism, high hopes have not been fulfilled due to disease progression and/or discontinuation

due to toxicity (Bowles *et al.*, 2016; Van Geel *et al.*, 2017; Bardia *et al.*, 2020). The most promising positive signal in the clinical application of PI3-Kinase inhibitors comes from SOLAR-1 breast cancer trial (André *et al.*, 2019). This study showed that ER+ breast cancer patients benefitted from concomitant PI3-Kinase alpha inhibition and fulvestrant, a selective estrogen receptor degrader. *PIK3CA* mutations occur in around 40% of hormone receptor positive breast cancer patients and a study conducted that mammary epithelial cells are very susceptible to *PIK3CA*^{H1047R} mediated transformation (Hart *et al.*, 2015). This indicates that breast and colon cells are wired differentially, resulting in a differential response to both PI3-Kinase pathway mutations, but also targeted therapy. The determining factor in these two cancer types may lie in their co-dependencies. In breast cancer, estrogen receptor signalling seems to sustain cancer growth alongside PI3-K signalling. Wnt signalling could have the same role in colorectal cancer. Wnt-signalling output inhibitors combined with PI3-Kinase inhibitors could therefore be trialled.

An important genetic alteration in CRC that I mentioned in the introduction, but did not elaborate further on, is loss of functional p53. *PIK3CA* and *TP53* mutations are mutually exclusively enriched in colorectal cancer patients, but co-mutation seems to drive worse overall survival and treatment response (Li *et al.*, 2018; Voutsadakis, 2021). The interaction between those pathways would therefore be interesting to investigate further. Mutual exclusivity of TP53 and PIK3CA mutation could indicate that they have redundant functions. Aberrant cell cycle progression and anti-apoptotic signalling could be some of those. *TP53* mutation has been shown to confer invasive properties to cells, akin to the phenotype observed in heterozygous PI3-Kinase mutants in this thesis. Finally, establishing the impact of *TP53* mutations on response to targeted treatment would be useful.

PIK3CA mutations significantly co-occur with BRAF mutation in human CRC (Voutsadakis, 2021). This implies that while there is a strong synergy with KRAS mutations, presumably in part due to their direct interaction, there is also a generic MAPK/PI3-K synergy in CRC. Relevance of this could be tested in mouse models by crossing the *Pik3ca*^{H1047R} allele to *Braf*^{V600E} mutant mice.

More precise quantification of signalling changes in response to mono-or bi-allelic mutation of the PI3-Kinase components will still be important to do. Gene-dosage

and IHC was used to describe the impact of the alleles on the mouse models. Ideally I would like to state exactly how and when PI3-Kinase signalling is changed in the different intestinal epithelial cell types before and after malignant transformation. There is an obvious propensity to lose the wildtype copy of *Apc* in intestinal epithelial cells e.g. upon *Pten* loss, or a selection to survive this process. Which cell type responds in what manner to drive this phenotype? Single cell sequencing could be performed on Villin-CreER^{T2}; *Pten*$^{fl/fl}$ mice directly after *Pten*-loss to capture cell type specific changes or changes in abundance of particular cell types. The nature of these changes would then inform hypothesis driven research into the most relevant pathways in the most relevant cell type. Furthermore, *Apc* wildtype crypt cultures could be used to dynamically measure the changes upon loss of *Pten* or introduction of mutant *Pik3ca*. I would expect PIP3 dynamics to change, ie accumulation of PIP3 and other phosphoinositides, resulting in aberrant localisation of downstream signalling proteins. Further investigation into the SI-specific tumour initiation phenotype would also be interesting, as there is no clear indication why the SI would be that much more permissive than the colon to PI3-Kinase driven tumour initiation.

A drawback of the purely PI3-Kinase driven models is that tumours arise almost exclusively in the SI. Since the modelled disease is colorectal cancer, induction of colonic tumours either by intracolonic injection of 4-OH tamoxifen or transplantation of organoid/spheroid cultures may be used to further refine this model and to elucidate colon-specific effects of PI3-Kinase signalling once tumours are established. I have already trialled the injection of 4-OH into the colon of Villin-CreER^{T2}; *Apc*$^{fl/fl}$; *Pten*$^{fl/fl}$ mice. This led to formation of tumours with a mixed population of *Pten* wildtype and KO cells. pAKT was high in a *Pten* dependent manner, indicating that *Pten* is also responsible for suppressing the PI3-Kinase signalling pathway in colonic tumours.

Combination treatment between the PI3-Kinase and MAPK pathways has been reported to be effective *in vitro*. *In Vivo*, on-target toxicity limits the utility of e.g. MEK1/2/PI3-Kinase alpha inhibitor combinations. Recently, *KRAS*^{G12C} specific inhibitors have been developed. Since these inhibitors are specific for the mutant protein, they are not toxic (Ishida *et al.*, 2021). This could lead to an opportunity for co-administration of KRAS^{G12C} and PI3-Kinase alpha inhibitors. We are now generating Villin-CreER^{T2}; *Apc*$^{fl/wt}$; *Kras*$^{G12C/wt}$; *Pik3ca*$^{H1047R/wt}$ mice with the aim to

first characterize the impact of co-mutation, and then sensitivity to the $KRAS^{G12C}$/PI3-Kinase alpha inhibitor combination.

I have mentioned earlier that mTORC1 activity is stimulated by lysosomal nutrient content and mTORC1 activity was sustained under ineffective treatments such as the PI3-Kinase alpha inhibitor. SLC7A5/LAT1 was previously shown to regulate cellular nutrient metabolism by exporting glutamine in favour of import of other essential amino acids, such as leucine. This was crucial to sustain the growth of KRAS mutant intestinal tumours, as genetic KO of *Slc7a5* resulted in a significant survival benefit (Figure 5-2 A). Furthermore, KO of *Slc7a5* sensitized *Kras* mutant tumours to Rapamycin (Najumudeen *et al.*, 2021). Interestingly, combined *Kras* and PI3-Kinase signalling hyperactivation resulted in a further robust expression of SLC7A5 (Figure 5-1). Furthermore, it was recently shown that prolonged Arginine or Leucine deprivation results in reduced mTORC1 activity, which can be overcome by PI3-Kinase and AKT signalling (Buel *et al.*, 2022). There is therefore a rationale to understand whether PI3-Kinase signalling can drive tumour initiation and outgrowth in *Kras* mutant, *Slc7a5*-KO mice. To this end, I generated Villin-$CreER^{T2}$; $Apc^{fl/wt}$; $Kras^{G12D/wt}$; $Pik3ca^{H1047R/wt}$; $Slc7a5^{fl/fl}$ and Villin-$CreER^{T2}$; $Apc^{fl/wt}$; $Kras^{G12D/wt}$; $Pik3ca^{H1047R/H1047R}$; $Slc7a5^{fl/fl}$ mice. Preliminary data indicates that the survival benefit observed in Villin-$CreER^{T2}$; $Apc^{fl/wt}$; $Kras^{G12D/wt}$ mice is diminished upon increased co-mutation of PI3-Kinase (Figure 5-2). This will be an opportunity to test whether co-administration of either PI3-Kinase inhibitors or Rapamycin will revert this effect.

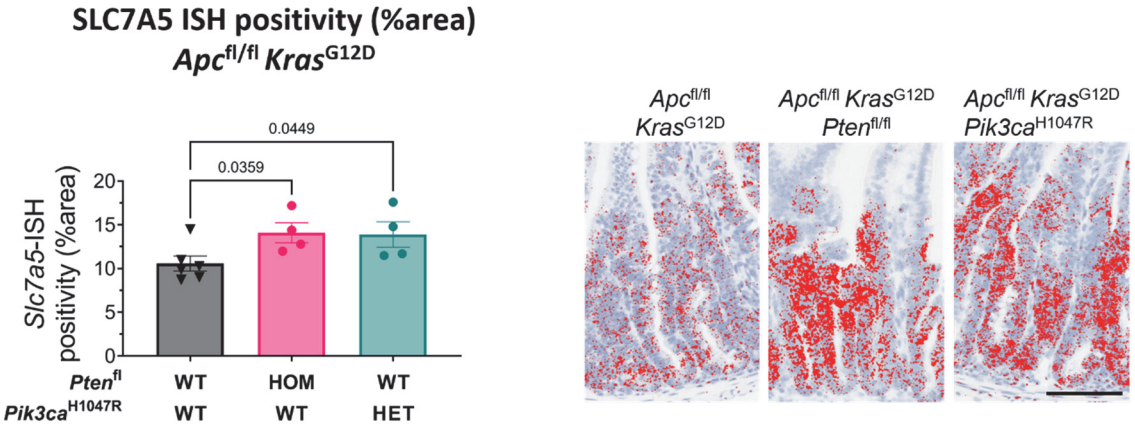

Figure 5-1: SLC7A5 ISH reveals increased positivity upon PI3-Kinase hyperactivation in *Apc*$^{fl/fl}$ *Kras*^{G12D} short term models. Mice were induced and sampled 3d post-inductions. RNA scope® (ISH) on SLC7A5 transcript was conducted and quantified using Halo software. Left – Quantification, right – representative images. Arafath Najumudeen from the Sansom laboratory has contributed to this data. Kurskal-Wallis test and uncorrected Dunn's multiple comparisons test.

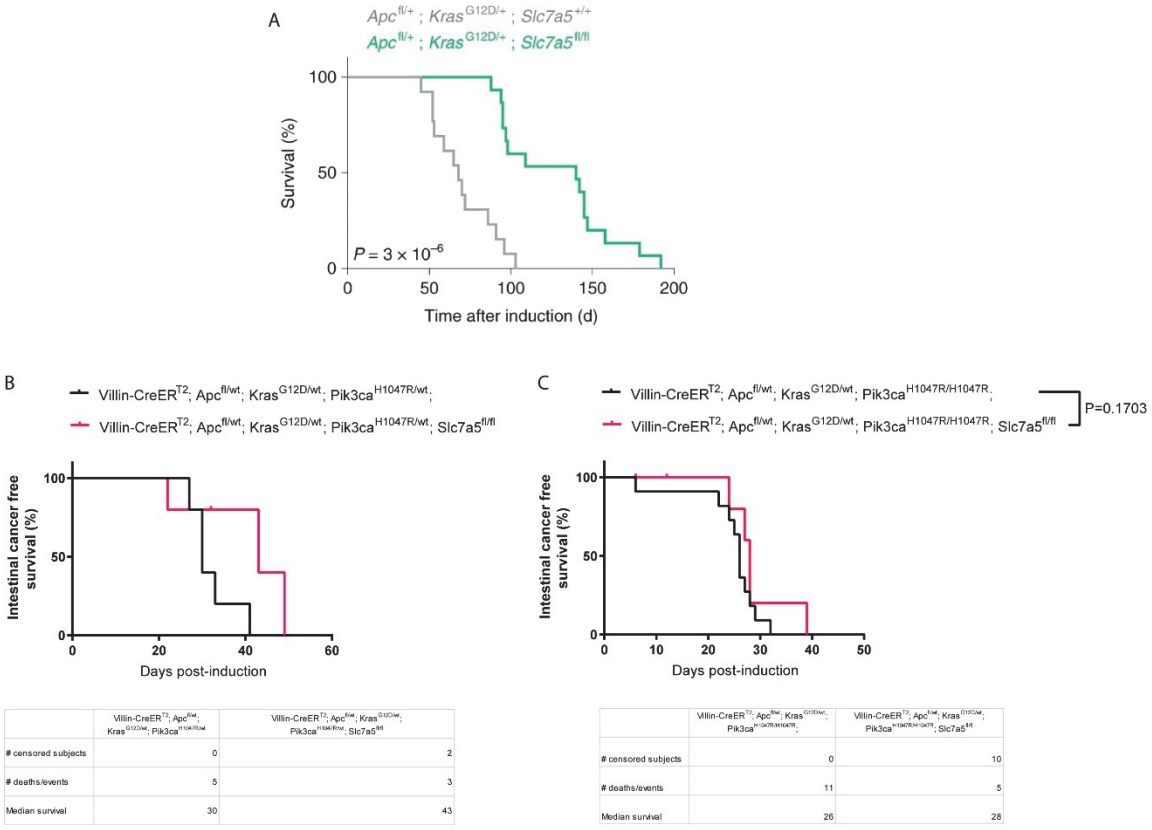

	Villin-CreER^{T2}; Apc$^{fl/wt}$; Kras$^{G12D/wt}$; Pik3ca$^{H1047R/wt}$;	Villin-CreER^{T2}; Apc$^{fl/wt}$; Kras$^{G12D/wt}$; Pik3ca$^{H1047R/wt}$; Slc7a5$^{fl/fl}$
# censored subjects	0	2
# deaths/events	5	3
Median survival	30	43

	Villin-CreER^{T2}; Apc$^{fl/wt}$; Kras$^{G12D/wt}$; Pik3ca$^{H1047R/H1047R}$;	Villin-CreER^{T2}; Apc$^{fl/wt}$; Kras$^{G12D/wt}$; Pik3ca$^{H1047R/H1047R}$; Slc7a5$^{fl/fl}$
# censored subjects	0	10
# deaths/events	11	5
Median survival	26	28

Figure 5-2: Preliminary data indicates diminishing effect of *Slc7a5*-KO in Villin-CreER^{T2}; *Apc*$^{fl/wt}$; *Kras*$^{G12D/wt}$; *Pik3ca*$^{H1047R/H1047R}$mice. A) Survival curve of Villin-CreER^{T2}; *Apc*$^{fl/wt}$; *Kras*$^{G12D/wt}$ and Villin-CreER^{T2}; *Apc*$^{fl/wt}$; *Kras*$^{G12D/wt}$ *Slc7a5*$^{fl/fl}$. Adapted from Najumudeen *et al.*, 2021. B, C) Survival curve of Villin-CreER^{T2}; *Apc*$^{fl/wt}$; *Kras*$^{G12D/wt}$; *Pik3ca*$^{H1047R/wt}$; *Slc7a5*$^{fl/fl}$, Villin-CreER^{T2}; *Apc*$^{fl/wt}$; *Kras*$^{G12D/wt}$; *Pik3ca*$^{H1047R/H1047R}$; *Slc7a5*$^{fl/fl}$, and Slc7a5$^{wt/wt}$ controls were induced and aged to clinical endpoint. Log-rank test.

In vitro studies to identify vulnerabilities in particular contexts have been crucial for the identification of druggable targets over the years (Behan *et al.*, 2019). In addition to understanding the disease itself, pre-clinical *in vivo* models are invaluable to test these hypotheses and account for unexpected organism-scale effects of drugs, such as PI3-Kinase inhibitors (Hopkins *et al.*, 2018). With the work presented in this thesis, I hope to have produced a set of mouse models valuable for testing the efficacy of treatments on PI3-Kinase hyperactive and *Kras*/PI3-Kinase co-mutated intestinal cancers *in vivo*, which will eventually accelerate the progression of promising therapeutic approaches to the clinic.

Bibliography

Al-Qassab, H. *et al.* (2009) 'Dominant Role of the p110ß Isoform of PI3K over p110α in Energy Homeostasis Regulation by POMC and AgRP Neurons', *Cell Metabolism*, 10(5), pp. 343–354. doi: 10.1016/J.CMET.2009.09.008.

Alessi, D. R. *et al.* (1996) 'Mechanism of activation of protein kinase B by insulin and IGF-1.', *The EMBO Journal*. John Wiley & Sons, Ltd, 15(23), pp. 6541–6551. doi: 10.1002/J.1460-2075.1996.TB01045.X.

Alimonti, A. *et al.* (2010) 'Subtle variations in Pten dose determine cancer susceptibility', *Nature Genetics*, 42(5), pp. 454–458. doi: 10.1038/NG.556.

Álvarez-Garcia, V. *et al.* (2019) 'Mechanisms of PTEN loss in cancer: It's all about diversity', *Seminars in Cancer Biology*. Academic Press, 59, pp. 66–79. doi: 10.1016/J.SEMCANCER.2019.02.001.

Amodio, V. *et al.* (2020) 'EGFR blockade reverts resistance to KRAS G12C inhibition incolorectal cancer', *Cancer discovery*. NIH Public Access, 10(8), p. 1129. doi: 10.1158/2159-8290.CD-20-0187.

André, F. *et al.* (2019) 'Alpelisib for *PIK3CA* -Mutated, Hormone Receptor–Positive Advanced Breast Cancer', *New England Journal of Medicine*. Massachussetts Medical Society, 380(20), pp. 1929–1940. doi: 10.1056/NEJMoa1813904.

Aylett, C. H. S. *et al.* (2016) 'Architecture of human mTOR complex 1', *Science*. American Association for the Advancement of Science, 351(6268), pp. 48–52. doi: 10.1126/SCIENCE.AAA3870/SUPPL_FILE/AYLETT.SM.PDF.

AZD8186 First Time In Patient Ascending Dose Study - Full Text View - ClinicalTrials.gov (no date). Available at: https://clinicaltrials.gov/ct2/show/NCT01884285 (Accessed: 28 February 2022).

Baba, Y. *et al.* (2011) 'Phosphorylated AKT expression is associated with PIK3CA mutation, low stage, and favorable outcome in 717 colorectal cancers', *Cancer*.

John Wiley & Sons, Ltd, 117(7), pp. 1399–1408. doi: 10.1002/CNCR.25630.

Baldus, S. E. *et al.* (2004) 'MUC1 and Nuclear ß-Catenin Are Coexpressed at the Invasion Front of Colorectal Carcinomas and Are Both Correlated with Tumor Prognosis', *Clinical Cancer Research*. American Association for Cancer Research, 10(8), pp. 2790–2796. doi: 10.1158/1078-0432.CCR-03-0163.

Bar-Peled, L. *et al.* (2012) 'Ragulator Is a GEF for the Rag GTPases that Signal Amino Acid Levels to mTORC1', *Cell*. Cell Press, 150(6), pp. 1196–1208. doi: 10.1016/J.CELL.2012.07.032.

Bar-Peled, L. *et al.* (2013) 'A tumor suppressor complex with GAP activity for the Rag GTPases that signal amino acid sufficiency to mTORC1', *Science*. American Association for the Advancement of Science, 340(6136), pp. 1100–1106. doi: 10.1126/SCIENCE.1232044/SUPPL_FILE/1232044BAR-PELED.SM.PDF.

Bardia, A. *et al.* (2020) 'Phase Ib Study of Combination Therapy with MEK Inhibitor Binimetinib and Phosphatidylinositol 3-Kinase Inhibitor Buparlisib in Patients with Advanced Solid Tumors with RAS/RAF Alterations', *The Oncologist*. Oxford Academic, 25(1), pp. e160–e169. doi: 10.1634/THEONCOLOGIST.2019-0297.

Barker, N. *et al.* (2007) 'Identification of stem cells in small intestine and colon by marker gene Lgr5', *Nature*. Nature Publishing Group, 449(7165), pp. 1003–1007. doi: 10.1038/nature06196.

Barlaam, B., Cosulich, S., Degorce, S., *et al.* (2015) 'Discovery of (R)-8-(1-(3,5-difluorophenylamino)ethyl)- N, N -dimethyl-2-morpholino-4-oxo-4 H -chromene-6-carboxamide (AZD8186): A potent and selective inhibitor of PI3Kß and PI3Kδ for the treatment of PTEN-deficient cancers', *Journal of Medicinal Chemistry*. American Chemical Society, 58(2), pp. 943–962. doi: 10.1021/JM501629P/SUPPL_FILE/JM501629P_SI_001.PDF.

Barlaam, B., Cosulich, S., Delouvrié, B., *et al.* (2015) 'Discovery of 1-(4-(5-(5-amino-6-(5-tert-butyl-1,3,4-oxadiazol-2-yl)pyrazin-2-yl)-1-ethyl-1,2,4-triazol-3-yl)piperidin-1-yl)-3-hydroxypropan-1-one (AZD8835): A potent and selective

inhibitor of PI3Kα and PI3Kδ for the treatment of cancers', *Bioorganic & Medicinal Chemistry Letters*. Pergamon, 25(22), pp. 5155–5162. doi: 10.1016/J.BMCL.2015.10.002.

Barrow, E. *et al.* (2008) 'Colorectal cancer in HNPCC: cumulative lifetime incidence, survival and tumour distribution. A report of 121 families with proven mutations', *Clinical Genetics*. John Wiley & Sons, Ltd, 74(3), pp. 233–242. doi: 10.1111/J.1399-0004.2008.01035.X.

Basu, A. and Lambring, C. B. (2021) 'Akt Isoforms: A Family Affair in Breast Cancer', *Cancers*. Multidisciplinary Digital Publishing Institute (MDPI), 13(14). doi: 10.3390/CANCERS13143445.

Behan, F. M. *et al.* (2019) 'Prioritization of cancer therapeutic targets using CRISPR–Cas9 screens', *Nature 2019 568:7753*. Nature Publishing Group, 568(7753), pp. 511–516. doi: 10.1038/s41586-019-1103-9.

Bennecke, M. *et al.* (2010) 'Ink4a/Arf and Oncogene-Induced Senescence Prevent Tumor Progression during Alternative Colorectal Tumorigenesis', *Cancer Cell*. Cell Press, 18(2), pp. 135–146. doi: 10.1016/J.CCR.2010.06.013.

Bentzinger, C. F. *et al.* (2008) 'Skeletal muscle-specific ablation of raptor, but not of rictor, causes metabolic changes and results in muscle dystrophy.', *Cell metabolism*. Elsevier, 8(5), pp. 411–24. doi: 10.1016/j.cmet.2008.10.002.

Beurel, E., Grieco, S. F. and Jope, R. S. (2015) 'Glycogen synthase kinase-3 (GSK3): regulation, actions, and diseases', *Pharmacol Ther*, 0, pp. 114–131. doi: 10.1016/j.pharmthera.2014.11.016.

Bhanot, P. *et al.* (1996) 'A new member of the frizzled family from Drosophila functions as a Wingless receptor', *Nature*, 382(6588), pp. 225–230. doi: 10.1038/382225a0.

Bignell, G. R. *et al.* (2010) 'Signatures of mutation and selection in the cancer genome', *Nature*, 463(7283), pp. 893–898. doi: 10.1038/NATURE08768.

Bjorge, J. D. *et al.* (1990) 'Activated type I phosphatidylinositol kinase is associated with the epidermal growth factor (EGF) receptor following EGF stimulation (tyrosine kinase/signal transduction)', *Proc. Nati. Acad. Sci. USA*, 87, pp. 3816–3820.

Bowles, D. W. *et al.* (2016) 'A Randomized, Phase II Trial of Cetuximab With or Without PX-866, an Irreversible Oral Phosphatidylinositol 3-Kinase Inhibitor, in Patients With Metastatic Colorectal Carcinoma', *Clinical colorectal cancer*. Clin Colorectal Cancer, 15(4), pp. 337-344.e2. doi: 10.1016/J.CLCC.2016.03.004.

Brabletz, T. *et al.* (1998) 'Nuclear overexpression of the oncoprotein ß-Catenin in colorectal cancer is localized predominantly at the invasion front', *Pathology Research and Practice*, 194(10), pp. 701–704. doi: 10.1016/S0344-0338(98)80129-5.

Braicu, C. *et al.* (2019) 'A Comprehensive Review on MAPK: A Promising Therapeutic Target in Cancer', *Cancers*. Multidisciplinary Digital Publishing Institute (MDPI), 11(10), p. 1618. doi: 10.3390/CANCERS11101618.

Brandmaier, A., Hou, S. Q. and Shen, W. H. (2017) 'Cell Cycle Control by PTEN', *Journal of Molecular Biology*. Academic Press, 429(15), pp. 2265–2277. doi: 10.1016/J.JMB.2017.06.004.

Brito, M. B., Goulielmaki, E. and Papakonstanti, E. A. (2015) 'Focus on PTEN regulation', *Frontiers in Oncology*. Frontiers Media S.A., 5(JUL), p. 166. doi: 10.3389/FONC.2015.00166/BIBTEX.

Browne, G. J. and Proud, C. G. (2004) 'A Novel mTOR-Regulated Phosphorylation Site in Elongation Factor 2 Kinase Modulates the Activity of the Kinase and Its Binding to Calmodulin', *Molecular and Cellular Biology*. American Society for Microbiology, 24(7), pp. 2986–2997. doi: 10.1128/MCB.24.7.2986-2997.2004/ASSET/154C8D65-03FF-4DE8-82E7-F77498941CDE/ASSETS/GRAPHIC/ZMB0070413960006.JPEG.

Buel, G. R. *et al.* (2022) 'Prolonged deprivation of arginine or leucine induces PI3K/Akt-dependent reactivation of mTORC1', *Journal of Biological Chemistry*.

Elsevier, p. 102030. doi: 10.1016/J.JBC.2022.102030.

Byun, D. S. *et al.* (2011) 'Intestinal epithelial-specific PTEN inactivation results in tumor formation', *American Journal of Physiology - Gastrointestinal and Liver Physiology*. American Physiological Society, 301(5), p. G856. doi: 10.1152/AJPGI.00178.2011.

Cammareri, P. *et al.* (2017) 'TGFβ pathway limits dedifferentiation following WNT and MAPK pathway activation to suppress intestinal tumourigenesis', *Cell Death & Differentiation 2017 24:10*. Nature Publishing Group, 24(10), pp. 1681–1693. doi: 10.1038/cdd.2017.92.

Castel, P. *et al.* (2021) 'The present and future of PI3K inhibitors for cancer therapy', *Nature cancer*. NIH Public Access, 2(6), p. 587. doi: 10.1038/S43018-021-00218-4.

Castellano, E. and Downward, J. (2011) 'RAS Interaction with PI3K: More Than Just Another Effector Pathway', *Genes & Cancer*. Impact Journals, LLC, 2(3), p. 261. doi: 10.1177/1947601911408079.

Castro-Martinez, F. *et al.* (2021) 'Rictor/Mammalian Target of Rapamycin Complex 2 Signaling Protects Colonocytes from Apoptosis and Prevents Epithelial Barrier Breakdown', *The American Journal of Pathology*. Elsevier, 191(9), pp. 1537–1549. doi: 10.1016/J.AJPATH.2021.06.004.

Caunt, C. J. and Keyse, S. M. (2013) 'Dual-specificity MAP kinase phosphatases (MKPs)', *The FEBS Journal*. John Wiley & Sons, Ltd, 280(2), pp. 489–504. doi: 10.1111/J.1742-4658.2012.08716.X.

Cetintas, V. B., Cetintas, V. B. and Batada, N. N. (2020) 'Is there a causal link between PTEN deficient tumors and immunosuppressive tumor microenvironment?', *Journal of Translational Medicine*. BioMed Central, 18(1), p. 45. doi: 10.1186/S12967-020-02219-W.

Chaker-Margot, M. *et al.* (2022) 'Structural basis of activation of the tumor suppressor protein neurofibromin', *Molecular Cell*. Cell Press. doi:

10.1016/J.MOLCEL.2022.03.011.

Champion, B. R., Fisher, K. and Seymour, L. (2016) ‘A PTENtial cause for the selectivity of oncolytic viruses?’, *Nature Publishing Group*. doi: 10.1038/ni.3394.

Chantranupong, L. *et al*. (2016) ‘The CASTOR Proteins Are Arginine Sensors for the mTORC1 Pathway’, *Cell*. Cell Press, 165(1), pp. 153–164. doi: 10.1016/J.CELL.2016.02.035.

Chen, X. *et al*. (2018) ‘Cryo-EM structure of human mTOR complex 2’, *Cell Research*. Nature Publishing Group, 28(5), pp. 518–528. doi: 10.1038/s41422-018-0029-3.

Cheng, H. and Leblond, C. P. (1974) ‘Origin, differentiation and renewal of the four main epithelial cell types in the mouse small intestine V. Unitarian theory of the origin of the four epithelial cell types’, *American Journal of Anatomy*. John Wiley & Sons, Ltd, 141(4), pp. 537–561. doi: 10.1002/AJA.1001410407.

Choi, J. *et al*. (1996) ‘Structure of the FKBP12-Rapamycin Complex Interacting with Binding Domain of Human FRAP’, *Science*. American Association for the Advancement of Science , 273(5272), pp. 239–242. doi: 10.1126/SCIENCE.273.5272.239.

Chong, H., Lee, J. and Guan, K. L. (2001) ‘Positive and negative regulation of Raf kinase activity and function by phosphorylation’, *The EMBO Journal*. John Wiley & Sons, Ltd, 20(14), pp. 3716–3727. doi: 10.1093/EMBOJ/20.14.3716.

Choudhury, A. D. *et al*. (2022) ‘A Phase I Study Investigating AZD8186, a Potent and Selective Inhibitor of PI3Kβ/δ, in Patients with Advanced Solid Tumors’, *Clinical Cancer Research*, pp. OF1–OF13. doi: 10.1158/1078-0432.CCR-21-3087.

Chow, C. W. and Davis, R. J. (2006) ‘Proteins Kinases: Chromatin-Associated Enzymes?’, *Cell*. Cell Press, 127(5), pp. 887–890. doi: 10.1016/J.CELL.2006.11.015.

Colakoglu, T. *et al*. (2008) ‘Clinicopathological significance of PTEN loss and the

phosphoinositide 3-kinase/Akt pathway in sporadic colorectal neoplasms: is PTEN loss predictor of local recurrence?', *The American Journal of Surgery*. Elsevier, 195(6), pp. 719–725. doi: 10.1016/J.AMJSURG.2007.05.061.

Cong, F., Schweizer, L. and Varmus, H. (2004) 'Wnt signals across the plasma membrane to activate the β-catenin pathway by forming oligomers containing its receptors, Frizzled and LRP', *Development*, 131(20), pp. 5103–5115. doi: 10.1242/DEV.01318.

Cox, A. D. *et al.* (2014) 'Drugging the undruggable RAS: Mission possible?', *Nature reviews. Drug discovery*. NIH Public Access, 13(11), pp. 828–51. doi: 10.1038/nrd4389.

CRUK (2022) *Bowel cancer statistics | Cancer Research UK. https://www.cancerresearchuk.org/health-professional/cancer-statistics/statistics-by-cancer-type/bowel-cancer#heading-One*. Available at: https://www.cancerresearchuk.org/health-professional/cancer-statistics/statistics-by-cancer-type/bowel-cancer#heading-One (Accessed: 5 August 2021).

Cuesta, C., Arévalo-Alameda, C. and Castellano, E. (2021) 'The Importance of Being PI3K in the RAS Signaling Network', *Genes 2021, Vol. 12, Page 1094*. Multidisciplinary Digital Publishing Institute, 12(7), p. 1094. doi: 10.3390/GENES12071094.

Cuevas, B. D. *et al.* (2001) 'Tyrosine Phosphorylation of p85 Relieves Its Inhibitory Activity on Phosphatidylinositol 3-Kinase', *Journal of Biological Chemistry*. Elsevier, 276(29), pp. 27455–27461. doi: 10.1074/JBC.M100556200.

Danielsen, S. A. *et al.* (2008) 'Novel mutations of the suppressor gene PTEN in colorectal carcinomas stratified by microsatellite instability- and TP53 mutation-status', *Human Mutation*. John Wiley & Sons, Ltd, 29(11), pp. E252–E262. doi: 10.1002/HUMU.20860.

Daston, M. M. *et al.* (1992) 'The protein product of the neurofibromatosis type 1 gene is expressed at highest abundance in neurons, Schwann cells, and

oligodendrocytes', *Neuron*. Cell Press, 8(3), pp. 415–428. doi: 10.1016/0896-6273(92)90270-N.

Davies, B. R. *et al*. (2007) 'AZD6244 (ARRY-142886), a potent inhibitor of mitogen-activated protein kinase/extracellular signal-regulated kinase kinase 1/2 kinases: mechanism of action in vivo, pharmacokinetic/pharmacodynamic relationship, and potential for combination in preclinical models', *Molecular Cancer Therapeutics*. American Association for Cancer Research, 6(8), pp. 2209–2219. doi: 10.1158/1535-7163.MCT-07-0231.

Davies, E. J. *et al*. (2014) '*PTEN* loss and *KRAS* activation leads to the formation of serrated adenomas and metastatic carcinoma in the mouse intestine', *The Journal of Pathology*. Wiley-Blackwell, 233(1), pp. 27–38. doi: 10.1002/path.4312.

Day, F. L. *et al*. (2013) 'PIK3CA and PTEN gene and exon mutation-specific clinicopathologic and molecular associations in Colorectal cancer', *Clinical Cancer Research*. American Association for Cancer Research, 19(12), pp. 3285–3296. doi: 10.1158/1078-0432.CCR-12-3614/85568/AM/PIK3CA-AND-PTEN-GENE-AND-EXON-MUTATION-SPECIFIC.

Deming, D. A. *et al*. (2013) 'mTOR Inhibition Elicits a Dramatic Response in PI3K-Dependent Colon Cancers', *PLoS ONE*. Edited by R. K. Srivastava, 8(4), p. e60709. doi: 10.1371/journal.pone.0060709.

Deming, D. A. *et al*. (2014) 'PIK3CA and APC mutations are synergistic in the development of intestinal cancers.', *Oncogene*. NIH Public Access, 33(17), pp. 2245–54. doi: 10.1038/onc.2013.167.

Deming, D. A. *et al*. (2016) 'A phase I study of selumetinib (AZD6244/ARRY-142866), a MEK1/2 inhibitor, in combination with cetuximab in refractory solid tumors and KRAS mutant colorectal cancer.', *Investigational new drugs*. NIH Public Access, 34(2), pp. 168–75. doi: 10.1007/s10637-015-0314-7.

Dibble, C. C. and Cantley, L. C. (2015) 'Regulation of mTORC1 by PI3K signaling', *Trends in Cell Biology*. Elsevier Current Trends, 25(9), pp. 545–555. doi:

10.1016/J.TCB.2015.06.002.

Ding, V. W., Chen, R.-H. and Mccormick, F. (2000) ‘Differential Regulation of Glycogen Synthase Kinase 3Î² by Insulin and Wnt Signaling*’. JBC Papers in Press. doi: 10.1074/jbc.M005342200.

Do, K. *et al*. (2015) ‘Biomarker-driven phase 2 study of MK-2206 and selumetinib (AZD6244, ARRY-142886) in patients with colorectal cancer HHS Public Access’, *Invest New Drugs*, 33(3), pp. 720–728. doi: 10.1007/s10637-015-0212-z.

Doble, B. W. *et al*. (2007) ‘Functional Redundancy of GSK-3α and GSK-3β in Wnt/β-Catenin Signaling Shown by Using an Allelic Series of Embryonic Stem Cell Lines’, *Developmental Cell*. Cell Press, 12(6), pp. 957–971. doi: 10.1016/J.DEVCEL.2007.04.001.

Downward, J. (2004) ‘PI 3-kinase, Akt and cell survival’, *Seminars in Cell & Developmental Biology*. Academic Press, 15(2), pp. 177–182. doi: 10.1016/J.SEMCDB.2004.01.002.

Driscoll, D. R. *et al*. (2016) ‘mTORC2 Signaling Drives the Development and Progression of Pancreatic Cancer.’, *Cancer research*. American Association for Cancer Research, 76(23), pp. 6911–6923. doi: 10.1158/0008-5472.CAN-16-0810.

Edimo, W. E. *et al*. (2016) ‘SHIP2 controls plasma membrane PI(4,5)P2 thereby participating in the control of cell migration in 1321 N1 glioblastoma cells’, *Journal of Cell Science*. Company of Biologists Ltd, 129(6), pp. 1101–1114. doi: 10.1242/JCS.179663/VIDEO-3.

Eid, W. *et al*. (2017) ‘mTORC1 activates SREBP-2 by suppressing cholesterol trafficking to lysosomes in mammalian cells’, *Proceedings of the National Academy of Sciences of the United States of America*. Proc Natl Acad Sci U S A, 114(30), pp. 7999–8004. doi: 10.1073/PNAS.1705304114.

Essers, M. A. G. *et al*. (2005) ‘Functional interaction between β-catenin and FOXO in oxidative stress signaling’, *Science*, 308(5725), pp. 1181–1184. doi: 10.1126/SCIENCE.1109083.

Faller, W. J. *et al.* (2015) 'MTORC1-mediated translational elongation limits intestinal tumour initiation and growth', *Nature*, 517(7535), pp. 497–500. doi: 10.1038/nature13896.

Fanger, G. R., Johnson, N. L. and Johnson, G. L. (1997) 'MEK kinases are regulated by EGF and selectively interact with Rac/Cdc42.', *The EMBO Journal*. European Molecular Biology Organization, 16(16), p. 4961. doi: 10.1093/EMBOJ/16.16.4961.

Fearon, E. R. (2011) 'Molecular Genetics of Colorectal Cancer', *Annual Review of Pathology: Mechanisms of Disease*. Annual Reviews , 6(1), pp. 479–507. doi: 10.1146/annurev-pathol-011110-130235.

Fearon, E. R. and Vogelstein, B. (1990) 'A genetic model for colorectal tumorigenesis', *Cell*. Cell Press, 61(5), pp. 759–767. doi: 10.1016/0092-8674(90)90186-I.

Fisher, N. C. *et al.* (2022) 'Biological Misinterpretation of Transcriptional Signatures in Tumor Samples can Unknowingly Undermine Mechanistic Understanding and Faithful Alignment with Preclinical Data', *Clinical Cancer Research*, pp. OF1–OF14. doi: 10.1158/1078-0432.CCR-22-1102.

Foley, T. M. *et al.* (2017) 'Dual PI3K/mTOR Inhibition in Colorectal Cancers with APC and PIK3CA Mutations.', *Molecular cancer research : MCR*. American Association for Cancer Research, 15(3), pp. 317–327. doi: 10.1158/1541-7786.MCR-16-0256.

Foukas, L. C. *et al.* (2006) 'Critical role for the p110α phosphoinositide-3-OH kinase in growth and metabolic regulation', *Nature*. Nature Publishing Group, 441(7091), pp. 366–370. doi: 10.1038/nature04694.

Frame, S., Cohen, P. and Biondi, R. M. (2001) 'A common phosphate binding site explains the unique substrate specificity of GSK3 and its inactivation by phosphorylation', *Molecular Cell*. Cell Press, 7(6), pp. 1321–1327. doi: 10.1016/S1097-2765(01)00253-2.

Fricke, S. L. *et al.* (2019) 'MTORC1/2 inhibition as a therapeutic strategy for PIK3CA mutant cancers', *Molecular Cancer Therapeutics*. American Association for Cancer Research Inc., 18(2), pp. 346–355. doi: 10.1158/1535-7163.MCT-18-0510/87725/AM/MTORC1-2-INHIBITION-AS-A-THERAPEUTIC-STRATEGY-FOR.

Fritsch, R. *et al.* (2013) 'RAS and RHO Families of GTPases Directly Regulate Distinct Phosphoinositide 3-Kinase Isoforms', *Cell*. Cell Press, 153(5), pp. 1050–1063. doi: 10.1016/J.CELL.2013.04.031.

Garami, A. *et al.* (2003) 'Insulin Activation of Rheb, a Mediator of mTOR/S6K/4E-BP Signaling, Is Inhibited by TSC1 and 2', *Molecular Cell*. Cell Press, 11(6), pp. 1457–1466. doi: 10.1016/S1097-2765(03)00220-X.

García-Martínez, J. M. and Alessi, D. R. (2008) 'mTOR complex 2 (mTORC2) controls hydrophobic motif phosphorylation and activation of serum- and glucocorticoid-induced protein kinase 1 (SGK1)', *Biochemical Journal*. Portland Press, 416(3), pp. 375–385. doi: 10.1042/BJ20081668.

Van Geel, R. M. J. M. *et al.* (2017) 'A phase Ib dose-escalation study of encorafenib and cetuximab with or without alpelisib in metastatic BRAF-mutant colorectal cancer', *Cancer Discovery*. American Association for Cancer Research Inc., 7(6), pp. 610–619. doi: 10.1158/2159-8290.CD-16-0795.

Gkeka, P. *et al.* (2014a) 'Investigating the Structure and Dynamics of the PIK3CA Wild-Type and H1047R Oncogenic Mutant', *PLoS Computational Biology*. Edited by B. L. de Groot. Public Library of Science, 10(10), p. e1003895. doi: 10.1371/journal.pcbi.1003895.

Gkeka, P. *et al.* (2014b) 'Investigating the Structure and Dynamics of the PIK3CA Wild-Type and H1047R Oncogenic Mutant', *PLoS Computational Biology*. Public Library of Science, 10(10), p. e1003895. doi: 10.1371/journal.pcbi.1003895.

Grasso, S. *et al.* (2014) 'Resistance to Selumetinib (AZD6244) in Colorectal Cancer Cell Lines is Mediated by p70S6K and RPS6 Activation', *Neoplasia (New York, N.Y.)*. Neoplasia Press, 16(10), p. 845. doi: 10.1016/J.NEO.2014.08.011.

Green, S., Trejo, C. L. and McMahon, M. (2015) 'PIK3CAH1047R Accelerates and Enhances KRASG12D-Driven Lung Tumorigenesis', *Cancer Research*. American Association for Cancer Research, 75(24), pp. 5378–5391. doi: 10.1158/0008-5472.CAN-15-1249.

Groom, L. A. *et al.* (1996) 'Differential regulation of the MAP, SAP and RK/p38 kinases by Pyst1, a novel cytosolic dual-specificity phosphatase.', *The EMBO Journal*. John Wiley & Sons, Ltd, 15(14), pp. 3621–3632. doi: 10.1002/J.1460-2075.1996.TB00731.X.

Gu, X. *et al.* (2017) 'SAMTOR is an S-adenosylmethionine sensor for the mTORC1 pathway', *Science*. American Association for the Advancement of Science, 358(6364), pp. 813–818. doi: 10.1126/SCIENCE.AAO3265/SUPPL_FILE/AAO3265_GU_SM.PDF.

Guertin, D. A. *et al.* (2009) 'mTOR Complex 2 Is Required for the Development of Prostate Cancer Induced by Pten Loss in Mice', *Cancer Cell*. Cell Press, 15(2), pp. 148–159. doi: 10.1016/J.CCR.2008.12.017.

Guichard, S. M. *et al.* (2015) 'AZD2014, an inhibitor of mTORC1 and mTORC2, is highly effective in ER+ breast cancer when administered using intermittent or continuous schedules', *Molecular Cancer Therapeutics*. American Association for Cancer Research Inc., 14(11), pp. 2508–2518. doi: 10.1158/1535-7163.MCT-15-0365/175572/AM/AZD2014-AN-INHIBITOR-OF-MTORC1-AND-MTORC2-IS.

Guillermet-Guibert, J. *et al.* (2008) 'The p110ß isoform of phosphoinositide 3-kinase signals downstream of G protein-coupled receptors and is functionally redundant with p110γ', *Proceedings of the National Academy of Sciences*. National Academy of Sciences, 105(24), pp. 8292–8297. doi: 10.1073/PNAS.0707761105.

Guinney, J. *et al.* (2015) 'The consensus molecular subtypes of colorectal cancer', *Nature Medicine*. Nature Publishing Group, 21(11), pp. 1350–1356. doi: 10.1038/nm.3967.

Gupta, S. *et al.* (2007) 'Binding of Ras to Phosphoinositide 3-Kinase p110α Is

Required for Ras- Driven Tumorigenesis in Mice', *Cell*. Cell Press, 129(5), pp. 957–968. doi: 10.1016/J.CELL.2007.03.051.

Guri, Y. *et al*. (2017) 'mTORC2 Promotes Tumorigenesis via Lipid Synthesis.', *Cancer cell*. Elsevier, 32(6), pp. 807-823.e12. doi: 10.1016/j.ccell.2017.11.011.

Hadac, J. N. *et al*. (2015) 'Colon Tumors with the Simultaneous Induction of Driver Mutations in APC, KRAS, and PIK3CA Still Progress through the Adenoma-to-carcinoma Sequence.', *Cancer prevention research (Philadelphia, Pa.)*. NIH Public Access, 8(10), pp. 952–61. doi: 10.1158/1940-6207.CAPR-15-0003.

Hancox, U. *et al*. (2015) 'Inhibition of PI3Kβ signaling with AZD8186 inhibits growth of PTEN-deficient breast and prostate tumors alone and in combination with docetaxel.', *Molecular cancer therapeutics*. American Association for Cancer Research, 14(1), pp. 48–58. doi: 10.1158/1535-7163.MCT-14-0406.

Hannan, K. M. *et al*. (2003) 'mTOR-Dependent Regulation of Ribosomal Gene Transcription Requires S6K1 and Is Mediated by Phosphorylation of the Carboxy-Terminal Activation Domain of the Nucleolar Transcription Factor UBF†', *Molecular and Cellular Biology*. American Society for Microbiology (ASM), 23(23), p. 8862. doi: 10.1128/MCB.23.23.8862-8877.2003.

Hardiman, K. M. *et al*. (2014) 'Rapamycin Inhibition of Polyposis and Progression to Dysplasia in a Mouse Model', *PLoS ONE*, 9(4), p. 96023. doi: 10.1371/journal.pone.0096023.

Hart, J. R. *et al*. (2015) 'The butterfly effect in cancer: a single base mutation can remodel the cell.', *Proceedings of the National Academy of Sciences of the United States of America*. National Academy of Sciences, 112(4), pp. 1131–6. doi: 10.1073/pnas.1424012112.

He, X. C. *et al*. (2007) 'PTEN-deficient intestinal stem cells initiate intestinal polyposis', *Nature Genetics*. NIH Public Access, 39(2), pp. 189–198. doi: 10.1038/ng1928.

Herms, A. *et al*. (2021) 'Levelling out differences in aerobic glycolysis

neutralizes the competitive advantage of oncogenic PIK3CA mutant progenitors in the esophagus', *bioRxiv*, p. 2021.05.28.446104. doi: 10.1101/2021.05.28.446104.

Hernández, A. R., Klein, A. M. and Kirschner, M. W. (2012) 'Kinetic responses of β-catenin specify the sites of Wnt control', *Science*. American Association for the Advancement of Science, 338(6112), pp. 1337–1340. doi: 10.1126/SCIENCE.1228734/SUPPL_FILE/HERNANDEZ.SM.REVISED.PDF.

Hofmann, M. H. *et al*. (2021) 'Bi-3406, a potent and selective sos1–kras interaction inhibitor, is effective in kras-driven cancers through combined mek inhibition', *Cancer Discovery*. American Association for Cancer Research Inc., 11(1), pp. 142–157. doi: 10.1158/2159-8290.CD-20-0142/333471/AM/BI-3406-A-POTENT-AND-SELECTIVE-SOS1-KRAS.

Home - Reactome Pathway Database (no date). Available at: https://reactome.org/ (Accessed: 26 May 2022).

Hopkins, B. D. *et al*. (2018) 'Suppression of insulin feedback enhances the efficacy of PI3K inhibitors', *Nature 2018 560:7719*. Nature Publishing Group, 560(7719), pp. 499–503. doi: 10.1038/s41586-018-0343-4.

Hudson, K. *et al*. (2016) 'Intermittent high-dose scheduling of AZD8835, a novel selective inhibitor of PI3Ka and PI3Kd, demonstrates treatment strategies for PIK3CA-dependent breast cancers', *Molecular Cancer Therapeutics*. American Association for Cancer Research Inc., 15(5), pp. 877–889. doi: 10.1158/1535-7163.MCT-15-0687/87082/AM/INTERMITTENT-HIGH-DOSE-SCHEDULING-OF-AZD8835-A.

Huu, T. N. *et al*. (2021) 'Redox Regulation of PTEN by Peroxiredoxins', *Antioxidants 2021, Vol. 10, Page 302*. Multidisciplinary Digital Publishing Institute, 10(2), p. 302. doi: 10.3390/ANTIOX10020302.

Inman, G. J. (2011) 'Switching TGFβ from a tumor suppressor to a tumor promoter', *Current Opinion in Genetics & Development*. Elsevier Current Trends, 21(1), pp. 93–99. doi: 10.1016/J.GDE.2010.12.004.

Inoki, K. *et al*. (2002) ‘TSC2 is phosphorylated and inhibited by Akt and suppresses mTOR signalling’, *Nature Cell Biology 2002 4:9*. Nature Publishing Group, 4(9), pp. 648–657. doi: 10.1038/ncb839.

Isella, C. *et al*. (2017) ‘Selective analysis of cancer-cell intrinsic transcriptional traits defines novel clinically relevant subtypes of colorectal cancer’, *Nature Communications*. Nature Publishing Group, 8, p. 15107. doi: 10.1038/ncomms15107.

Ishida, K. *et al*. (2021) ‘Nonclinical Safety Profile of Sotorasib, a KRASG12C-Specific Covalent Inhibitor for the Treatment of KRAS p.G12C-Mutated Cancer’, *International Journal of Toxicology*. SAGE Publications Inc., 40(5), pp. 427–441. doi: 10.1177/10915818211022965.

Jaaks, P., Coker, Elizabeth A, *et al*. (2022) ‘Effective drug combinations in breast, colon and pancreatic cancer cells.’, *Nature*. doi: 10.1038/S41586-022-04437-2.

Jaaks, P., Coker, Elizabeth A., *et al*. (2022) ‘Effective drug combinations in breast, colon and pancreatic cancer cells’, *Nature*. Nature Publishing Group, 603(7899), p. 166. doi: 10.1038/S41586-022-04437-2.

Jackson, E. L. *et al*. (2001) ‘Analysis of lung tumor initiation and progression using conditional expression of oncogenic K-ras’, *Genes & Development*. Cold Spring Harbor Laboratory Press, 15(24), pp. 3243–3248. doi: 10.1101/GAD.943001.

Jackstadt, R. *et al*. (2019) ‘Epithelial NOTCH Signaling Rewires the Tumor Microenvironment of Colorectal Cancer to Drive Poor-Prognosis Subtypes and Metastasis’, *Cancer Cell*. Cell Press, 36(3), pp. 319-336.e7. doi: 10.1016/J.CCELL.2019.08.003.

Jackstadt, R. and Sansom, O. J. (2016) ‘Mouse models of intestinal cancer’, *The Journal of Pathology*. John Wiley & Sons, Ltd, 238(2), pp. 141–151. doi: 10.1002/path.4645.

Jänne, P. A. *et al.* (2017) 'Selumetinib Plus Docetaxel Compared With Docetaxel Alone and Progression-Free Survival in Patients With KRAS-Mutant Advanced Non–Small Cell Lung Cancer: The SELECT-1 Randomized Clinical Trial', *JAMA*. American Medical Association, 317(18), pp. 1844–1853. doi: 10.1001/JAMA.2017.3438.

Janssen, K. *et al.* (2006) 'APC and Oncogenic KRAS Are Synergistic in Enhancing Wnt Signaling in Intestinal Tumor Formation and Progression', *Gastroenterology*. W.B. Saunders, 131(4), pp. 1096–1109. doi: 10.1053/J.GASTRO.2006.08.011.

Jean, S. and Kiger, A. A. (2014) 'Classes of phosphoinositide 3-kinases at a glance.', *Journal of cell science*. Company of Biologists, 127(Pt 5), pp. 923–8. doi: 10.1242/jcs.093773.

Jehan, Z. *et al.* (2009) 'Frequent PIK3CA gene amplification and its clinical significance in colorectal cancer', *The Journal of pathology*. J Pathol, 219(3), pp. 337–346. doi: 10.1002/PATH.2601.

Jhaveri, K. *et al.* (2020) 'Phase I Basket Study of Taselisib, an Isoform-Selective PI3K Inhibitor, in Patients with *PIK3CA* -Mutant Cancers', *Clinical Cancer Research*. Clin Cancer Res, p. clincanres.2657.2020. doi: 10.1158/1078-0432.CCR-20-2657.

Jiang, Q. *et al.* (2022) 'S6K1-mediated phosphorylation of PDK1 impairs AKT kinase activity and oncogenic functions', *Nature Communications 2022 13:1*. Nature Publishing Group, 13(1), pp. 1–14. doi: 10.1038/s41467-022-28910-8.

Johansson, J. *et al.* (2019) 'RAL GTPases Drive Intestinal Stem Cell Function and Regeneration through Internalization of WNT Signalosomes', *Cell Stem Cell*. Cell Press, 24(4), pp. 592-607.e7. doi: 10.1016/J.STEM.2019.02.002.

Jung, J., Genau, H. M. and Behrends, C. (2015) 'Amino Acid-Dependent mTORC1 Regulation by the Lysosomal Membrane Protein SLC38A9', *Molecular and Cellular Biology*. American Society for Microbiology, 35(14), pp. 2479–2494. doi: 10.1128/MCB.00125-15/SUPPL_FILE/ZMB99910887SO1.PDF.

Jung, S. H. *et al*. (2019) ‘mTOR kinase leads to PTEN-loss-induced cellular senescence by phosphorylating p53’, *Oncogene*. Nature Publishing Group, 38(10), p. 1639. doi: 10.1038/S41388-018-0521-8.

Kaidanovich-Beilin, O. and Woodgett, J. R. (2011a) ‘GSK-3: Functional Insights from Cell Biology and Animal Models’, *Frontiers in Molecular Neuroscience*. Frontiers, 0, p. 40. doi: 10.3389/FNMOL.2011.00040.

Kaidanovich-Beilin, O. and Woodgett, J. R. (2011b) ‘GSK-3: Functional Insights from Cell Biology and Animal Models’, *Frontiers in Molecular Neuroscience*. Frontiers Media SA, 4. doi: 10.3389/FNMOL.2011.00040.

Karakas, D. and Ozpolat, B. (2020) ‘Eukaryotic elongation factor-2 kinase (eEF2K) signaling in tumor and microenvironment as a novel molecular target’, *Journal of Molecular Medicine 2020 98:6*. Springer, 98(6), pp. 775–787. doi: 10.1007/S00109-020-01917-8.

Kararli, T. T. and Searle, G. D. (1995) ‘Comparison of the gastrointestinal anatomy, physiology, and biochemistry of humans and commonly used laboratory animals’, *Biopharmaceutics & Drug Disposition*. John Wiley & Sons, Ltd, 16(5), pp. 351–380. doi: 10.1002/BDD.2510160502.

Karlsson, M. *et al*. (2021) ‘A single–cell type transcriptomics map of human tissues’, *Science Advances*. American Association for the Advancement of Science, 7(31). doi: 10.1126/SCIADV.ABH2169.

Kim, E. *et al*. (2008) ‘Regulation of TORC1 by Rag GTPases in nutrient response’, *Nature Cell Biology 2008 10:8*. Nature Publishing Group, 10(8), pp. 935–945. doi: 10.1038/ncb1753.

Kim, E. *et al*. (2016) ‘Systematic functional interrogation of rare cancer variants identifies oncogenic alleles’, *Cancer Discovery*. American Association for Cancer Research Inc., 6(7), pp. 714–726. doi: 10.1158/2159-8290.CD-16-0160/333313/AM/SYSTEMATIC-FUNCTIONAL-INTERROGATION-OF-RARE-CANCER.

Kim, J. and Guan, K.-L. (2019) ‘mTOR as a central hub of nutrient signalling and

cell growth', *Nature Cell Biology 2019 21:1*. Nature Publishing Group, 21(1), pp. 63–71. doi: 10.1038/s41556-018-0205-1.

Kinzler, K. W. *et al*. (1991) 'Identification of FAP Locus Genes from Chromosome 5q21', *Science*. American Association for the Advancement of Science , 253(5020), pp. 661–665. doi: 10.1126/SCIENCE.1651562.

Knight, J. R. P. *et al*. (2021) 'MNK inhibition sensitizes KRAS-Mutant colorectal cancer to mTORC1 inhibition by reducing eIF4E phosphorylation and C-MYC expression', *Cancer Discovery*. American Association for Cancer Research Inc., 11(5), pp. 1228–1247. doi: 10.1158/2159-8290.CD-20-0652/333524/AM/MNK-INHIBITION-SENSITIZES-KRAS-MUTANT-COLORECTAL.

Kopetz, S. *et al*. (2019) ' Encorafenib, Binimetinib, and Cetuximab in BRAF V600E–Mutated Colorectal Cancer ', *New England Journal of Medicine*. Massachusetts Medical Society, 381(17), pp. 1632–1643. doi: 10.1056/NEJMOA1908075/SUPPL_FILE/NEJMOA1908075_DATA-SHARING.PDF.

Kosako, H. *et al*. (2009) 'Phosphoproteomics reveals new ERK MAP kinase targets and links ERK to nucleoporin-mediated nuclear transport', *Nature Structural & Molecular Biology 2009 16:10*. Nature Publishing Group, 16(10), pp. 1026–1035. doi: 10.1038/nsmb.1656.

Koyama, S. and Kikuchi, A. (2001) 'Ras interaction with Ra1GDS effector targets', *Methods in Enzymology*. Academic Press, 332, pp. 127–138. doi: 10.1016/S0076-6879(01)32197-3.

Kulkarni, S. *et al*. (2011) 'PI3Kβ plays a critical role in neutrophil activation by immune complexes', *Science Signaling*. American Association for the Advancement of Science, 4(168). doi: 10.1126/SCISIGNAL.2001617/SUPPL_FILE/4_RA23_SM.PDF.

Lambert, J. M. *et al*. (2002) 'Tiam1 mediates Ras activation of Rac by a PI(3)K-independent mechanism', *Nature Cell Biology 2002 4:8*. Nature Publishing Group, 4(8), pp. 621–625. doi: 10.1038/ncb833.

Lannagan, T. R. *et al.* (2021) ‘Advances in colon cancer research: in vitro and animal models’, *Current Opinion in Genetics & Development*. Elsevier, 66, p. 50. doi: 10.1016/J.GDE.2020.12.003.

Lavoie, H. and Therrien, M. (2015) ‘Regulation of RAF protein kinases in ERK signalling’. doi: 10.1038/nrm3979.

Lee, D. W. *et al.* (2015) ‘KRAS Mutation is Associated with Worse Prognosis in Stage III or High-risk Stage II Colon Cancer Patients Treated with Adjuvant FOLFOX’, *Annals of Surgical Oncology*. Springer New York LLC, 22(1), pp. 187–194. doi: 10.1245/S10434-014-3826-Z/FIGURES/3.

Leedham, S. J. *et al.* (2012) ‘A basal gradient of Wnt and stem-cell number influences regional tumour distribution in human and mouse intestinal tracts.’, *Gut*, 62(1), pp. 83–93. doi: 10.1136/GUTJNL-2011-301601.

Leystra, Alyssa A *et al.* (2012) ‘Mice expressing activated PI3K rapidly develop advanced colon cancer.’, *Cancer research*. NIH Public Access, 72(12), pp. 2931–6. doi: 10.1158/0008-5472.CAN-11-4097.

Leystra, A. A. *et al.* (2012) ‘Mice Expressing Activated PI3K Rapidly Develop Advanced Colon Cancer’, *Cancer Research*, 72(12), pp. 2931–2936. doi: 10.1158/0008-5472.CAN-11-4097.

Li, A. J. *et al.* (2018) ‘PIK3CA and TP53 mutations predict overall survival of stage II/III colorectal cancer patients’, *World Journal of Gastroenterology*. Baishideng Publishing Group Inc, 24(5), p. 631. doi: 10.3748/WJG.V24.I5.631.

Li, J. *et al.* (1997) ‘PTEN, a putative protein tyrosine phosphatase gene mutated in human brain, breast, and prostate cancer’, *Science*. American Association for the Advancement of Science , 275(5308), pp. 1943–1947. doi: 10.1126/SCIENCE.275.5308.1943/ASSET/07AC2F8A-192A-4B43-AC65-83E79A7DFDB0/ASSETS/GRAPHIC/SE137495204A.JPEG.

Li, J., Kim, S. G. and Blenis, J. (2014) ‘Rapamycin: One Drug, Many Effects’, *Cell Metabolism*. Cell Press, 19(3), pp. 373–379. doi: 10.1016/J.CMET.2014.01.001.

Lim, K. H. and Counter, C. M. (2005) ‘Reduction in the requirement of oncogenic Ras signaling to activation of PI3K/AKT pathway during tumor maintenance’, *Cancer Cell*. Cell Press, 8(5), pp. 381–392. doi: 10.1016/J.CCR.2005.10.014.

Liu, C. *et al*. (2002) ‘Control of β-Catenin Phosphorylation/Degradation by a Dual-Kinase Mechanism’, *Cell*. Cell Press, 108(6), pp. 837–847. doi: 10.1016/S0092-8674(02)00685-2.

Liu, P. *et al*. (2015) ‘PtdIns(3,4,5)P3-Dependent Activation of the mTORC2 Kinase Complex.’, *Cancer discovery*. NIH Public Access, 5(11), pp. 1194–209. doi: 10.1158/2159-8290.CD-15-0460.

Lone, M. U. D. *et al*. (2019) ‘Direct physical interaction of active Ras with mSIN1 regulates mTORC2 signaling’, *BMC Cancer*. BioMed Central Ltd., 19(1). doi: 10.1186/s12885-019-6422-6.

Long, X. *et al*. (2005) ‘Rheb Binds and Regulates the mTOR Kinase’, *Current Biology*. Cell Press, 15(8), pp. 702–713. doi: 10.1016/J.CUB.2005.02.053.

Lowenstein, E. J. *et al*. (1992) ‘The SH2 and SH3 domain-containing protein GRB2 links receptor tyrosine kinases to ras signaling’, *Cell*. Cell Press, 70(3), pp. 431–442. doi: 10.1016/0092-8674(92)90167-B.

Lozano, J. *et al*. (2003) ‘Deficiency of Kinase Suppressor of Ras1 Prevents Oncogenic Ras Signaling in Mice 1’, *CANCER RESEARCH*, 63, pp. 4232–4238. Available at: http://aacrjournals.org/cancerres/article-pdf/63/14/4232/2505391/4232.pdf (Accessed: 16 May 2022).

Lucas, C. L. *et al*. (2014) ‘Heterozygous splice mutation in PIK3R1 causes human immunodeficiency with lymphoproliferation due to dominant activation of PI3K.’, *The Journal of experimental medicine*. The Rockefeller University Press, 211(13), pp. 2537–47. doi: 10.1084/jem.20141759.

Luo, Q. *et al*. (2020) ‘KRAS and PIK3CA bi-mutations predict a poor prognosis in colorectal cancer patients: A single-site report’, *Translational Oncology*. Elsevier, 13(12), p. 100874. doi: 10.1016/J.TRANON.2020.100874.

Madsen, R. R. *et al*. (2019) 'Oncogenic PIK3CA promotes cellular stemness in an allele dose-dependent manner', *Proceedings of the National Academy of Sciences of the United States of America*. National Academy of Sciences, 116(17), pp. 8380–8389. doi: 10.1073/pnas.1821093116.

Madsen, R. R. and Vanhaesebroeck, B. (2020) 'Cracking the context-specific PI3K signaling code', *Science Signaling*. American Association for the Advancement of Science. doi: 10.1126/scisignal.aay2940.

Malek, M. *et al*. (2017) 'PTEN Regulates PI(3,4)P 2 Signaling Downstream of Class I PI3K', *Molecular cell*. Mol Cell, 68(3), pp. 566-580.e10. doi: 10.1016/J.MOLCEL.2017.09.024.

Manning, B. D. *et al*. (2002) 'Identification of the Tuberous Sclerosis Complex-2 Tumor Suppressor Gene Product Tuberin as a Target of the Phosphoinositide 3-Kinase/Akt Pathway', *Molecular Cell*. Cell Press, 10(1), pp. 151–162. doi: 10.1016/S1097-2765(02)00568-3.

Manning, B. D. and Toker, A. (2017) 'AKT/PKB Signaling: Navigating the Network', *Cell*. NIH Public Access, 169(3), p. 381. doi: 10.1016/J.CELL.2017.04.001.

Mao, C. *et al*. (2012) 'PIK3CA exon 20 mutations as a potential biomarker for resistance to anti-EGFR monoclonal antibodies in KRAS wild-type metastatic colorectal cancer: a systematic review and meta-analysis', *Annals of Oncology*. Oxford University Press, 23(6), pp. 1518–1525. doi: 10.1093/annonc/mdr464.

El Marjou, F. *et al*. (2004) 'Tissue-specific and inducible Cre-mediated recombination in the gut epithelium', *genesis*. John Wiley & Sons, Ltd, 39(3), pp. 186–193. doi: 10.1002/GENE.20042.

Marques, M. *et al*. (2020) 'Combined MEK and PI3K/p110β inhibition as a novel targeted therapy for malignant mesothelioma displaying sarcomatoid features', *Cancer Research*. American Association for Cancer Research Inc., 80(4), pp. 843–856. doi: 10.1158/0008-5472.CAN-19-1633/653852/AM/COMBINED-MEK-AND-PI3K-P110B-INHIBITION-AS-A-NOVEL.

Martini, E. *et al.* (2017) 'Mend Your Fences: The Epithelial Barrier and its Relationship With Mucosal Immunity in Inflammatory Bowel Disease', *Cellular and Molecular Gastroenterology and Hepatology*. Elsevier, 4(1), pp. 33–46. doi: 10.1016/J.JCMGH.2017.03.007.

Matallanas, D. *et al.* (2011) 'Raf Family Kinases: Old Dogs Have Learned New Tricks', *Genes & Cancer*. Impact Journals, LLC, 2(3), p. 232. doi: 10.1177/1947601911407323.

Maunoury, R. *et al.* (1992) 'Developmental regulation of villin gene expression in the epithelial cell lineages of mouse digestive and urogenital tracts', *Development*. The Company of Biologists, 115(3), pp. 717–728. doi: 10.1242/DEV.115.3.717.

McManus, E. J. *et al.* (2005) 'Role that phosphorylation of GSK3 plays in insulin and Wnt signalling defined by knockin analysis', *The EMBO Journal*. European Molecular Biology Organization, 24(8), p. 1571. doi: 10.1038/SJ.EMBOJ.7600633.

Mei, Z. *et al.* (2016) 'Prognostic role of tumor PIK3CA mutation in colorectal cancer: a systematic review and meta-analysis', *Annals of Oncology*. Oxford University Press, 27(10), p. 1836. doi: 10.1093/ANNONC/MDW264.

Misale, S. *et al.* (2012) 'Emergence of KRAS mutations and acquired resistance to anti-EGFR therapy in colorectal cancer', *Nature 2012 486:7404*. Nature Publishing Group, 486(7404), pp. 532–536. doi: 10.1038/nature11156.

Molinari, F. and Frattini, M. (2014) 'Functions and regulation of the PTEN gene in colorectal cancer', *Frontiers in Oncology*. Frontiers Research Foundation, 4 JAN, p. 326. doi: 10.3389/FONC.2013.00326/BIBTEX.

Mora, A. *et al.* (2004) 'PDK1, the master regulator of AGC kinase signal transduction', *Seminars in Cell & Developmental Biology*. Academic Press, 15(2), pp. 161–170. doi: 10.1016/J.SEMCDB.2003.12.022.

Moser, A. R., Pitot, H. C. and Dove, W. F. (1990) 'A dominant mutation that predisposes to multiple intestinal neoplasia in the mouse.', *Science (New York,*

N.Y.), 247(4940), pp. 322–4. Available at: http://www.ncbi.nlm.nih.gov/pubmed/2296722 (Accessed: 17 March 2018).

Murphy, N. *et al.* (2019) 'Lifestyle and dietary environmental factors in colorectal cancer susceptibility', *Molecular Aspects of Medicine*. Pergamon, 69, pp. 2–9. doi: 10.1016/J.MAM.2019.06.005.

Muzny, D. M. *et al.* (2012) 'Comprehensive molecular characterization of human colon and rectal cancer', *Nature 2012 487:7407*. Nature Publishing Group, 487(7407), pp. 330–337. doi: 10.1038/nature11252.

Myant, K. B. *et al.* (2013) 'ROS production and NF-κB activation triggered by RAC1 facilitate WNT-driven intestinal stem cell proliferation and colorectal cancer initiation.', *Cell stem cell*. Elsevier, 12(6), pp. 761–73. doi: 10.1016/j.stem.2013.04.006.

Mysore, V. P. *et al.* (2021) 'A structural model of a Ras–Raf signalosome', *Nature Structural & Molecular Biology 2021 28:10*. Nature Publishing Group, 28(10), pp. 847–857. doi: 10.1038/s41594-021-00667-6.

Najumudeen, A. K. *et al.* (2021) 'The amino acid transporter SLC7A5 is required for efficient growth of KRAS-mutant colorectal cancer', *Nature Genetics 2021 53:1*. Nature Publishing Group, 53(1), pp. 16–26. doi: 10.1038/s41588-020-00753-3.

Nicklin, P. *et al.* (2009) 'Bidirectional Transport of Amino Acids Regulates mTOR and Autophagy', *Cell*. Cell Press, 136(3), pp. 521–534. doi: 10.1016/J.CELL.2008.11.044.

Van Noort, M. *et al.* (2002) 'Wnt Signaling Controls the Phosphorylation Status of β-Catenin', *Journal of Biological Chemistry*. Elsevier, 277(20), pp. 17901–17905. doi: 10.1074/JBC.M111635200.

Nosho, K. *et al.* (2008) 'PIK3CA mutation in colorectal cancer: relationship with genetic and epigenetic alterations.', *Neoplasia (New York, N.Y.)*. Neoplasia Press, 10(6), pp. 534–41. Available at:

http://www.ncbi.nlm.nih.gov/pubmed/18516290 (Accessed: 9 May 2019).

Ogino, S. *et al.* (2013) 'Discovery of colorectal cancer PIK3CA mutation as potential predictive biomarker: power and promise of molecular pathological epidemiology', *Oncogene 2014 33:23*. Nature Publishing Group, 33(23), pp. 2949–2955. doi: 10.1038/onc.2013.244.

Okamura, T. *et al.* (2020) 'Clinicopathologic and molecular characteristics of familial adenomatous polyposis-associated traditional serrated adenoma', *American Journal of Surgical Pathology*. Lippincott Williams and Wilkins, 44(9), pp. 1282–1289. doi: 10.1097/PAS.0000000000001502.

Olsen, J. V. *et al.* (2006) 'Global, In Vivo, and Site-Specific Phosphorylation Dynamics in Signaling Networks', *Cell*. Cell Press, 127(3), pp. 635–648. doi: 10.1016/J.CELL.2006.09.026.

Overview | Colorectal cancer | Guidance | NICE (no date). Available at: https://www.nice.org.uk/guidance/ng151 (Accessed: 25 May 2022).

Pacold, M. E. *et al.* (2000) 'Crystal Structure and Functional Analysis of Ras Binding to Its Effector Phosphoinositide 3-Kinase γ', *Cell*. Cell Press, 103(6), pp. 931–944. doi: 10.1016/S0092-8674(00)00196-3.

Park, J. M. *et al.* (2016) 'The ULK1 complex mediates MTORC1 signaling to the autophagy initiation machinery via binding and phosphorylating ATG14', *Autophagy*. Taylor and Francis Inc., 12(3), pp. 547–564. doi: 10.1080/15548627.2016.1140293/SUPPL_FILE/KAUP_A_1140293_SM1719.DOCX.

Pause, A. *et al.* (1994) 'Insulin-dependent stimulation of protein synthesis by phosphorylation of a regulator of 5'-cap function', *Nature 1994 371:6500*. Nature Publishing Group, 371(6500), pp. 762–767. doi: 10.1038/371762a0.

Phase I, Dose Study to Look at the Safety and Pharmacokinetics of AZD8835 in Patients With Advanced Solid Tumours - Full Text View - ClinicalTrials.gov (no date). Available at: https://clinicaltrials.gov/ct2/show/NCT02260661 (Accessed: 28 February 2022).

Pickering, K. A. *et al*. (2021) 'A RAC-GEF network critical for early intestinal tumourigenesis', *Nature Communications*. Nature Research, 12(1). doi: 10.1038/S41467-020-20255-4.

Pierre, S., Bats, A. S. and Coumoul, X. (2011) 'Understanding SOS (Son of Sevenless)', *Biochemical Pharmacology*. Elsevier, 82(9), pp. 1049–1056. doi: 10.1016/J.BCP.2011.07.072.

Pinson, K. I. *et al*. (2000) 'An LDL-receptor-related protein mediates Wnt signalling in mice', *Nature 2000 407:6803*. Nature Publishing Group, 407(6803), pp. 535–538. doi: 10.1038/35035124.

Porstmann, T. *et al*. (2008) 'SREBP Activity Is Regulated by mTORC1 and Contributes to Akt-Dependent Cell Growth', *Cell Metabolism*. Elsevier, 8(3–3), p. 224. doi: 10.1016/J.CMET.2008.07.007.

Potter, C. J., Pedraza, L. G. and Xu, T. (2002) 'Akt regulates growth by directly phosphorylating Tsc2', *Nature Cell Biology 2002 4:9*. Nature Publishing Group, 4(9), pp. 658–665. doi: 10.1038/ncb840.

Prenen, H. *et al*. (2009) 'PIK3CA mutations are not a major determinant of resistance to the epidermal growth factor receptor inhibitor cetuximab in metastatic colorectal cancer', *Clinical Cancer Research*. American Association for Cancer Research, 15(9), pp. 3184–3188. doi: 10.1158/1078-0432.CCR-08-2961/346934/P/PIK3CA-MUTATIONS-ARE-NOT-A-MAJOR-DETERMINANT-OF.

Prossomariti, A. *et al*. (2020) 'Are Wnt/β-Catenin and PI3K/AKT/mTORC1 Distinct Pathways in Colorectal Cancer?', *Cellular and Molecular Gastroenterology and Hepatology*. Elsevier, 10(3), pp. 491–506. doi: 10.1016/J.JCMGH.2020.04.007.

Rad, R. *et al*. (2013) 'A Genetic Progression Model of BrafV600E-Induced Intestinal Tumorigenesis Reveals Targets for Therapeutic Intervention', *Cancer Cell*. Cell Press, 24(1), pp. 15–29. doi: 10.1016/J.CCR.2013.05.014.

Rademacher, S. and Eickholt, B. J. (2019) 'PTEN in Autism and

Neurodevelopmental Disorders', *Cold Spring Harbor Perspectives in Medicine*. Cold Spring Harbor Laboratory Press, 9(11), p. a036780. doi: 10.1101/CSHPERSPECT.A036780.

Rebsamen, M. *et al.* (2015) 'SLC38A9 is a component of the lysosomal amino acid sensing machinery that controls mTORC1', *Nature 2015 519:7544*. Nature Publishing Group, 519(7544), pp. 477–481. doi: 10.1038/nature14107.

Rex, D. K. *et al.* (2012) 'Serrated Lesions of the Colorectum: Review and Recommendations From an Expert Panel', *The American Journal of Gastroenterology*. Nature Publishing Group, 107(9), pp. 1315–1329. doi: 10.1038/ajg.2012.161.

Rim, E. Y., Clevers, H. and Nusse, R. (2022) 'The Wnt Pathway: From Signaling Mechanisms to Synthetic Modulators'. doi: 10.1146/annurev-biochem-040320.

Rodriguez-Viciana, P., Sabatier, C. and McCormick, F. (2004) 'Signaling Specificity by Ras Family GTPases Is Determined by the Full Spectrum of Effectors They Regulate', *Molecular and Cellular Biology*. American Society for Microbiology, 24(11), pp. 4943–4954. doi: 10.1128/MCB.24.11.4943-4954.2004/ASSET/6B63B5D5-2CD6-42A2-879A-53E792E4460F/ASSETS/GRAPHIC/ZMB0110441110006.JPEG.

Román-Fernández, Á. *et al.* (2018) 'The phospholipid PI(3,4)P2 is an apical identity determinant', *Nature Communications 2018 9:1*. Nature Publishing Group, 9(1), pp. 1–17. doi: 10.1038/s41467-018-07464-8.

Samuels, Y. *et al.* (2004) 'High Frequency of Mutations of the PIK3CA Gene in Human Cancers', *Science*. American Association for the Advancement of Science, 304(5670), pp. 554–554. doi: 10.1126/SCIENCE.1096502.

Sancak, Y. *et al.* (2008) 'The rag GTPases bind raptor and mediate amino acid signaling to mTORC1', *Science*. American Association for the Advancement of Science , 320(5882), pp. 1496–1501. doi: 10.1126/SCIENCE.1157535/SUPPL_FILE/SANCAK.SOM.PDF.

Sancak, Y. *et al.* (2010) 'Ragulator-Rag complex targets mTORC1 to the lysosomal surface and is necessary for its activation by amino acids', *Cell*. NIH Public Access, 141(2), p. 290. doi: 10.1016/J.CELL.2010.02.024.

Sansom, O. J. *et al.* (2004) 'Loss of Apc in vivo immediately perturbs Wnt signaling, differentiation, and migration.', *Genes & development*, 18(12), pp. 1385–90. doi: 10.1101/gad.287404.

Sansom, O. J. *et al.* (2006) 'Loss of Apc allows phenotypic manifestation of the transforming properties of an endogenous K-ras oncogene in vivo.', *Proceedings of the National Academy of Sciences of the United States of America*. National Academy of Sciences, 103(38), pp. 14122–7. doi: 10.1073/pnas.0604130103.

Sansom, O. J. *et al.* (2007) 'Myc deletion rescues Apc deficiency in the small intestine.', *Nature*, 446(7136), pp. 676–9. doi: 10.1038/nature05674.

Sarbassov, D. D. *et al.* (2005) 'Phosphorylation and regulation of Akt/PKB by the rictor-mTOR complex.', *Science (New York, N.Y.)*. American Association for the Advancement of Science, 307(5712), pp. 1098–101. doi: 10.1126/science.1106148.

Sato, T. *et al.* (2009) 'Single Lgr5 stem cells build crypt-villus structures in vitro without a mesenchymal niche.', *Nature*, 459(7244), pp. 262–5. doi: 10.1038/nature07935.

Schmid, P. *et al.* (2017) 'A study of vistusertib in combination with selumetinib in patients with advanced cancers: TORCMEK phase Ib results.', *Journal of Clinical Oncology*. Wolters Kluwer, 35(15_suppl), p. 2548. doi: 10.1200/JCO.2017.35.15_suppl.2548.

Schmidt, K. M. *et al.* (2017) 'Inhibition of mTORC2 component RICTOR impairs tumor growth in pancreatic cancer models', *Oncotarget*. Impact Journals, 8(15), pp. 24491–24505. doi: 10.18632/ONCOTARGET.15524.

Schreiber, K. H. *et al.* (2015) 'Rapamycin-mediated mTORC2 inhibition is determined by the relative expression of FK506-binding proteins', *Aging Cell*.

Wiley-Blackwell, 14(2), p. 265. doi: 10.1111/ACEL.12313.

Search of: AZD2014 - List Results - ClinicalTrials.gov (no date). Available at: https://clinicaltrials.gov/ct2/results?term=AZD2014 (Accessed: 28 February 2022).

Search of: AZD6244 | Colorectal Cancer - List Results - ClinicalTrials.gov (no date). Available at: https://clinicaltrials.gov/ct2/results?term=AZD6244&cond=Colorectal+Cancer (Accessed: 16 May 2022).

Serebriiskii, I. G. *et al.* (2022) 'Comprehensive characterization of PTEN mutational profile in a series of 34,129 colorectal cancers', *Nature Communications 2022 13:1*. Nature Publishing Group, 13(1), pp. 1–17. doi: 10.1038/s41467-022-29227-2.

Shi, J. *et al.* (2012) 'Microsomal glutathione transferase 1 protects against toxicity induced by silica nanoparticles but not by zinc oxide nanoparticles', *ACS Nano*. American Chemical Society, 6(3), pp. 1925–1938. doi: 10.1021/NN2021056/SUPPL_FILE/NN2021056_SI_001.PDF.

Shibata, H. *et al.* (1997) 'Rapid colorectal adenoma formation initiated by conditional targeting of the APC gene', *Science*. American Association for the Advancement of Science, 278(5335), pp. 120–133. doi: 10.1126/SCIENCE.278.5335.120/ASSET/91835449-3697-4D9F-90D7-1BA8B9F011D1/ASSETS/GRAPHIC/SE3975756004.JPEG.

Shor, B. *et al.* (2010) 'Requirement of the mTOR Kinase for the Regulation of Maf1 Phosphorylation and Control of RNA Polymerase III-dependent Transcription in Cancer Cells', *The Journal of Biological Chemistry*. American Society for Biochemistry and Molecular Biology, 285(20), p. 15380. doi: 10.1074/JBC.M109.071639.

Siena, S. *et al.* (2009) 'Biomarkers Predicting Clinical Outcome of Epidermal Growth Factor Receptor–Targeted Therapy in Metastatic Colorectal Cancer', *JNCI: Journal of the National Cancer Institute*. Oxford Academic, 101(19), pp.

1308–1324. doi: 10.1093/JNCI/DJP280.

Sjolander, A. *et al.* (1991) ‘Association of p21(ras) with phosphatidylinositol 3-kinase’, *Proceedings of the National Academy of Sciences of the United States of America*, 88(18), pp. 7908–7912. doi: 10.1073/PNAS.88.18.7908.

Smith, S. F., Collins, S. E. and Charest, P. G. (2020) ‘Ras, PI3K and mTORC2 – three’s a crowd?’, *Journal of Cell Science*. Company of Biologists Ltd, 133(19). doi: 10.1242/JCS.234930/226141.

Solberg, N. T. *et al.* (2018) ‘TANKYRASE inhibition enhances the antiproliferative effect of PI3K and EGFR inhibition, mutually affecting ß-CATENIN and AKT signaling in colorectal cancer’, *Molecular Cancer Research*. American Association for Cancer Research Inc., 16(3), pp. 543–553. doi: 10.1158/1541-7786.MCR-17-0362/193023/AM/TANKYRASE-INHIBITION-ENHANCES-THE-ANTI.

Song, Y. *et al.* (2022) ‘Double-edged roles of protein tyrosine phosphatase SHP2 in cancer and its inhibitors in clinical trials’, *Pharmacology & Therapeutics*. Pergamon, 230, p. 107966. doi: 10.1016/J.PHARMTHERA.2021.107966.

Sottoriva, A. *et al.* (2015) ‘A Big Bang model of human colorectal tumor growth’, *Nature Genetics*, 47(3), pp. 209–216. doi: 10.1038/ng.3214.

Sphyris, N., Hodder, M. C. and Sansom, O. J. (2021) ‘Subversion of Niche-Signalling Pathways in Colorectal Cancer: What Makes and Breaks the Intestinal Stem Cell’, *Cancers 2021, Vol. 13, Page 1000*. Multidisciplinary Digital Publishing Institute, 13(5), p. 1000. doi: 10.3390/CANCERS13051000.

Su, L. K. *et al.* (1992) ‘Multiple intestinal neoplasia caused by a mutation in the murine homolog of the APC gene.’, *Science (New York, N.Y.)*, 256(5057), pp. 668–670. doi: 10.1126/SCIENCE.1350108.

Suire, S. *et al.* (2006) ‘Gβγs and the Ras binding domain of p110γ are both important regulators of PI(3)Kγ signalling in neutrophils’, *NATURE CELL BIOLOGY*, 8. doi: 10.1038/ncb1494.

Sumigray, K. D., Terwilliger, M. and Lechler, T. (2018) ‘Morphogenesis and Compartmentalization of the Intestinal Crypt’, *Developmental Cell*. Cell Press, 45(2), pp. 183-197.e5. doi: 10.1016/J.DEVCEL.2018.03.024.

Suzuki, A. *et al.* (2001) ‘T Cell-Specific Loss of Pten Leads to Defects in Central and Peripheral Tolerance’, *Immunity*. Cell Press, 14(5), pp. 523–534. doi: 10.1016/S1074-7613(01)00134-0.

Szwed, A., Kim, E. and Jacinto, E. (2021) ‘Regulation and metabolic functions of mTORC1 and mTORC2’, *Physiological reviews*. NLM (Medline), 101(3), pp. 1371–1426. doi: 10.1152/PHYSREV.00026.2020/ASSET/IMAGES/LARGE/PHYSREV.00026.2020_F008.JPEG.

Tee, A. R. *et al.* (2003) ‘Tuberous Sclerosis Complex Gene Products, Tuberin and Hamartin, Control mTOR Signaling by Acting as a GTPase-Activating Protein Complex toward Rheb’, *Current Biology*. Cell Press, 13(15), pp. 1259–1268. doi: 10.1016/S0960-9822(03)00506-2.

Tenbaum, S. P. *et al.* (2012) ‘ß-catenin confers resistance to PI3K and AKT inhibitors and subverts FOXO3a to promote metastasis in colon cancer’, *Nature Medicine 2012 18:6*. Nature Publishing Group, 18(6), pp. 892–901. doi: 10.1038/nm.2772.

Ternet, C. and Kiel, C. (2021) ‘Signaling pathways in intestinal homeostasis and colorectal cancer: KRAS at centre stage’, *Cell Communication and Signaling : CCS*. BioMed Central, 19(1). doi: 10.1186/S12964-021-00712-3.

Das Thakur, M. *et al.* (2013) ‘Modelling vemurafenib resistance in melanoma reveals a strategy to forestall drug resistance’, *Nature*, 494(7436), pp. 251–255. doi: 10.1038/NATURE11814.

Therrien, M. *et al.* (1995) ‘KSR, a Novel Protein Kinase Required for RAS Signal Transduction’, *Cell*, 83, pp. 879–888.

Thobe, K., Sers, C. and Siebert, H. (2017) ‘Unraveling the regulation of mTORC2

using logical modeling', *Cell Communication and Signaling*. BioMed Central Ltd., 15(1), p. 6. doi: 10.1186/s12964-016-0159-5.

Thorpe, L. M., Yuzugullu, H. and Zhao, J. J. (2015) 'PI3K in cancer: divergent roles of isoforms, modes of activation and therapeutic targeting', *Nature Reviews Cancer*. Nature Publishing Group, 15(1), pp. 7–24. doi: 10.1038/nrc3860.

Tian, H. *et al.* (2011) 'A reserve stem cell population in small intestine renders Lgr5-positive cells dispensable', *Nature 2011 478:7368*. Nature Publishing Group, 478(7368), pp. 255–259. doi: 10.1038/nature10408.

Trotman, L. C. *et al.* (2003) 'Pten dose dictates cancer progression in the prostate', *PLoS Biology*, 1(3). doi: 10.1371/JOURNAL.PBIO.0000059.

Valvezan, A. J. *et al.* (2017) 'mTORC1 couples nucleotide synthesis to nucleotide demand resulting in a targetable metabolic vulnerability', *Cancer cell*. NIH Public Access, 32(5), p. 624. doi: 10.1016/J.CCELL.2017.09.013.

Vanhaesebroeck, B. *et al.* (2021) 'PI3K inhibitors are finally coming of age', *Nature Reviews Drug Discovery 2021 20:10*. Nature Publishing Group, 20(10), pp. 741–769. doi: 10.1038/s41573-021-00209-1.

Vasan, N. *et al.* (2019) 'Double PIK3CA mutations in cis increase oncogenicity and sensitivity to PI3Kα inhibitors', *Science (New York, N.Y.)*. Science, 366(6466), pp. 714–723. doi: 10.1126/SCIENCE.AAW9032.

Vermeulen, L. *et al.* (2009) 'The versatile role of MSKs in transcriptional regulation', *Trends in Biochemical Sciences*. Elsevier Current Trends, 34(6), pp. 311–318. doi: 10.1016/J.TIBS.2009.02.007.

Voutsadakis, I. A. (2021) 'The Landscape of PIK3CA Mutations in Colorectal Cancer', *Clinical Colorectal Cancer*. Elsevier, 20(3), pp. 201–215. doi: 10.1016/J.CLCC.2021.02.003.

Wang, S. *et al.* (2015) 'Lysosomal amino acid transporter SLC38A9 signals arginine sufficiency to mTORC1', *Science*. American Association for the

Advancement of Science, 347(6218), pp. 188–194. doi: 10.1126/SCIENCE.1257132/SUPPL_FILE/1257132.WANG.SM.PDF.

Wang, X. *et al*. (2007) 'NEDD4-1 Is a Proto-Oncogenic Ubiquitin Ligase for PTEN', *Cell*. Cell Press, 128(1), pp. 129–139. doi: 10.1016/J.CELL.2006.11.039.

Wang, X. *et al*. (2022) 'Identification of MRTX1133, a Noncovalent, Potent, and Selective KRASG12DInhibitor', *Journal of Medicinal Chemistry*. American Chemical Society, 65(4), pp. 3123–3133. doi: 10.1021/ACS.JMEDCHEM.1C01688/SUPPL_FILE/JM1C01688_SI_002.CSV.

Waniczek, D. *et al*. (2013) 'PTEN expression profiles in colorectal adenocarcinoma and its precancerous lesions', *Polish Journal of Pathology*. Termedia, 64(1), pp. 15–20. doi: 10.5114/PJP.2013.34598.

Webb, A. E. and Brunet, A. (2014) 'FOXO transcription factors: Key regulators of cellular quality control', *Trends in Biochemical Sciences*. Elsevier Ltd, 39(4), pp. 159–169. doi: 10.1016/J.TIBS.2014.02.003.

Wee, S. *et al*. (2008) 'PTEN-deficient cancers depend on PIK3CB.', *Proceedings of the National Academy of Sciences of the United States of America*. National Academy of Sciences, 105(35), pp. 13057–62. doi: 10.1073/pnas.0802655105.

Welch, H. C. E. *et al*. (2002) 'P-Rex1, a PtdIns(3,4,5)P3- and Gβγ-Regulated Guanine-Nucleotide Exchange Factor for Rac', *Cell*. Cell Press, 108(6), pp. 809–821. doi: 10.1016/S0092-8674(02)00663-3.

Whitmarsh, A. J. (2007) 'Regulation of gene transcription by mitogen-activated protein kinase signaling pathways', *Biochimica et Biophysica Acta (BBA) - Molecular Cell Research*. Elsevier, 1773(8), pp. 1285–1298. doi: 10.1016/J.BBAMCR.2006.11.011.

Wilkinson, J. E. *et al*. (2012) 'Rapamycin slows aging in mice', *Aging cell*. NIH Public Access, 11(4), p. 675. doi: 10.1111/J.1474-9726.2012.00832.X.

Wolfson, R. L. *et al*. (2016) 'Sestrin2 is a leucine sensor for the mTORC1

pathway', *Science*. American Association for the Advancement of Science, 351(6268), pp. 43–48. doi: 10.1126/SCIENCE.AAB2674/SUPPL_FILE/AAB2674-WOLFSON-SM.PDF.

Wyant, G. A. *et al.* (2017) 'mTORC1 Activator SLC38A9 Is Required to Efflux Essential Amino Acids from Lysosomes and Use Protein as a Nutrient', *Cell*. Cell Press, 171(3), pp. 642-654.e12. doi: 10.1016/J.CELL.2017.09.046.

Xenou, L. and Papakonstanti, E. A. (2020) 'p110δ PI3K as a therapeutic target of solid tumours', *Clinical Science*. Portland Press, 134(12), pp. 1377–1397. doi: 10.1042/CS20190772.

Yaeger, R. *et al.* (2018) 'Clinical Sequencing Defines the Genomic Landscape of Metastatic Colorectal Cancer.', *Cancer cell*. Elsevier, 33(1), pp. 125-136.e3. doi: 10.1016/j.ccell.2017.12.004.

Yamauchi, M. *et al.* (2012) 'Assessment of colorectal cancer molecular features along bowel subsites challenges the conception of distinct dichotomy of proximal versus distal colorectum', *Gut*. BMJ Publishing Group, 61(6), pp. 847–854. doi: 10.1136/GUTJNL-2011-300865.

Yang, H. *et al.* (2016) '4.4 Å Resolution Cryo-EM structure of human mTOR Complex 1', *Protein and Cell*. Higher Education Press, 7(12), pp. 878–887. doi: 10.1007/S13238-016-0346-6/FIGURES/5.

Yang, H. *et al.* (2017) 'Structural Mechanisms of mTORC1 activation by RHEB and inhibition by PRAS40', *Nature*. NIH Public Access, 552(7685), p. 368. doi: 10.1038/NATURE25023.

Yang, S. H., Sharrocks, A. D. and Whitmarsh, A. J. (2013) 'MAP kinase signalling cascades and transcriptional regulation', *Gene*. Elsevier, 513(1), pp. 1–13. doi: 10.1016/J.GENE.2012.10.033.

Yueh, A. E. *et al.* (2016) 'Colon Cancer Tumorigenesis Initiated by the H1047R Mutant PI3K', *PLoS ONE*. Public Library of Science, 11(2), p. e0148730. doi: 10.1371/JOURNAL.PONE.0148730.

Yui, S. *et al*. (2018) 'YAP/TAZ-Dependent Reprogramming of Colonic Epithelium Links ECM Remodeling to Tissue Regeneration', *Cell Stem Cell*. Cell Press, 22(1), pp. 35-49.e7. doi: 10.1016/J.STEM.2017.11.001.

Zeng, H., Dvorak, H. F. and Mukhopadhyay, D. (2001) 'Vascular Permeability Factor (VPF)/Vascular Endothelial Growth Factor (VEGF) Receptor-1 Down-modulates VPF/VEGF Receptor-2-mediated Endothelial Cell Proliferation, but Not Migration, through Phosphatidylinositol 3-Kinase-dependent Pathways', *Journal of Biological Chemistry*. Elsevier, 276(29), pp. 26969–26979. doi: 10.1074/JBC.M103213200.

Zhang, H. *et al*. (2007) 'PDGFRs are critical for PI3K/Akt activation and negatively regulated by mTOR', *The Journal of Clinical Investigation*, 117. doi: 10.1172/JCI28984.

Zhao, L. and Vogt, P. K. (2008) 'Helical domain and kinase domain mutations in p110α of phosphatidylinositol 3-kinase induce gain of function by different mechanisms', *Proceedings of the National Academy of Sciences*. National Academy of Sciences, 105(7), pp. 2652–2657. doi: 10.1073/PNAS.0712169105.

Zoncu, R. *et al*. (2011) 'mTORC1 senses lysosomal amino acids through an inside-out mechanism that requires the vacuolar H+-ATPase', *Science*. American Association for the Advancement of Science, 334(6056), pp. 678–683. doi: 10.1126/SCIENCE.1207056/SUPPL_FILE/ZONCU.SOM.PDF.